

The Pennsylvania State University

The Graduate School

College of Engineering

ULTRAFILTRATION OF PEGYLATED PROTEINS

A Dissertation in

Chemical Engineering

by

Jessica R. Molek

© 2008 Jessica R. Molek

Submitted in Partial Fulfillment
of the Requirements
for the Degree of

Doctor of Philosophy

December 2008

The dissertation of Jessica R. Molek was reviewed and approved* by the following:

Andrew L. Zydney
Head of the Department of Chemical Engineering
Walter L. Robb Chair and Professor of Chemical Engineering
Dissertation Advisor
Chair of Committee

Wayne R. Curtis
Professor of Chemical Engineering

Darrell Velegol
Associate Professor of Chemical Engineering

Erwin A. Vogler
Professor of Materials Science and Engineering

*Signatures are on file in the Graduate School

ABSTRACT

There is considerable clinical interest in the use of "second-generation" therapeutics produced by conjugation of a native protein with various polymers including polyethylene glycol (PEG). PEG–protein conjugates, so-called PEGylated proteins, can exhibit enhanced stability, half-life, and bioavailability. One of the challenges in the commercial production of PEGylated proteins is the purification required to remove unreacted polymer, native protein, and in many cases PEGylated proteins with non-optimal degrees of conjugation. The overall objective of this thesis was to examine the use of ultrafiltration for the purification of PEGylated proteins. This included: (1) analysis of size-based separation of PEGylated proteins using conventional ultrafiltration membranes, (2) use of electrically-charged membranes to exploit differences in electrostatic interactions, and (3) examination of the effects of PEGylation on protein fouling. The experimental results were analyzed using appropriate theoretical models, with the underlying physical properties of the PEGylated proteins evaluated using size exclusion chromatography, capillary electrophoresis, dynamic light scattering, and reverse phase chromatography.

PEGylated proteins were produced by covalent attachment of activated PEG to a protein via primary amines on the lysine residues. A simple model was developed for the reaction kinetics, which was used to explore the effect of reaction conditions and mode of operation on the distribution of PEGylated products. The effective size of the PEGylated proteins was evaluated using size exclusion chromatography, with appropriate correlations developed for the size in terms of the molecular weight of the native protein and attached PEG. The electrophoretic mobility of the PEGylated proteins were

evaluated by capillary electrophoresis with the data in good agreement with a simple model accounting for the increase in protein size and the reduction in the number of protonated amine groups in the PEGylated proteins.

Ultrafiltration experiments were performed using PEGylated α -lactalbumin, ovalbumin, and bovine serum albumin. In contrast to the size exclusion chromatography data, the sieving coefficient of the PEGylated proteins depended upon both the number and size of the attached PEG chains due to the elongation or deformation of the PEG associated with the filtrate flux. Sieving coefficients at low filtrate flux were in good agreement with predictions of available hydrodynamic models, with significant elongation occurring when the Deborah number for the PEG chain exceeded 0.001. The effects of electrostatic interactions on the ultrafiltration of PEGylated proteins were examined using electrically-charged membranes generated by covalent attachment of sulphonic acid groups to the base cellulosic membrane. Transmission of PEGylated proteins through charged membranes was dramatically reduced at low ionic strength due to strong electrostatic interactions, despite the presence of the neutral PEG. The experimental results were in good agreement with model calculations developed for the partitioning of charged spheres into charged cylindrical pores. The experimental and theoretical results provide the first quantitative analysis of the effects of PEGylation on transport through semipermeable ultrafiltration membranes.

The results from small-scale ultrafiltration experiments were used to develop a two-stage diafiltration process to purify PEGylated α -lactalbumin. The first-stage used a neutral membrane to remove the unreacted protein by exploiting differences in size. The second stage used a negatively-charged membrane to remove hydrolyzed PEG, with the

PEGylated product retained by strong electrostatic interactions. This process provided a purification factor greater than 1000 with respect to the unreacted protein and greater than 20-fold with respect to the PEG with an overall yield of PEGylated α -lactalbumin of 78%. These results provide the first demonstration of the potential of using ultrafiltration for the purification of protein-polymer conjugates.

TABLE OF CONTENTS

LIST OF TABLES	xi
LIST OF FIGURES	xiii
ACKNOWLEDGEMENTS	xxiv
Chapter 1. INTRODUCTION.....	1
1.1 Biotechnology	1
1.1.1 Post-Translational Modifications	2
1.1.2 Purification of Biotherapeutics	3
1.2 PEGylation.....	4
1.2.1 Benefits of PEGylation.	8
1.2.2 Mechanisms of Increased <i>In Vivo</i> Activity	10
1.2.3 Current Separation Techniques.....	13
1.2.3.1 Ion Exchange	17
1.2.3.2 Reverse Phase	18
1.2.3.3 Size Exclusion.....	19
1.3 Ultrafiltration	19
1.4 Thesis Summary.....	22
1.4.1 Overall Objectives	22
1.4.2 Thesis Outline	23
Chapter 2. THEORETICAL BACKGROUND	26
2.1 Introduction.....	26
2.2 Bulk Mass Transport.....	26
2.2.1 Stagnant Film Model.....	28
2.2.2 Mass Transfer Coefficient.....	30
2.3 Solvent Transport.....	31
2.3.1 Permeability	32
2.3.2 Electrostatic Effects on Solvent Flow	32
2.4 Solute Transport.....	35
2.4.1 Hydrodynamic Transport Parameters	39
2.4.2 Electrostatic Effects on the Partition Coefficient.....	41
2.5 Log-Normal Pore Size Distribution	44
2.6 Solute Deformation.....	46
Chapter 3. MATERIALS AND METHODS	49
3.1 Experimental Materials.....	49
3.1.1 Polyethylene Glycol.....	49
3.1.2 Activated Polyethylene Glycol	50
3.1.3 Proteins	51
3.1.4 Protein Modifications.....	53

3.1.4.1 PEGylated Protein Reaction	53
3.1.4.2 Protein Acetylation	56
3.1.5 Dextrans	57
3.1.6 Buffers.....	58
3.1.7 Ultrafiltration Membranes	59
3.2 Experimental Methods	61
3.2.1 Ultrafiltration Set-up.....	61
3.2.2 Membrane Hydraulic Permeability.....	62
3.2.3 Sieving Experiments	63
3.2.4 Diafiltration.....	64
3.2.5 Membrane Characterization.....	64
3.2.5.1 Pore Size Distribution	64
3.2.5.2 Membrane Charge Characterization	65
3.3 Assays	67
3.3.1 UV Spectrophotometry	67
3.3.2 Size Exclusion Chromatography.....	68
3.3.3 Reverse Phase High Performance Liquid Chromatography	73
3.3.4 Dynamic Light Scattering.....	74
3.3.5 Capillary Electrophoresis.....	75
3.3.6 Mass Spectrometry.....	76
 Chapter 4. PEGYLATED PROTEIN REACTIONS	 78
4.1 Introduction.....	78
4.2 Reaction Chemistry.....	78
4.2.1 Primary Amines – Lysine	79
4.2.2 Sulfides – Cysteine	81
4.2.3 Carboxylic Acid – C terminal amino acid	81
4.2.4 Other Reaction Chemistries	82
4.3 Materials and Methods.....	83
4.3.1 Materials	83
4.3.2 Reactions.....	83
4.4 PEGylation Reaction.....	85
4.5 Effect of Solution Parameters on Reaction Yield.....	89
4.5.1 Molar Ratio	89
4.5.2 Solution pH	90
4.5.3 Ionic Strength.....	92
4.5.4 Reactant Concentration.....	93
4.6 Reaction Schemes	94
4.7 Conclusions.....	101
 Chapter 5. SIZE EXCLUSION CHROMATOGRAPHY OF PEGYLATED PROTEINS	 104
5.1 Introduction.....	104
5.2 Theory	105
5.2.1 Size Exclusion Chromatography.....	105

5.2.2 Dynamic Light Scattering	106
5.3. Materials and Methods.....	108
5.3.1 Materials	108
5.3.2 Size Exclusion Chromatography.....	109
5.3.3 Dynamic Light Scattering	109
5.4 Results.....	109
5.4.1 Protein and PEG Standards.....	109
5.4.2 PEGylated Proteins	113
5.4.3 Modeling of the Partition Coefficient	117
5.4.4 Dynamic Light Scattering	121
5.4 Conclusions.....	124
Chapter 6. CAPILLARY ELECTROPHORESIS OF PEGYLATED PROTEINS	127
6.1 Introduction.....	127
6.2 Theory	129
6.2.1 Background.....	129
6.2.2 PEGylated Proteins	132
6.3 Materials and Methods.....	138
6.3.1 Materials	138
6.3.2 Capillary Electrophoresis.....	138
6.4 Results and Analysis	139
6.4.1 Effects of Buffer Additives.....	139
6.4.2 Effects of PEGylation on Protein Mobility.....	143
6.4.3 Electrophoretic Mobility of PEGylated Proteins	146
6.4.3.1 Effect of the Number of Substitutions	146
6.4.3.2 Effect of Ionic Strength.....	149
6.4.4 Drag Ratio.....	151
6.5 Conclusions.....	158
Chapter 7. ULTRAFILTRATION CHARACTERISTICS OF PEGYLATED PROTEINS	161
7.1 Introduction	161
7.2 Materials and Methods.....	162
7.2.1 Protein PEGylation	162
7.2.2 Ultrafiltration	163
7.3 Results.....	164
7.3.1 Observed Sieving Behavior	164
7.3.2 Comparison of Different PEG Configurations	168
7.3.3 Stagnant Film Model Calculations.....	171
7.3.4 Model Calculations for a Hard Sphere.....	173
7.3.5 Deviations from the Stagnant Film Model.....	176
7.3.6 Scaled Sieving Coefficient.....	180
7.3.7 Deborah Number.....	182
7.4 Conclusions.....	185

Chapter 8. ULTRAFILTRATION OF PEGYLATED PROTEINS USING CHARGE MODIFIED MEMBRANES	188
8.1 Introduction.....	188
8.2 Materials and Methods.....	191
8.2.1 Materials	191
8.2.2 Methods.....	192
8.3 Results.....	193
8.3.1 Membrane Charge.....	193
8.3.2 Effect of Ionic Strength on Sieving	196
8.3.3 Effect of pH on PEGylated Protein Transport	209
8.3.4 Effect of Membrane Charge.....	211
8.4 Conclusions.....	213
 Chapter 9. SEPARATION OF PEGYLATED PROTEINS FROM UNREACTED PRECURSORS	 216
9.1 Introduction.....	216
9.2 Materials and Methods.....	217
9.2.1 Protein PEGylation	217
9.2.2 Ultrafiltration Membranes / Apparatus.....	218
9.2.3 Ultrafiltration Sieving Experiments.....	218
9.2.4 Diafiltration.....	219
9.2.5 Assays	220
9.3 Results.....	221
9.3.1 Sieving Experiments	221
9.3.1.1 Uncharged Membranes	221
9.3.1.2 Charged Membrane Separations.....	224
9.3.2 Diafiltration.....	231
9.3.3 Purification – Yield Analysis.....	239
9.4 Conclusions.....	242
 Chapter 10. FOULING AND CONCENTRATION POLARIZATION DURING ULTRAFILTRATION OF PEGYLATED PROTEINS	 246
10.1 Introduction.....	246
10.2 Materials and Methods.....	249
10.2.1 Protein PEGylation	249
10.2.2 Ultrafiltration	249
10.2.3 Protein Characterization.....	251
10.3 Results.....	252
10.3.1 Regenerated Cellulose Membranes.....	252
10.3.2 Polyethersulfone Membranes.....	259
10.3.3 Electrostatic Interactions.....	264
10.4 Conclusions.....	267
 Chapter 11. CONCLUSIONS AND FUTURE WORK	 269
11.1 Introduction.....	269

11.2 PEGylation Reactions	270
11.3 Size Characterization	271
11.4 Charge Characterization.....	272
11.5 Ultrafiltration and PEG Elongation Effects	274
11.6 Ultrafiltration and Electrostatic Effects	276
11.7 Purification of PEGylated Proteins	278
11.8 Membrane Fouling.....	280
11.9 Recommendations.....	281
REFERENCES	287
Appendix A. NOMENCLATURE.....	313
Appendix B. ANALYSIS OF MEMBRANE PORE SIZE USING POLYDISPERSED DEXTRANS	319
Appendix C. CHARGE REGULATION THEORY.....	328

LIST OF TABLES

Table 1.1:	Commercially available PEGylated proteins.	7
Table 1.2:	Purification techniques for a range of PEGylated proteins – Chromatographic methods.	15
Table 1.3:	Purification techniques for a range of PEGylated proteins – Nonchromatographic methods.	16
Table 2.1:	Expansion coefficients for the K_t and K_s functions in Equation 2.38 and Equation 2.39.	40
Table 3.1:	Physico-chemical properties of proteins.	53
Table 3.2:	Components for different buffers used in experiments.	59
Table 3.3:	Molecular weight of PEG, α -lactalbumin and PEGylated α - lactalbumin as determined by MALDI-TOF.	77
Table 4.1:	Rate constants for reaction of α -lactalbumin with 5 kDa mPEG-SPA and mPEG-SMB in a 10 mM Bis Tris (pH 7.0) buffer.	88
Table 4.2:	Rate constants for reaction of 10 kDa mPEG-SPA with α - lactalbumin in a 10 mM Bis Tris pH 7.0 buffer.	98
Table 6.1:	Theoretical expressions for drag ratios using physical models discussed in Section 6.2.2.	154
Table 7.1:	Mass transfer coefficient (k_m) and actual sieving coefficients (S_a) of ovalbumin, PEG, and PEGylated forms of ovalbumin through a 30 kDa Ultracel TM membrane.	172
Table 8.1:	Zeta potential and charge density for 30 kDa and 100 kDa Ultracel TM membranes charged for 0, 12, or 24 hours.	195
Table 8.2:	Physical properties of α -lactalbumin, PEG, and PEGylated α -lactalbumin in 10 mM pH 7.0 Bis Tris buffer.	199
Table 8.3:	Physical parameters of the 100 kDa Ultracel TM membrane charged for 12 hours.	199
Table 8.4:	Calculated electronic charge (number of free electrons) based on the published amino acid sequence (Brew et al., 1970).	210

Table 9.1:	Feed concentration of 20 kDa PEG, native α -lactalbumin, and PEGylated α -lactalbumin for the ultrafiltration and diafiltration experiments.	218
Table 9.2:	Sieving coefficients for α -lactalbumin, 20 kDa PEG, and PEGylated protein for the first and second stage diafiltration.	235
Table 10.1:	Membrane, fouling layer, and polarization resistances through Ultracel TM membranes.....	258
Table 10.2:	Membrane, fouling layer, and polarization resistances for ultrafiltration experiments with Biomax TM membranes.	262
Table C.1:	Number and pKa values for the dissociable amino acids in α -lactalbumin (Brew, et al., 1970).....	329

LIST OF FIGURES

Figure 1.1:	Concentration of α -interferon in the body as a function of time for the PEGylated and native forms. The PEGylated form shows a relatively constant concentration profiles while the native form shows significant variations. Taken from Harris (2001).....	9
Figure 1.2:	Comparison of the <i>in vitro</i> and <i>in vivo</i> activity of a PEGylated molecule as a function of the mass of PEG added. Curves are simple fits to clarify the trend of the data. Adapted from Bailon and Berthold (1998).....	13
Figure 2.1:	Schematic of concentration polarization in solution above a membrane. The highest solute concentration is at the membrane surface. C_b , C_w , and C_f represent the concentration of the solute in the bulk solution, at the membrane surface (wall), and in the filtrate solution. Adapted from Bohonak (2006).....	28
Figure 2.2:	Hydrodynamic functions, G and K^{-1} as a function of the solute to pore ratio, λ	41
Figure 3.1:	Chemical structure of polyethylene glycol.	49
Figure 3.2:	Chemical structures of activated polyethylene glycols used for protein PEGylation.....	51
Figure 3.3:	Structure of globular proteins: α -lactalbumin, ovalbumin, and human serum albumin.	52
Figure 3.4:	Scaled schematic of PEGylated α -lactalbumin with 5 kDa or 20 kDa total molecular weight of PEG and BSA with 12 kDa of PEG attached.	55
Figure 3.5:	Acetylation reaction between the primary amine on a protein and acetic anhydride.	56
Figure 3.6:	Chemical structure of dextran. Adapted from Burns (2000).	57
Figure 3.7:	SEM image of the cross section of an Ultracel 100 kDa membrane produced by Millipore Corporation (2008a).....	60
Figure 3.8:	Schematic of reaction chemistry used to make negatively charged membranes.	61

Figure 3.9: Schematic of ultrafiltration stirred cell set-up.	62
Figure 3.10: Streaming potential apparatus used to determine the membrane surface charge. Adapted from Mehta (2006).	66
Figure 3.11: Calibration curve of α -lactalbumin using UV absorbance at 280 nm.	68
Figure 3.12: Schematic of size exclusion chromatography set-up.	70
Figure 3.13: Calibration curve for PEG using refractive index detection.	71
Figure 3.14: Calibration curves for α -lactalbumin using both refractive index and UV absorbance.	71
Figure 3.15: Dextran molecular weight calibration for the G2000SW column.	73
Figure 3.16: MALDI-TOF results with a 5 kDa PEG conjugated to α -lactalbumin.	77
Figure 4.1: The reaction between PEG-SPA (an NHS derivative) and a primary amine group occurs under mild conditions in aqueous buffer (15-30°C and pH 7.0-8.5).	79
Figure 4.2: The reaction between 2-fluoro-1-methylpyridinium toluene-4-sulfonate PEG occurs under mild conditions in aqueous buffer (4 °C and pH 7 - 8).	80
Figure 4.3: The reaction between PEG-maleimide and a protein under mild conditions in aqueous buffer (pH 7.5-8.5).	81
Figure 4.4: The reaction between PEG-hydrazine and a protein in aqueous buffer (pH 4.5-5.0) in the presence of N-(3-dimethyl aminopropyl)-N'-ethylcarbodiimide.	82
Figure 4.5: The reaction between PEG-isocyanate and a peptide containing no available primary amines (lysine residues).	82
Figure 4.6: Reaction between an alkyne-activated PEG and a para-azidophenylalanine amino acid added into a protein.	83
Figure 4.7: Concentration of α -lactalbumin, 5 kDa PEG, and 5 kDa PEGylated α -lactalbumin as a function of time. Solid curves represent model calculations as discussed in the text.	86

Figure 4.8: Equilibrium concentration of PEG, protein, and PEGylated proteins as a function of the PEG to α -lactalbumin ratio. Data obtained at pH 7 using a 10 g/L α -lactalbumin solution in 10 mM Bis Tris buffer. Solid curves are simple spline fits to the data.....	90
Figure 4.9: Effect of pH on the concentration of PEG, protein, and PEGylated protein using a 0.5 to 1 molar ratio of PEG to protein. Solid curves are spline fits to the data.	92
Figure 4.10: Effect of reactant concentration on the fraction of activated PEG that participates in the PEGylation reaction. Data obtained at pH 7, 10 mM Bis Tris, using a 0.5 to 1 molar ratio of PEG to α -lactalbumin. Solid curve is spline fit to the data.	94
Figure 4.11: Theoretical concentration (g/L) of the 5 kDa PEGylated species with either one or two PEG branches as a function of the molar ratio of PEG to protein added. The initial α -lactalbumin concentration is 14.6 g/L.....	96
Figure 4.12: Comparison of the concentration of PEGylated reaction products for a batch and a fed-batch process. Kinetic parameters for the model curves are shown in Table 4.2.	97
Figure 4.13: Reaction-separation process for PEGylation of α -lactalbumin using a 10 kDa mPEG-SPA. Solid curves are model calculations using the rate constants in Table 4.2 for a separation system with a 12% loss of α -lactalbumin during every cycle. The curves end when 88% of the α -lactalbumin is assumed to be in the product stream.	101
Figure 5.1: Autocorrelation function for a 96 nm standard sample (Taken from Brookhaven, 2004).....	107
Figure 5.2: Calibration curves for the Superdex 200 G/L column for the PEG and protein standards.....	110
Figure 5.3: Partition coefficient of PEG and globular proteins as a function of the molecular weight. Curves are exponential fits to the data given by Equations 5.6 and 5.7.	111
Figure 5.4: Partition coefficient as a function of the solute radius. The solid curve is a model calculation for the partitioning of a hard sphere into a cylindrical pore.....	113

Figure 5.5:	Chromatogram for a mixture of α -lactalbumin PEGylated with 5 kDa mPEG. PEG # refers to the number of 5 kDa branches of PEG added to the α -lactalbumin.	115
Figure 5.6:	Partition coefficient as a function of molecular weight for native protein, unmodified PEG, and PEGylated versions of α -lactalbumin, ovalbumin, and bovine serum albumin. Solid curves are given by Equation 5.10.....	116
Figure 5.7:	Comparison of models and experimental data for the hydrodynamic radius of PEGylated BSA and α -lactalbumin.....	121
Figure 5.8:	Hydrodynamic radius of α -lactalbumin, ovalbumin, and BSA determined using size exclusion chromatography and dynamic light scattering. Error bars represent plus/minus one standard deviation of the experimental data.	122
Figure 5.9:	Hydrodynamic radii of PEGylated α -lactalbumin calculated using SEC and dynamic light scattering.	124
Figure 6.1:	Electropherogram of a 20 kDa PEGylated α -lactalbumin with two different running buffers: Bis Tris (pH 7.0, 10 mM), and Bis Tris with Glycine (pH 7.0, 11 mM).....	142
Figure 6.2:	Electropherograms of acetylated α -lactalbumin (lower curve) and α -lactalbumin PEGylated with 5 kDa mPEG-SPA (upper curve). The first peak corresponds to the neutral marker (mesityl oxide), while the subsequent peaks in the PEGylated sample correspond to samples with decreasing amount of PEG. The acetylated peaks each differ by one reacted lysine group, with the first peak representing the native α -lactalbumin.	145
Figure 6.3:	Electrophoretic mobility of the acetylated and PEGylated α -lactalbumin in 10 mM pH 8.1 Tris-Glycine running buffer as a function of the number of substituted lysine groups. Error bars represent plus/minus one standard deviation of the experimental data.	148
Figure 6.4:	The effect of ionic strength on the mobility of α -lactalbumin and PEGylated α -lactalbumin with one 5 kDa PEG or one 20 kDa PEG. Error bars represent plus/minus one standard deviation of the experimental data. Solids curves are spline fits to the data.....	150

Figure 6.5:	The effect of ionic strength on the mobility of PEGylated α -lactalbumin with 20 kDa total PEG molecular weight. Electrophoretic mobility is shown for molecules with one, two, or four branches. Error bars represent plus/minus one standard deviation of the experimental data.	151
Figure 6.6:	Drag coefficient as a function the hydrodynamic radius for PEGylated proteins containing 2, 5, 10, 20 and 30 kDa branches. Error bars represent plus/minus one standard deviation of the experimental data. The solid curve is a spline fit to the data.	153
Figure 6.7:	Theoretical drag coefficient for PEGylated proteins as a function of the PEGylated protein radius. Experimental results are listed for comparison.	155
Figure 6.8:	Theoretical drag ratio of a 20 kDa PEGylated α -lactalbumin as a function of the κ_2/κ_1 ratio where κ_2 is the inverse Debye length in the bulk fluid and κ_1 is the inverse Debye length in the PEG layer.	158
Figure 7.1:	The observed sieving coefficient of PEG, protein, and PEGylated proteins as a function of the molecular weight. The upper panel shows the sieving data for PEGylated α -lactalbumin (5 kDa and 10 kDa series) and the lower panel shows the sieving data for PEGylated ovalbumin (5 kDa and 10 kDa series). Error bars represent plus/minus one standard deviation for at least three repeat experiments.	166
Figure 7.2:	The observed sieving coefficient as a function of the effective radius determined by SEC for PEG, globular proteins, and PEGylated proteins. Error bars represent plus/minus one standard deviation for at least three repeat experiments.	168
Figure 7.3:	The observed sieving coefficient as a function of molecular weight for PEGylated α -lactalbumin (upper panel) and ovalbumin (lower panel) formed using 10 kDa and 5 kDa mPEG-SPA. Error bars represent plus/minus one standard deviation for at least three repeat experiments.	170

Figure 7.4: Observed sieving coefficient as a function of flux for ovalbumin and PEGylated forms of ovalbumin with 5 kDa PEG branches. Curves are model calculations using the stagnant film theory with best fit values of the actual sieving coefficient given in Table 7.1. Error bars represent plus/minus one standard deviation for at least three repeat experiments.....	173
Figure 7.5: Actual sieving coefficient through the 30 kDa Ultracel™ membrane for PEGylated α -lactalbumin formed with 5 kDa and 10 kDa PEG chains. Data for a series of globular proteins, α -lactalbumin, ovalbumin, and bovine serum albumin, are shown for comparison. Results are plotted as a function of the effective radius determined by size exclusion chromatography. Error bars represent plus/minus one standard deviation for at least three repeat experiments.....	174
Figure 7.6: Observed sieving coefficient of PEGylated α -lactalbumin with four 5 kDa PEG and two 10 kDa PEG chains through an Ultracel™ 30 kDa membrane at a stirring speed of 600 rpm. The solid curve is the model calculation as described in the text. Error bars represent plus/minus one standard deviation for the experimental data.	177
Figure 7.7: Observed sieving coefficients of PEGylated α -lactalbumin with four 5 kDa PEG chains and one 20 kDa PEG chain through an Ultracel™ 100 kDa membrane at a stirring speed of 1200 rpm. The solid curve is the model calculation as described in the text.	179
Figure 7.8: Scaled sieving coefficient as a function of flux for PEGylated α -lactalbumin. Data for the protein with two 10 kDa PEGylated samples were obtained using a 30 kDa Ultracel™ membrane while that with one 20 kDa PEG was obtained using a 100 kDa Ultracel™ membrane.....	182
Figure 8.1: Schematic of electrically charged membrane used for the separation of negatively charged molecules from neutral molecules (adapted from Mehta, 2006).	189
Figure 8.2: Streaming potential as a function of applied transmembrane pressure for the 100 kDa Ultracel™ membranes charged for different periods of time.....	195

Figure 8.3:	Observed sieving coefficient of a 5 kDa PEG, α -lactalbumin, and a PEGylated α -lactalbumin with different numbers of PEG chains as a function of ionic strength at a flux of 8 $\mu\text{m/s}$. Error bars represent plus/minus one standard deviation of the experimental data. Error bars that are smaller than the symbols are not shown.....	197
Figure 8.4:	Actual sieving coefficient of α -lactalbumin, PEG and, PEGylated α -lactalbumin as a function of ionic strength. Model calculations using the Smith and Deen analysis are shown as solid curves.....	201
Figure 8.5:	Effect of pore size distribution on the calculated values of the actual sieving coefficient of PEG, α -lactalbumin, and PEGylated α -lactalbumin. Dashed curves represent model calculations with $\sigma/\bar{r}=0.10$ and 0.30 ; bold curves represents results with $\sigma/\bar{r}=0.20$	202
Figure 8.6:	Effect of mean pore size on the actual sieving coefficient of PEG, α -lactalbumin, and PEGylated α -lactalbumin. Dashed curves represent model calculations with $\bar{r}=5.0$ and 7.0 nm. The bold curves represent the model calculation with $\bar{r}=6.0$ nm.	204
Figure 8.7:	Effect of membrane surface charge density on actual sieving coefficient of PEG, α -lactalbumin, and PEGylated α -lactalbumin. Dashed curves represent model calculations with membrane charge of $0.6 \times 10^{-3} \text{ C/m}^2$ and $3.0 \times 10^{-3} \text{ C/m}^2$. The bold curves represent model calculations with membrane charge of $1.3 \times 10^{-3} \text{ C/m}^2$	205
Figure 8.8:	Effect of protein surface charge density on the predicted values of the actual sieving coefficient of PEG, α -lactalbumin, and PEGylated α -lactalbumin. Dashed curves represent model calculations in which the solute charge was varied by $\pm 15\%$. The bold curves represent the model calculation in which the solute charge was calculated directly from the published amino acid sequence.	206
Figure 8.9:	Actual sieving coefficient as a function of ionic strength for α -lactalbumin PEGylated with 20 kDa total molecular weight of PEG in one 20 kDa branch, two 10 kDa branches, or four 5 kDa branches. Error bars represent plus/minus standard deviation of at least three repeat experiments. Solid curves are model calculations as described in the text.....	208

Figure 8.10: The actual sieving coefficient of 5 kDa PEG, α -lactalbumin, and PEGylated α -lactalbumin as a function of pH. Solid curves are model calculations as described in text.211

Figure 8.11: Actual sieving coefficient as a function of the solution ionic strength for membranes that were charged for either 12 or 24 hr (charge densities of -1.4×10^{-3} and -1.7×10^{-3} C/m²). Error bars represent plus/minus one standard deviation of the experimental data.212

Figure 9.1: Observed sieving coefficients for PEGylated α -lactalbumin, native α -lactalbumin, and 20 kDa polyethylene glycol as a function of filtrate flux through a 30 kDa UltracelTM membrane at pH 7 and 10 mM total ionic strength. Error bars represent plus/minus one standard deviation of the experimental data.222

Figure 9.2: Selectivity between the PEGylated protein and α -lactalbumin and between the PEGylated protein and the 20 kDa PEG using the 30 kDa UltracelTM membrane at pH 7 and 10 mM ionic strength. Error bars represent plus/minus one standard deviation of the experimental data.224

Figure 9.3: Observed sieving coefficients for PEGylated α -lactalbumin, native α -lactalbumin, and hydrolyzed 20 kDa polyethylene glycol as a function of ionic strength using a negatively-charged 100 kDa UltracelTM membrane at pH 7 and a filtrate flux of 17 μ m/s. Error bars represent plus/minus one standard deviation of the experimental data.227

Figure 9.4: Selectivity between the PEGylated protein and α -lactalbumin and between the PEGylated protein and the 20 kDa PEG for the 100 kDa UltracelTM membrane charged for 24 hrs at pH 7 and 17 μ m/s.228

Figure 9.5: Observed sieving coefficient as a function of pH for native α -lactalbumin, PEGylated α -lactalbumin, and 20 kDa PEG through a negatively charged 100 kDa membrane at a flux of 31 μ m/s. Error bars represent plus/minus one standard deviation of the experimental data.230

Figure 9.6: Selectivity between the PEGylated protein and α -lactalbumin and between the PEGylated protein and the 20 kDa PEG for the 100 kDa Ultracel TM membrane charged for 24 hrs at 10 mM ionic strength and a flux of 31 $\mu\text{m/s}$. Error bars represent plus/minus one standard deviation of the experimental data.	231
Figure 9.7: Normalized concentrations of the PEGylated α -lactalbumin, native α -lactalbumin, and hydrolyzed 20 kDa polyethylene glycol as a function of the number of diavolumes for a diafiltration performed with a 30 kDa Ultracel TM membrane at pH 7, 500 mM ionic strength, and a filtrate flux of 9 $\mu\text{m/s}$. Solid lines are model calculations using the best fit values of the sieving coefficients as shown in Table 9.2.	233
Figure 9.8: Size exclusion chromatograms showing the initial feed and final retentate for the first-stage diafiltration using a 30 kDa Ultracel TM membrane at pH 7, 500 mM ionic strength, and a filtrate flux of 9 $\mu\text{m/s}$. Detection is by UV at 280 nm.	236
Figure 9.9: Normalized concentrations of the PEGylated α -lactalbumin and free 20 kDa polyethylene glycol as a function of the number of diavolumes for a diafiltration performed with a negatively-charged 100 kDa Ultracel TM membrane at pH 7, 2.5 mM total ionic strength, and a filtrate flux of 21 $\mu\text{m/s}$. Solid lines are model calculations using the best fit values of the sieving coefficients shown in Table 9.2.	238
Figure 9.10: Yield versus purification factor for the PEGylated α -lactalbumin based on native α -lactalbumin as the impurity. Data for a diafiltration using a 30 kDa Ultracel TM membrane at pH 7, 500 mM ionic strength, and a filtrate flux of 9 $\mu\text{m/s}$. The solid curve is the model calculation using a selectivity of $\psi_{\text{protein}} = 530$	240
Figure 9.11: Yield versus purification factor for the PEGylated α -lactalbumin based on the 20 kDa PEG as the impurity. Data for a diafiltration using a negatively-charged 100 kDa Ultracel TM membrane at pH 7, 2.5 mM ionic strength, and a filtrate flux of 21 $\mu\text{m/s}$. Solid curve is model calculation using a selectivity of $\psi_{\text{PEG}} = 43$	242

Figure 10.1: Flux decline for ultrafiltration of 1 g/L solutions of native BSA and the 12 kDa PEGylated BSA at pH 7 and 10 mM ionic strength through 100 kDa Ultracel™ membranes at a constant pressure of 35 kPa (upper panel) and 140 kPa (lower panel). Data for $t > 1800$ s (upper panel) and $t > 5400$ s (lower panel) are the buffer flux through the fouled membranes.	253
Figure 10.2: Flux decline for ultrafiltration of 1 g/L solutions of native BSA and the 12 kDa PEGylated BSA at pH 7 and 10 mM ionic strength through 30 kDa Ultracel™ membranes at a constant pressure of 120 kPa. Data for $t > 3600$ s are the buffer flux through the fouled membranes.	256
Figure 10.3: Flux decline for ultrafiltration of 1 g/L solutions of native BSA and the 12 kDa PEGylated BSA at pH 7 and 10 mM ionic strength through 100 kDa Biomax™ membranes at a constant pressure of 28 kPa. Data for $t > 1800$ s are the buffer flux through the fouled membranes.	260
Figure 10.4: Flux decline for ultrafiltration of 1 g/L solutions of native BSA and the 12 kDa PEGylated BSA at pH 7 and 10 mM ionic strength through the 300 kDa Biomax™ membranes at a constant pressure of 14 kPa. Data for $t > 3600$ s are the buffer flux through the fouled membranes.	261
Figure 10.5: Reverse phase chromatography for BSA and the 12 kDa PEGylated BSA on a C4 column using a gradient of trifluoroacetic acid (TFA) in water and TFA in acetonitrile.....	263
Figure 10.6: Effect of solution pH and salt concentration on the flux decline for BSA (top panel) and the 5 kDa PEGylated BSA (bottom panel) through 100 kDa Biomax™ membranes at a constant pressure of 103 kPa. Data for $t > 5400$ s are the buffer flux through the fouled membranes.	266
Figure B.1: Actual Sieving coefficient as a function of the dextran molecular weight in a 100 kDa Ultracel™ membrane that was charged modified for 24 hours.....	321
Figure B.2: Sum of squared residuals (SSR) between the theoretical and experimental actual sieving coefficient for various values of mean pore radius and Z ratio.	322

Figure C.1: Calculated net charge of α -lactalbumin and an α -lactalbumin with 1 or 2 substituted lysine groups as a function of the solution pH.....331

ACKNOWLEDGEMENTS

First, I would like to thank my advisor, Dr. Andrew Zydney for his valuable comments and input at all stages of my research project. His help has been essential to the completion of this thesis. I am forever amazed by his knowledge on such a wide range of topics and his ability to patiently help others understand with relative ease. I would also like to thank my entire doctoral committee: Dr. Velegol, Dr. Pishko, Dr. Curtis, and Dr. Vogler for generously spending their time helping me to improve this work. I would especially like to thank Dr. Vogler for spending so much time working with me on my comprehensive project.

I have really enjoyed working with everyone in the lab group while I've been at PSU. Dave Bohonak and Suzanne Wolff helped to teach me the basics in lab and made me immediately feel part of the group, for which I am sincerely grateful. Late nights in the lab could have become very tedious, if it wasn't for the camaraderie provided by Amit Mehta and Martin Chandler. I would like to especially thank Suma Rao for being both a mentor and a friend to me during my graduate studies. Since my transition back from Genentech, It's been great to working with a new group of labmates. I hope that I have been able to pass on some of what I've learned during my first years in the lab to the new members. I would like to express my appreciation to Mahsa Rohani for being such an understanding officemate as all the thesis resources have been placed in every free space available. It has been great working with Dave Latulippe on the project of the deformation of biomolecules as we found our seemingly unrelated work beginning to intertwine. I would like to especially thank and recognize Dr. Boksoon Kwon, who was a post-doc in our laboratory for a year. She worked with me in the area of PEGylated

protein fouling and I would like to thank her for her specific contributions to Chapter 10. I've been lucky to have an amazing number of very capable undergraduate students – Ben Smith, Melissa Bebb, Aileen Dinin, Abasha Lewis, Alison Harter, Steve Benner, and Colleen Cruetz who also contributed to this work.

Personally, I would like to thank Eric Hauck, my husband, for all his love and encouragement. He has been there for me on both the good and the bad research days, making each of those days better. I would also like thank my family especially my mom, Carol Shefrin for all her support and encouragement throughout the years and my grandfather, Joe Shefrin for being my inspiration to be an engineer.

Chapter 1

INTRODUCTION

1.1 Biotechnology

The advent of biologically-derived pharmaceuticals began in the 1970s with the production of human insulin from recombinant bacterial cells developed by cloning the human insulin gene into the bacteria. The use of protein-based therapeutics provides opportunities for much more targeted therapies with fewer side effects by exploiting the unique three-dimensional structure, binding properties, and biological activity of these macromolecules. Currently, therapeutic proteins are used to treat a wide variety of diseases including cancers, AIDS, hepatitis B and C, infectious diseases, diabetes, arthritis, and cardiovascular ailments (Walsh, 2006).

The first recombinant protein products were highly active hormones such as human-growth hormone, clotting factors such as erythropoietin, insulin, colony stimulating factors, and α -, β -, and γ -interferons. The past decade has seen the development of monoclonal antibodies as a major class of biotherapeutics for the treatment of cancer, rheumatoid arthritis, and acute organ transplant rejection (Rang, 2001). Overall revenues for the biotech industry have risen from \$7.6 billion in 1996 (Paugh and Lafrance, 1997) to more than \$54 billion in 2004 (Mirasol, 2005) and more than \$80 billion in 2007 (Ernest and Young, 2008) while the number of FDA approved biological products has increased from 30 (Paugh and Lafrance, 1997) to over 230 (Mirasol, 2005) from 1997 to 2005.

1.1.1 Post-Translational Modifications

Although all of the early recombinant therapeutic products were designed to provide exact copies of the native protein, several recent studies have demonstrated the clinical potential of using "second generation" therapeutics produced by conjugation of the native protein with various natural or synthetic polymers including polyethylene glycol (Asahina, et al., 2007; Hamidi, et al., 2006; Heredia and Maynard, 2007; Muller, et al., 2000), polysaccharides (Mehvar, 2003), or other synthetic polymers made from divinyl ether, maleic anhydride, and lauric acid (Shibata, et al., 2004; Shibata, et al., 2005). The resulting protein-polymer conjugates can have a significantly longer biological half-life and lower immunogenicity than the native protein, particularly for smaller proteins that are rapidly cleared by the kidney. In addition, the use of chemically-modified proteins can provide active targeting of the therapeutic agent to tumors or reticuloendothelial tissues (Mehvar, 2003). These protein-polymer conjugates can have much greater clinical efficacy, allowing less frequent dosing at lower concentrations with greater therapeutic effectiveness. More detailed information on the use and performance of protein-polyethylene glycol conjugates is provided in Section 1.2.

1.1.2 Purification of Biotherapeutics

Biologically derived pharmaceuticals are typically produced using either recombinant mammalian cells (e.g., Chinese Hamster Ovary cells) or bacteria (e.g., *E. coli*). Recombinant products can also be produced using yeast, plant, or insect cell lines, and there have been a number of studies using transgenic plants and animals. In each case, the desired protein product must be purified from the host cells, host cell proteins, DNA, and cell debris to the very high levels of purity. Intravenous or subcutaneous administered biologically-derived products must contain less than 0.1 % of protein impurities and less than 100 picograms of nucleic acid per dose (Blanch and Clark, 1997). Purification is usually performed through a series of steps including centrifugation, chromatography (usually a mixture of protein A, ion exchange, and hydrophobic interaction), and membrane filtration steps. Additional steps are used to ensure that there are no active viruses present in the final product, including viral inactivation by pH or heat and virus filtration. A thorough review of biological purification processes and more specifically the chromatography techniques for bioseparations is given by Jungbauer (2005).

Although there is considerable variability in the economics for different therapeutic products, Blanch and Clark (1997) reported that up to 80% of the total production cost for large-scale manufacture is attributed to the downstream purification process. The high cost is a result of low product yield in the initial reaction mixture as well as the necessity to remove impurities through multiple processing steps. In recent years, the titer of biological products has increased as much as an order of magnitude

(Butler, 2005), which has created new challenges with respect to the overall capacity and throughput of the downstream purification process.

Production of second-generation therapeutic proteins is currently accomplished in two distinct steps. First, the native recombinant protein is made and purified from the original cell culture fluid. The purified protein is then conjugated to the desired polymer, e.g., to appropriate molecular weight polyethylene glycol chain(s). The desired conjugated product must then be purified from unreacted polymer, native protein, and any reaction by-products. In some cases, the desired conjugated protein must also be purified from protein conjugates with non-optimal degrees of conjugation. The presence of unreacted (native) protein can provoke an undesired immunological response that can affect both the native and modified forms of the therapeutic protein (Bailon and Berthold, 1998). The presence of unreacted polymer can also have an adverse impact on the biological response of the therapeutic product. The final purification of the protein-polymer conjugate is thus essential for the successful commercial production of these second-generation biotherapeutics. The purification of the optimal form of the modified protein from other forms, as well as from the unreacted precursors, can have a significant impact on the overall economics due to the high value of the product.

1.2 PEGylation

One of the most common polymers used for conjugation to therapeutic proteins is polyethylene glycol (PEG). PEG is attractive because of its compatibility with biological tissue and the wide range of chemical strategies that can be used to couple PEG to specific sites on the native protein (Abuchowski et al., 1977b). A number of PEG-protein

conjugates have been approved by the FDA: Adagen in 1990, Oncaspar in 1994, Miralax in 1999, and Cimzia in 2008 (Food and Drug Administration, 2008).

PEG can be produced as a linear polymer or with specific branched structures. Polymers with low molecular weight (0.2 - 35 kDa) are generally referred to as polyethylene glycol while high molecular weight species (> 35 kDa) are typically referred to as polyethylene oxide; the term PEG will be used throughout this thesis for any polymer with ethylene glycol monomer units. PEG is usually produced by anionic polymerization, which provides superior control of the polymer molecular weight. Activated forms of PEG are created by attaching facile leaving groups that will react with specific moieties on the protein (e.g., lysine amino groups) under mild conditions. More details on different activated groups and the corresponding chemical reactions are given in Chapter 4.

The covalent attachment of PEG to a protein is called PEGylation. The use of PEG as a method to increase the half-life and reduce the immunogenicity of a protein *in vivo* was first discussed by (Abuchowski et al., 1977a). They demonstrated that the concentration of PEGylated bovine serum albumin (BSA) injected into rabbits stayed at a higher level for a longer period of time than that for un-modified BSA, which was attributed to the shielding of the PEGylated protein from the immune system. Abuchowski et al. (1977b) also showed that the activity of a PEGylated liver catalase enzyme in rabbits was comparable to that of the native protein but with much slower degradation. The first clinically approved PEGylated protein was Adagen, a PEGylated adenosine deaminase introduced by Enzon Pharmaceutical in 1990. Many other PEGylated products have since been approved including PEGylated interferon α -2a,

PEGylated interferon α -2b, PEGylated human granulocyte colony-stimulating factor, and PEGylated L-asparaginase (Food and Drug Administration, 2008). All of these PEGylated proteins have shown marked improvements in therapeutic efficacy compared to the native proteins (Foser et al., 2003; Michallet et al., 2004; Muller et al., 2000; van der Auwera et al., 2001). For example, the half life of interferon α -2b was increased from 4 to 40 hr by conjugation with a 40 kDa PEG (Michallet, et al., 2004). The half-life of growth releasing factor was increased from approximately 20 minutes to more than 70 hr by conjugation with 42-46 kDa of PEG (Parkinson, et al., 2003), eliminating the need for using a continuous intravenous feed.

Table 1.1 provides a list of FDA approved PEGylated proteins currently on the market, including company information, the primary indication, and data on the biological half-life. The total molecular weight of PEG conjugated to the protein is provided in the second to last column.

Table 1.1. Commercially available PEGylated proteins.

Commercial Name	Scientific Name	Company	Indication	FDA Approval	BLA #	Half Life of PEGylated form	Half life increase	Amount PEG added	References
Adagen	ademase bovine	Enzon	Sever Combined Immuno-deficiency	1990	19818	1 - 5 days		5 kDa	Enzon Pharmaceuticals 2008; Food and Drug Administration, 2008
Oncaspar	asparagase	Enzon	Leukemia	1994	103411	50 hrs	33x	100 kDa	Enzon Pharmaceuticals 2008; Food and Drug Administration, 2008; Kodera, et al., 1998
Pegintron	interferon a-2b	Schering-Plough	Hepatitis C	2001	103949	40 hrs	10x	12 kDa - 40 kDa	Food and Drug Administration, 2008; Wang, et al., 2002; Wylie, et al., 2001
Neulasta	filgrastim	Amgen	Neutropenia	2002	125031	15 - 80 hrs		6 kDa - 30 kDa	Amgen, 2008; Food and Drug Administration, 2008; Kinstler, et al., 2002; Kodera, et al., 1998; Piedmonte and Treuheit, 2008
Pegasys	interferon a-2a	Hoffman-LaRoche	Hepatitis C	2002	103964	77 hrs	8.5x	20 kDa - 40 kDa	Food and Drug Administration, 2008; Foser, et al., 2003; Michallet, et al., 2004; Reddy, et al., 2002; Yun, et al., 2005b
Somavert	visomant	Pharmacia-Upjohn	Acromegaly	2003	21106	70hrs	210x	5 kDa - 46 kDa	Esposito, et al., 2003; Food and Drug Administration, 2008; Parkinson, et al., 2003; Piquet, et al., 2002; Youn, et al., 2004
Macugen	aptanib sodium	Osi EyeTech	Wet Macular Degeneration	2004	21756	10 days		20 kDa	Food and Drug Administration, 2008; Pfizer and (OSI)Eyetech, 2006
Cimizia	certolizumab	UCB Inc.	Crohns' Disease	2008	125160	14 days		40 kDa	Food and Drug Administration, 2008; UCB Group, 2008

Although PEG has been used most extensively for conjugation to therapeutic proteins, a number of other polymers such as polyacrylamide, poly(vinyl pyrrolidone), and poly(acryloyl morpholine) have also shown promise. The resulting protein-polymer conjugates have shown comparable improvement in circulation half-life to PEGylated proteins. One of the biggest challenges associated with using these polymers is developing appropriate activated groups to facilitate attachment to the protein under mild reaction conditions (Torchilin and Trubetskoy, 1995).

1.2.1 Benefits of PEGylation

As discussed previously, PEGylated proteins can have significantly longer half-lives than the native product, particularly for small therapeutic proteins. This increase in half-life can reduce the number and frequency of the required dosing leading to improved patient compliance (Wang, et al., 2002) and reduced side effects. For example, Figure 1.1 shows data for the concentration of α -interferon and PEGylated α -interferon, Pegasys, in the body as a function of time. The unmodified α -interferon was dosed three times per week, with the *in vivo* concentration varying by well over an order of magnitude between the doses. In contrast, the concentration of PEGylated α -interferon stays relatively constant over a full week after only a single injection (Harris, 2001). The increased stability and solubility of PEGylated proteins can also provide opportunities for using subcutaneous or intramuscular injection instead of the traditional intravenous administration used for most therapeutic proteins (Chapman, 2002). Recent studies have

also shown that PEGylated proteins may be attractive in oral formulations (Chapman, 2002).

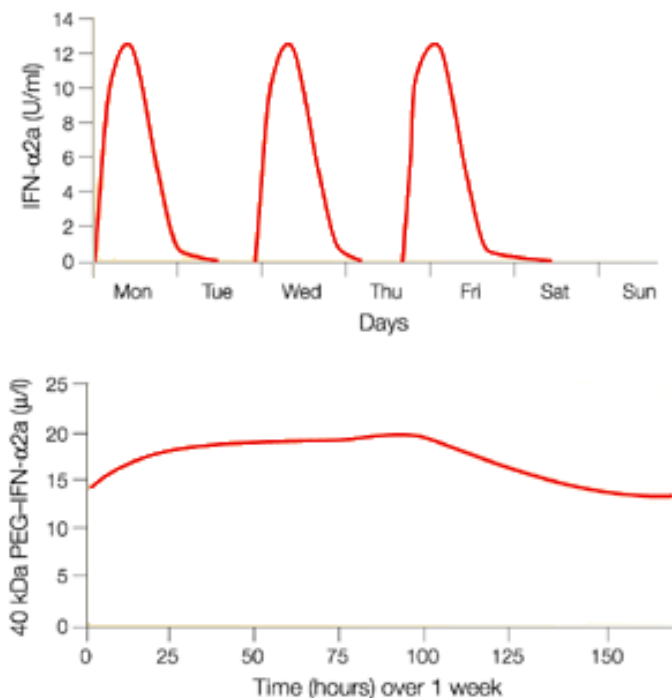


Figure 1.1. Concentration of α -interferon in the body as a function of time for the PEGylated and native forms. The PEGylated form shows a relatively constant concentration profiles while the native form shows significant variations. Taken from Harris, (2001).

PEGylation also causes a shift in the biodistribution of the therapeutic protein among different tissues. Bioaccumulation in the liver and spleen is typically reduced for PEGylated proteins (Zalipsky, 1995), with increased accumulation in the lymph nodes. This makes PEGylated compounds especially effective in treating lymphatic cancers but they tend to be less effective in treating ailments of the liver and spleen, although this can be compensated for by attachment of specific targeting moieties (Caliceti and Veronese, 2003). Many studies have shown that PEGylated molecules tend to accumulate in tumors

due to the leaky vascular structure in the rapidly growing tumor tissue. A number of PEGylated molecules have been examined that specifically target tumor growth suppression (Ton, et al., 2005); although there is also evidence that large PEGylated molecules may not be able to penetrate throughout the tumor (Ton, et al., 2005).

Free PEG has been shown to be non-immunogenic in numerous studies (Kodera, et al., 1998), which is usually attributed to the absence of biospecific antigenic sites. PEG is highly flexible and interacts strongly with water, which may also reduce the immune response (Kopelman et al., 2002). In general, linear PEG has a lower immunological response than branched versions, which is probably related to the greater flexibility of the linear molecule (Caliceti and Veronese, 2003). PEGylation suppresses protein immunogenicity (Abuchowski et al., 1977b) by “hiding” antigenic sites on the protein surface especially when the PEGylation site is located near the antigenic site (Kopelman et al., 2002). For example, the antigenic character of asparaginase was reduced by 10-fold by attachment of 10 kDa PEG (Caliceti and Veronese, 2003). PEG has also been shown to effectively block an immunological response to liposomes (Torchilin and Trubetskoy, 1995). The use of a branched PEG appears to provide better immunoprotection since its umbrella-like structure can more effectively cover antigenic sites on the protein.

1.2.2 Mechanisms of Increased *In Vivo* Activity

The therapeutic efficacy of PEGylated proteins compared to their native counterparts is determined by changes in the protein half-life, the biodistribution within the body (i.e., the fraction of the product that actually reaches the appropriate therapeutic

site), and the intrinsic activity of the biomolecule. Proteins are cleared from the body by a variety of mechanisms including proteolysis, renal ultrafiltration, liver clearance, and the immune system (Chapman, 2002), all of which can be altered by PEGylation (Caliceti and Veronese, 2003). However, the resulting increase in circulation time can be offset by a reduction in biological activity. PEGylation can partially block the active site of the protein, potentially causing a significant reduction in activity. The optimal degree of PEGylation thus reflects a balance between reducing clearance while maintaining the intrinsic biological activity.

One of the major benefits of PEGylation is the reduction in glomerular (renal) filtration, particularly for smaller molecular weight proteins. The extent of renal filtration is controlled primarily by the size of the molecule, with smaller effects associated with the chemical composition and charge. Proteins greater than 70 kDa in size are retained by the kidney, with smaller proteins excreted in the urine. Experimental studies with unmodified PEG show nearly complete retention for PEG molecules larger than about 30 kDa reflecting the much more open configuration of the PEG compared to that of a globular protein (Caliceti and Veronese, 2003).

Quantitative studies of the effects of PEGylation on glomerular filtration are somewhat contradictory (Caliceti and Veronese, 2003). Nakaoka (1997) found that the clearance of PEGylated proteins was independent of the molecular weight of added PEG, although this was attributed to differences in immune degradation. PEGylated proteins with highly branched PEG chains tend to have lower rate of immune degradation but greater kidney clearance than PEGylated proteins with a single linear PEG chain (Caliceti and Veronese, 2003). The rate of glomerular filtration is also affected by protein charge

with more highly charged molecules showing greater retention by the kidneys (Caliceti and Veronese, 2003). PEGylation can directly alter the protein charge through the covalent reaction, and it can also physically shield the effective surface charge (Caliceti and Veronese, 2003). These phenomena are discussed in more detail in Chapter 6.

PEGylation often decreases the rate of liver degradation, although again the results are contradictory (Caliceti and Veronese, 2003). For example, Caliceti (1999) found that the conjugation of a 5 kDa PEG to Uricase reduced accumulation in the liver but the reverse was true for conjugation to 10 kDa of PEG (Caliceti and Veronese, 2003). The change in liver accumulation may be related to a shift in biodistribution, with the PEGylated proteins preferentially partitioning in the blood stream (Zalipsky, 1995). In addition, the PEG may inhibit degradation by hepatocytes.

The site of PEGylation affects the immunological response of the PEG-protein complex (Francis, et al., 1998). In addition, the conformation of PEG may also be a factor. For example, PEGylation of IgM and IgG with branched PEG caused a greater reduction in immune response than a linear PEG (Caliceti, et al., 2001). However, there is also evidence that anti-PEG antibodies can be created causing an increased immunological clearance in some cases (Caliceti and Veronese, 2003).

Several studies have shown that the intrinsic *in vitro* activity of PEGylated proteins is often reduced due to steric hindrance of the active site and to a much lesser extent a physical change in three-dimensional structure of the PEGylated molecule. For example, (Digilio et al., 2002) examined the effect of PEGylation on human growth-hormone releasing factor using NMR and found no change in protein structure. However, any small decrease in activity is usually more than compensated for by a

decrease in clearance. This is clearly shown in the data in Figure 1.2 for erythropoietin (Bailon and Berthold, 1998; Bailon, 2000), with PEGylation providing a significant increase in *in vivo* activity despite the reduction in *in vitro* activity.

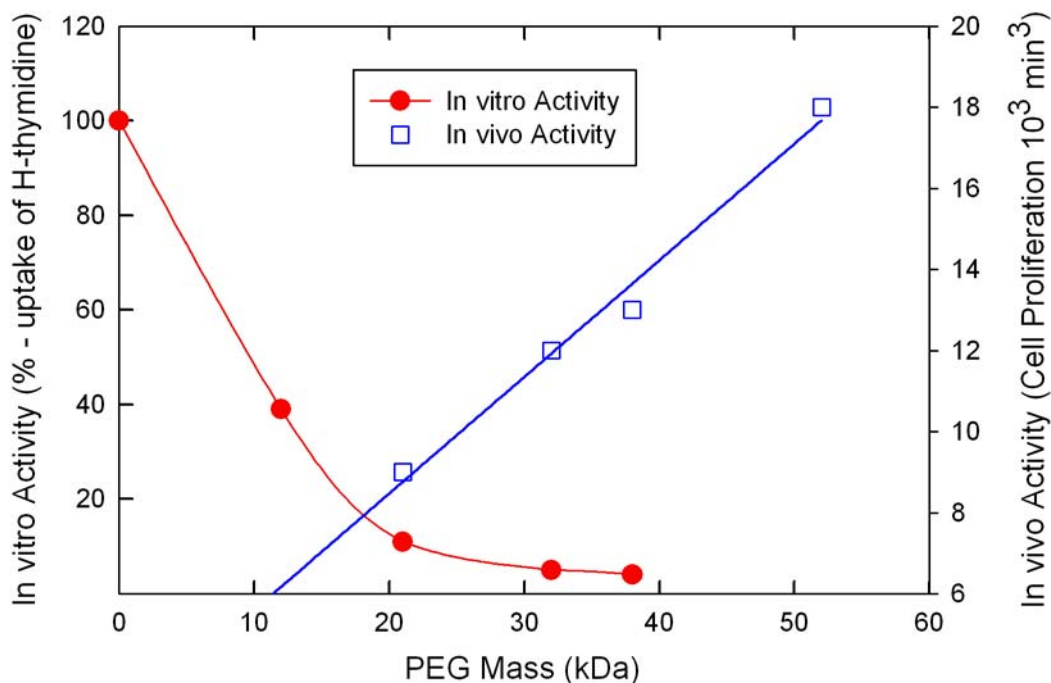


Figure 1.2. Comparison of the *in vitro* and *in vivo* activity of a PEGylated erythropoietin as a function of the mass of PEG added. Curves are simple fits to clarify the trend of the data. Adapted from Bailon and Berthold (1998).

1.2.3 Current Separation Techniques

In order to obtain the benefits of PEGylation, it is necessary to separate the desired form of the PEGylated protein from the unreacted (native) protein, from any hydrolyzed PEG generated during the conjugation process, and possibly from other forms of the PEGylated protein with reduced activity (Esposito et al., 2003). This can be very difficult due to the inherent heterogeneity in both the number and position of attached PEG molecules (Fee and Van Alstine, 2006). A number of methods have been examined

for the purification of PEGylated proteins including two phase aqueous partitioning (Delgado et al., 1992), capillary and gel electrophoresis (Li et al., 2001; Veronese et al., 2001), and a variety of chromatographic techniques such as ion exchange (Piquet et al., 2002), hydrophobic interaction (Vincentelli et al., 1999), reverse phase (Calceti et al., 2004; Esposito et al., 2003), and size exclusion (Lee et al., 1999b; Veronese, 2001) chromatography. This wide range of purification strategies reflects the changes in size, electrical charge, and hydrophobicity associated with the attachment of the polyethylene glycol chain (Fee and Van Alstine, 2006). Table 1.2 and Table 1.3 shows a list of purification techniques used for different PEGylated proteins, including both small (analytical) and preparative scale separations.

Table 1.2. Purification techniques for a range of PEGylated proteins – Chromatographic methods.

Technique	PEGylated proteins purified	Purpose of Purification	References
Size Exclusion Chromatography	Alpha-interferon 2b, Alpha-lactalbumin, Anti-interleukin-8, Anti-tumour Necrosis Factor-Alpha scFC fragment, Beta-interferon, Beta-lactoglobulin, BSA, Calcitonin, Carboxypeptidase A, Epidermal Growth Factor, Gelonin, Granulocyte Colony-stimulating Factor (human), Immunoglobulin Antigen Binding Domains, Immunoglobulins, Insulin, Lysozyme, Methioninase, Parathyroid Hormone, Ovalbumin, Staphylokinase, Tumor Necrosis Factor-Alpha, Uricase	Analytical fractionation of different PEGylated forms, Buffer exchange, Preparative fractionation of different PEGylated forms, Reaction during separation, Removal of unreacted PEG and protein	Arduini, et al., 2004; Arpicco, et al., 2002; Brumeanu, et al., 1995; Calceti, et al., 2004; Fee, 2003; Fee and Van Alstine, 2004; Johnson, et al., 2003; Kinstler, et al., 2002; Koumenis, et al., 2000; Lee and Park, 2003; Lee and Park, 2002a; Lee, et al., 1999a; Lee, et al., 1999b; Li, et al., 2007; Molek and Zydny, 2006; Moreadith and Collen, 2003; Na, et al., 2004; Pabst, et al., 2007; Pettit, et al., 1997; Schiavon, et al., 2000; Tan, et al., 1998; Ton, et al., 2005; Veronese, 2001; Wang, et al., 2002; Yamamoto, et al., 2003; Yang, et al., 2003; Yun, et al., 2006; Yun, et al., 2005b; Zhang, et al., 2007
Anion Exchange Chromatography	BSA, Granulocyte Colony-stimulating Factor (human), Hemoglobin, Immunoglobulins, Methioninase, Myelopoietin	Analytical fractionation of different PEGylated forms, Removal of PEG and protein	Brumeanu, et al., 1995; Hall, 2004; Manjula, et al., 2003; Pabst, et al., 2007; Tan, et al., 1998; Yun, et al., 2005b
Cation Exchange Chromatography	Alpha-interferon 2a, Alpha-interferon 2b, Anti-interleukin-8, Beta-interferon, Beta-lactoglobulin, Chymopapain, Granulocyte Colony-stimulating Factor (human), Granulocyte Hormone Releasing Factor, Growth Hormone Releasing Factor 1-29 Analogue, Human Growth Hormone, Interleukin-1 Receptor Antagonist, Interleukin-2, Myelopoietin, Staphylokinase, Trichosanthin, Tumor Necrosis factor-RI	Analytical fractionation of different PEGylated forms, Concentration, Reaction during separation, Removal of PEG, Separation of positional isomers	Arduini, et al., 2004; Azarkan, et al., 2003; Azarkan, et al., 1996; Edwards, et al., 2003; Esposito, et al., 2003; Hall, 2004; He, et al., 1999; Jiang, et al., 2005; Johnson, et al., 2003; Kinstler, et al., 2002; Koumenis, et al., 2000; Lee and Lee, 2004; Moreadith and Collen, 2003; Olson, et al., 1997; Piquet, et al., 2002; Reddy, et al., 2002; Sato, 2002; Wang, et al., 2002; Wylie, et al., 2001; Yun, et al., 2006; Yun, et al., 2005b
Hydrophobic Interaction Chromatography	Beta-lactoglobulin, BSA, Caricain, Chymopapain, Lysozyme	Analytical fractionation of different PEGylated forms	Azarkan, et al., 2003; Nijs, et al., 1997; Vincentelli, et al., 1999
Reverse Phase Chromatography	Calcitonin, Epidermal Growth Factor, Growth Hormone Releasing Factor, Insulin	Analytical fractionation of different PEGylated forms, Separation of positional isomers	Lee and Park, 2002a; Lee, et al., 1999b; Veronese, 2001; Youn, et al., 2004; Zhang, et al., 2007
Affinity Chromatography	Asparaginase, Basic Fibroblast Growth Factor, Catalase, Immunoaderhin, Recombinant Human Necrosis Factor Receptor	Analytical fractionation of different PEGylated forms, Reaction protection of the active site, Removal of unreacted PEG	Baran, et al., 2003; Chamow, et al., 1994; Pettit et al. 1997; Wu et al. 2007

Table 1.3. Purification techniques for a range of PEGylated proteins – Nonchromatographic methods.

Technique	PEGylated proteins purified	Purpose of Purification	References
Capillary Electrophoresis	Calcitonin, Human Tumor Necrosis Factor-alpha, Lysozyme, Ribonuclease A	Analytical fractionation of different PEGylated forms	Li, et al., 2002; Li, et al., 2001; Na, et al., 2001
Ultrafiltration	Alpha-lactalbumin, Beta-interferon, BSA, Gelonin, Growth Hormone Releasing Factor, Immunoglobulins, Lysozyme, Methioninase, Ovalbumin, Tumor Necrosis Factor-RI	Concentration of purified product, Removal of unreacted PEG	Arduini, et al., 2004; Arpicco, et al., 2002; Brumeanu, et al., 1995; Caliceti and Veronese, 2003; Edwards, et al., 2003; Esposito, et al., 2003; Molek and Zydney, 2006; Molek and Zydney, 2007; Tan, et al., 1998; Veronese, 2001
Dialysis	Alpha-lactalbumin, Beta-lactoglobulin, Epidermal Growth Factor, Immunoglobulins, Insulin, Lysozyme, Tumor Necrosis Factor-RI	Buffer Exchange, Removal of PEG and protein	Brumeanu, et al., 1995; Edwards, et al., 2003; Hinds, 2002; Kim, et al., 2002; Lee and Park, 2003; Molek and Zydney, 2007; Nijs, et al., 1997; Veronese, 2001
MALDI-TOF	Calcitonin, Granyulocyte Colony-Simulating Factor (human), Human Growth Hormone Anatagonist, Interferon Alpha-2b	Identification of PEGylated forms, Identification of Positional Isomers	Li, et al., 2007; Liu, et al., 2002; Na, et al., 2001; Olson, et al., 1997; Yun, et al., 2006; Yun, et al., 2005b

1.2.3.1 Ion Exchange

Ion exchange chromatography has probably been used most frequently for the purification of PEGylated proteins, but implementation of this technology at large scale can be difficult due to the low capacity of the ion exchange resins for most PEGylated proteins associated with steric hindrance and charge-shielding by the PEG (Fee and Van Alstine, 2006; Pabst et al., 2007; Piquet et al., 2002; Snider et al., 1992; Wylie et al., 2001; Yamamoto et al., 2003). For example, the dynamic binding capacity of BSA PEGylated with a 12 kDa polyethylene glycol chain on a Capto Q resin (GE Healthcare, Piscataway, NJ) was only 37 g/L, which is nearly a factor of 4 smaller than the capacity of the un-modified protein under the same conditions (Pabst et al., 2007). In contrast, (Hall, 2004) found that PEGylation had little affect on the dynamic binding capacity of myelopietin on SP or Q Sepharose (GE Healthcare, Piscataway, NJ) ion exchange resins, which may be due to the specific surface charge and binding characteristics of this particular molecule.

Ion exchange can be used for the separation of PEGylated proteins containing different numbers of added chains as well as the removal of unreacted precursors. Ion exchange chromatography has been used for the purification of PEGylated GRF (Monkarsh et al., 1997), PEGylated insulin (Zhang et al., 2007), PEGylated rhG-CSF (Yun et al., 2005b), and PEGylated C-IFN (Yun et al., 2006) including removal of both the unmodified (native) protein and undesired PEGylated forms. In all cases the more heavily PEGylated species eluted first in the presence of a salt gradient, with the unreacted protein being the most strongly retained (Zhang et al., 2007). Yun (2005a) obtained improved separation using cation and anion exchange chromatography in series.

In this case, the native protein was bound during the first cation exchange step while the PEGylated proteins were captured and then selectively eluted from an anion exchange resin using a salt gradient (Yun et al., 2005a). There is even some evidence for separation of "isomers" of the PEGylated protein, species containing the same total amount of PEG but with different sites for covalent attachment, although this has not yet been demonstrated on a preparative scale. For example, Monkarsh (1997) identified 11 different mono-PEGylated isomers of interferon α -2a using cation exchange chromatography, although not with baseline resolution.

1.2.3.2 Reverse Phase

Alternatives to ion exchange chromatography include reverse phase and hydrophobic interaction chromatography, although the successful separation performance is highly variable and most of the studies have been limited to small analytical scale separations (Snider et al., 1992; Youn et al., 2006; Youn et al., 2004; Zhang et al., 2007). For example, Youn et al. (2004) used a C-8 reverse phase column for purification of PEGylated growth hormone releasing factor, with the native protein eluting first and the most PEGylated species eluting last in an acetonitrile gradient, suggesting the PEG made the protein more hydrophobic (PEGylated protein interacts less with the water than the native protein). Similar results were obtained by Zhang et al. (2007) for the separation of PEGylated insulin using a C-18 column with an acetonitrile gradient. It is also possible to use ion exchange and reverse chromatography in series (Esposito et al., 2003). For example, Zhang et al. (2007) obtained enhanced separation of PEGylated insulin on an

analytical scale using ion exchange to remove the PEG prior to separating the protein from the PEGylated protein using reverse phase chromatography.

1.2.3.3 Size Exclusion

Size exclusion chromatography is used extensively for small analytical scale separations, but applications at large scale are more limited due to the very large columns and processing times needed for the separation (Snider, et al., 1992; Vestling, et al., 1992). Fundamental studies of PEGylated proteins using size exclusion chromatography have examined the affect of PEGylation on the protein partition coefficient providing a measure of the effective size of the PEGylated species (Fee and Van Alstine, 2004). These results are discussed in more detail in Chapter 5. Ton (2005) showed that PEGylated carboxypeptidase could be separated from unreacted PEG and protein using preparative size exclusion chromatography, although this was probably not viable at a commercial scale.

1.3 Ultrafiltration

Ultrafiltration is used for both concentration and formulation (i.e., concentration in combination with buffer exchange) in the large-scale production of nearly all recombinant protein products. Although ultrafiltration developed in the 1920's, widespread use of the technology didn't begin until the late 1960's with the commercialization of asymmetric ultrafiltration membranes (Howell, 1993). These asymmetric or anisotropic membranes have a thin skin layer that provides the membrane

its selectivity but with much less resistance than for a homogeneous (isotropic) membrane, and a support layer with an open structure that provides the membrane its mechanical stability.

The type of membrane chosen for a separation process is usually based on the size of the species to be separated. Some common types of membranes used for separation of liquid streams include: ultrafiltration, microfiltration, reverse osmosis, and nanofiltration. Ultrafiltration membranes typically have pore size between about 1 and 20 nm and are thus used to retain macromolecules. In contrast, microfiltration membranes typically have pore size between 0.1 and 10 μm although these limits are somewhat arbitrary. Microfiltration is used extensively in bioprocessing for sterile filtration of final products, for initial clarification of cell broths, and for removal of aggregates and debris throughout the downstream process (Subramanian, 1998). Reverse osmosis membranes have pore size below about 0.5 nm and are used primarily for desalination. Reverse osmosis can also be used to concentrate and possibly even fractionate very small solutes (Subramanian, 1998). Nanofiltration membranes have pore size between reverse osmosis and ultrafiltration, providing opportunities for selective removal of divalent salts for water softening and for concentration of organic compounds with molecular weights above 200 Da (Subramanian, 1998).

Most membranes are produced from organic polymers, although inorganic membranes made from metals, ceramics, and zeolites have also been developed typically for use in high pressure or high temperature applications (Shah, et al., 2007). A variety of polymers are used commercially including: polypropylene, polytetrafluoroethylene (PTFE), polyvinylidene fluoride (PVDF), cellulose nitrate, cellulose acetate, cellulose

triacetate, aliphatic polyamides, aromatic polyamides, polysulfone, polyethersulfone, polyimide, polyvinyl alcohol, polyacrylonitrile, polycarbonate, and polyetheretherketone. Cellulosic membranes are very hydrophilic, leading to low levels of protein adsorption, but they are less stable to extremes of pH, cleaning agents, and temperature (Howell, 1993). The membrane properties can often be improved by using polymer blends, e.g., polyvinylpyrrolidone is often added to polysulfone membranes to improve hydrophilicity and facilitate pore formation.

Membrane separations are well suited for use with biomolecules since they typically cause little degradation or denaturation of the biological product. They are able to separate a wide variety of molecules with vastly disparate sizes, and the membrane properties (pore size and surface chemistry) can be tailored to improve separations. Scale-up is generally straight-forward if the proper modular structures are available (Howell, 1993). Ultrafiltration is typically performed using tangential flow (also known as cross flow) filtration, in which the feed solution is circulated across the membrane and perpendicular to the direction of filtration. Tangential flow filtration systems maintain higher filtrate flux over longer processing times since the retained species are continually removed from the membrane by the flow (Ratledge and Kristiansen, 2001). Diafiltration is used for buffer exchange and desalting, with a diafiltration buffer continuously added to the feed solution as filtrate is removed (Subramanian, 1998). Typical challenges with membrane separations are low selectivity, particularly compared with chromatographic separations, and membrane fouling, the irreversible decline in membrane performance due to interactions between the feed and membrane. Membrane fouling can often be reduced by using more hydrophilic surfaces, either by proper selection of the base

polymer or by surface modification after membrane formation by chemical reaction, plasma treatment, or adsorptive coatings (Howell, 1993).

Recent experimental and theoretical work has shown that membrane selectivity can be dramatically improved by exploiting electrostatic interactions between the naturally charged proteins and intentionally charged membranes (Burns and Zydney, 2001; Mehta and Zydney, 2006; Pujar and Zydney, 1994; Saksena and Zydney, 1994; van Eijndhoven et al., 1995; van Reis, 2006; Zulkali et al., 2005). Charged membranes have been successfully used for fractionation of whey proteins (Cheang and Zydney, 2003), for purification of recombinant therapeutic proteins (van Reis et al., 1999), and for selective retention of small molecules in blood (Nakajima et al., 2001). Optimization of these membrane separations typically involves selection of the appropriate solution ionic strength, pH, and membrane charge to control the extent of the electrostatic interactions.

1.4 Thesis Summary

1.4.1 Overall Objectives

Previous work on ultrafiltration of PEGylated proteins is quite limited. A few studies (Arduini et al., 2004; Brumeanu et al., 1995; Edwards et al., 2003; Lee and Park, 2002a; Nijs et al., 1997; Pabst et al., 2007) have reported the use of ultrafiltration for concentration and buffer exchange in the formulation of purified PEGylated products, but there have been no prior studies examining the potential use of ultrafiltration for the purification of PEGylated proteins from unreacted precursors.

The overall objective of this thesis was to examine the use of ultrafiltration as a method to separate PEGylated protein from unreacted precursors and from PEGylated species with different numbers of PEG chains. This included: (1) analysis of size-based separation of PEGylated proteins using electrically neutral membranes, (2) examination of the use of electrically-charged membranes for purification of PEGylated proteins by exploiting electrostatic interactions, and (3) development of appropriate models for the separation of PEGylated proteins. As part of this effort, a number of techniques were used to evaluate the underlying physical properties of the PEGylated proteins and to relate these to the observed separation characteristics. In particular, size exclusion chromatography and dynamic light scattering were used to evaluate the effective size of the PEGylated proteins and capillary electrophoresis was used to examine the electrophoretic mobility and effective surface charge.

1.4.2 Thesis Outline

The general theoretical background used to analyze the ultrafiltration results is presented in Chapter 2. This includes theoretical models for solvent and solute transport for idealized membranes consisting of a parallel array of cylindrical pores with the solutes described as uniformly charged spheres. The relative contributions of convective, diffusive, and electrophoretic solute transport are also discussed.

Chapter 3 presents the basic experimental systems, materials, and methods used throughout the thesis for size exclusions chromatography, capillary electrophoresis, ultrafiltration, and diafiltration.

Chapter 4 provides a description of the reaction system used to produce the PEGylated proteins. Data are presented for the effects of solution pH, ionic strength, and ratio of PEG to protein on the degree and uniformity of the PEGylation. Both the extent of reaction and the kinetics are explored as well as different reaction schemes.

Chapters 5 and 6 show results for the characterization of PEGylated proteins by size exclusion chromatography and capillary electrophoresis, respectively. The effective sizes of the PEGylated proteins were determined from the measured partition coefficient in a size exclusion chromatography resin by comparison with results for appropriate molecular standards. Electrophoretic mobility data for the PEGylated proteins were used to evaluate the effective protein charge including the possibility of charge shielding by the PEG.

The behavior of PEGylated proteins in ultrafiltration systems is explored in Chapters 7 and 8. Chapter 7 examines the behavior during ultrafiltration through electrically-neutral membranes, with a specific focus on the effects of the ultrafiltration flux on the elongation or deformation of the PEG chains. Chapter 8 examines the effects of electrostatics on the transport of PEGylated proteins using electrically-charged membranes generated by covalent attachment of sulfonic acid groups to the base cellulosic membrane.

Chapter 9 shows results for the separation of PEGylated α -lactalbumin from native α -lactalbumin and hydrolyzed PEG using a two-stage diafiltration process to selectively remove the different impurities. This process provided a PEGylated α -lactalbumin product with a purification factor greater than 100 and a yield of 78%.

Chapter 10 examines the fouling characteristics of PEGylated proteins using both hydrophilic and hydrophobic membranes. The results clearly demonstrate that PEGylation of bovine serum albumin increases the extent of fouling with hydrophobic membranes due to the reduced hydrophilicity of the PEGylated protein.

A summary of the final conclusion and implications of the results are presented in Chapter 11 along with a discussion of appropriate future studies that build directly on the work presented in this thesis.

Chapter 2

THEORETICAL BACKGROUND

2.1 Introduction

This chapter reviews the theoretical models used to describe the basic mass transport and separation phenomena that govern the behavior of ultrafiltration systems. Previous reviews of this theoretical background have been presented by Zeman and Zydney (1996), Pujar (1996), and Rao (2007); the discussion in this chapter draws heavily from these prior discussions. The theoretical framework used to analyze results from the size exclusion chromatography and capillary electrophoresis experiments are discussed in the specific chapters focused on those results.

The overall rate of solute transport in ultrafiltration is determined by both the rate of transport from the bulk solution to the membrane and the rate of transport through the membrane pores. These phenomena are discussed separately in the following sections, including both the rate of solvent and protein transport through the membrane. Transport in the bulk solution is controlled by the system hydrodynamics while transport through the membrane has contributions from thermodynamics (possibly including electrostatic interactions) and hydrodynamics.

2.2 Bulk Mass Transport

The transport of solute molecules to the membrane surface during pressure-driven filtration reflects the balance between the convective flow toward the membrane and

diffusion away from the region of higher concentration of retained solutes that develops near the membrane surface. This phenomenon is often referred to as concentration polarization. Figure 2.1 shows a graphical depiction of the concentration polarization phenomenon, including the expected concentration profile. The concentration profile through the membrane is discussed in more detail later in this chapter.

The increase in solute concentration at the surface of the membrane can reduce the filtration rate by three distinct mechanisms. First, the accumulated solute can give rise to a large osmotic pressure on the feed side of the membrane (Denisov, 1994), reducing the effective pressure driving force for filtration. This effect tends to be most significant for small solutes since osmotic pressure is a colligative property, but it can also be important for some proteins due to the non-linear dependence of the osmotic pressure on the protein concentration. Second, the solute can form a dense cake or gel layer that provides an additional hydraulic resistance to the solvent flow (Bowen and Jenner, 1995). Third, the high solute concentration at the surface of the membrane can lead to irreversible fouling both on and within the membrane pores (Palecek and Zydney, 1994).

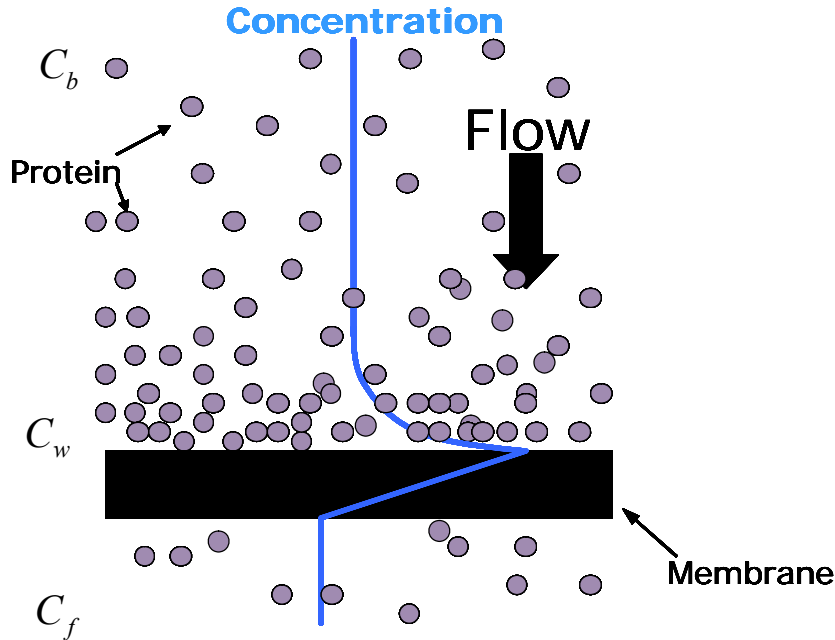


Figure 2.1. Schematic of concentration polarization in solution above a membrane. The highest solute concentration is at the membrane surface. C_b , C_w , and C_f represent the concentration of the solute in the bulk solution, at the membrane surface (wall), and in the filtrate solution Adapted from Bohonak (2006).

2.2.1 Stagnant Film Model

The most common approach used to describe the effects of concentration polarization is through the stagnant film model. This model assumes that solute transport occurs in a stagnant film above the membrane surface. In the basic stagnant film model particle-particle interactions are neglected and the solute diffusivity and viscosity are both assumed to be constant (independent of the solute concentration). At steady state, the solute flux through the membrane and into the filtrate solution is equivalent to the net solute flux towards the membrane as described by Equation 2.1.

$$-J_v C_f = -J_v C - D_\infty \frac{dC}{dz} \quad (2.1)$$

where J_v is the filtrate flux (volumetric filtrate flow rate divided by the membrane area), C_f is the concentration of solute in the filtrate, C is the local solute concentration at a positive position, z , above the membrane, and D_∞ is the solute diffusivity. Equation 2.1 can be integrated over the thickness of the concentration polarization boundary layer (δ) with the solute concentration at the surface of the membrane ($z = 0$) equal to C_w while the solute concentration at the outer edge of the boundary layer is C_b (see Figure 2.1):

$$J_v = \frac{D_\infty}{\delta} \ln \left(\frac{C_w - C_f}{C_b - C_f} \right) \quad (2.2)$$

A more detailed analysis of this model, including the validity of the one-dimensional transport analysis, is provided by Zydney (1997).

In addition to altering the filtrate flux, concentration polarization also affects the rate of solute transport through the membrane. This is typically described in terms of the observed sieving coefficient, which is defined as the ratio of the solute concentration in the filtrate solution to that in the bulk solution well above the membrane ($S_o = C_f / C_b$). The observed sieving coefficient can be related to the actual sieving coefficient (S_a), which is defined as the ratio of the solute concentration in the filtrate to that at the membrane surface or "wall" ($S_a = C_f / C_w$), by rearranging Equation 2.2 to give:

$$S_o = \frac{S_a \exp \left(\frac{J_v}{D_\infty / \delta} \right)}{1 - S_a + S_a \exp \left(\frac{J_v}{D_\infty / \delta} \right)} \quad (2.3)$$

2.2.2 Mass Transfer Coefficient

The ratio of the solute diffusion coefficient (D_∞) to the boundary layers thickness (δ) in Equations 2.2 and 2.3 is typically defined as the solute mass transfer coefficient, k_m . The mass transfer coefficient is a function of the solute diffusivity and the hydrodynamics of the particular membrane device. A semi-empirical equation for the mass transfer coefficient in a stirred cell was developed by Smith et al. (1968) based on the rate of benzoic acid dissolution:

$$Sh = A(\text{Re})^d (Sc)^{0.33} \quad (2.4)$$

where $Sh = k_m b / D_\infty$ is the Sherwood number, $\text{Re} = \omega b^2 / \nu$ is the Reynolds number, $Sc = \nu / D_\infty$ is the Schmidt number, b is the radius of the stirred cell, ω is the stirring speed, ν is the kinematic viscosity, and D_∞ is the solute diffusion coefficient.

The solute diffusion coefficient can be evaluated using the Stokes-Einstein equation:

$$D_\infty = \frac{k_B T}{f} = \frac{k_B T}{6\pi\eta a} \quad (2.5)$$

where k_B is Boltzmann's constant ($k_B = 1.38 \times 10^{-23}$ J/K), T is temperature, f is the frictional coefficient, η is the solution viscosity, and a is the hydrodynamic radius of the solute. The protein radius can be estimated based on the molecular weight using Equation 2.6

$$R_{h,protein} = 0.082 \times MW_{pro}^{1/3} \quad (\text{Young, et al., 1980}) \quad (2.6)$$

with an analogous expression for polyethylene glycol given as

$$R_{h,PEG} = 0.01912 \times MW_{PEG}^{0.559} \quad (\text{Singh, et al., 1998}) \quad (2.7)$$

where the hydrodynamic radius (R_h) is in nm and the molecular weight (MW) is in Da. Equations 2.6 and 2.7 are valid for infinitely dilute solutions, with no dependence of D_∞ on the solute concentration or ionic strength. This approximation is not always valid experimentally and can lead to significant discrepancies between the data and model correlations (Rautenbach and Holtz, 1980).

The value of A in Equation 2.4 has been determined experimentally and is a weak function of the stirred cell geometry. Colton (1969) calculated the value of A to be 0.285 based on the dissolution of benzoic acid in a turbulent flow system. Opong and Zydney (1991) calculated the value of A to be 0.23 for laminar flow in a 25 mm Amicon stirred cell (which is the system used in most of the experiments performed in this thesis). The value of d varies with Re from a value of 0.567 in the laminar region (for $Re < 10,000$) to a value of 0.746 in the turbulent region (for $Re > 60,000$). Reynolds numbers between 10,000 and 60,000 are in the transition region. The appropriate value of d in this region is typically determined by linear interpolation between the values for laminar and turbulent flow.

2.3 Solvent Transport

The rate of solute and solvent transport through porous membranes can be described using hydrodynamic theories presented in Anderson and Quinn (1974) and Deen (1987) for membranes modeled as an array of well-defined, typically cylindrical, pores. The advantage of the hydrodynamic models is that the key transport parameters can be calculated directly in terms of the physical properties of the solute and the pores.

The available hydrodynamic models for spherical solutes in cylindrical pores are discussed in more detail in the following sections.

2.3.1 Permeability

The hydraulic permeability (L_p) of the membrane is defined experimentally as:

$$L_p = \frac{\eta J_v}{\Delta P} \quad (2.8)$$

where ΔP is the transmembrane pressure, η is the solution viscosity, and J_v is the volumetric filtrate flux (volumetric flow rate per total membrane area). For a membrane with a uniform array of cylindrical pores, the flux can be evaluated using the Hagen-Poiseuille equation:

$$J_v = \frac{\varepsilon r_p^2 \Delta P_{TM}}{8 \eta \delta} \quad (2.9)$$

where r_p is the pore radius and ε is the porosity of the membrane. Equation 2.9 assumes that end effects are negligible, which is valid for typical ultrafiltration membranes since the membrane thickness is typically more than 100 times greater than the pore radius. In some cases a tortuosity factor is added to Equation 2.9 to account for the irregular flow path through the membrane.

2.3.2 Electrostatic Effects on Solvent Flow

The fluid flow characteristics through a charged membrane are considerably more complicated. The fluid flow through the charged pores generates an electrical (streaming) potential due to interactions between the flow and the ions in the electrical

double layer. This induced streaming potential causes a net electrophoretic flux of ions that exerts stresses on the fluid, a phenomenon known as counter electro-osmosis.

The one dimensional momentum equation describing fluid flow through the cylindrical pore can be written as (Newman, 1991):

$$\frac{\eta}{r} \frac{d}{dr} \left(r \frac{dv_z}{dr} \right) + \rho_e E_z - \frac{dP}{dz} = 0 \quad (2.10)$$

where r is the radial position within the pore, v_z is the axial velocity, E_z is the axial electric field, dP/dz is the pressure gradient, and ρ_e is the local charge density of the electrolyte solution defined as:

$$\rho_e = F \sum_i z_i C_i \quad (2.11)$$

where F is Faraday's constant, z_i is the ion valence number, and C_i is the ion concentration. The velocity profile within the pore is determined by integrating Equation 2.10 over the radial direction with boundary conditions that $v_z = 0$ at $r = r_p$ and v_z and Φ are finite at $r = 0$ giving (Newman, 1991):

$$v_z = E_z \frac{\varepsilon_0 \varepsilon_r}{\eta} \left(\Phi - \Phi_{r=r_p} \right) - \frac{dP}{dz} \frac{r_p^2 - r^2}{4\eta} \quad (2.12)$$

where ε_0 is the permittivity of a vacuum, ε_r is the relative permeability of the buffer solution, Φ is the potential at radial position r , and $\Phi_{r=r_p}$ is the potential at the surface of the pore.

The electrical potential gradient is typically evaluated by solving the linearized form of the Poisson-Boltzmann equation in cylindrical coordinates.

$$\frac{1}{r} \frac{\partial}{\partial r} \left(r \frac{\partial \Phi}{\partial r} \right) = - \frac{\rho_e}{\varepsilon_0 \varepsilon_r} \quad (2.13)$$

The local charge density is evaluated in terms of the potential from the constraint that the net ion flux in the radial direction is zero:

$$N_i = D_i \frac{\partial C_i}{\partial r} - \frac{D_i}{RT} z_i F \frac{\partial \Phi}{\partial r} = 0 \quad (2.14)$$

where D_i is the ion diffusion coefficient and $\frac{\partial \Phi}{\partial r}$ is the radial electric field. Integrating

Equation 2.14 over the radius of the pore gives the Boltzmann distribution:

$$C_i = C_i^0 \exp\left[-\frac{z_i F}{RT}(\Phi - \Phi_{r=0})\right] \quad (2.15)$$

where the exponential term can be approximated using the first term in a Taylor series expansion, $1 - \frac{z_i F}{RT}(\Phi - \Phi_{r=0})$, at low potentials. The electrical potential is evaluated by

solving the Poisson-Boltzmann equation (Equations 2.11, 2.13, and 2.15) to give:

$$(\Phi - \Phi_{r=0}) = \left(\frac{q_p}{\varepsilon_0 \varepsilon_r \kappa}\right) \left[\frac{I_0(\kappa r) - 1}{I_1(\kappa r)}\right] \quad (2.16)$$

where q_p is the constant surface charge density of the pore and κ^{-1} is the Debye length defined as:

$$\kappa^{-1} = \left(\frac{\varepsilon_0 \varepsilon_r RT}{F^2 \sum z_i^2 C_i}\right)^{1/2} \quad (2.17)$$

where R is the ideal gas constant. Equation 2.16 is valid at low surface potentials and is typically referred to as the Debye Huckel approximation.

The average fluid velocity can be calculated by integrating Equation 2.12 over the pore radius with the electrostatic potential evaluated from Equation 2.16:

$$J_v = \left(\frac{\varepsilon_r^2}{8\eta\delta}\right) \Delta P_{TM} + \left(\frac{q_p}{\kappa\eta}\right) \left[\frac{I_2(\kappa a)}{I_1(\kappa a)}\right] E_z \quad (2.18)$$

where $I_1(\kappa a)$ and $I_2(\kappa a)$ are the modified Bessel Functions of the first kind of order 1 and 2, respectively. The effects of counter-osmosis are described by the second term in Equation 2.18. A more detailed review of the fluid flow through electrically-charged membranes is provided by Burns (2000) and Pujar (1996).

2.4 Solute Transport

The solute flux (N_s) through the membrane has contributions from the diffusive, convective, and electrophoretic transport as described by Equation 2.19.

$$N_s = -K^{-1}D_\infty \nabla C_s + GVC_s - K^{-1}D_\infty \frac{C_s}{RT} \nabla \psi \quad (2.19)$$

where K and G are hindrance factors for diffusion and convection, respectively. K and G are both complex functions of the pore size, solute size, and electrostatic interactions as discussed in more detail in Section 2.4.1. V is the velocity of the fluid with respect to the pore wall, ψ is the electrical potential energy of interaction, and C_s is the solute concentration in the pore at a specified z and r coordinate. Equation 2.19 assumes that the solute activity coefficient is unity and thus neglects any nonidealities associated with solute-solute interactions. A detailed derivation of this equation is presented by Pujar and Zydney (1994).

The overall solute flux through the pore is evaluated by integrating Equation 2.19 over the cross sectional area of the pore to give:

$$\langle N_s \rangle = \frac{\int_0^1 N_s \beta d\beta}{\int_0^1 \beta d\beta} = 2 \int_0^{1-\lambda} N_s \beta d\beta \quad (2.20)$$

where β is the dimensionless radial position ($\beta = r / r_p$) and λ is the ratio of the solute to pore radii ($\lambda = r_s / r_p$). The upper bound of the integral represents the maximum distance away from the pore center for a given solute molecule accounting for the steric exclusion of the solute from the region within one solute radius of the pore wall. Substitution of Equation 2.19 into Equation 2.20 and performing the integration gives:

$$\langle N_s \rangle = -2D_\infty \int_0^{1-\lambda} K^{-1} \frac{\partial C_s}{\partial z} \beta d\beta - 2D_\infty \int_0^{1-\lambda} K^{-1} \frac{C_s}{RT} \frac{\partial \Psi}{\partial z} \beta d\beta + 2 \int_0^{1-\lambda} G C_s V \beta d\beta \quad (2.21)$$

The radial concentration profile in the pore is assumed to follow a Boltzmann distribution:

$$C_s(\beta) = C_s(\beta=0) \exp\left[-\frac{\psi(\beta) - \psi(\beta=0)}{RT}\right] \quad (2.22)$$

where $\psi(\beta=0)$ and $C_s(\beta=0)$ are the potential energy and the solute concentration at the center of the pore.

Substitution of Equation 2.22 into Equation 2.21 gives the following expression for the radially averaged solute flux:

$$\langle N_s \rangle = K_c \langle V \rangle \langle C_s \rangle - K_d D_\infty \frac{d\langle C_s \rangle}{dz} \quad (2.23)$$

where $\langle V \rangle$, $\langle C_s \rangle$, and $\left\langle \frac{\partial \psi}{\partial z} \right\rangle$ are the radially averaged velocity, concentration, and

potential energy. The coefficients K_c and K_d are given as:

$$K_c = \frac{\int_0^{1-\lambda} G V \exp\left(-\frac{\psi(\beta)}{RT}\right) \beta d\beta}{\left[\int_0^{1-\lambda} \exp\left(-\frac{\psi(\beta)}{RT}\right) \beta d\beta \right] \left[2 \int_0^1 V \beta d\beta \right]} \quad (2.24)$$

$$K_d = \frac{\int_0^{1-\lambda} K^{-1} \exp\left(-\frac{\psi(\beta)}{RT}\right) \beta d\beta}{\int_0^{1-\lambda} \exp\left(-\frac{\psi(\beta)}{RT}\right) \beta d\beta} \quad (2.25)$$

The exact forms of the hydrodynamic parameters G and K will be discussed in Section 2.4.1.

Equation 2.23 is expressed in terms of the radially averaged solute concentration within the pore. The concentration in the pore can be related to the concentration in the solution immediately outside the membrane pore using the equilibrium partition coefficient:

$$\phi = \frac{\langle C_s \rangle_{z=0}}{C_w} = \frac{\langle C_s \rangle_{z=\delta m}}{C_f} = 2 \int_0^{1-\lambda} \exp\left(-\psi/k_b T\right) \beta d\beta \quad (2.26)$$

The partition coefficient for a hard sphere in a cylindrical pore in the absence of any electrostatic interactions becomes:

$$\phi = (1 - \lambda)^2 \quad (2.27)$$

which describes the steric exclusion of the solute from the region within one solute radius of the pore wall.

The solute flux can be related to the solute concentrations in the solution outside the membrane by integrating Equation 2.23 across the membrane with the boundary conditions at the upper ($z = 0$) and lower ($z = \delta$) surfaces of the membrane evaluated using Equation 2.26 to give (Opong and Zydney, 1991):

$$\langle N_s \rangle = S_\infty C_w \langle V \rangle \frac{\left[1 - \left(\frac{C_f}{C_w} \right) \exp[-Pe_m] \right]}{[1 - \exp[-Pe_m]]} \quad (2.28)$$

where

$$S_{\infty} = \phi K_c = 4 \int_0^{1-\lambda} G(1-\beta)^2 \exp\left[\frac{-\psi}{k_b T}\right] \beta d\beta \quad (2.29)$$

$$\frac{D_{eff}}{D_{\infty}} = \phi K_d = 2 \int_0^{1-\lambda} K^{-1} \exp\left[\frac{-\psi}{k_b T}\right] \beta d\beta \quad (2.30)$$

$$\langle V \rangle = -\frac{r_p^2}{8\eta} \frac{dP}{dz} \quad (2.31)$$

$$Pe_m = \left(\frac{S_{\infty}}{\phi K_d} \right) \left(\frac{\langle V \rangle \delta}{D_{\infty}} \right) \quad (2.32)$$

The convective contribution to the solute flux is described by the asymptotic sieving coefficient (S_{∞}). At very high filtration velocities, the solute flux across the membrane reduces to $\langle N_s \rangle = S_{\infty} \langle V \rangle C_w$. The membrane Peclet number describes the relative contributions of the convective and diffusive fluxes. In the limit of very low Peclet numbers (corresponding to low filtration velocities), solute transport is dominated by diffusion with the solute flux given as $\langle N_s \rangle = \phi K_D D_{\infty} (C_w - C_f)$.

The solute flux through the membrane (as given by Equation 2.28) is equal to the solute flux into the filtrate solution $\langle N_s \rangle = \langle V \rangle C_f$. Substitution of this expression into Equation 2.28 gives upon rearrangement an expression for the actual sieving coefficient, S_a .

$$S_a = \frac{S_{\infty} \exp(Pe_m)}{S_{\infty} + \exp(Pe_m) - 1} \quad (2.33)$$

where S_a is defined as the ratio of the solute concentration in the filtrate solution (C_f) to that at the upstream surface of the membrane (C_w). Equation 2.33 predicts that the actual sieving coefficient decreases from a value of one at very low Pe_m to a constant

asymptotic sieving coefficient at high filtration velocities, in good agreement with experimental observations (Zeman and Zydney, 1996).

2.4.1 Hydrodynamic Transport Parameters

The expressions for K_c and K_d are given as integrals involving the lag coefficient $[G(\lambda, \beta)]$ and the enhanced drag coefficient $[K(\lambda, \beta)]$, both of which are related to properties of the membrane and the solute. These terms are typically evaluated using the centerline approximation which assumes that the solute is located at the axis of the pore (Deen, 1987) in which case the integrals simply become:

$$K_c = G(\lambda, 0) \left(2 - (1 - \lambda)^2 \right) \quad (2.34)$$

$$K_d = K^{-1}(\lambda, 0) \quad (2.35)$$

Expressions for $G(\lambda, 0)$ and $K(\lambda, 0)$ were developed by Bungay and Brenner (1973) for all values of λ using matched asymptotic expansions with the results expressed as (Brenner and Gaydos, 1977; Bungay and Brenner, 1973; Deen, 1987):

$$G(\lambda, 0) = \frac{K_s}{2K_t} \quad (2.36)$$

$$K^{-1}(\lambda, 0) = \frac{6\pi}{K_t} \quad (2.37)$$

where K_s and K_t are given by Equation 2.38 and Equation 2.39 with the expansion coefficients provided in Table 2.1.

$$K_t = \frac{9}{4} \pi^2 \sqrt{2} (1 - \lambda)^{-5/2} \left[1 + \sum_{n=1}^2 a_n (1 - \lambda)^n \right] + \sum_{n=3}^7 a_n \lambda^{n-3} \quad (2.38)$$

$$K_s = \frac{9}{4} \pi^2 \sqrt{2} (1 - \lambda)^{-5/2} \left[1 + \sum_{n=1}^2 b_n (1 - \lambda)^n \right] + \sum_{n=3}^7 b_n \lambda^{n-3} \quad (2.39)$$

Table 2.1 Expansion coefficients for the K_r and K_s functions in Equation 2.38 and Equation 2.39.

Subscript n	a_n	b_n
1	-73/60	7/60
2	77293/50400	-2227/50400
3	-22.5083	4.0180
4	-5.6117	-3.9788
5	-.3363	-1.9215
6	-1.216	4.392
7	1.647	5.006

K_c varies between 1.47 and 1 depending on the value of λ . The value of K_c is greater than one because the solute flux is expressed in terms of the area averaged velocity while the velocity at the pore centerline is twice the average velocity. The hindrance factor for diffusion (K_d) is much smaller than K_c , particularly for large values of λ , due to the greater hydrodynamic interactions associated with solute diffusion. Figure 2.2 shows the hydrodynamic functions, G and K^{-1} , as a function λ . Both G and K^{-1} decrease with increasing λ due to the increased drag on the solute due to the pore wall. The value of K^{-1} decreases to 0 as λ goes to 1 since the hydrodynamic drag becomes infinitely large. The value of G approaches 0.5 as λ approaches 1 because the solute will move at the average solution velocity, equivalent to one-half of the maximum velocity in the pore.

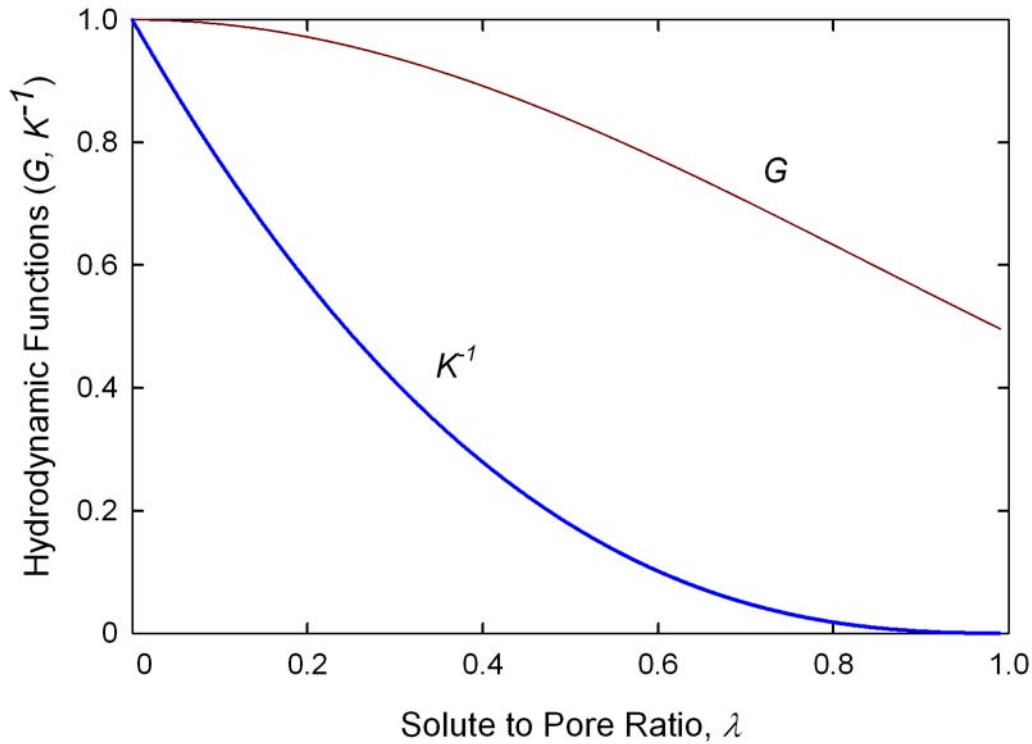


Figure 2.2. Hydrodynamic functions, G and K^{-1} as a function of the solute to pore ratio, λ .

2.4.2 Electrostatic Effects on the Partition Coefficient

The presence of electrostatic interactions can influence both the equilibrium partition coefficient and the hindrance factors for convection and diffusion. Smith and Deen (1980; 1983) evaluated the partition coefficient by solving the linearized Poisson-Boltzmann equation (Equation 2.40) for a charged sphere in a charged cylindrical pore:

$$\nabla^2 \psi = (\kappa r_p) \psi \quad (2.40)$$

Equation 2.40 is valid at low electrical potentials (< 25 mV) due to the linearization of the exponential in the Boltzmann distribution (i.e. the Debye-Huckel approximation). Smith and Deen (1980) solved Equation 2.40 using matched asymptotic expansions in

spherical and cylindrical coordinates. The dimensionless interaction energy (V_σ) was determined using the procedure described by Verwey and Overbeek (1948) as:

$$V_\sigma = \frac{A_s \sigma_s^2 + A_{sp} \sigma_s \sigma_p + A_p \sigma_p^2}{[\pi \tau (1 + \tau \lambda)] \exp(-\tau \lambda) - M_0 h(\tau \lambda)} \quad (2.41)$$

where

$$A_s = \frac{4\pi \lambda^4 e^{\tau \lambda} M_0}{1 + \tau \lambda} \quad (2.42)$$

$$A_{sp} = \frac{4\pi^2 \lambda^2}{I_1(\tau)} \quad (2.43)$$

$$A_p = \frac{\pi^2 h(\tau \lambda)}{\tau^2 I_1^2(\tau)} \quad (2.44)$$

where $\tau = \kappa r_p$ is the dimensionless pore size, I_1 is the Bessel function of the first kind order 1, and σ_s and σ_p are the dimensionless solute and pore surface charge densities, respectively:

$$\sigma_s = \frac{F r_p q_s}{\epsilon_o \epsilon_r RT} \quad (2.45)$$

$$\sigma_p = \frac{F r_p q_p}{\epsilon_o \epsilon_r RT} \quad (2.46)$$

where q_s and q_p are the dimensional charge densities. The functions $h(\tau \lambda)$ and M_0 are shown in Equation 2.47 and Equation 2.48.

$$h(\tau \lambda) = (1 + \tau \lambda) e^{-\tau \lambda} - (1 - \tau \lambda) e^{\tau \lambda} \quad (2.47)$$

$$M_0 = \int_0^\infty \frac{K_1 \left[(\tau^2 + \alpha^2)^{1/2} \right]}{I_1 \left[(\tau^2 + \alpha^2)^{1/2} \right]} d\alpha \quad (2.48)$$

where I_1 and K_1 are the Bessel functions of the first and second kind, respectively. The integral in Equation 2.48 can be approximated as (Smith and Deen, 1980)

$$M_0 = \frac{\pi}{2} \left(\frac{\pi}{\tau} \right)^{1/2} e^{-2\tau} \left[\tau + \frac{15}{16} - \frac{39}{512\tau} + O\left(\frac{1}{\tau^2}\right) \right] \quad (2.49)$$

for $\tau \geq 3$. The potential energy of interaction is directly related to the dimensionless interaction energy (V_σ):

$$\psi(0) = r_p \varepsilon_o \varepsilon_r \left[\frac{RT}{F} \right]^2 V_\sigma \quad (2.50)$$

The potential energy of interaction Equation 2.41 is represented as the sum of three separate contributions: the energy associated with the deformation of the electrical double layer surrounded by the solute, the deformation of the double layer within the pore, and the direct charge-charge interaction between the pore and the solute. The change in energy due to the deformation of the electrical double layer surrounding the solute or the pore always increases the potential energy, leading to a reduction in the magnitude of the partition coefficient, while the direct interaction term is positive if the membrane pore and solute have like charges and is negative if they are oppositely charged.

The analysis of the potential energy of interaction has been extended to account for off-center positions within the pore (Smith and Deen, 1983), constant surface potential boundary conditions (Smith and Deen, 1980), and the effects of charge regulation (Pujar and Zydney, 1997). A more detailed discussion of these results is provided by Pujar (1996).

2.5 Log-Normal Pore Size Distribution

The previous sections describe the transport of solvent and solute through a single pore. In order to apply these equations to real membranes it is necessary to account for the distribution of pore sizes within the membrane. A number of previous studies have examined the effects of a pore size distribution on both solute and solvent transport (Mochizuki and Zydney, 1993; Saksena and Zydney, 1995). This section briefly reviews these analyses.

Most studies of membrane pore size distributions have used a log-normal density function (Causserand et al., 1996; Mochizuki and Zydney, 1993; Saksena and Zydney, 1995):

$$f_R(r) = \frac{1}{r_p \sqrt{2\pi b}} \exp \left[-\frac{\left(\ln \frac{r_p}{\bar{r}} + \frac{b}{2} \right)^2}{2b} \right] \quad (2.51)$$

with

$$b = \ln \left[1 + \left(\frac{\sigma}{\bar{r}} \right)^2 \right] \quad (2.52)$$

where r_p is the pore radius, \bar{r} is the mean pore radius, and σ is the standard deviation. The log-normal pore size distribution is convenient for this analysis because it is only defined for positive values of the pore radius (in contrast to the Gaussian distribution which is defined for $-\infty < r_p < \infty$).

The average velocity through the membrane is evaluated by integrating the velocity for each pore over the pore size distribution.

$$\bar{V} = \frac{\int_0^{\infty} \langle V \rangle n(r_p) \pi r_p^2 dr_p}{\int_0^{\infty} n(r_p) \pi r_p^2 dr_p} \quad (2.53)$$

where \bar{V} is the average velocity through the membrane, $\langle V \rangle$ is the average velocity in a single pore with radius r_p , and n is number of pores with radius (r_p). The weighting of the integrals by πr_p^2 accounts for the cross-sectional area of the pore. The average solute flux \bar{N}_s is evaluated in an analogous fashion as:

$$\bar{N}_s = \frac{\int_0^{\infty} \langle N_s \rangle n(r_p) \pi r_p^2 dr_p}{\int_0^{\infty} n(r_p) \pi r_p^2 dr_p} \quad (2.54)$$

where $\langle N_s \rangle$ is the flux through a single pore. Equation 2.53 and Equation 2.28 can be combined to develop an expression for the average asymptotic sieving coefficient:

$$\bar{S}_{\infty} = \frac{\bar{N}_s}{C_w \bar{V}} = \frac{\int_0^{\infty} S_{\infty}(r_p) n(r_p) r_p^4 dr_p}{\int_0^{\infty} n(r_p) r_p^4 dr_p} \quad (2.55)$$

The hydraulic permeability for a membrane with a pore size distribution (assuming no electrostatic interactions) is shown in Equation 2.56.

$$L_p = \frac{\varepsilon}{8\eta\delta} \frac{\int_0^{\infty} n(r_p) r_p^4 dr}{\int_0^{\infty} n(r_p) r_p^2 dr} \quad (2.56)$$

The r^4 dependence in the numerator comes from the Hagen-Poiseuille equation (Equation 2.9) while the r^2 dependence in the denominator comes from the circular cross sectional area of the cylindrical pores.

2.6 Solute Deformation

All of the discussion in this Chapter has implicitly assumed that the solutes are unaffected by the fluid flow, which ignores the possibility of any deformation or elongation of the solutes during ultrafiltration. This assumption is typically valid for most proteins due to their highly globular structure, but this may not be valid for the PEGylated proteins examined in this thesis. The degree of flow-induced polymer deformation is typically characterized in terms of the Deborah number (De):

$$De = \frac{\tau_0}{\gamma^{-1}} = \tau_0 \cdot \dot{\gamma} \quad (2.57)$$

where τ_0 is the time scale for polymer relaxation and γ^{-1} is the time scale characteristic of the fluid flow. The elongation of molecules is generally thought to become significant at $De \geq 1$ although some studies have reported deformation effects at De as small as 0.05 (Long and Anderson, 1984).

The relaxation time is the longest time required for a polymer chain to return to its natural equilibrium state after elongation, which is typically calculated using the chain like bead-spring model originally developed by Rouse (1953) and modified by Zimm (1956). Alternatively, τ_0 can be evaluated experimentally using transient analysis of the post-stretching recovery using electric birefringence (Thompson and Gill, 1967), flow dichroism (Callis and Davidson, 1969), creep recovery (Klotz and Zimm, 1972), or

microscopy (Perkins, et al., 1997). The time-scale for the fluid flow is typically set equal to the inverse shear rate (γ^{-1}), which is proportional to the volumetric flow rate through the membrane and inversely proportional to the characteristic distance to the third power:

$$\gamma \approx \left(\frac{Q_p}{L^3} \right) \quad (2.58)$$

where Q_p is the flow rate through a single pore and L is the characteristic distance. The flow rate Q_p can be related to the filtrate flux (J_v) as:

$$Q_p = \frac{J_v \pi r_p^2}{\varepsilon} \quad (2.59)$$

Daoudi and Brochard (1978) argued that the critical distance from the pore entrance where deformation effects become significant should be evaluated using the solute radius of gyration (R_G) giving:

$$\gamma \approx \left(\frac{J_v \cdot r_p^2}{\varepsilon \cdot R_G^3} \right) \quad (2.60)$$

In contrast, Long and Anderson (1984) assumed that the critical distance was equal to the membrane pore radius giving:

$$\gamma \approx \left(\frac{Q_p}{r_p^3} \right) = \left(\frac{J_v}{\varepsilon \cdot r_p} \right) \quad (2.61)$$

which has a totally different dependence on both the pore and solute radius. The use of these models is discussed in more detail in Chapter 7.

In general, the Zimm model is typically used for very dilute polymer solutions where each polymer segment is modeled as a bead in a chain. The Rouse model is more

appropriate for polymer melts that are not strongly intertwined. Equation 2.62 shows the characteristic time given by the Zimm model:

$$\tau \approx \frac{\eta \cdot R_G^3}{k_B T} \quad (2.62)$$

where η is the fluid viscosity, k_B is the Boltzmann constant, and T is the absolute temperature. The Rouse model is shown in Equation 2.63:

$$\tau = S[\eta_o] \eta \frac{MW}{RT} \quad (2.63)$$

where $[\eta_o]$ is the intrinsic viscosity, MW is the polymer molecular weight, and R is the ideal gas constant.

The intrinsic viscosity for a PEG system was determined experimentally by Singh (1998):

$$[\eta_o] = 4.9 \times 10^{-4} M^{0.672} \quad (2.64)$$

The Zimm model was chosen for use in this study as discussed in more detail in Chapter 7.

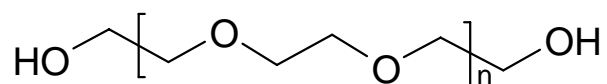
Chapter 3

MATERIALS AND METHODS

3.1 Experimental Materials

3.1.1 Polyethylene Glycol

Polyethylene glycol (PEG) is a linear or branched polymer made of ethylene glycol monomer units with terminal hydroxyl groups as shown in Figure 3.1. The most common method of production of PEG is through the anionic polymerization of ethylene glycol. PEG is biocompatible and has been approved for intravenous applications for MW > 400 Da. Lower molecular weight species (< 300 kDa) have been shown to result in complete respiratory arrest of canines at concentrations above 3 g/kg (Working et al., 1997).



Polyethylene Glycol

Figure 3.1. Chemical structure of polyethylene glycol.

The hydrodynamic radius (R_h) of the PEG used in this study was estimated using the correlation developed by Singh (1998) based on intrinsic viscosity data for molecules up to 35 kDa in molecular weight (Equation 2.7). Polyethylene glycols were obtained from Sigma (St. Louis, MO) and Fluka (Busch, Switzerland) with nominal molecular weights ranging from 1,450 to 35,000.

3.1.2 Activated Polyethylene Glycol

A number of methods have been used for the covalent attachment of PEG to different chemical groups on proteins including the N-terminus or C-terminus, primary or secondary amines, cysteines, and saccharides (Roberts, et al., 2002). Each method requires somewhat different activation of the PEG to allow the reaction to proceed under mild conditions. The specific reaction chemistry used in this thesis is described in Chapter 4.

In this study, activated polyethylene glycol molecules with nominal molecular weight ranging from 2 to 30 kDa were used to produce PEGylated proteins. Two forms of activated PEG were used: N-hydroxysuccinimide esters (NHS) or maleimide which react with primary amines or free cysteine groups, respectively. PEG activated with NHS were obtained from Nektar Therapeutics (Huntsville, AL) and NOF Corporation (Tokyo, Japan). Two commercial forms were used: methoxyPEG succinimidyl propionic acid (mPEG-SPA) and methoxyPEG succinimidyl α -methylbutanoate (mPEG-SMB) with chemical formula shown in Figure 3.2. The hydrolysis rates of mPEG-SPA and mPEG-SMB were 16.5 minutes and 44 minutes, respectively, when placed in DI water at room temperature at pH 8.1 (Olson, et al., 1997). The maleimide activated form, methoxy

polyethylene glycol – maleimide (mPEG-MAL) was obtained from NOF Corporation (Tokyo, Japan). All activated PEG samples were kept at -20°C surrounded by calcium sulfate desiccants when not in use to limit the amount of hydrolysis of the activated group. The polydispersity of each sample was less than 1.05 and the diol concentration was less than 4% as provided by the manufacturer.

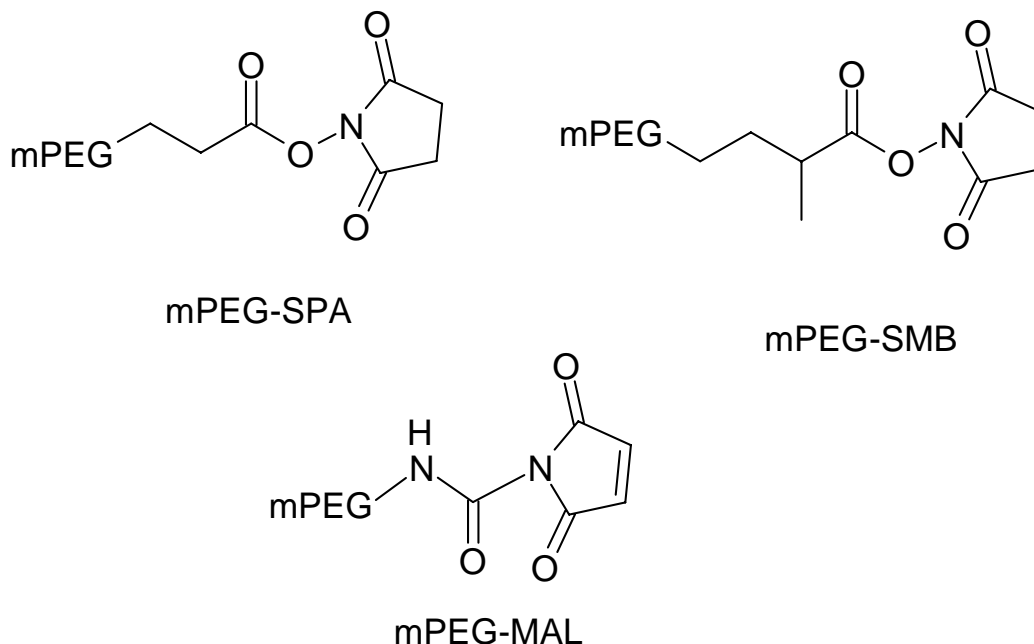


Figure 3.2. Chemical structures of activated polyethylene glycols used for protein PEGylation.

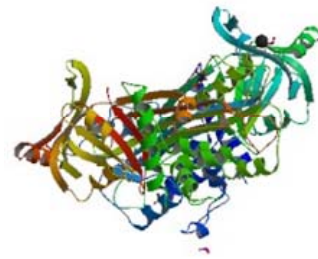
3.1.3 Proteins

α -lactalbumin, ovalbumin, and bovine serum albumin were used as model proteins. All proteins were obtained from Sigma Chemical (St. Louis, MO) with catalog numbers shown in Table 3.1. These proteins were chosen due to their availability, high stability over a wide range of pH and ionic strength, and well defined physical properties. Figure 3.3 shows the 3D stereoview of the protein structures (Chrysina et al., 2000; Stein

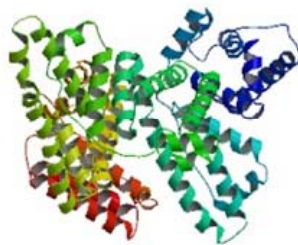
et al., 1991; Sugio et al., 1999). Note that the structure of human serum albumin is shown, but it is similar to bovine serum albumin both in the number of disulfide bonds and the amino acid sequence (Peters, 1996). Table 3.1 shows key physical properties of these proteins. The number of lysine groups was taken from the published amino acid sequences (Bairoch et al., 2005). The hydrodynamic radii were calculated from the molecular weight using the expression developed by Young et al. (1980) as given in Equation 2.6. The diffusion coefficients were calculated from the hydrodynamic radii using the Stokes-Einstein equation.



α -lactalbumin (Chrysina et al., 2000)



Ovalbumin (Stein et al., 1991)



Human Serum Albumin (Sugio et al., 1999)

Figure 3.3. Structure of globular proteins: α -lactalbumin, ovalbumin, and human serum albumin.

Table 3.1 Physico-chemical properties of proteins.

Property	α-Lactalbumin	Ovalbumin	BSA
<i>Catalog Number (Sigma)</i>	L5385	A5503	A7906
<i>Molecular Weight (Da)</i>	14,200	42,750	69,300
<i>D_w (m²/s)</i>	1.06×10^{-10}	7.8×10^{-11}	6.0×10^{-11}
<i>Stokes Radius (nm)</i>	1.9	2.7	3.2
<i>Isoelectric Point</i>	4.6	4.5	4.9
<i># Lysine Groups</i>	12	20	60

Protein solutions were prepared by dissolving pre-weighed quantities of dry protein into the appropriate buffer. The pH of the protein solution was measured using a Model 402 Thermo Orion pH meter (Beverly, MA). The proteins were then filtered through a 0.2 μ m Pall Acrodisc Syringe Filter (Supor Membranes) to remove any large aggregates prior to each experiment. Proteins were stored at 4°C when not in use. Protein solutions were used within ten days of preparation.

3.1.4 Protein Modifications

3.1.4.1 PEGylated Protein Reaction

PEGylated proteins were produced by reaction of a globular protein with an activated form of mPEG. The protein of interest was dissolved in an appropriate buffer (pH above 6.5) with concentration between 2 and 30 g/L. The activated mPEG was then added at a desired ratio (usually ranging from 0.5 to 10 moles of PEG per mole of protein) and slowly stirred at room temperature (21-24°C) for a minimum of 8 hours to allow the reaction to go essentially to completion. The resulting product solution, which contained the PEGylated protein, the un-reacted protein and any residual mPEG, the

hydrolyzed PEG reagent, and n-hydroxysuccinimide (produced from hydrolysis of the mPEG-SPA or mPEG-SMB), was then diluted approximately four-fold with the same buffer. The solution was pre-filtered through a 0.2 μm pore size Acrodisc syringe filter (Pall Corporation, Ann Arbor, MI) to remove any particulate matter and larger aggregates prior to use. The solution ionic strength was adjusted to the desired value by addition of 1 M KCl or NaCl containing the buffer species of interest or the solution was diafiltered through a 10 kDa Ultracel membrane using an appropriate diafiltration buffer. PEGylated proteins were stored at 4°C when not in use. PEGylated proteins were used within 25 days of preparation. More details on the PEGylation reaction are given in Chapter 4.

PEGylated BSA, formed by attachment of a single 12 kDa PEG to the free sulfhydryl group on BSA, was provided by Pfizer Inc. (St. Louis, MO) in a 20 mM Bis Tris propane solution containing 10 mM NaCl. This 12 kDa PEG-BSA conjugate was purified by Pfizer Inc. (St. Louis, MO) to remove both unreacted protein and hydrolyzed PEG. 12 kDa PEGylated BSA was used for fouling experiments discussed in Chapter 10. Additional PEGylated BSA was produced in our laboratory using either an activated mPEG-SPA to obtain species with multiple PEG branches (attached at the lysine amino groups) or using maleimide to obtain a PEGylated BSA with one PEG branch (attached at the single free cysteine).

Typical PEGylated α -lactalbumin was produced with PEG branches ranging from 5 kDa to 20 kDa. PEGylated ovalbumin was produced with 5 kDa and 10 kDa PEG branches and PEGylated BSA was produced with a 12 kDa PEG branch. Scaled schematics of some of the PEGylated proteins used in this study are shown in Figure 3.4

with the darker circle representing the protein with fixed negative surface charges and the lightly shaded outer circle representing the PEG.

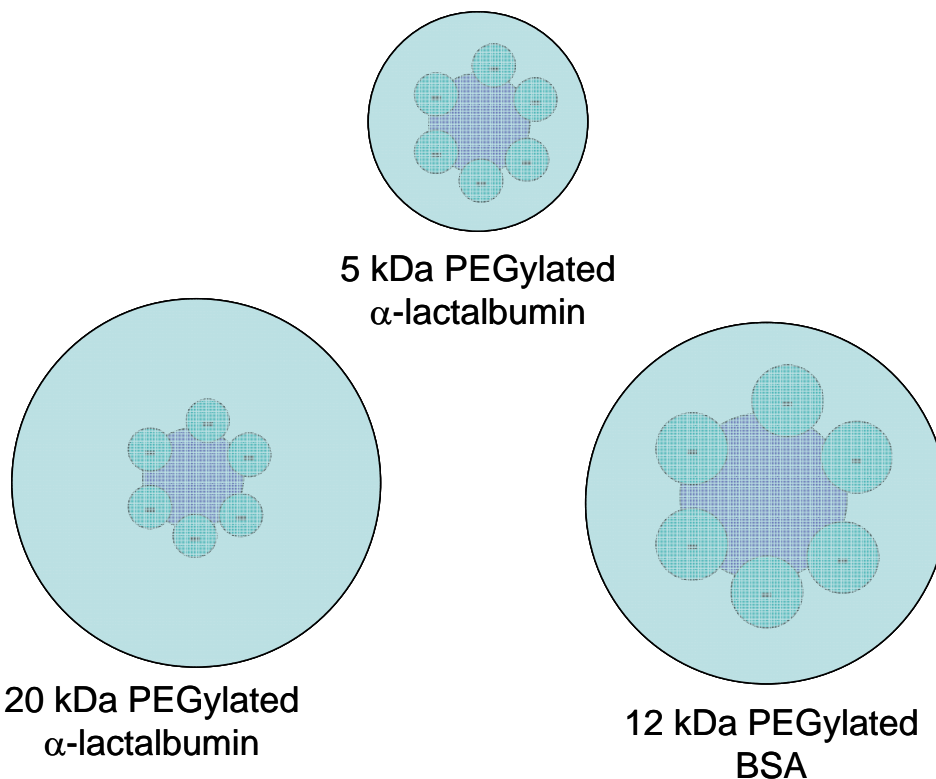


Figure 3.4. Scaled schematic of PEGylated α -lactalbumin with 5 kDa or 20 kDa total molecular weight of PEG and BSA with 12 kDa of PEG attached.

In order to reduce the amount of PEGylated protein required in the ultrafiltration experiments, the PEGylated proteins were re-used for multiple experiments by performing an ultrafiltration / diafiltration to re-adjust the concentration, pH, and conductivity to the desired values. Diafiltration was performed using 10 kDa UltracelTM membranes for 10 diavolumes using the procedures described in Section 3.2.4. The pH, conductivity, and composition of the final solution were evaluated immediately before use in the ultrafiltration experiments. There was no degradation of the PEGylated protein as determined by SEC.

3.1.4.2 Protein Acetylation

Acetylated proteins were synthesized using the general procedure described by Gao and Whitesides (1997). This involved reaction of the protein with acetic anhydride, which converts the free amine groups on lysine to the corresponding amide as shown in Figure 3.5. The acetylated proteins were created by first adding 2 g/L of protein to deionized water and chilling in an ice bath to 5°C. The solution pH was adjusted to 12 by the addition of 0.1 M NaOH. Four molar equivalents of acetic anhydride (as a 9.75 g/L solution in dioxane) were then added to the protein solution. The reaction mixture was stirred continuously for 15 minutes while adding 0.1 M NaOH to maintain the pH at 12. The reaction mixture was quenched by adding 0.5 M HCl to rapidly reduce the pH to approximately 6. The resulting solution was placed in an ultrafiltration cell containing a 10 kDa Ultracel™ membrane (Millipore Corp., Bedford, MA). A constant volume diafiltration was performed using a 10 mM Bis Tris buffer for a minimum of five diavolumes to remove acetic acid, unreacted acetic anhydride, and other small impurities using a flux of 14 μm/s (50 L m⁻² hr⁻¹). The resulting solution was then filtered through a 0.2 μm Pall Supor Acrodisc syringe filter prior to use.

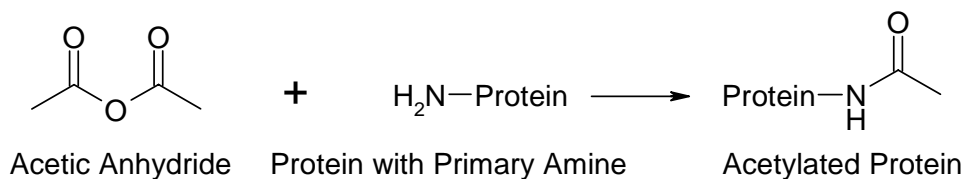


Figure 3.5. Acetylation reaction between the primary amine on a protein and acetic anhydride.

3.1.5 Dextrans

Dextrans are neutral polymers of glucose joined via α -1,6 linkages with possible branches occurring at the α -1,3 linkage as shown in Figure 3.6. Dextran is synthesized naturally by certain lactic acid bacteria. Dextrans of specific molecular weight are typically produced by partial hydrolysis of the natural product. Dextran diffusion coefficients were evaluated using the correlation presented by Granath (1958) for molecular weights between 21,600 and 526,000 Da.

$$\text{Log}(D_{\infty}) = -4.1154 - 0.47752\text{Log}(MW) \quad (3.1)$$

where D_{∞} is in cm^2/s . and MW is in g/mol .

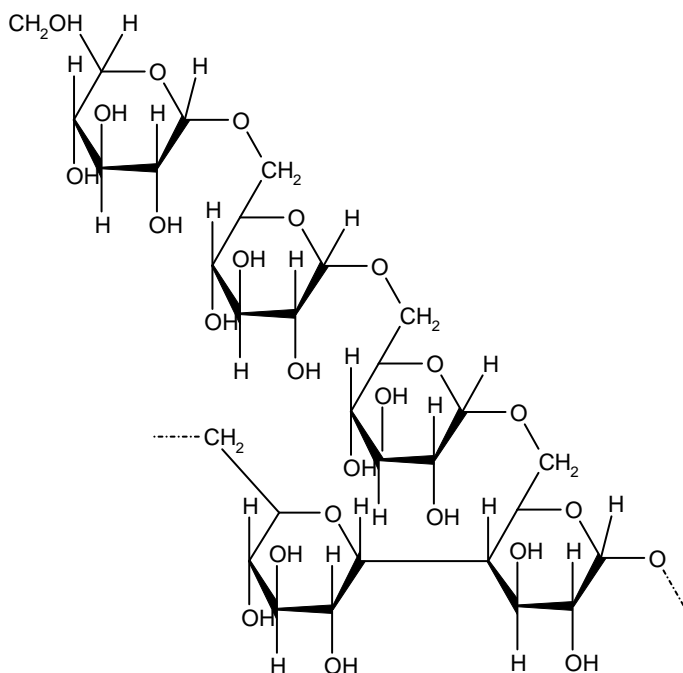


Figure 3.6 Chemical structure of dextran. Adapted from Burns (2000).

Dextran solutions were prepared by dissolving powdered dextran (Sigma Chemical, St. Louis, MO) in the desired buffer. Narrow molecular weight dextran standards were used for calibration in size exclusion chromatography while polydisperse dextrans with either 40 kDa or 75 kDa average molecular weight were used to characterize the pore size distribution of the ultrafiltration membranes. Blue dextran with 1,000,000 Da molecular weight (Catalog number D5751 from Sigma, St. Louis, MO) was used as a fully excluded solute in size exclusion chromatography.

3.1.6 Buffers

Buffers were used to control the pH and ionic strength of the protein and PEG solutions. All buffers were prepared using the methods described by Beylon and Easterby (1996) with the ionic strength (I) evaluated as

$$I = \frac{1}{2} \sum_i z_i^2 C_i \quad (3.2)$$

where z_i is the the valence charge and C_i is the total concentration of a buffer species. Buffers were prepared by dissolving the desired buffer components in deionized water obtained from a NANOpure Diamond water purification system (Barnstead Thermolyne Corporation, Dubuque, IA) with resistivity greater than 18.0 M Ω -cm. All salts were certified ACS grade or higher and obtained from Sigma (St. Louis, MO) unless otherwise noted. The solution pH was measured using a Model 402 Thermo Orion pH meter (Beverly, MA) and was adjusted by addition of 1.0 or 0.5 M hydrochloric acid, potassium hydroxide, or sodium hydroxide as required. The solution conductivity was evaluated using a Model 105 Thermo Orion conductivity meter referenced to 25°C. Buffer solutions were filtered through a 0.2 μ m Pall Supor200 47 mm filter with a vacuum pump

to remove any particulate matter before use. The concentrations of buffer components used in the most common buffers are shown in Table 3.2.

Table 3.2. Components for different buffers used in experiments.

Buffer	Ionic Strength	pH	Acid	Acid (mol/L)	Base	Base (mol/L)	Salt	Salt (g/L)
Bis Tris	10mM	7.0	HCl	0.002	Bis Tris	0.008	KCl	0.564
Bis Tris	500mM	7.0	HCl	0.010	Bis Tris	0.007	KCl	37.059
Bis Tris	10mM	6.0	HCl	0.008	Bis Tris	0.002	KCl	0.177
Acetate	10mM	5.0	CH ₃ COOH	0.003	NaCH ₂ COO	0.007	KCl	0.254
Tris	10mM	8.0	HCl	0.005	Trizma Base	0.005	KCl	0.353
Tris	10 mM	8.5	HCl	0.003	Trizma Base	.007	KCl	0.531
Phosphate	150mM	7.0	NaPO ₂ (OH) ₂	0.019	Na ₂ PO ₃ OH•7H ₂ O	0.031	NaCl	2.318
Phosphate	200mM	7.0	NaPO ₂ (OH) ₂	0.197	Na ₂ PO ₃ OH•7H ₂ O	0.030	NaCl	5.147

3.1.7 Ultrafiltration Membranes

Ultrafiltration and diafiltration experiments were performed using UltracelTM composite regenerated cellulose membranes with nominal molecular weight cut-offs (MWCO) of 30 kDa or 100 kDa (Millipore Corp., Bedford, MA). Fouling experiments were performed with UltracelTM membranes as well as BiomaxTM polyethersulfone membranes (MWCO of 100 kDa or 300 kDa) also provided by Millipore Corp. (Bedford, MA). The nominal molecular weight cut-off refers to the molecular weight of a solute which has a 90% rejection as determined by the manufacturer. UltracelTM membranes with 10 kDa molecular weight cut off were used for buffer exchange. These ultrafiltration membranes all have an asymmetric structure with a thin skin on a thicker more porous substrate (Figure 3.7). The skin thickness is approximately 1.0 μm while the total membrane thickness is approximately 0.018 to 0.038 cm (Millipore, 2008b).

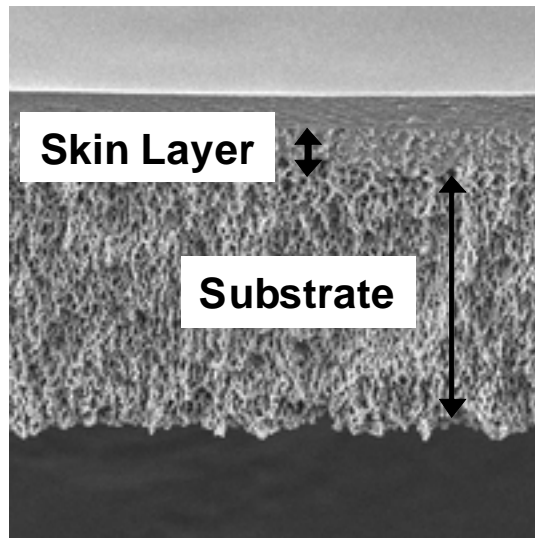


Figure 3.7. SEM image of the cross section of an Ultracel 100 kDa membrane produced by Millipore Corporation (2008a)

Membrane disks were cut from large flat sheets using a specially designed cutting tool. All membranes were soaked in isopropanol for 45 minutes to remove any wetting / storage agents prior to use. The membranes were then thoroughly rinsed with at least 40 L/m² of DI water and 40 L/m² of the working buffer.

Negatively charged versions of the UltracelTM membranes were created by covalently attaching sulfonic acid groups to the membrane surface using the base activated chemistry described by van Reis (2006) as shown in Figure 3.8. Membranes were initially soaked in 0.1 M NaOH for at least 12 hours. The negatively-charged membrane was made by immersing the membrane in a 2 M solution of 3-bromopropanesulfonic acid sodium salt (Catalog #B2912, Sigma Chemical) in 0.1 N NaOH for a specified amount of time. The membrane was then thoroughly washed with 0.1 M NaOH followed by DI water, 0.2 M acetic acid, DI water again, and finally the buffer solution that was to be used in the ultrafiltration experiments.

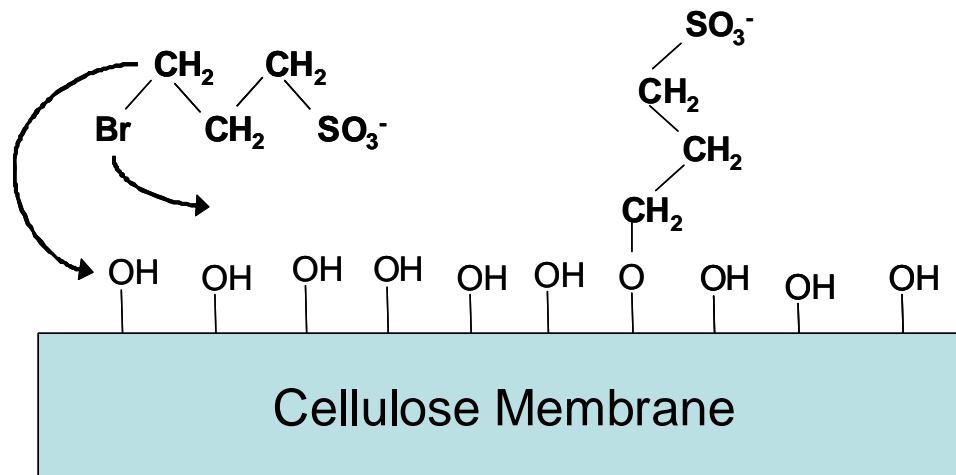


Figure 3.8. Schematic of reaction chemistry used to make negatively charged membranes.

3.2 Experimental Methods

3.2.1 Ultrafiltration Set-up

Ultrafiltration experiments were performed in Amicon 8003, Amicon 8010, or Amicon 8200 stirred cells with effective membrane areas of 0.9, 4.1, and 28.7 cm², respectively (Millipore Corp., Bedford, MA). UltracelTM and BiomaxTM membranes were placed in the bottom of the stirred cell directly on top of a porous layer of Tyvek[®] that was used to minimize deformation of the membrane at higher pressures. The membrane was held in place by a rubber o-ring that provided a leak-free seal. A stir bar was placed directly above the membrane, suspended from the top of the stirred cell module, and rotated at 600 rpm unless otherwise stated to minimize the effects of concentration polarization. The stirring speed was controlled by a VWR 205 Autostirrer magnetic stir plate and adjusted to 600 rpm using a Strobotac 1531-AB phototachometer (General Radio Company, Concord, MA). The stirred cell was air-pressurized, with the

filtrate flux controlled by a pressure regulator (Scott Specialty gases, Plumsteadville, PA). The pressure was measured by an Ashcroft model 0518 (0-30 psi) or model 8920 (0-15 psi) pressure gauge. More accurate control of the filtrate flux was obtained in some experiments by connecting the filtrate exit line directly to a Rabbit-Plus peristaltic pump (Rainin Instrument Co. Woburn, MA) as shown in Figure 3.9.

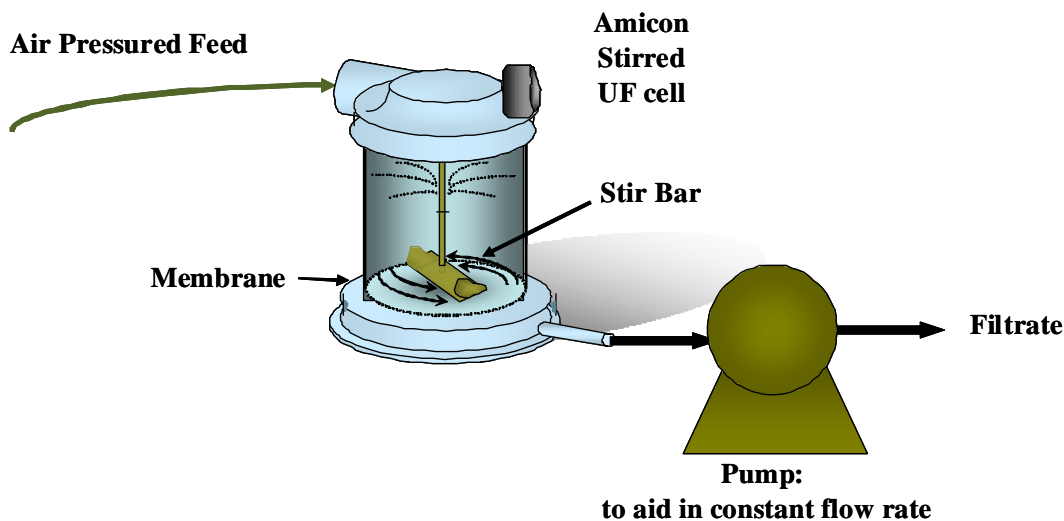


Figure 3.9. Schematic of ultrafiltration stirred cell set-up.

3.2.2 Membrane Hydraulic Permeability

The membrane hydraulic permeability (L_p) was evaluated by measuring the filtrate flux as a function of transmembrane pressure for at least five pressures using a 10 mM Bis Tris buffer unless otherwise stated. Filtrate flux was determined by timed mass collection of the filtrate using a Mettler Toledo AG104 digital balance. The hydraulic permeability of the charge-modified membrane was also evaluated using a 500 mM KCl buffer solution containing 10 mM Bis Tris to minimize the contribution of counter-electroosmosis. The permeability was calculated from the slope of the data using

Equation 2.8. In each case, the solution was filtered through the membrane for approximately 25 min to insure stable operation. The membrane permeability was re-evaluated after this initial adsorption step using the same method described above and then again after completion of the experiment. The decrease in permeability provided a measure of the extent of undesired fouling during the experiments.

3.2.3 Sieving Experiments

Sieving experiments were performed with proteins, PEG, and PEGylated proteins. Immediately after evaluating the membrane permeability, the stirred cell was emptied and re-filled with the desired feed solution. The system was equilibrated at 4°C for a minimum of 10 hr prior to use to minimize transients during ultrafiltration. The stirred cell was then emptied and refilled with a fresh feed solution. An initial ultrafiltration was performed for approximately 25 min at low flux (below 11 $\mu\text{m/s}$). The pressure / flux were then readjusted, and a minimum of 2 ml of filtrate collected to washout the dead volume beneath the membrane and to insure stable operation. Selected experiments were run using a variable speed, 10 roller peristaltic pump (Rabbit-Plus, Rainin Instrument Co. Woburn, MA) connected to the filtrate line to insure a constant flux. The filtrate flux was evaluated by timed collection and small samples of the filtrate and bulk solutions were collected for subsequent analysis by size exclusion chromatography or UV spectrophotometry as described in Section 3.3. After each measurement, the stirred cell was opened and refilled with feed solution. In order to reduce the amount of PEGylated protein required for these experiments, the feed solution was re-used for multiple experiments by performing an ultrafiltration / diafiltration to re-adjust the concentration,

pH, and conductivity to the desired values (see Section 3.2.4). Diafiltration was performed using the 10 kDa UltracelTM membranes for 10 diavolumes, with the pH, conductivity, and composition of the resulting solution evaluated before use in subsequent ultrafiltration experiments. No degradation of the protein molecules were observed by SEC for the re-used feed.

3.2.4 Diafiltration

Diafiltration was used for the actual separation of NHS, PEG, PEGylated protein, and α -lactalbumin. The diafiltration system was identical to the apparatus shown in Figure 3.9 except a buffer reservoir was attached to the feed side of the stirred cell to provide diafiltration buffer at the same rate that the permeate solution was drawn through the membrane. The buffer reservoir was air pressured to the appropriate value. The filtrate flux was measured by timed collection with small adjustments made to the applied pressure to maintain the flux at an essentially constant value (within 0.5 $\mu\text{m/s}$). Small samples were taken periodically from both the collected filtrate and the stirred cell for subsequent analysis of the solute concentrations. More details on the diafiltration of the PEGylated protein solution are given in Chapter 9.

3.2.5 Membrane Characterization

3.2.5.1 Pore Size Distribution

The pore size distribution of select membranes was determined by dextran sieving measurements using polydisperse dextrans. Dextrans with an average molecular weight of 40 kDa were used to characterize the 30 kDa membranes while dextrans of 75 kDa

average molecular weight were used to characterize the 100 kDa membranes. A 5 g/L solution of the polydisperse dextran was placed in a stirred cell and air pressurized to obtain the desired flux. Approximately 2 ml of solution were passed through the membrane to washout the dead volume, with samples of retentate and filtrate then collected and analyzed by size exclusion chromatography as described in Section 3.3.

3.2.5.2 Membrane Charge Characterization

The membrane surface charge was determined using streaming potential measurements. The membrane was placed between two chambers, each filled with the buffer solution of interest, as shown in Figure 3.10 (Mehta, 2006). Ag/AgCl electrodes were inserted into the end of each chamber to measure the voltage difference across the membrane. O-rings were used to seal the electrodes in place and prevent leakage.

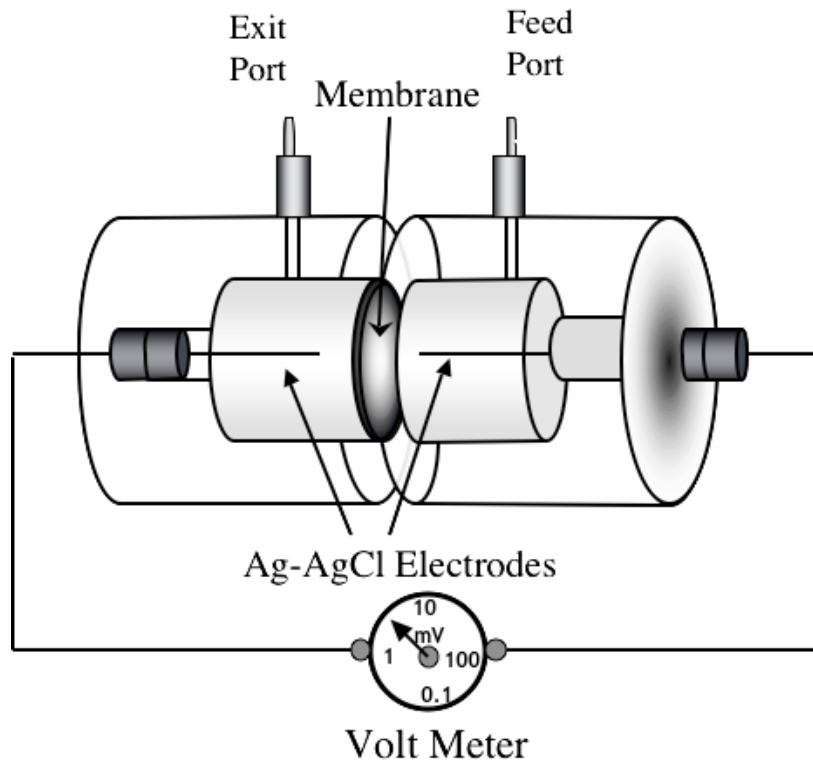


Figure 3.10. Streaming potential apparatus used to determine the membrane surface charge. Adapted from Mehta (2006).

The Ag/AgCl electrodes were prepared by reducing pieces of pure silver wire (1 mm radius) in a 1 M KCl solution. The silver wires were first lightly sanded and placed in a beaker of concentrated nitric acid for 10 s. The wire was then washed with DI water and placed in a beaker containing 1 M KCl. A DC power source was then connected to the silver electrode and a steel wire in a separate beaker containing 1 M KCl. A commercial Kimwipe was used as a salt bridge. A current of 20 mA was maintained for 20 minutes to reduce the silver to AgCl. The same process was repeated for the second silver electrode. Electrodes were stored in 0.5 M KCl between experiments.

To measure the streaming potential of the membrane, the streaming potential apparatus was assembled, a solution reservoir was attached to one chamber, and a drain

was connected to the other insuring no air bubbles were trapped in either chamber. A small pressure was applied across the membrane by either adjusting the height of the feed reservoir or by air pressurization. The system was allowed to equilibrate for 5 min, and the voltage then measured using a Keithley 200 multimeter. The voltage was measured continuously every 5 min until equilibrium was attained. Data were obtained at several discrete pressures with the zeta potential (ζ) evaluated from the change in streaming potential as a function of the applied pressure using the Helmholtz-Smoluchowski equation (Hunter, 1981):

$$\zeta = \frac{\eta c}{\varepsilon_0 \varepsilon} \frac{dE_z}{dP} \quad (3.3)$$

where η is the solution viscosity, c is the conductivity, ε_0 is the permittivity of a vacuum, and ε is the relative permittivity of the solution. Note that Equation 3.3 is developed by assuming that the double layer is small compared to the pore radius, a condition that is not strictly valid in these experiments. dE_z/dP was evaluated from the slope of the streaming potential as a function of the applied transmembrane pressure. More details on the stream potential measurements and analysis are given in Chapter 8.

3.3 Assays

3.3.1 UV Spectrophotometry

Concentration of individual (pure) proteins were measured using a UV spectrophotometer model 1240 (Shimadzu, Columbia, MD) at a wavelength of 280 nm, which is the natural absorbance of the protein aromatic groups. A calibration curve was

created for each protein from protein standards generated by serial dilution using at least five different concentrations (Figure 3.11). The limit of detection for α -lactalbumin was 0.005 g/L. Measurements were obtained by placing approximately 1 ml of sample in a 1.5 ml cuvette (model number 759165, Plastibrand Wertheim, Germany) to evaluate the absorbance. The observed sieving coefficient was evaluated directly from the ratio of the solute concentration in the feed and filtrate solutions.

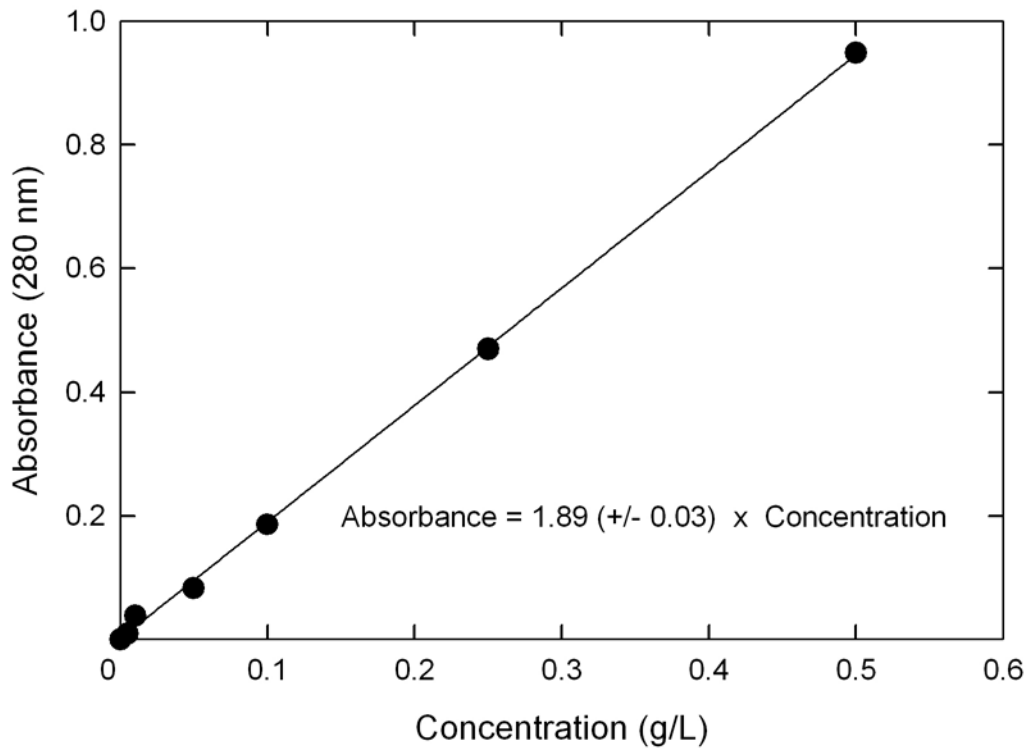


Figure 3.11. Calibration curve of α -lactalbumin using UV absorbance at 280 nm.

3.3.2 Size Exclusion Chromatography

The concentrations of the different components in the feed containing the PEGylated protein, the native protein, n-hydroxysuccinimide, and the unreacted

polyethylene glycol were determined using size exclusion chromatography with an Agilent 1100 HPLC system as shown in Figure 3.12. The same approach was used to evaluate the molecular weight distribution of the polydisperse dextrans. The chromatography system was operated using Chemstation software version A.04.08 (Agilent Technologies).

The PEG and protein samples were analyzed using a Superdex 200, 10/300 gel permeation column (13 μm particle size, 1×10^5 MW exclusion limit) obtained from GE Healthcare (Uppsala, Sweden). The mobile phase was a 50 mM phosphate buffer at pH 7 containing 0.15 M NaCl with a flow rate of 0.3 ml/min. The column was initially flushed with a minimum of 2 column volumes of running buffer to insure equilibration. 100 μl samples were injected over a period of 30 s. Sample detection was performed using an Agilent 1100 series refractive index detector and an Agilent 1200 series UV-Vis detector at 280 nm, with the two detectors operated in series. The PEG was effectively invisible to the UV detector, providing much more accurate measurements of the protein concentrations. The concentrations of PEG and the PEGylated protein could be accurately measured to within 0.02 g/L (with baseline resolution of the peaks) using the RI detector; the α -lactalbumin and NHS concentrations could be accurately measured to ± 0.002 g/L using the UV detector. Calibration curves were constructed using samples of known concentration, with the peak areas determined by numerical integration. Overlapping peaks were simply split at the location of the minimum.

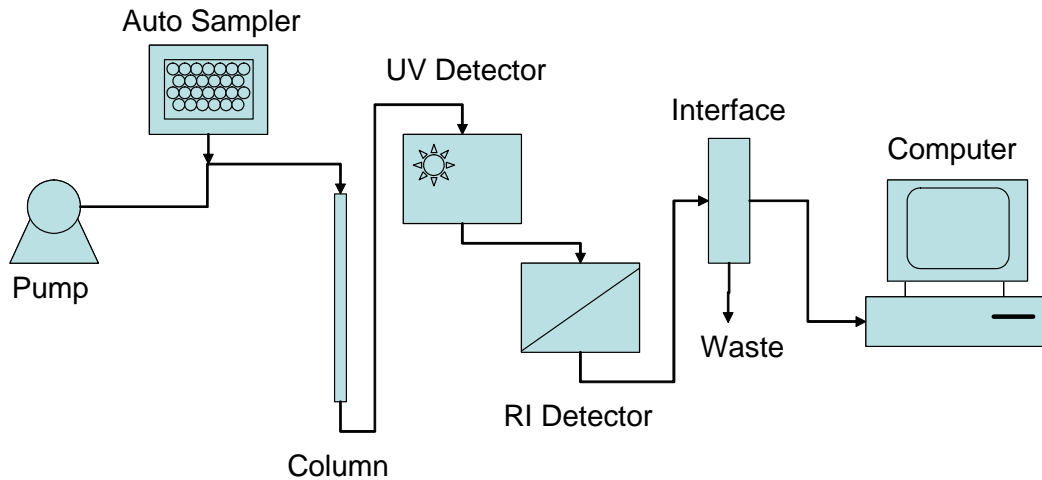


Figure 3.12. Schematic of size exclusion chromatography set-up.

Concentrations of the PEGylated proteins were evaluated from the peak areas assuming that the total RI response (n_{RI}) was determined by the contribution of each species weighted by its specific response (Kunitani et al., 1991):

$$n_{RI} = \left(\frac{dn_{RI}}{dc} \right)_{pro} C_{pro} + \left(\frac{dn_{RI}}{dc} \right)_{PEG} C_{PEG} \quad (3.4)$$

where $(dn_{RI}/dc)_{pro}$ and $(dn_{RI}/dc)_{PEG}$ are the specific RI response for the pure PEG (2.78×10^6 nRIU/g/L) and pure protein (3.78×10^6 nRIU/g/L). The use of Equation 3.4 is discussed in more detail by Kunitani et al. (1991) and Li et al. (2005). Figure 3.13 and Figure 3.14 show calibration curves for the PEG and α -lactalbumin.

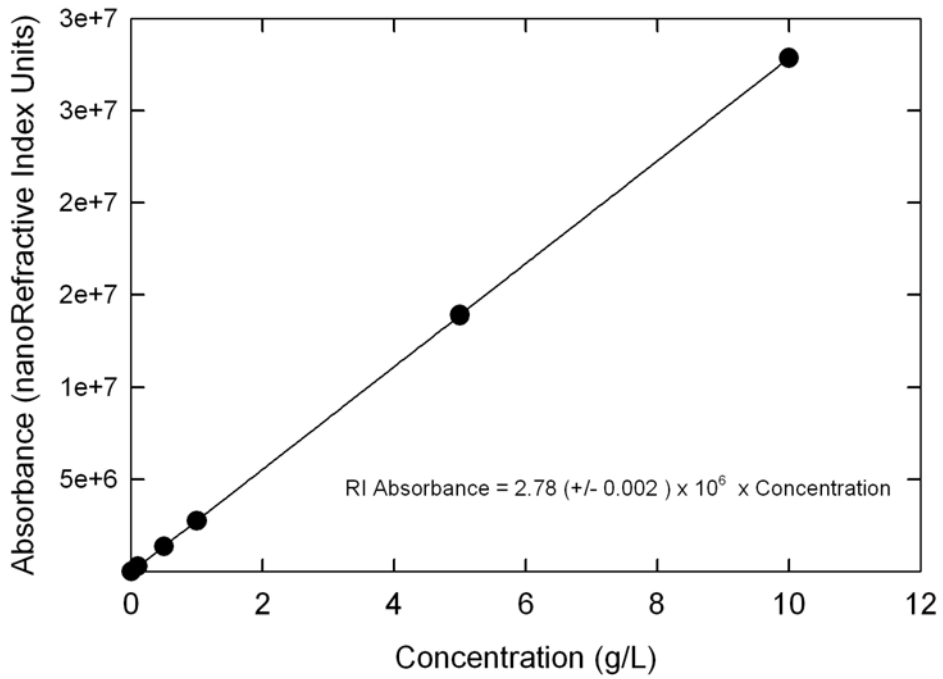


Figure 3.13. Calibration curve for PEG using refractive index detection.

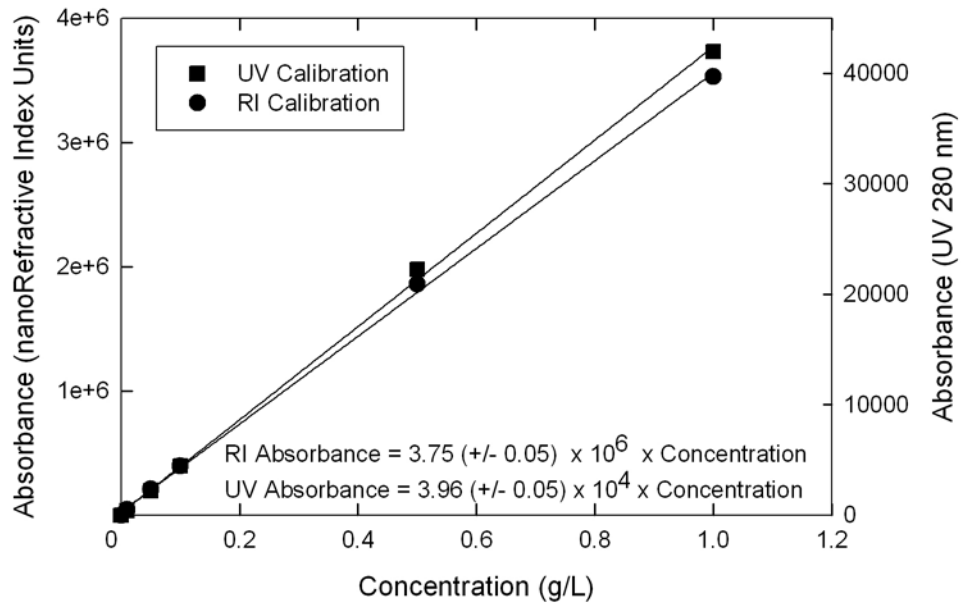


Figure 3.14. Calibration curves for α -lactalbumin using both refractive index and UV absorbance.

Dextran samples were analyzed using a G2000SW TOSOH (Montgomeryville, PA) silica gel permeation column for the 40 kDa dextran and a G3000SW TOSOH (Montgomeryville, PA) for the 75 kDa dextran. The columns were calibrated before each experiment using a set of narrow molecular mass dextran standards (4.4 kDa, 9.9 kDa, 18.5 kDa, 20.5 kDa, 27.5 kDa, 42.8 kDa, 78.8 kDa, 102.0 kDa, 123.4 kDa, 165.5 kDa) obtained from America Polymer Standards (Mentor, OH). A calibration curve for the TSK gel 2000SW column is shown in Figure 3.15. Data were obtained using 50 mM phosphate buffer at pH 7 containing 0.15 M NaCl as the mobile phase at a flow rate of 0.8 ml/min. The sample size and injection rate were the same as for the PEGylated protein mixtures. A sieving curve was constructed by analyzing the dextran peak at fixed intervals (~1 min) corresponding to a range in dextran molecular weight. The sieving coefficient for each molecular weight dextran was evaluated directly from the ratio of the dextran concentration in the filtrate and retentate solutions. The membrane pore size distribution was determined from the dextran sieving data as described in Appendix B.

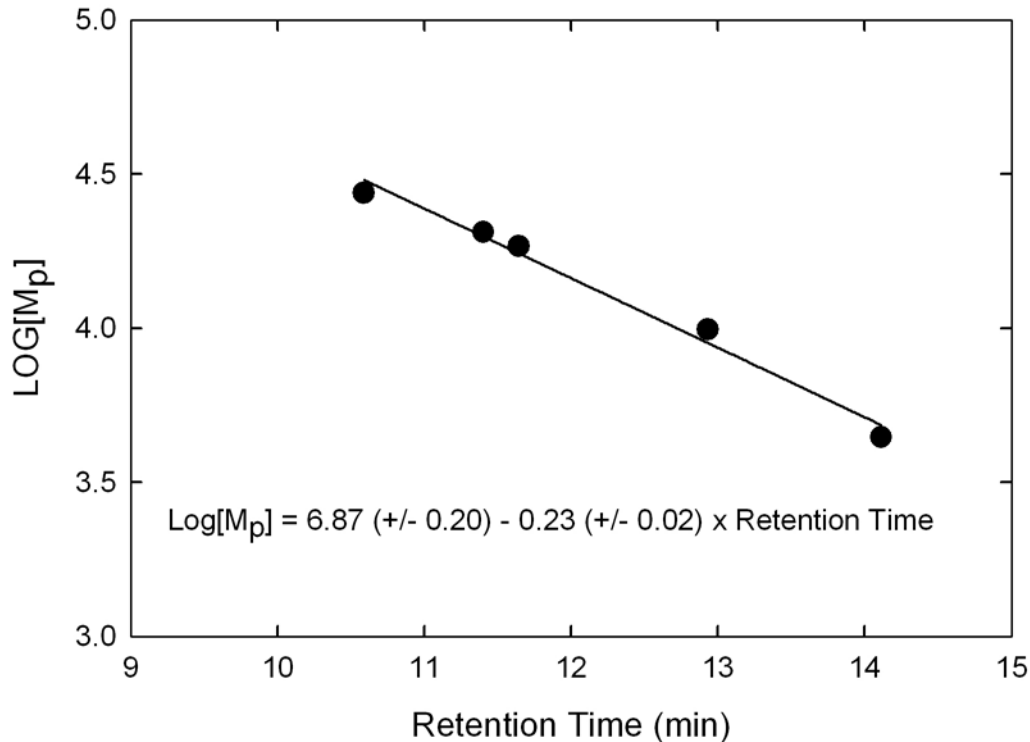


Figure 3.15. Dextran molecular weight calibration for the G2000SW column.

3.3.3 Reverse Phase High Performance Liquid Chromatography

The relative degree of hydrophobic interactions between the BSA or PEGylated BSA and a C4 hydrophobic resin was characterized using reverse-phase HPLC with the Symmetry 300TM C4 column (4.6 mm × 50 mm, 30 nm pore size, 5 μm particle size from Waters, Milford, MA). The set-up was similar to that shown in Figure 3.9, except no RI detector was employed. The mobile phase was a mixture of: (A) 0.1% v/v trifluoroacetic acid (TFA) in water and (B) 0.1% TFA in acetonitrile. Prior to sample injection the column was equilibrated with two column volumes of (A). Injection volume was 100 μL and the mobile phase flow rate was constant at 0.75 mL/min. Once the sample was

injected, the column was washed for 5 min with mobile phase (A) to remove molecules with no specific interactions to the hydrophobic resin. The mobile phase was quickly increased to 30% B and then run in a gradient mode from 30-50% B for 35 min. At the end of the gradient the mobile phase was held at 50% B for 5 min and then quickly increased to 100% B to remove any tightly bound aggregates. The specific gradient chosen was based on the measured protein resolution over a range of experimental conditions. Initial experiments showed that the BSA and PEGylated BSA eluted in the range of 40-45% B under a gradient mode from 0 to 100% B for 40 min.

3.3.4 Dynamic Light Scattering

Dynamic light scattering was performed using the Zetasizer Nano ZS (Malvern Instruments, Worcestershire, United Kingdom) to determine the average size of the proteins and PEGylated proteins. Data were obtained using 1 g/L solutions in 10 mM Bis Tris at a scattering angle of 173° with the solution temperature maintained at 25°C . The particle size was calculated from the homodyne intensity-intensity correlation function $G(q, t)$, with q (scattering vector) given by $q = (4\pi n_0 / \lambda_0) \sin(\theta / 2)$, where n_0 is the refractive index of the medium, λ_0 is the wave-length of the excitation light in a vacuum, and θ is the scattering angle. The correlation time was approximately 1 minute per run and 3 runs were performed per measurement. The autocorrelation function was analyzed using the CONTIN algorithm for monomodal samples. The autocorrelation function was converted to a diffusion coefficient, D_∞ , which was used to calculate the particle hydrodynamic radius, R_h , using the Stokes-Einstein equation, $R_h = k_B T / 6\pi\eta D_\infty$,

where, k_B is the Boltzmann constant, T is the absolute temperature, and η is the viscosity of the solvent.

3.3.5 Capillary Electrophoresis

Capillary electrophoresis was used to analyze samples containing multiple PEGylated species and to understand how the protein electrophoretic mobility is affected by PEGylation. Data were obtained using an Agilent G1600 capillary electrophoresis system equipped with a dual-polarity variable high voltage DC supply (0-30 kV) and a diode array UV/visible absorbance detector (214 nm wavelength for detection). Experiments were performed with fused-silica capillaries (inner diameter of 0.5 μm) with a total length of 80.5 cm (effective length to the detection window of 70.2 cm) or 64.5 cm (effective length of 52 cm). The capillary and solution reservoirs were filled with the buffered electrolyte solution. Protein samples (approximately 65- 140 nL) containing 5 mM of mesityl oxide as a neutral marker were injected for 3 or 25 seconds at a pressure of 4000 Pa. Data were obtained at a constant applied electric field of 25 kV, with the field direction chosen so that the direction of the bulk flow was toward the detector (and cathode). The current was less than 45 μA , so Joule heating was negligible. The electrophoretic mobility (μ) was calculated from the migration times of the protein and neutral marker:

$$\mu = \frac{L_d}{E_z} \left(\frac{1}{t_o} - \frac{1}{t} \right) \quad (3.5)$$

where E_z is the applied electric field, L_d is the length of the capillary, and t and t_o are the times for the protein and neutral marker to reach the detector.

3.3.6 Mass Spectrometry

A Waters micromass Matrix Assisted Laser Desorption Ionization Time of Flight (MALDI-TOF) mass spectrometer was used to confirm the molecular weight and identity of the individual PEGylated proteins. Sinapinic acid from Waters Corporation (Milford, MA) was used as the matrix to aid in ionization of the PEGylated proteins. The device was operated in a positive linear mode in a mass range of 5,000 to 50,000 m/z. The use of a matrix causes less fragmentation of larger biomolecules than other mass spectrometry ionization techniques such as electron or chemical ionization (both of which are used primarily for smaller organic molecules). The ionization was performed using a nitrogen laser at 355 nm. MALDI was chosen over methods such as electrospray ionization due to the significant polydispersivity of the PEG that is difficult to analyze when multiply charged molecules are produced. Previously PEGylated proteins have also been successfully analyzed using MALDI-TOF (Chowdhury et al., 1995; Na et al., 2001; Na et al., 2003). Figure 3.16 shows typical results for a 5 kDa PEGylated α -lactalbumin molecule run with MALDI-TOF. The graph shows the percent total mass as a function of the species molecular weight. The peaks from left to right include α -lactalbumin (15301 Da), α -lactalbumin covalently bonded to a single 5 kDa nominal molecular weight mPEG (19818 Da), α -lactalbumin with two 5 kDa mPEG branches (25318 Da), α -lactalbumin with three 5kDa mPEG (30795 Da), and α -lactalbumin with four 5 kDa mPEG (36446 Da). Table 3.3 shows the experimentally determined molecular weights of the PEGylated proteins and the standard deviations obtained using at least 3 repeat measurements.

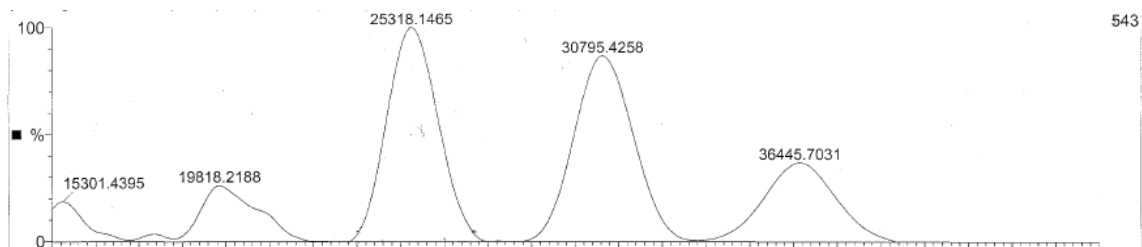


Figure 3.16. MALDI-TOF results with a 5 kDa PEG conjugated to α -lactalbumin.

Table 3.3. Molecular weight of PEG, α -lactalbumin and PEGylated α -lactalbumin as determined by MALDI-TOF.

	Average Molecular Weight (kDa)	Standard Deviation (kDa)
5 kDa PEG	5.53	0.10
α -lactalbumin	14.18	0.17
5 kDa PEGylated α -lactalbumin	19.80	0.78
2 - 5 kDa PEGylated α -lactalbumin	25.59	0.49
3 - 5 kDa PEGylated α -lactalbumin	30.84	0.33
4 - 5 kDa PEGylated α -lactalbumin	36.42	0.34

Chapter 4

PEGYLATED PROTEIN REACTIONS

4.1 Introduction

PEGylated proteins are produced by the covalent attachment of polyethylene glycol (PEG) to specific sites on a protein. This chapter discusses the reaction chemistry, basic kinetics, effects of solution conditions, and physical reaction schemes that were examined as part of this work. Some initial modeling work is also presented and suggestions are provided on how this work could be expanded in the future to obtain a more quantitative description of the PEGylation process. The possibility of performing a combined reaction and separation is also discussed, with focus on the potential advantages of this approach. The overall goal of the work presented in this chapter is to provide the basic understanding of the reaction between activated PEG and protein needed to produce consistent PEGylated protein feed solutions for use in the experimental studies described in subsequent chapters of this thesis.

4.2 Reaction Chemistry

A variety of different conjugation chemistries have been examined for the covalent attachment of PEG to a therapeutic protein. Each conjugation method offers distinct advantages and disadvantages for different protein products. The conjugation chemistries include attachment of the PEG to primary amines, carboxyl groups, free cysteine residues, hydroxyl groups, and azidophenylalanine (Deiters et al., 2004; Roberts

et al., 2002; Veronese 2001). Each method requires a slightly different functionalization (activation) of the PEG and in some cases more than one form of activated PEG can be used for the same covalent linkage (Li and Kao, 2003).

4.2.1 Primary Amines - Lysine

The most common covalent attachment site of PEG to a protein is through the primary amine of a lysine group. The reaction is usually performed with PEG containing an N-hydroxysuccinimide (NHS) ester, an electrophilic leaving group, as shown in Figure 4.1 (Fee, 2003; Roberts and Harris, 1998; Wang et al., 2002). Other activated PEG compounds that react with primary amines include PEG-p-nitrophenyl carbonate, PEG trichlorophenyl carbonate, PEG-oxycarbonylimidazole, and PEG-benzotriazole carbonate (Veronese, 2001). PEG-1-3-dioxocompounds can react with arginine amino acids, but the reaction rate is relatively slow compared to the attachment of PEG at a lysine amino acid (Veronese, 2001).

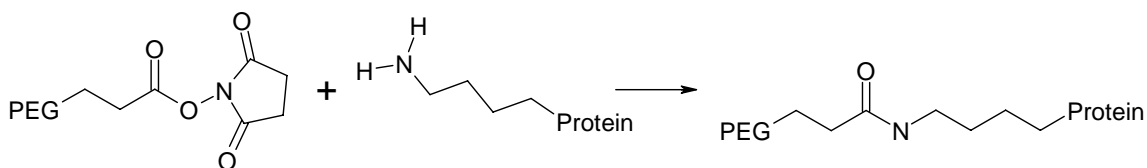


Figure 4.1. The reaction between PEG-SPA (an NHS derivative) and a primary amine group occurs under mild conditions in aqueous buffer (15-30°C and pH 7.0-8.5).

For the NHS ester compounds, the rate of reaction is a strong function of the number of methylene groups between the active ester and the PEG. The number of methylene groups also controls the rate of hydrolysis of the activated PEG. For example, the half life of an activated PEG containing 3 methylene groups between the PEG and N-

hydroxysuccinimide group is 23 hours at pH 8 and 25 °C while the half life of an activated PEG containing only one methylene group between the PEG and NHS is 0.75 hours at the same conditions (Bentley et al., 2004; Harris and Antoni, 1997).

Since lysine amino acids often compose up to 10% of a protein, many PEGylation sites are available under standard conditions using PEG activated with NHS esters. This can be a disadvantage because the number of possible substitution sites is often greater than the optimal number and the extent of reaction can be difficult to control (Esposito et al., 2003). In most cases, PEG will covalently bond to the least sterically hindered lysine groups first, but there are often a number of amino sites on the protein with similar accessibility.

It is also possible to specifically target the terminal amine group of a protein (compared to the lysine amino groups). Attachment of PEG to a terminal amine can be performed using a 2-fluoro-1-methylpyridinium toluene – 4 sulfonate group as shown in Figure 4.2 (Yun et al., 2005). The advantage of using a terminal amine reaction site is that only one reaction site is available, although the specificity is not 100% (Veronese, 2001).

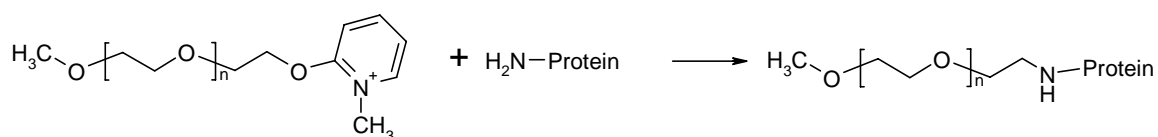


Figure 4.2. The reaction between 2-fluoro-1-methylpyridinium toluene-4-sulfonate PEG and a terminal amine occurs under mild conditions in aqueous buffer (4°C and pH 7 - 8).

4.2.2 Sulfides - Cysteine

Another common method of conjugation between a protein and PEG is through a free cysteine amino acid. The reaction can be performed using a PEG-orthopyridyl-disulphide, or more commonly PEG-maleimide as shown in Figure 4.3 (Veronese, 2001). Cysteine conjugation can be very specific, especially since many proteins have only a single free cysteine residue. If no free cysteine exists in the protein, it is possible to add a cysteine at a specific location (typically away from the active site) through site-directed mutagenesis (Veronese, 2001). Despite these advantages, reproducibility and yield of the reactions with cysteine are typically low (Esposito et al., 2003).

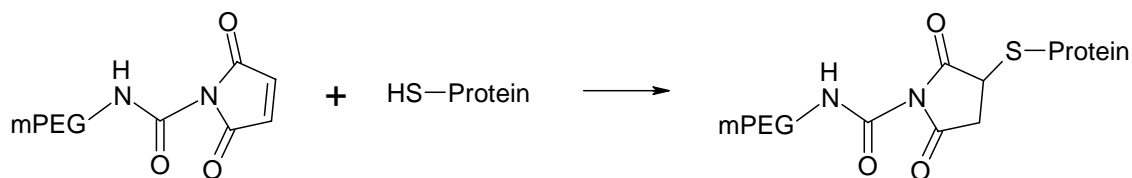


Figure 4.3. The reaction between PEG-maleimide and a protein under mild conditions in aqueous buffer (pH 7.5-8.5).

4.2.3 Carboxylic Acid – C terminal amino acid

PEG can also be conjugated to the protein through a primary carboxylic acid. This is usually performed using an amino PEG or a PEG-hydrazide (as shown in Figure 4.4), typically involving the addition of either N-(3-dimethyl aminopropyl)-N'-ethylcarbodiimide or N-ethylcarbodiimide hydrochloride, respectively. N-(3-dimethyl aminopropyl)-N'-ethylcarbodiimide cannot be used when both amino and carboxyl groups are present because cross linking will occur. Cross linking between the amines

and carboxylic acids can be avoided by operating at pH between 4.5 and 5 with N-ethylcarbodiimide hydrochloride (Veronese, 2001). Conjugation to a carboxylic acid is often performed when attachment to an amine would greatly shield the active site of the protein. Reactions with carboxylic acids are not commonly used because these typically cause a significant reduction in biological activity (Esposito et al., 2003).

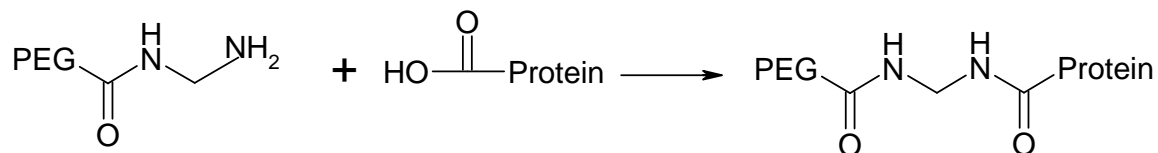


Figure 4.4. The reaction between PEG-hydrazine and a protein in aqueous buffer (pH 4.5-5.0) in the presence of N-(3-dimethyl aminopropyl)-N'-ethylcarbodiimide.

4.2.4 Other Reaction Chemistries

PEG can be covalently bonded to a hydroxyl group using PEG-isocyanate (Veronese, 2001) as shown in Figure 4.5. PEG-isocyanate will also react with primary amines that are present; thus, this chemistry is most useful for small peptides that do not contain primary amines. This approach is rarely used for proteins due to the presence of large numbers of lysine residues.

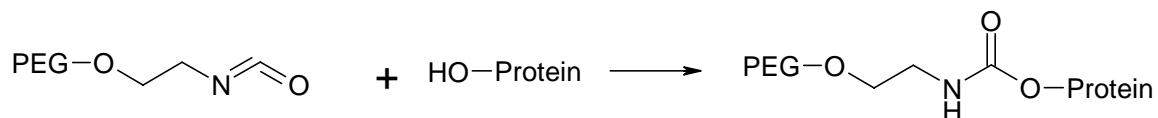


Figure 4.5. The reaction between PEG-isocyanate and a peptide containing no available primary amines (lysine residues).

PEG can be attached to a para-azidophenylalanine by the use of a cycloaddition reaction with an alkyne-activated PEG as shown in Figure 4.6. This artificial amino acid

can be introduced into a protein sequence at a specific location by site specific incorporation. The reaction is highly selective to this artificial amino acid (Deiters et al., 2004).

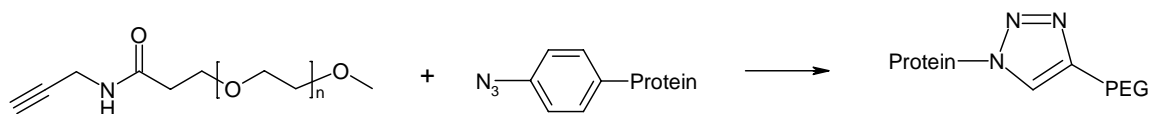


Figure 4.6. Reaction between an alkyne-activated PEG and a para-azidophenylalanine amino acid added into a protein.

4.3 Materials and Methods

4.3.1 Materials

The model protein used for the reaction studies was α -lactalbumin as described in Chapter 3. Two activated PEG molecules were used: methoxyPEG succinimidyl propionic acid (mPEG-SPA) and methoxyPEG succinimidyl α -methylbutanoate (mPEG-SMB). The structure of these activated PEG molecules are shown in Figure 3.2. The methoxyPEG succinimidyl propionic acid (mPEG-SPA) and methoxyPEG succinimidyl α -methylbutanoate (mPEG-SMB) are *n*-hydroxylsuccinimide derivatives that react with the primary amines on a protein.

4.3.2 Reactions

Reactions were performed by mixing the desired concentration of activated PEG and protein in an aqueous buffer solution of specific ionic strength and pH. Samples were removed at specified time intervals to determine the concentration of reactants and products by size exclusion chromatography. The PEGylation reaction was quenched by

the addition of 0.1 M HCl (volume equal to the sample volume) for at least 5 minutes followed by re-equilibration with the starting buffer using about a 4:1 volume ratio of buffer to the quenched sample. Reactions were performed at different solution pH, ionic strength, protein concentration, and ratio of PEG to protein. PEG and protein were reacted in an aqueous buffer, unless otherwise specified.

In addition to the simple batch reaction, experiments were also performed using a fed-batch reactor and a combined reaction-separation system. The fed-batch reaction was performed by first dissolving the protein in buffer and then adding very small volumes of 10 kDa mPEG-SPA dissolved in dioxane throughout the reaction time. Samples were taken after each mPEG-SPA addition to evaluate the reactant and product concentrations. The combined reaction-separation was performed using a fed-batch reaction, with the PEGylated protein and most of the PEG separated from the unreacted protein after each addition of the mPEG-SPA. The separation was performed using diafiltration through a 30 kDa UltracelTM membrane using 5 diavolumes of a 10 mM Bis Tris buffer. The filtrate was then concentrated back to the original volume by ultrafiltration through a 10 kDa UltracelTM membrane. A small amount of activated PEG in dioxane was then added to the reaction mixture and the entire procedure repeated. The reaction in the retentate was quenched with 0.1 M HCl, with the resulting solution diafiltered through a 10 kDa UltracelTM membrane using a pH 7.0 Bis Tris buffer.

4.4 PEGylation Reaction

Figure 4.7 shows the concentration of PEG, protein, and PEGylated proteins as a function of time for a reaction between α -lactalbumin and either a 5 kDa mPEG-SPA (upper panel) or 5 kDa mPEG-SMB (lower panel) in a 5 to 1 molar ratio. The reaction was performed in a 10 mM Bis Tris (pH 7.0) buffer with an initial α -lactalbumin concentration of 10 g/L. The reactant and product concentrations at each time point were obtained by removing a small sample from the reaction vessel, quenching it by rapid addition of 0.1 M HCl to drop the pH below 4.0, and then analyzing the resultant solution by size exclusion chromatography. The concentration of PEG and α -lactalbumin decreased over time as expected. The concentration of the PEGylated species with one 5 kDa branch (PEG 1) increased rapidly at the start of the experiment but then went through a maximum around $t = 5.5$ minutes for the mPEG-SPA sample and $t = 38$ minutes for the mPEG-SMB sample. At longer times, the concentration of singly PEGylated species decreased as it was converted to the doubly (PEG 2) and triply (PEG 3) PEGylated products.

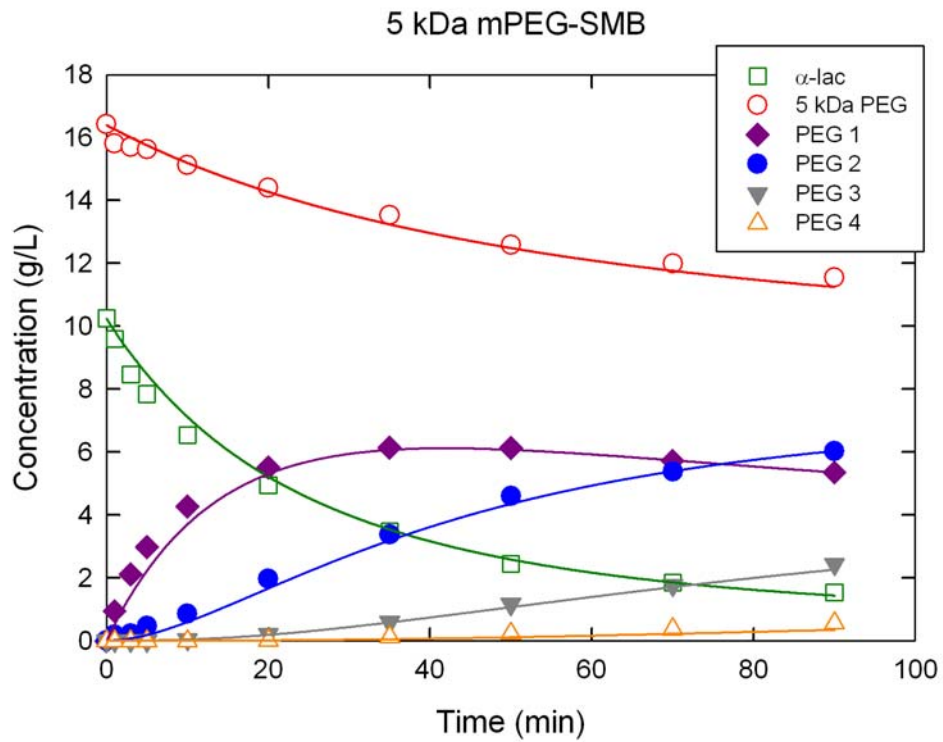
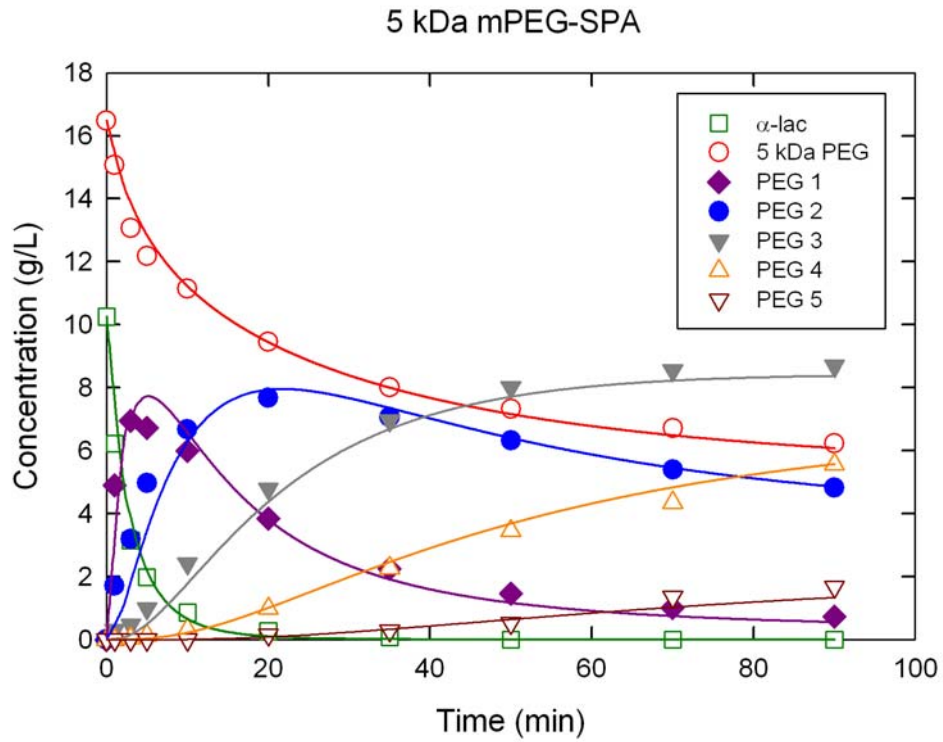


Figure 4.7. Concentration of α -lactalbumin, 5 kDa PEG, and 5 kDa PEGylated α -lactalbumin as a function of time. Solid curves represent model fits as discussed in the text.

The solid curves in Figure 4.7 were evaluated using a simple kinetic model accounting for the formation and reaction of the first five PEGylated species (the concentration of higher order PEGylated products was sufficiently small that these species were neglected in the mathematical analysis). The differential equations describing the species concentrations are shown in Equations 4.1 thru 4.8.

$$\frac{dC_{P1}}{dt} = k_1 C_{alac} C_{PEG} - k_2 C_{P1} C_{PEG} \quad (4.1)$$

$$\frac{dC_{P2}}{dt} = k_2 C_{P1} C_{PEG} - k_3 C_{P2} C_{PEG} \quad (4.2)$$

$$\frac{dC_{P3}}{dt} = k_3 C_{P2} C_{PEG} - k_4 C_{P3} C_{PEG} \quad (4.3)$$

$$\frac{dC_{P4}}{dt} = k_4 C_{P3} C_{PEG} - k_5 C_{P4} C_{PEG} \quad (4.4)$$

$$\frac{dC_{P4}}{dt} = k_5 C_{P4} C_{PEG} \quad (4.5)$$

$$\frac{dC_{PEG}}{dt} = -k_1 C_{alac} C_{PEG} - k_2 C_{P1} C_{PEG} - k_3 C_{P2} C_{PEG} - k_4 C_{P3} C_{PEG} - k_5 C_{P4} C_{PEG} - k_{PEG} C_{PEG} \quad (4.6)$$

$$\frac{dC_{alac}}{dt} = -k_1 C_{alac} C_{PEG} \quad (4.7)$$

$$\frac{dC_{HydroPEG}}{dt} = k_{PEG} C_{PEG} \quad (4.8)$$

where C is the concentration of each species and k_i is the rate constant associated with that particular step in the reaction. $P1$, $P2$, $P3$, $P4$, and $P5$ represent the PEGylated species with 1, 2, 3, 4 or 5 branches, respectively. PEG , and $alac$ represent the activated PEG and the native α -lactalbumin respectively. $HydroPEG$ represents the hydrolyzed

form of the activated PEG. The hydrolyzed form of the PEG cannot be differentiated from the active form in the SEC analysis so the concentration of these species is reported in all subsequent graphs simply as the sum of $C_{PEG} + C_{HydroPEG}$.

The differential equations were solved numerically using the Runge-Kutta-Fehlberg method with *Polymath* v. 5.1 software. The best fit values of the rate constants were estimated by minimizing the sum of the squared residuals between the data and model calculations using experimental results for the concentration of all reactants and products. The best fit values of the rate constants for the reactions with mPEG-SPA and mPEG-SMB are shown in Table 4.1. The rate constants for the mPEG-SPA reaction are larger than the rate constants for the mPEG-SMB reaction (Figure 4.7), although the equilibrium product distributions in the two systems are similar.

Table 4.1. Rate constants for reaction of α -lactalbumin with 5 kDa mPEG-SPA and mPEG-SMB in a 10 mM Bis Tris (pH 7.0) buffer.

	mPEG-SPA	mPEG-SMB
PEG hydrolysis	0.01 min ⁻¹	0.008 min ⁻¹
1- 5 Da PEGylated	0.11 L mol ⁻¹ min ⁻¹	0.012 L mol ⁻¹ min ⁻¹
2 – 5kDa PEGylated	0.04 L mol ⁻¹ min ⁻¹	0.008 L mol ⁻¹ min ⁻¹
3 – 5 kDa PEGylated	0.022 L mol ⁻¹ min ⁻¹	0.0045 L mol ⁻¹ min ⁻¹
4 – 5 kDa PEGylated	0.014 L mol ⁻¹ min ⁻¹	0.0025 L mol ⁻¹ min ⁻¹
5 – 5 kDa PEGylated	0.007 L mol ⁻¹ min ⁻¹	---

The rate constants for the reactions with the activated PEG are smaller for the more highly substituted PEGylated species, which could be due to differences in the accessibility / reactivity of the different PEGylation sites and / or to a reduction in the rate of reaction associated with the presence of the attached PEG chain(s). There is well over

an order of magnitude difference in rate constants for PEGylation of the native protein compared to that for the PEGylated product with five PEG chains.

4.5 Effect of Solution Parameters on Reaction Yield

It is also possible to control the rate and extent of PEGylation by adjusting the pH, temperature, and ionic strength of the solution (Monkarsh et al., 1997; Nijs et al., 1997; Orsatti and Veronese, 1999; Wang et al., 2002). The effects of the molar ratio, total protein concentration, pH, and ionic strength on the extent of reaction of α -lactalbumin with 5 kDa mPEG-SPA were examined in this section. All results were obtained after the reaction between the PEG and protein proceeded essentially to completion (greater than 12 hours reaction time), at which point the concentration of mPEG-SPA was negligible due to the combination of the PEGylation reaction and the hydrolysis of the activated PEG species.

4.5.1 Molar Ratio

Experiments were performed with molar ratios of PEG to protein from 0.1:1 to 5:1 using a 10 mM Bis Tris buffer (pH 7.0) and an α -lactalbumin concentration of 10 g/L. Figure 4.8 shows the concentration of each compound as a function of the PEG to α -lactalbumin ratio in the initial reaction mixture. The solid curves are spline fits to the data. Increasing the ratio of PEG to protein increased the conversion of α -lactalbumin as expected. The concentration of the PEGylated species containing a single 5 kDa PEG branch (PEG 1) initially increased with increasing concentration of PEG but then went through a maximum at a PEG to protein ratio of approximately 2:1. Higher

concentrations of PEG resulted in the conversion of the singly PEGylated protein into α -lactalbumin species containing two or more 5 kDa branches (PEG 2 and PEG 3).

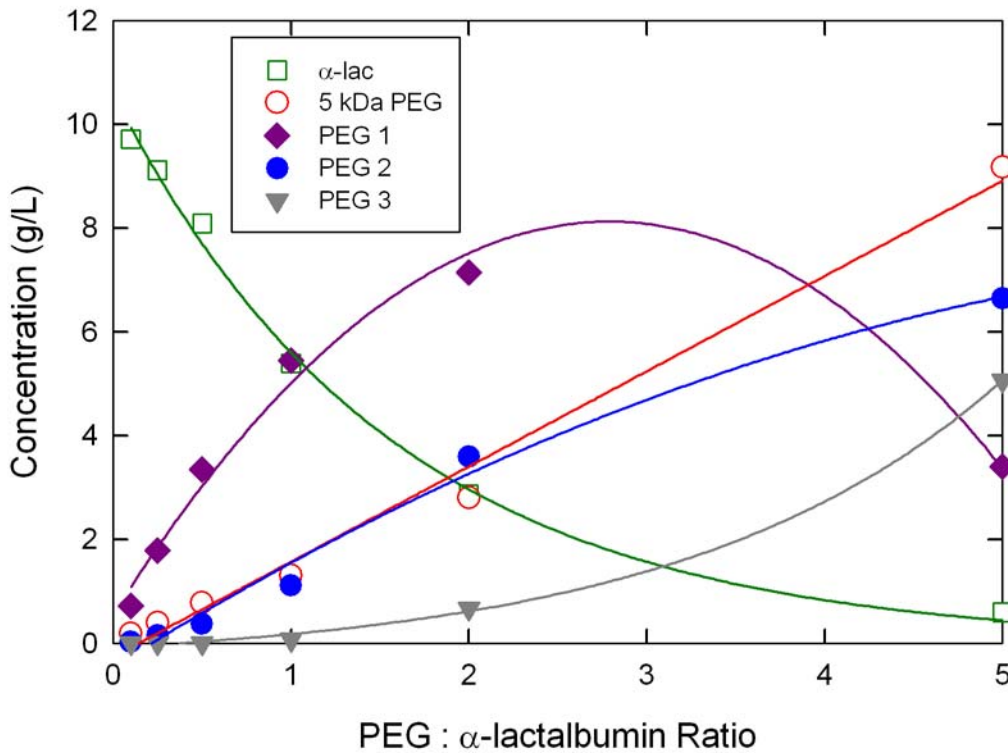


Figure 4.8. Equilibrium concentration of PEG, protein, and PEGylated proteins as a function of the PEG to α -lactalbumin ratio. Data obtained at pH 7 using a 10 g/L α -lactalbumin solution in 10 mM Bis Tris buffer. Solid curves are simple spline fits to the data.

4.5.2 Solution pH

Figure 4.9 shows the final concentration of PEG, α -lactalbumin and PEGylated α -lactalbumin as a function of the solution pH. The experiments were performed using a 0.5 to 1 molar ratio of mPEG-SPA to α -lactalbumin with an α -lactalbumin concentration of 10 g/L. The solution pH was adjusted by using different buffers: a 10 mM acetate buffer was used at pH 5.0, a 10 mM Bis Tris buffer was used at pH 6.0 and 7.0, and a 10

mM Tris buffer was used at pH 8.0. Specific buffer compositions are given in Chapter 3. The product concentrations are nearly independent of solution pH over this range of pH, with a slight increase in the concentration of the PEGylated products at the highest pH. Note that several other studies have shown a significant effect of pH on the PEGylation reaction. For example Besselink (1993) found that the half-life of NHS activated N-t-BOC glycine decreased almost ten fold by changing the pH from 6.0 to 8.0. Zhang et al. (2007) reported a low yield of PEGylated insulin at pH 9.0 compared to results at pH 8.0. Thus, the effects of pH seem to depend on both the nature of the activated PEG and possibly the detailed properties of the protein, although it should also be noted that the data in Figure 4.9 reflect the final equilibrium concentrations of the various components and thus provide no information on the detailed kinetics of the reactions.

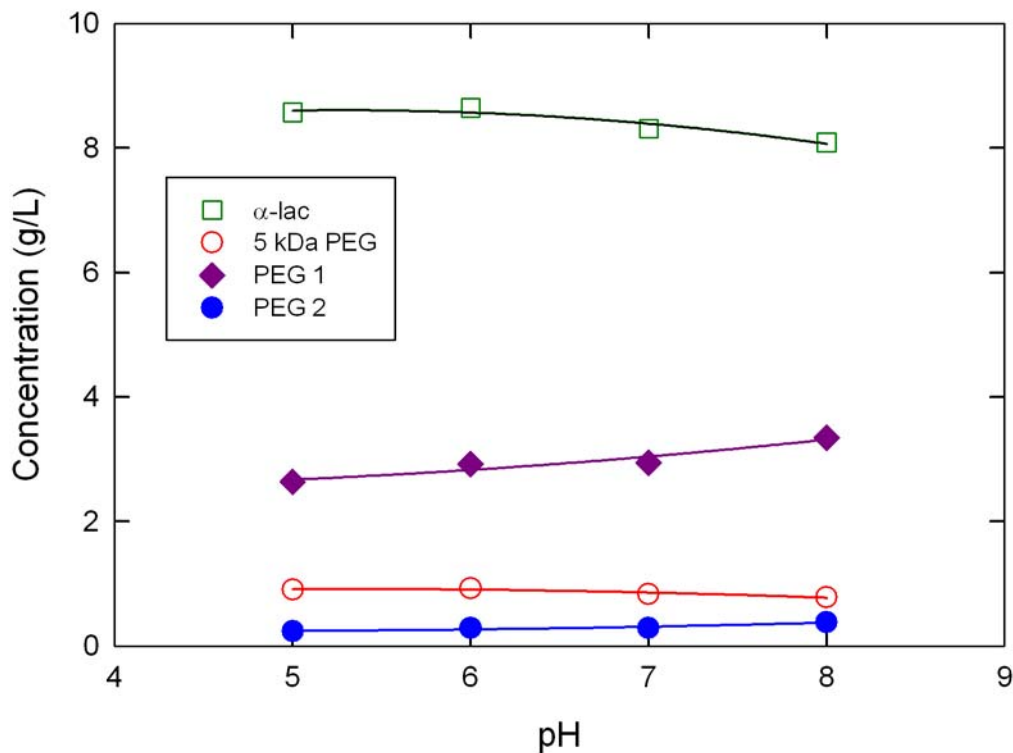


Figure 4.9. Effect of pH on the concentration of PEG, protein, and PEGylated protein using a 0.5 to 1 molar ratio of PEG to protein. Solid curves are spline fits to the data.

4.5.3 Ionic Strength

The effect of ionic strength on the PEGylation reaction was examined over a range from 1 to 500 mM using a 5 mM Bis Tris buffer with the ionic strength adjusted by addition of KCl. Data were obtained with the PEG to protein ratio fixed at 0.5 to 1 and with an α -lactalbumin concentration of 10 g/L. The final concentrations of the different PEGylated proteins were essentially independent of the ionic strength, with a slight increase in the concentration of the PEG 2 species and a corresponding decrease in PEG 1 at the highest ionic strength.

4.5.4 Reactant Concentration

The effect of reactant concentration on the PEGylation reaction was examined by performing a series of experiments with different mPEG-SPA and α -lactalbumin concentrations with the PEG to protein ratio fixed at 0.5:1 and with a 10 mM Bis Tris buffer at pH 7. Figure 4.10 shows the percentage of PEG that has reacted with protein (rather than hydrolyzing) as a function of the concentration of α -lactalbumin in the solution. At low α -lactalbumin concentrations, relatively little PEG was involved in the formation of the PEGylated proteins suggesting the PEGylation reaction is bimolecular (first order in both PEG and protein) while the rate of hydrolysis is first order. Thus, most of the mPEG-SPA hydrolyzes before it reacts with the protein. The use of higher reactant concentrations increases the relative rate of the PEGylation reactions, increasing the yield of both the singly and doubly PEGylated products. However, the final ratio of the concentrations of PEGylated α -lactalbumin with a single 5 kDa PEG chain to that with two 5 kDa PEG chains was nearly independent of the initial α -lactalbumin in the feed mixture for reactions formed at a constant ratio of the two reactants.

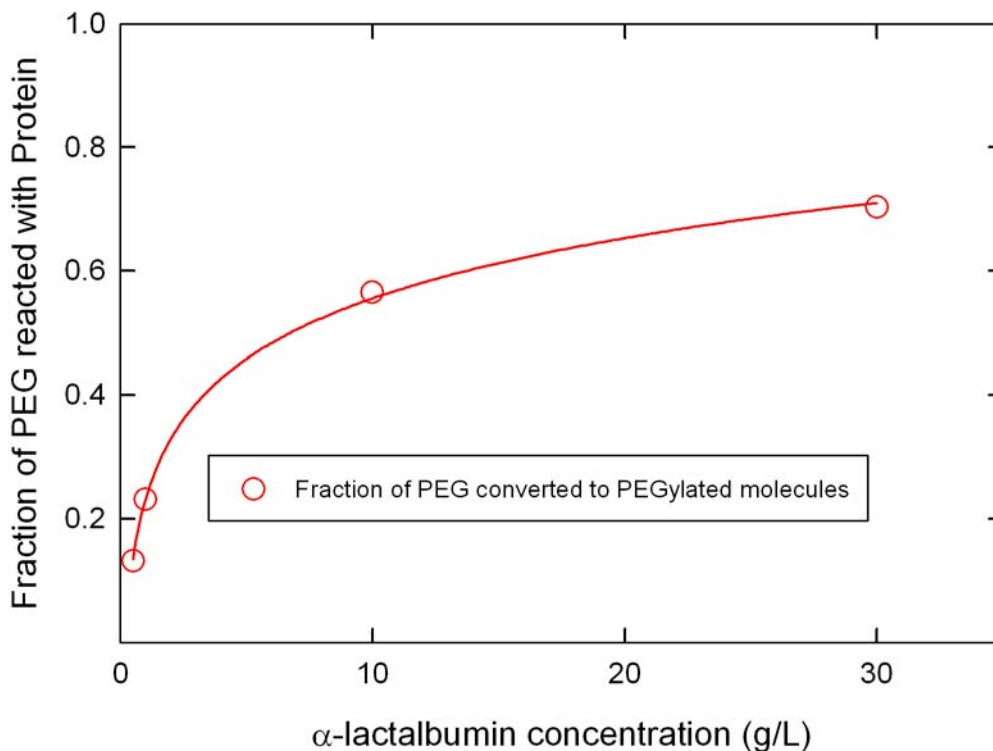


Figure 4.10. Effect of reactant concentration on the fraction of activated PEG that participates in the PEGylation reaction. Data obtained at pH 7, 10 mM Bis Tris, using a 0.5 to 1 molar ratio of PEG to α -lactalbumin. Solid curve is spline fit to the data.

4.6 Reaction Schemes

It is typically desirable if the activated PEG can be covalently linked to the protein at only a single site since more highly substituted species tend to have lower biological activity due to steric hindrance or blockage of the active site. Two different reaction schemes were analyzed both theoretically and experimentally to explore opportunities for increasing the yield of the desired (singly) PEGylated product. Calculations were performed using the rate constants determined for the reaction between mPEG-SPA and α -lactalbumin. First, a fed-batch system was examined in which the

activated PEG was added to the α -lactalbumin solution in small increments with the PEGylated reaction allowed to go to completion between each addition. In this case, the PEG was added at a molar ratio of 0.15 moles of activated PEG to each mole of native protein remaining in solution at the end of the prior step. Second, a reaction-separation scheme was examined in which the PEG and PEGylated products were removed from the reaction mixture (after the reaction had gone to completion), with the native α -lactalbumin recycled for subsequent reaction with additional fresh PEG. Theoretical calculations were performed assuming ideal separation at each step. Three different addition ratios were analyzed: adding PEG at a ratio of 0.40 moles of PEG for every mole of native protein remaining in solution, adding PEG at a ratio of 0.15 moles of PEG for every mole of native protein, and adding PEG at a ratio of 0.02 moles of PEG for every mole of native protein. All calculations were performed using Polymath v. 5.1.

Figure 4.11 shows the theoretical results for the concentrations of the singly and doubly PEGylated species using both the fed-batch and reaction-separation schemes (with 0.40, 0.15, and 0.02 addition ratios). The results are plotted as a function of the ratio of total PEG to protein added to the system. The results for the fed-batch system are identical to those for the corresponding batch reaction since all of the reactions have a first order dependence on the concentration of activated PEG. In contrast, the ideal reaction-separation scheme increases the yield of the singly PEGylated species, with a corresponding reduction in the amount of the more highly substituted PEGylated species, since the PEGylated products are removed from the reactor after each step in the reaction-separation scheme. The yield of the singly PEGylated species increases as the number of reaction-separation cycles is increased since this reduces the likelihood that

the singly PEGylated product is able to encounter an activated PEG. At a total PEG:protein ratio of 1:1, the selectivity for the singly PEGylated protein is approximately 74% when adding 0.15 moles of PEG for every mole of native protein compared to a selectivity of only 28% for the fed-batch and batch reaction systems.

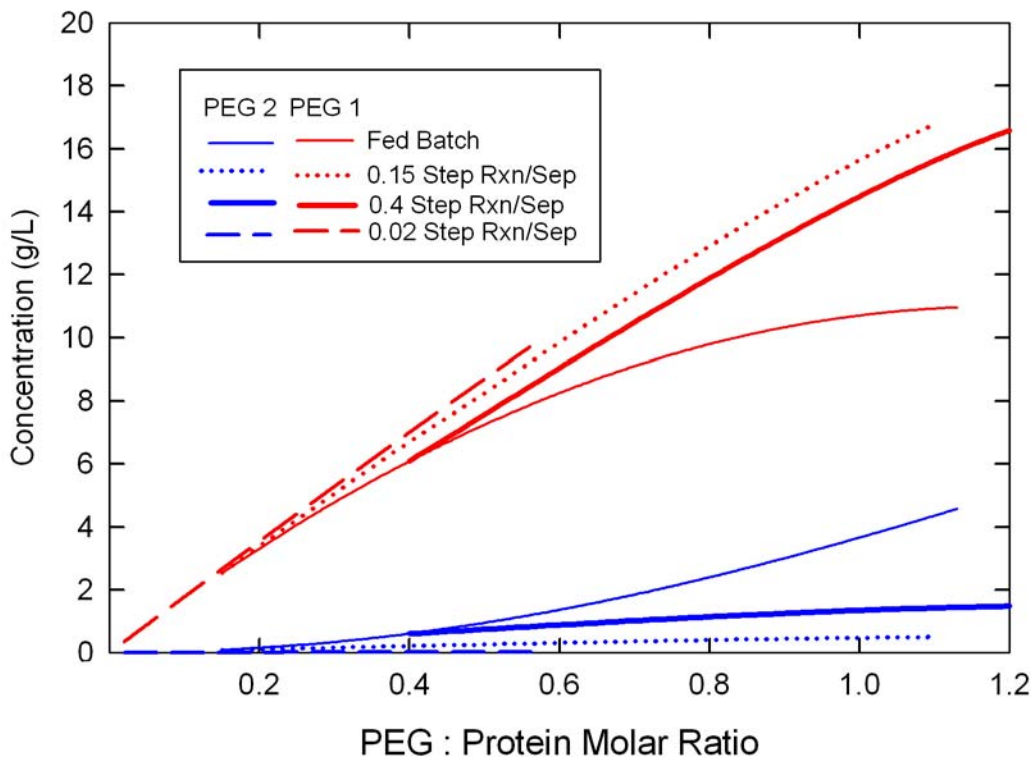


Figure 4.11. Theoretical concentration (g/L) of the 5 kDa PEGylated species with either one or two PEG branches as a function of the molar ratio of PEG to protein added. The initial α -lactalbumin concentration is 14.6 g/L.

Experimental studies of the fed-batch and reaction-separation systems were conducted using a 10 kDa mPEG-SPA with α -lactalbumin (in contrast to the 5 kDa PEG examined in Figure 4.11). The fed-batch reaction was performed by making a 15 g/L solution of α -lactalbumin and adding the 10 kDa mPEG-SPA in a molar ratio of

0.15 moles of PEG to each mole native protein remaining in the reaction system. Results are shown in Figure 4.12 for the concentration of the α -lactalbumin, the hydrolyzed PEG, and the singly and doubly PEGylated proteins at the end of a 50 minute reaction. The data are plotted as a function of the total molar ratio of added PEG to protein, with the open symbols representing data from a corresponding batch reaction. The results for the batch and fed-batch systems were very similar, within the accuracy of the experimental measurements, in good agreement with the model fits in Figure 4.11.

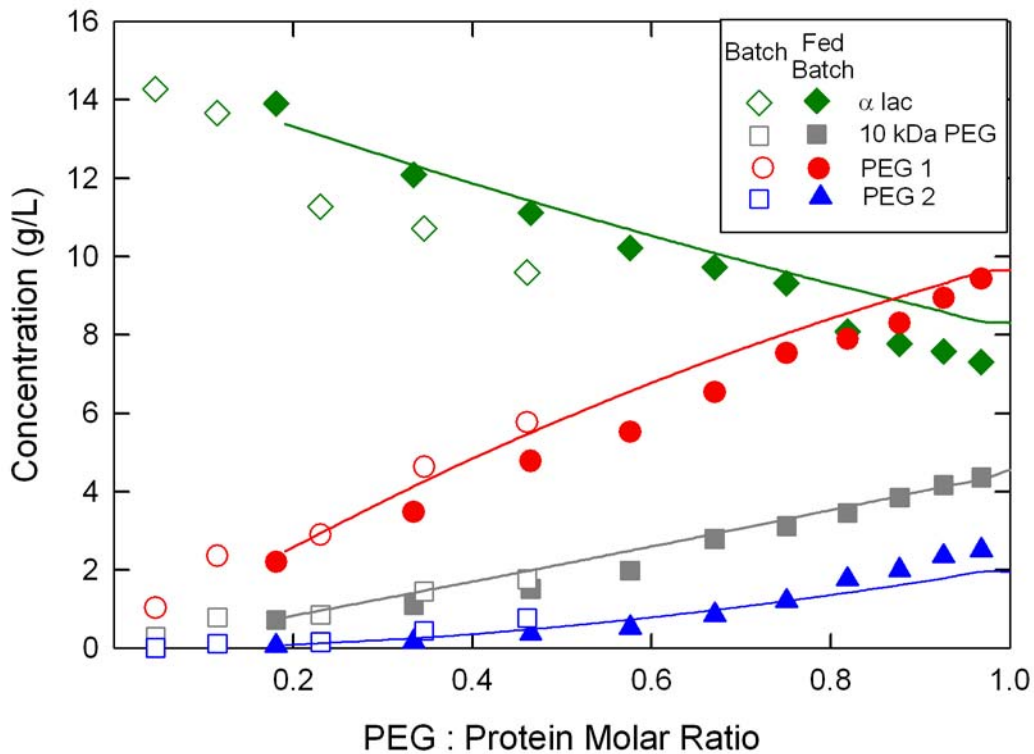


Figure 4.12. Comparison of the concentration of PEGylated reaction products for a batch and a fed-batch process. Kinetic parameters for the model curves are shown in Table 4.2.

It was not possible to describe the experimental results in Figure 4.12 for reaction with the 10 kDa mPEG-SPA using the rate constants determined previously for the 5 kDa

mPEG-SPA due to the significantly different reaction rates in the two systems. Instead, the solid curves in Figure 4.12 were evaluated by fitting a new set of rate constants to the same kinetic model, with the best fit values shown in Table 4.2. The rate constant for the hydrolysis reaction for the 10 kDa mPEG-SPA was assumed to be identical to that for the 5 kDa mPEG-SPA to reduce the number of fitted parameters. The rate constant for the first PEGylation reaction with the 10 kDa mPEG-SPA was approximately 8 times smaller than the corresponding rate constant for the 5 kDa mPEG-SPA. A similar reduction in rate constant was seen for all of the other PEGylation reactions. This reduction in rate of PEGylation may be related to steric hindrance effects or possible mass transfer limitations associated with the larger size of the 10 kDa mPEG-SPA. The model fits are in good agreement with the experimental data for all of the PEGylated species.

Table 4.2. Rate constants for reaction of 10 kDa mPEG-SPA with α -lactalbumin in a 10 mM Bis Tris pH 7.0 buffer.

	10 kDa mPEG-SPA
PEG hydrolysis	0.01 min ⁻¹
1- 5 Da PEGylated	0.014 L mol ⁻¹ min ⁻¹
2 – 5kDa PEGylated	0.006 L mol ⁻¹ min ⁻¹
3 – 5 kDa PEGylated	0.003 L mol ⁻¹ min ⁻¹

Experimental studies were also performed using the reaction-separation scheme with the 10 kDa mPEG-SPA. Experiments were performed by reacting a small quantity of PEG with the native α -lactalbumin solution (initial protein concentration of 15 g/L) followed by a 5 diavolume diafiltration through a 30 kDa UltracelTM membrane to collect the PEGylated protein (with the bulk of the PEG) while the large majority of the unreacted protein was removed in the filtrate. For each cycle approximately 12 % of the

native α -lactalbumin remained in the retentate after the diafiltration and about 14% of the hydrolyzed PEG was removed from the retentate. The details of the diafiltration process are discussed in Chapter 9. After the separation, the α -lactalbumin in the filtrate was concentrated using a 10 kDa UltracelTM membrane to its original volume, and the entire procedure was repeated multiple times. In each case, approximately 0.10 moles of fresh activated PEG were added to the reaction vessel per mole of recovered α -lactalbumin. The product (retentate) streams from the reaction-separation scheme were pooled and concentrated to the original volume, with the data in Figure 4.13 representing the concentrations in the final pool. The filled symbols represent results from a corresponding fed-batch reaction shown for comparison. The yield of the singly PEGylated product in the reaction-separation system is slightly larger than that obtained in the fed-batch system, although the difference was quite small for the relatively low values of the PEG to protein ratio examined in this experiment. The increase in selectivity towards the singly PEGylated product is somewhat less than that shown previously in Figure 4.11 due to the incomplete separation during the diafiltration process.

The solid curves in Figure 4.13 are model simulations for the reaction-separation scheme using the rate constants in Table 4.2 (obtained from data obtained in the batch and fed-batch experiments). The calculations were performed assuming that the sieving coefficients of α -lactalbumin, PEG, were constant throughout each diafiltration with values of 0.42, and 0.03 based on small scale experiments. The sieving coefficient of the PEGylated protein is assumed to be negligible. The model calculations are in good agreement with the experimental data for both the singly and doubly PEGylated proteins.

The small difference between the model calculations and experimental data are presumably due in part to some loss of solution volume during the transfer of the feed solution between the reaction and separation steps. The model calculations were relatively independent of the α -lactalbumin sieving coefficient since the simulations were performed by adding 0.10 moles of fresh PEG per mole of α -lactalbumin in the reactant solution. Thus, any increase in α -lactalbumin retention during the diafiltration was at least partially compensated for by a corresponding reduction in the amount of mPEG-SPA added in the next reaction step. The final concentration of the singly PEGylated species formed after removal of 88% of the α -lactalbumin from the reaction mixture (initial concentration of 15 g/L) is predicted to be 6.5 g/L, which is less than half the value assuming complete conversion of the α -lactalbumin into the desired PEGylated species.

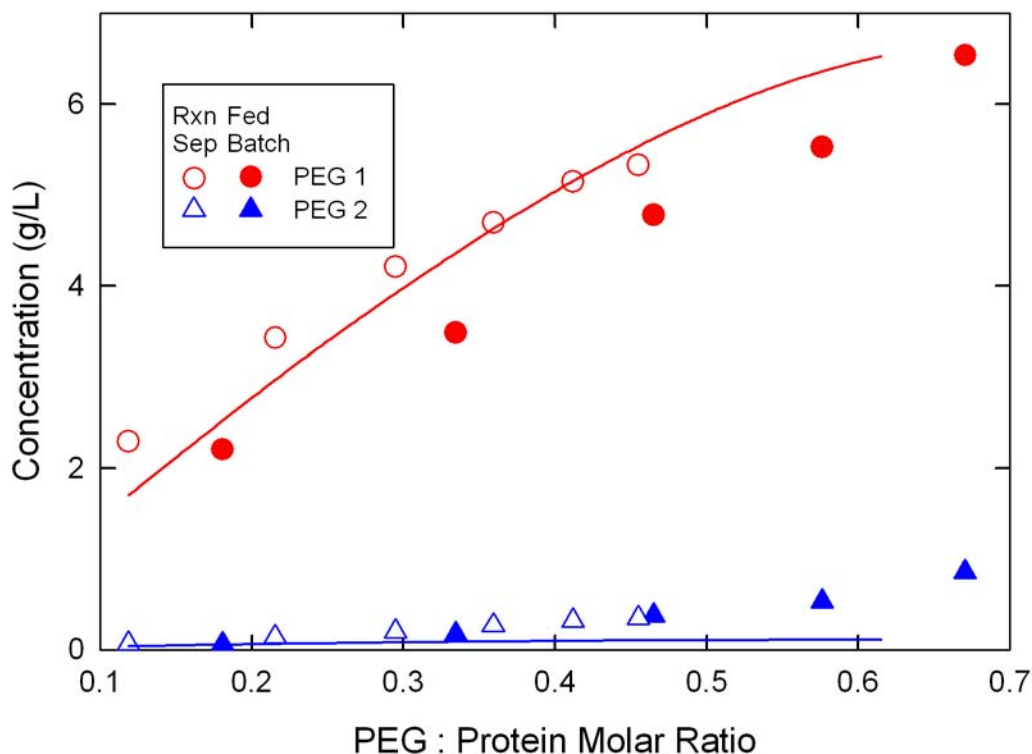


Figure 4.13. Reaction-separation process for PEGylation of α -lactalbumin using a 10 kDa mPEG-SPA. Solid curves are model calculations using the rate constants in Table 4.2 for a separation system with a 12 % loss of α -lactalbumin during every cycle. The curves end when 88% of the α -lactalbumin is assumed to be in the product stream.

4.7 Conclusions

The experimental studies described in this chapter examined the key factors controlling the extent and selectivity of the reaction between the amino groups on the lysine residues in α -lactalbumin and an activated PEG with an N-hydroxylsuccinimide ester as the leaving group. The solution pH and ionic strength had very little effect on the selectivity of the PEGylation reaction, with the dominant variables being the total reactant concentration and the molar ratio of PEG to protein in the initial feed. Robust

reaction conditions were identified that could provide a final product solution with consistent composition, which was critical for use in the characterization and separation experiments discussed in Chapters 5-10 of this thesis.

The batch reaction data for PEGylation of the α -lactalbumin with 5 kDa mPEG-SPA and mPEG-SMB were well-described using a kinetic model assuming all reactions are first order in the key reactants. The rate constants for the attachment of PEG to the PEGylated protein decreased with the number of previously attached PEG groups, which is likely due to the reduced accessibility and reactivity of the reaction sites. This simple kinetic model provides a framework for the analysis of alternative reaction schemes, e.g., fed-batch and combined reaction-separation. The fed-batch and batch systems were predicted to provide equivalent yield of the singly PEGylated protein, and this was confirmed experimentally using a 10 kDa mPEG-SPA. It was possible to increase the selectivity for the singly PEGylated species using a reaction-separation scheme, although experimental results showed only marginal improvements due to the incomplete separation of the PEGylated product and unreacted α -lactalbumin which limited the maximum attainable ratio of PEG to protein.

Future improvements in the membrane separation step should provide opportunities for increasing the yield of the desired singly PEGylated product by using a reaction-separation scheme similar to that presented in this Chapter. However, significant improvements in selectivity would require the development of membranes, or alternative separation methods, that could rapidly separate the singly PEGylated product from the un-reacted PEG to minimize the formation of the more highly PEGylated species. In contrast, the membrane diafiltration process used in the reaction-separation

scheme examined in this Chapter only provided effective removal of the un-reacted α -lactalbumin, with the PEG remaining with the PEGylated protein.

Chapter 5

SIZE EXCLUSION CHROMATOGRAPHY OF PEGYLATED PROTEINS

5.1 Introduction

As discussed previously, one of the primary benefits of PEGylation is the reduction in the rate of kidney clearance associated with the increase in effective size of the PEGylated proteins. The objective of this chapter was to quantitatively evaluate the effect of PEGylation on protein size using both size exclusion chromatography (SEC) and dynamic light scattering (DLS). The results are discussed in terms of available theoretical models for the partitioning of hard spheres. The implications of these results on the behavior of PEGylated proteins during ultrafiltration and electrophoresis are discussed in Chapters 6 through 9.

Size exclusion chromatography (SEC) is a well-established technique for protein separations and for the analysis of the effective size of biological molecules (Ogez et al., 1989). SEC has also been used extensively for the analysis of PEGylated proteins (Snider et al., 1992; Vestling et al., 1992) as discussed in Chapter 1. Fee and Van Alstine (2004) used size exclusion chromatography to evaluate the effective size of a variety of PEGylated proteins as a function of the molecular weight of the protein and PEG. These data are discussed in more detail later in this Chapter.

Dynamic light scattering provides a more direct measure of the effective size from transient decay in scattering intensity arising from the random thermal (Brownian)

motion of the particles (Pecora, 1985; Pike and Abbiss, 1997). McGoff (1988) obtained limited data for the effective size of PEGylated superoxide dismutase by dynamic light scattering, although the results were complicated by the polydispersivity of the PEG. Many studies have reported successful analysis of large PEGylated particles, e.g., PEGylated liposomes and nanoparticles, using dynamic light scattering (Lee et al., 2005; Miyamoto et al., 2008).

5.2 Theory

5.2.1 Size Exclusion Chromatography

In size exclusion chromatography, molecules are separated by the extent to which they partition into the pores of the stationary resin. Most analyses assume that diffusion is very rapid, with the solute concentration in the stationary and mobile phases in equilibrium at any point in the column. Larger solutes pass quickly through the column as they are excluded from most of the pore space, while small solutes have access to the entire pore volume. The largest molecules will have a retention volume equal to the external fluid volume while the smallest molecules will have a retention volume equal to the external fluid volume plus the pore volume. The equilibrium partition coefficient (ϕ) between the pore volume and the external fluid volume is evaluated as:

$$\phi_{SEC} = \frac{(V_r - V_i)}{(V_v - V_i)} \quad (5.1)$$

where V_r is the retention volume of the species of interest. The interstitial (excluded) volume (V_i) can be evaluated using a very large (fully excluded) solute while the total void volume (V_v) can be evaluated using a very small solute like NaCl. The partition

coefficient ranges from zero to one with a value of zero for the largest molecules that do not enter into the pore structure of the resin and a value of one for the smallest molecules that can penetrate all resin space.

5.2.2 Dynamic Light Scattering

Dynamic light scattering is used to calculate the effective particle size from measurements of the diffusion coefficient based on the Stokes Einstein equation.

$$R_h = k_B T / 6\pi\eta D_\infty \quad (5.2)$$

where k_B is the Boltzmann constant, T is the absolute temperature, and η is the viscosity of the solvent. The diffusion coefficient is evaluated experimentally by measuring the time-dependent fluctuations in the scattered intensity from a laser using a photomultiplier tube and correlator. It is critical that the temperature be uniform to insure constant viscosity and to minimize free convection. Other factors that may have an effect on the diffusion coefficient are the ionic strength, intermolecular interactions, and solute surface structure (Grigsby et al., 2000; Junfeng et al., 2005). Data are typically obtained using relatively dilute solutions to avoid scattering from multiple solutes.

The correlator analyzes the variation of scattered light intensity as a function of time. At short times, the measured signal is similar to the initial scattering, but this decays to zero as the particle locations become random due to diffusion. Measurements are typically taken over 100 ns to 1 s depending on the particle size and solution viscosity. The scattering intensity data are used to fit an autocorrelation function $G(\tau)$ as discussed by Pecora (1985):

$$G(\tau) = \frac{I(t_o)I(t_o + \tau)}{I(t_o)^2} = A + \beta_0 \exp(-2\Gamma \tau) \quad (5.3)$$

where t_o is the initial time, τ is the time step, and A , β_0 , and Γ are fit to the experimental data. Figure 5.1 shows the autocorrelation function for a monodisperse suspension of 96 nm spheres in water. If the particles are monodispersed then the autocorrelation function can be defined by the exponential decay of the correlator time delay (Γ). Since most samples are not perfectly monodisperse more complex schemes are used for fitting. CONTNIN, the fitting analysis used in the Zetasizer nano, fits multiple exponential correlation functions to obtain a distribution of sizes.

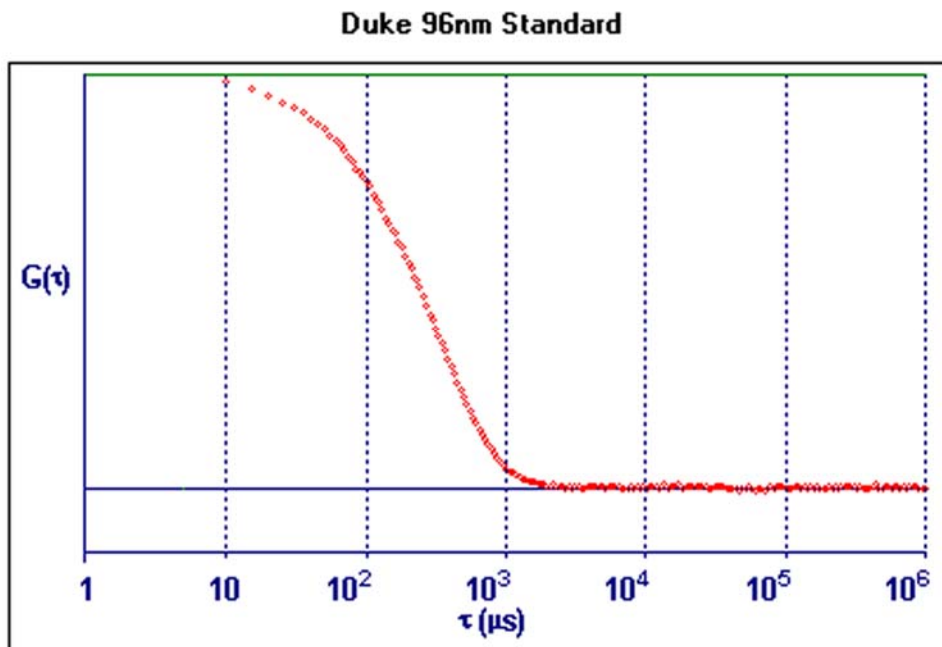


Figure 5.1. Autocorrelation function for a 96 nm standard sample (taken from Brookhaven, 2004).

The diffusion coefficient (D_∞) is related to the time delay (Γ) by the scattering intensity (q):

$$D_\infty = \frac{\Gamma}{q^2} \quad (5.4)$$

where the intensity of the scattering (q) is dependent on the refractive index of the solvent (n), the wavelength of light from the laser (λ), and the scattering angle (θ):

$$q = \frac{4\pi n}{\lambda} \sin\left(\frac{\theta}{2}\right) \quad (5.5)$$

Equations 5.4 and 5.5 are discussed in more detail by Pecora (1985).

5.3. Materials and Methods

5.3.1 Materials

PEGylated protein samples were prepared by dissolving 10 g/L of protein in a 150 mM phosphate buffer and then adding the desired amount of mPEG-SPA. Two to one molar ratios were used to obtain PEGylated proteins with 1, 2, and 3 branches while a five to one molar ratio was used to obtain PEGylated proteins with 2, 3, 4, and 5 branches. Experiments were performed with ovalbumin, α -lactalbumin, and bovine serum albumin (BSA). A detailed discussion of the preparation of the PEGylated proteins is provided in Chapters 3 and 4. PEGylated BSA with a single 12 kDa branch was obtained from Pfizer in a 10 mM Bis Tris Propane buffer. PEG standards ranging from 1.45 kDa to 35 kDa (Fluka, Steinheim, Germany) were used to generate a calibration curve for the SEC system. PEG standards were dissolved in a 150 mM phosphate buffer at a concentration of 1 g/L.

5.3.2 Size Exclusion Chromatography

PEG, protein, and PEGylated protein samples were tested on an Agilent 1100 Series HPLC system with a Superdex 200 10/300 gel permeation column (GE Healthcare) as discussed in Chapter 3. PEG standards (5 to 35 kDa) and protein standards (α -lactalbumin, ovalbumin, and bovine serum albumin) were run before each set of experiments to verify consistency of the column. A calibration curve was constructed from a plot of the logarithm of the PEG molecular weight as a function of the solute elution time. The column was only used when the r^2 value for the standard plot of the log of the molecular weight as a function of the retention time was greater than 0.98.

5.3.3 Dynamic Light Scattering

A Zetasizer Nano ZS (Malvern Instruments, Worcestershire, United Kingdom) was used for the dynamic light scattering experiments. Data were obtained using 1 g/L solutions in a 150 mM phosphate buffer. The calculated value for the solute diffusion coefficient was used to evaluate the effective hydrodynamic radius, R_h , using the Stokes-Einstein equation.

5.4 Results

5.4.1 Protein and PEG Standards

Figure 5.2 shows a plot of the molecular weight versus retention time for the protein and PEG standards, with the molecular weight taken from the certificate of

analysis provided by the manufacturer. In both cases, the retention time increases with decreasing molecular weight due to the greater accessibility of the pore space by the smaller size (i.e., smaller molecular weight) solutes. The data are linear when plotted in this fashion, with $r^2 > 0.98$. The absolute value of the slope for the proteins is somewhat greater than that for the PEG due to the different conformation of these macromolecules.

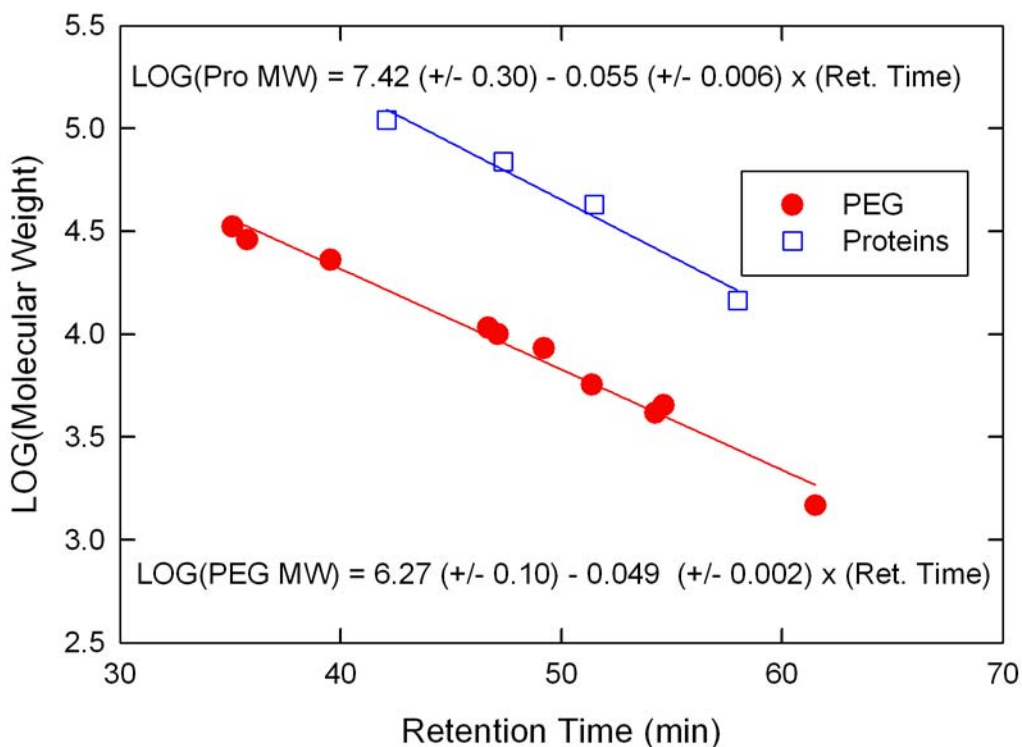


Figure 5.2. Calibration curves for the Superdex 200 G/L column for the PEG and protein standards.

The experimental data in Figure 5.2 are re-plotted in Figure 5.3 in terms of the solute partition coefficients evaluated from Equation 5.1 with the retention volume equal to the retention time multiplied by the constant flow rate of 0.3 ml/min. The interstitial volume ($V_i = 8.19 \text{ cm}^3$) was determined using the retention time of a blue dextran and the

total void volume ($V_v = 21.35 \text{ cm}^3$) was determined using NaCl. The protein partition coefficients are uniformly larger than those of the PEG (at the same molecular weight) reflecting the much larger size of the PEG caused by the open structure arising from the high degree of hydration (Branca et al., 2002). For example, the 5 kDa PEG has a partition coefficient that is very similar to that of ovalbumin, a 43 kDa globular protein, and the partition coefficient of the 10 kDa PEG ($\phi_{\text{SEC}} = 0.47$) is significantly smaller than that for α -lactalbumin with a molecular weight of 14.6 kDa ($\phi_{\text{SEC}} = 0.73$).

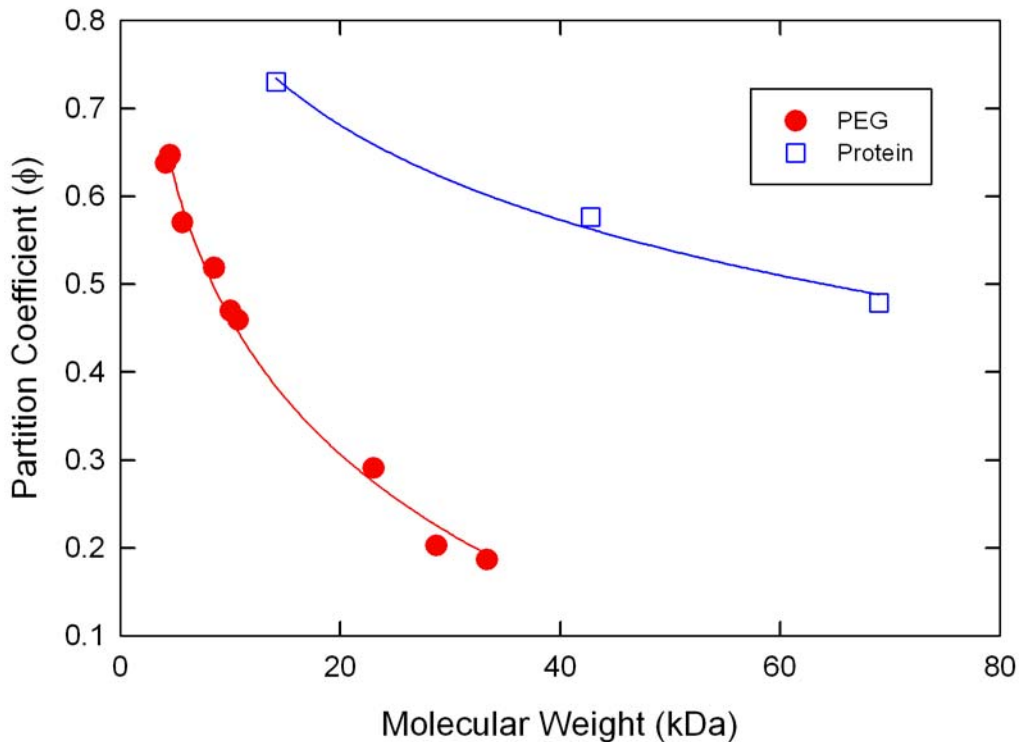


Figure 5.3. Partition coefficient of PEG and globular proteins as a function of the molecular weight. Curves are fits to the data given by Equations 5.6 and 5.7.

The solid curves in Figure 5.3 are fits to the experimental data to give the partition coefficient (ϕ) as a function of the molecular weight (kDa) of each compound.

$$\phi_{PEG} = -0.229\{\pm 0.009\}Ln(MW_{PEG}) + 0.992\{\pm 0.023\} \quad (5.6)$$

$$\phi_{Pro} = -0.156\{\pm 0.015\}Ln(MW_{Pro}) + 1.147\{\pm 0.053\} \quad (5.7)$$

The experimental data for the solute partition coefficients have been re-plotted in Figure 5.4 as a function of the solute hydrodynamic radius, which was determined from empirical correlations for the radius as a function of MW developed using measurements of the diffusion coefficient and intrinsic viscosity for both globular proteins (Equation 2.6) and PEG (Equation 2.7). The partition coefficient data collapse to a single curve when plotted in this manner, consistent with previous studies showing that the partition coefficient in SEC is a unique function of the hydrodynamic radius even for molecules with significantly different shape, size, or flexibility (Grubisic et al., 1967).

The solid curve in Figure 5.4 represents the theoretical results for the partition coefficient of a hard sphere in a porous media consisting of an array of uniform cylindrical pores:

$$\phi = (1 - \lambda)^2 \quad (5.8)$$

where λ is the ratio of the hydrodynamic radius of the solute (r_s) to the radius of the pore (r_p). The best fit values of the pore radius were determined by minimizing the sum of the squared residuals between the model calculations and the experimental data giving $r_p = 11$ nm for the hard-sphere model. The experimental data are in good agreement with the model calculations, consistent with prior results obtained by Pujar and Zydney (1998) for a series of globular proteins.

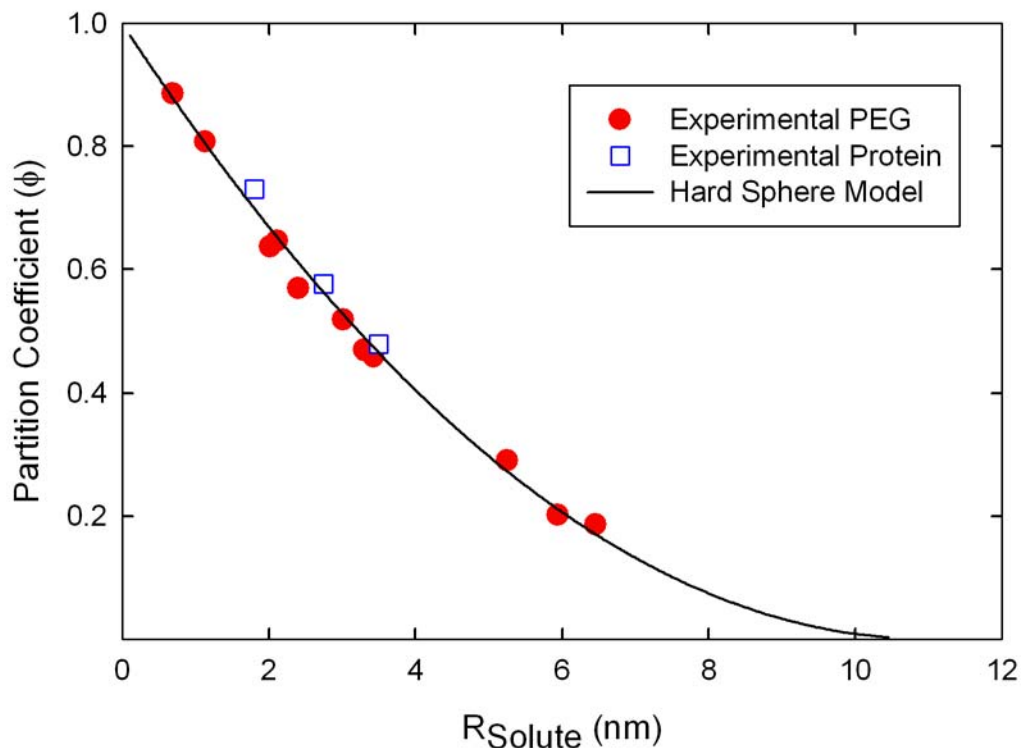


Figure 5.4. Partition coefficient as a function of the solute radius. The solid curve is a model fits for the partitioning of a hard sphere into a cylindrical pore.

5.4.2 PEGylated Proteins

A typical SEC chromatogram for a PEGylated protein mixture produced by reaction of the 5 kDa mPEG-SPA and α -lactalbumin is shown in Figure 5.5. The first four peaks (from left to right) are the PEGylated proteins: the first peak (PEG 4) corresponds to α -lactalbumin having four covalently bonded 5 kDa nominal molecular weight PEG groups (total PEG molecular weight of approximately 20 kDa), the second peak corresponds to α -lactalbumin with three covalently bonded 5 kDa PEG groups (PEG 3), and so on. The concentration of α -lactalbumin with only a single covalently

bonded PEG was quite low due to the relatively high concentration of activated PEG (5:1 molar ratio of mPEG-SPA to protein) used in the original reaction mixture. It was not possible to resolve peaks with more than five PEG groups for the 5 kDa PEGylated α -lactalbumin species using the Superdex 200 G/L column, although very low concentrations of species with higher molecular weight were identified using MALDI-TOF in the tail that exits at the leading edge of the first peak. The fifth peak corresponds to the native (non-activated) 5 kDa PEG that was added to the mixture after reaction, and the last peak corresponds to the unmodified α -lactalbumin (MW = 14.2 kDa). The relatively broad peak seen for the PEG is a direct result of the larger polydispersity of the unmodified PEG (approximately 1.12) compared to that of the activated mPEG-SPA (polydispersity of 1.02).

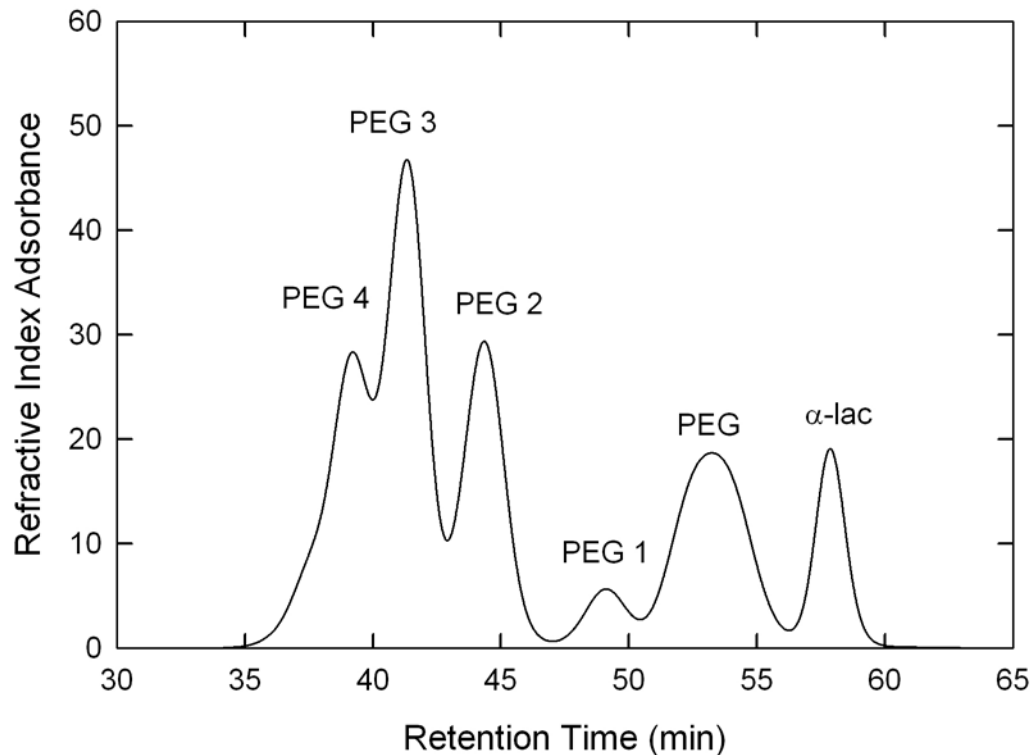


Figure 5.5 Chromatogram for a mixture of α -lactalbumin PEGylated with 5 kDa mPEG. PEG # refers to the number of 5 kDa branches of PEG added to the α -lactalbumin.

The identities of the peaks corresponding to the PEG and α -lactalbumin were confirmed by running samples of the pure components alone, with the retention volumes being identical to those seen in Figure 5.5 (95% confidence interval). This also indicates that there were no measurable intramolecular interactions between the PEG, protein, and PEGylated species in the complex reaction mixture. The smaller retention volume for the 5 kDa PEG compared to that of the 14 kDa α -lactalbumin arises from the very different conformations of these species as discussed previously.

The retention time data for the different PEGylated proteins were used to calculate the equilibrium partition coefficient using Equation 5.1, with the results shown

as a function of solute molecular weight in Figure 5.6 for data obtained with α -lactalbumin, ovalbumin, and BSA. The data were highly reproducible, with partition coefficients varying by less than 1.0 % for repeat runs performed with different mixtures of the PEGylated proteins. The calculated values of the partition coefficients for the PEGylated α -lactalbumins are similar to those reported previously by Fee and Van Alstine (2004) using a Superdex 200 resin, with the small differences likely arising from differences in column packing and resin lots for the SEC experiments. The partition coefficients of the PEGylated proteins lie between the values for the PEG and proteins (when plotted as a function of the solute molecular weight), consistent with the intermediate conformation of these composite molecules.

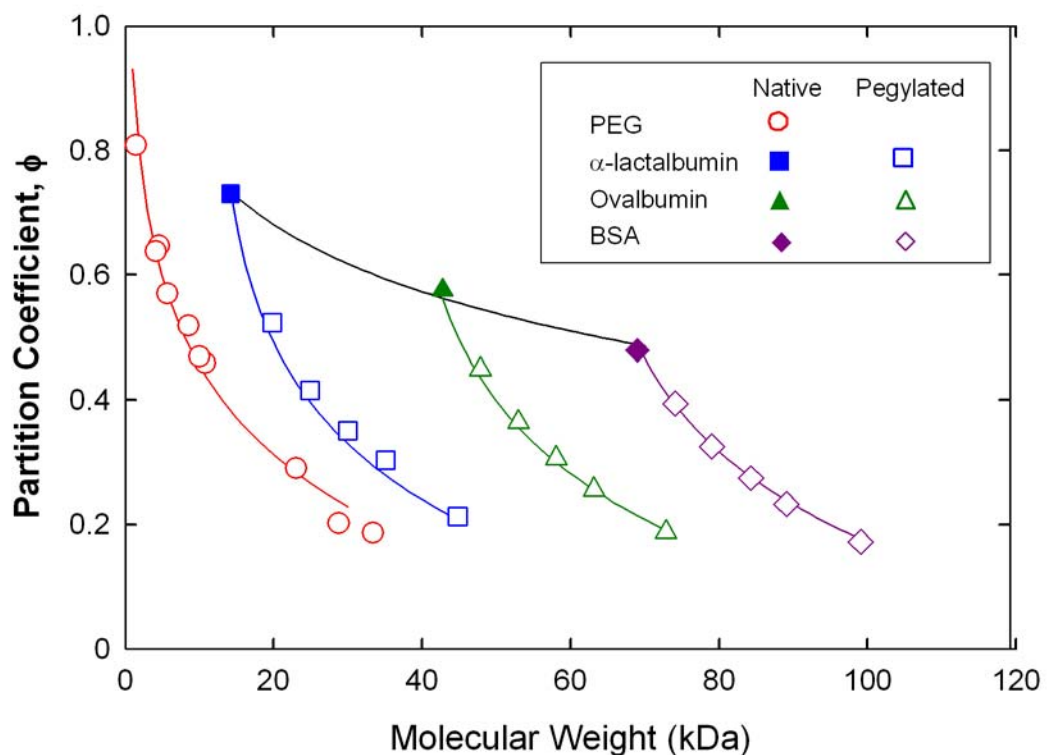


Figure 5.6 Partition coefficient as a function of molecular weight for native protein, unmodified PEG, and PEGylated versions of α -lactalbumin, ovalbumin, and bovine serum albumin. Solid curves are given by Equation 5.10.

The molecular weight dependence of the partition coefficient for both the PEG and PEGylated proteins is much stronger than that for the unmodified proteins. The partition coefficients for PEGylated proteins with the same total molecular weight were identical, independent of the number of attached PEG groups, in good agreement with previous observations by Fee and Van Alstine (2004). For example, the partition coefficient for α -lactalbumin with four 5 kDa PEG chains is 0.287 ± 0.017 compared to a value of 0.282 ± 0.006 for α -lactalbumin with two 10 kDa PEG chains. This behavior is very different than what is seen with the protein sieving coefficients as discussed in Chapter 7.

5.4.3 Modeling of the Partition Coefficient

The data in Figure 5.6 for the PEG and the different PEGylated proteins show a very similar dependence on the molecular weight of the PEG portion of the molecule, with the curves for the different proteins shifted down and to the right based on the molecular weight and partition coefficient of the base protein. This suggests re-plotting the partition coefficient data as a function of an effective solute molecular weight, which is determined from the sum of the molecular weight of the attached PEG and the “effective” molecular weight of the protein. In this case, the equivalent molecular weight of the protein is calculated from its partition coefficient using a calibration curve for ϕ as a function of molecular weight constructed from data for the unmodified PEG (Equation 5.6 and Equation 5.7):

$$\ln(MW_{effective}) = 0.68\{\pm 0.01\}\ln(MW_{protein}) - 0.68\{\pm 0.37\} \quad (5.9)$$

where $MW_{effective}$ is the molecular weight (kDa) of a PEG molecule with the same partition coefficient as a protein having a molecular weight (kDa) $MW_{protein}$. This allows a general correlation to be developed for the partition coefficient of the PEGylated proteins based on the molecular weight of the protein and PEG components:

$$\phi_{SEC} = -0.23\{\pm 0.01\}\ln(MW_{PEG} + MW_{effective}) + 0.99\{\pm 0.02\} \quad (5.10)$$

The solid curves in Figure 5.6 are model calculations based on Equation 5.10. The model is in excellent agreement with the data for the PEG, the proteins, and the PEGylated proteins over the full range of PEGylation tested with an absolute deviation of less than 10%. Although Equation 5.10 provides a good fit for the experimental data obtained in this study, care must be taken in extrapolating this correlation to other proteins or to a broader range of PEG molecular weights.

Several different theoretical approaches were used to examine the partitioning behavior of the PEGylated proteins in terms of the effective hydrodynamic radius of the PEG and protein. The simplest approach was to assume that the total volume of the PEGylated protein is equal to the sum of the volume of the isolated PEG and protein components in which case the effective hydrodynamic radius is given as:

$$R_{Pegylated} = [R_{PEG}^3 + R_{Pro}^3]^{1/3} \quad (5.11)$$

Fee and Van Alstine (2004) assumed that the surface area to volume ratio of the PEG portion of the PEGylated molecule remains constant, with the hydrodynamic radius of the PEGylated protein given as:

$$R_{pegylated} = \frac{A}{6} + \frac{2}{3A}R_{PEG}^2 + \frac{R_{PEG}}{3} \quad (5.12)$$

where

$$A = \left[108R_{Pro}^3 + 8R_{PEG}^3 + 12(81R_{Pro}^6 + 12R_{Pro}^3 R_{PEG}^3)^{1/2} \right]^{1/3} \quad (5.13)$$

with R_{PEG} and R_{Pro} in Equation 5.12 and Equation 5.13 evaluated for the isolated PEG and protein, respectively.

These different models are compared with the experimental results for PEGylated α -lactalbumin and PEGylated BSA in Figure 5.7. The experimental values of the hydrodynamic radius were calculated from the measured partition coefficients using Equation 5.8 with the best fit value of the pore radius ($r_p = 11$ nm) determined by fitting the data for the PEG and protein standards. The solid curve represents the calculated values of the hydrodynamic radius determined using the empirical correlation for the partition coefficient in terms of the PEG and protein molecular weight (Equation 5.10), with the radius calculated from Equation 5.8. This empirical fit is in excellent agreement with the data for both the PEGylated α -lactalbumin (standard deviation of 1.72) and the PEGylated BSA (standard deviation of 1.53). The equation developed by Fee and Van Alstine (2004) based on the assumption of a constant PEG surface area to volume ratio (Equation 5.12) slightly over predicts the data but properly describes the general behavior as well as the curvature (standard deviation of 2.71 and 2.14 for α -lactalbumin and BSA respectively). The model based on the additivity of the PEG and protein volumes (Equation 5.11) slightly under predict the data, especially at low molecular weights of PEG (standard deviation of 1.97 and 4.44 for α -lactalbumin and BSA respectively). Despite the differences between the experimental data and the models, an analysis of the variance of the empirical model compared to the variance of the other possible models

suggest that it is not possible to determine if one model is better than another with any significant (>95%) degree of certainty with the given experimental data.

The deviation between the volume based on the additivity of the volumes and the experimental data suggests that the conformation of the PEG is effected, at least to some degree, by the covalent attachment to the protein. This effect may simply be related to the loss flexibility associated with the attachment of one end of the PEG chain to the globular protein, or it could be related to specific interactions between the ethylene glycol groups and the amino acid residues on the surface of the protein. Although the Fee and Van Alstine model is in good agreement with the experimental results, there is no obvious reason why the surface area to volume ratio of the PEG should remain constant upon attachment to the protein. Additional work is needed to develop a more fundamental understanding of the volume / conformational changes associated with protein PEGylation.

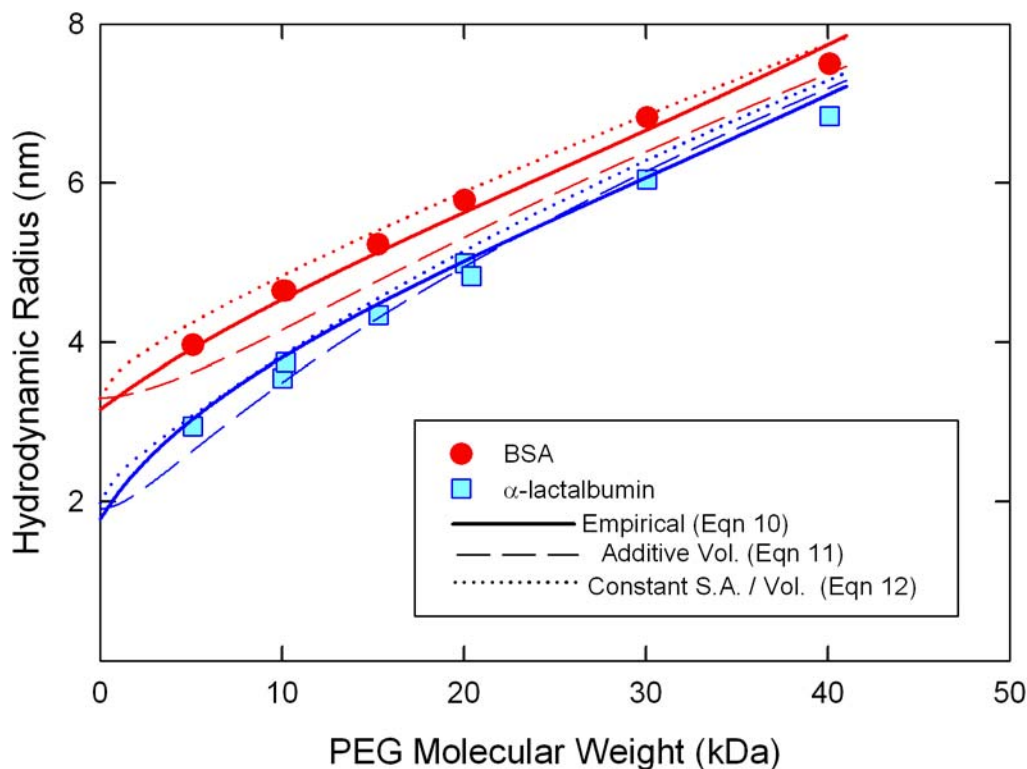


Figure 5.7. Comparison of models and experimental data for the hydrodynamic radius of PEGylated BSA and α -lactalbumin.

5.4.4 Dynamic Light Scattering

The hydrodynamic radius of the protein and PEGylated proteins were also determined using dynamic light scattering. Data were obtained using dilute (1 g/L) solutions in a 150 mM phosphate buffer at pH 7.0 to minimize protein-protein interactions and electrostatic effects. Figure 5.8 shows the calculated values of the hydrodynamic radius of α -lactalbumin, ovalbumin, and BSA determined from both light scattering and size exclusion chromatography. Error bars are shown for a minimum of three repeat measurements using the dynamic light scattering system. Error bars are not

shown for the size exclusion chromatography system since the errors are similar in size to the actual data point. There was good agreement between the calculated radii determined from these independent experimental methods, demonstrating the consistency of the two methods.

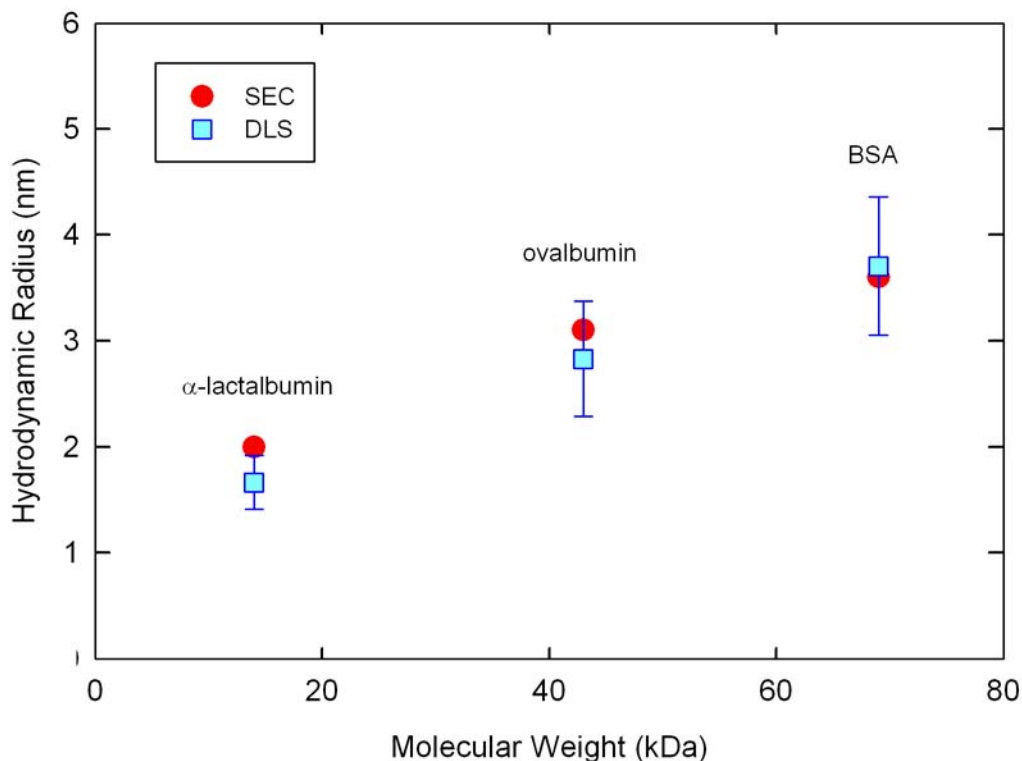


Figure 5.8. Hydrodynamic radius of α -lactalbumin, ovalbumin, and BSA determined using size exclusion chromatography and dynamic light scattering. Error bars represent plus/minus one standard deviation of the experimental data.

It was considerably more difficult to obtain accurate measurements of the hydrodynamic radius of the PEGylated proteins by dynamic light scattering. Initial studies using mixtures of the differently PEGylated species were unsuccessful since it was impossible to interpret the data from the measured autocorrelation function. Subsequent experiments were performed with purified samples of the individual

PEGylated proteins separated by size exclusion chromatography using a Superdex 200 G/L column following the procedures discussed in Chapter 3 with one 500 μ L injection volume. The eluent was collected in 0.3 ml fractions, with the two fractions containing the highest concentration of a given PEGylated species pooled. The fractions collected from three identical SEC runs were combined to obtain sufficient material for use in the dynamic light scattering experiments.

Figure 5.9 shows the calculated radii of the different PEGylated α -lactalbumin species determined by both SEC and light scattering. The results are in good qualitative agreement, although there are some small deviations between the measurements. However, the data were insufficient to draw any conclusions about possible differences in the hydrodynamic radius of the PEGylated proteins determined by dynamic light scattering and size exclusion chromatography. The use of larger PEG or protein components may provide more complete information regarding differences in the size of these molecules measured using SEC and DLS.

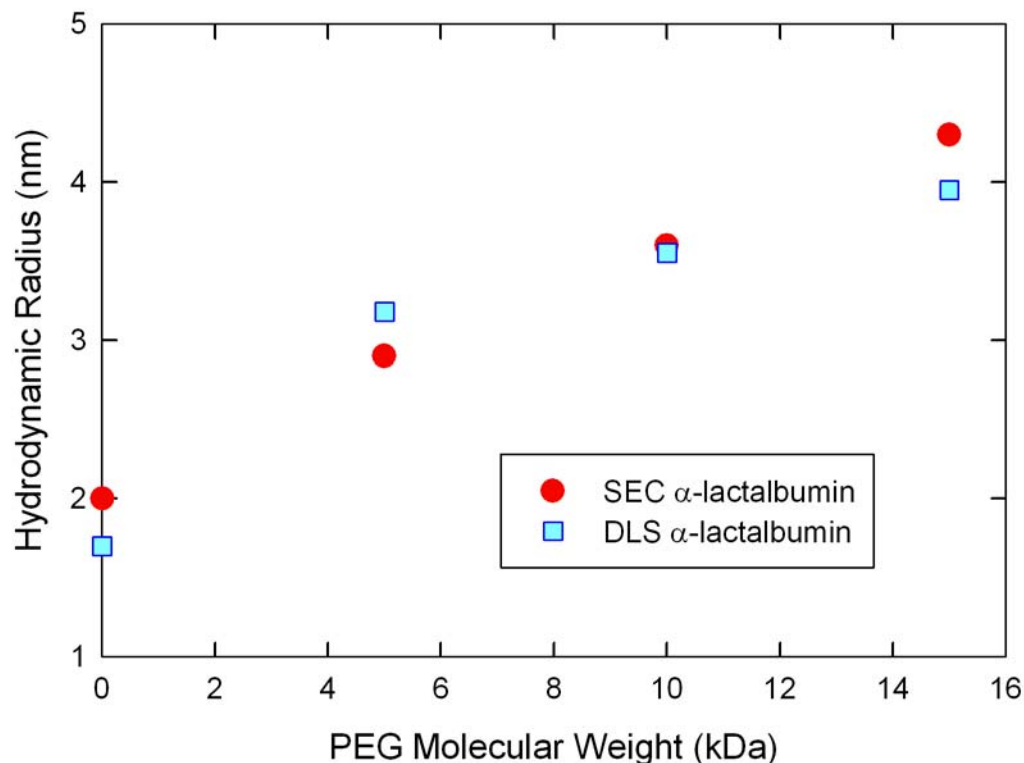


Figure 5.9. Hydrodynamic radii of PEGylated α -lactalbumin calculated using SEC and dynamic light scattering.

5.4 Conclusions

The experiments performed in this chapter provide quantitative data for the effective size of PEGylated α -lactalbumin, ovalbumin, and BSA based on measurements of the equilibrium partition coefficient in size exclusion chromatography. PEG itself has a much more open and flexible structure than the globular proteins, resulting in smaller values for the equilibrium partition coefficient, corresponding to a larger effective size, for a PEG chain compared to a protein of equal molecular weight. The effective size of the PEGylated proteins were between those of the PEG and protein, reflecting the

composite structure of these protein-polymer conjugates. In addition, the effective size of the PEGylated proteins was determined entirely by the molecular weight of the base protein and the total molecular weight of the attached PEG, independent of the number of PEG groups attached to the protein. Thus, PEGylated α -lactalbumin with two 5 kDa PEG groups had an identical partition coefficient, and thus identical size, to that of a PEGylated α -lactalbumin with a single 10 kDa PEG. This behavior is in sharp contrast to the results obtained in the ultrafiltration studies discussed later in Chapter 7.

An empirical correlation was developed for the effective hydrodynamic radius of the PEGylated protein in terms of the molecular weight of the protein and PEG components in the protein-PEG conjugate. This empirical model provides a very good agreement with the experimental data. It was possible to describe the results using two fairly simple geometric models: the model proposed by Fee and Van Alstine (2004) in which the surface area to volume ratio of the PEG was assumed to remain constant upon attachment to the protein and a hydrodynamic volume model in which the volumes of the PEG and protein in the PEGylated molecule are assumed to be unchanged from those of the isolated components. The data suggest that there is some increase of PEG volume in the composite molecule, probably due to a change in conformation of the PEG chain associated with the covalent linkage of one end of the molecule to the protein and / or to some non-specific interactions between the PEG chain and the surface of the protein.

The hydrodynamic radius of the PEGylated proteins were also evaluated using dynamic light scattering. The calculated radii for α -lactalbumin and ovalbumin determined by dynamic light scattering were in excellent agreement with the results from size exclusion chromatography, demonstrating the viability of the two methods. Results

for the PEGylated proteins showed very similar trends but there were some significant deviations between the values determined by dynamic light scattering and SEC. This may simply reflect the experimental challenges in evaluating the effective size using dynamic light scattering, particularly the possible presence of protein oligomers, species with different degrees of PEGylation, and the inherent polydispersity of the added PEG. Future studies using more highly purified samples would be needed to determine if there are any significant differences in the effective radius for a PEGylated protein as determined from the partition coefficient in SEC and the diffusion coefficient in dynamic light scattering.

Chapter 6

CAPILLARY ELECTROPHORESIS OF PEGYLATED PROTEINS

6.1 Introduction

Capillary electrophoresis has become a well-established technique for evaluating the composition and concentrations of a wide range of protein samples (Carbeck et al., 1998; Corradini 1997; Na et al., 2001; Watzig et al., 1998). In addition, capillary electrophoresis can be used to study a variety of protein properties including the net protein charge (Gao and Whitesides, 1997), the extent of ion binding (Menon and Zydney, 1998), and the presence of specific biomolecular interactions (Caravella et al., 1999; Martinez-Gomez et al., 2007; Safi et al., 2007).

Several investigators have used capillary electrophoresis for analysis of PEGylated protein samples. Semi-aqueous capillary electrophoresis has been used to resolve the different PEGylated forms of ribonuclease A (Li and Su, 2004), lysozyme (Corradini et al., 2005), and recombinant TNF- α (Li et al., 2002). Li and Su (2004) used capillary electrophoresis to measure the extent of aggregation of PEGylated ribonuclease A under different storage conditions. More recently, Na et al. (2008) used SDS capillary gel electrophoresis to check the purity of PEGylated α -interferon with both single and multiple PEG chains. In addition, Sharma and Carbeck (2005) used capillary electrophoresis to calculate the effective size of PEGylated lysozyme using Henry's equation, implicitly assuming that the electrical charge on the native protein is displaced

to the outer radius of a PEGylated sphere. The calculated values of this effective spherical radius were in good agreement with results from partitioning in size exclusion chromatography, although the authors provided no physical basis for the use of this model.

In this chapter, quantitative data on the resolution and mobility of PEGylated α -lactalbumin molecules using capillary electrophoresis are reported including the effects of buffer additives on the behavior of the PEGylated proteins. The electrophoretic mobility data for the PEGylated proteins are compared with results for acetylated forms of α -lactalbumin to account for the change in charge associated with the PEGylated reaction. Acetylated forms of the protein were generated by covalent modification of the same lysine amino groups used in the PEGylation reaction but without any significant change in the protein molecular weight due to the small size of the ligand. Mobility data are analyzed using available theoretical models for the electrophoretic mobility of composite objects to obtain additional insights into the underlying structure of the PEGylated proteins. These results provide important information on the use of capillary electrophoresis for analysis of PEGylated proteins as well as a basis for understanding the effect of electrostatic interactions on the transmission of PEGylated proteins through charged ultrafiltration membranes (Chapter 9) and the extent of fouling with both hydrophilic and hydrophobic membranes (Chapter 10).

6.2 Theory

6.2.1 Background

The wide range of applications of capillary electrophoresis for the separation and analysis of protein samples is possible, at least in part, because of the strong theoretical foundation for describing the electrophoretic mobility of globular proteins. The electrophoretic mobility reflects the balance between the electrical forces arising from the applied electric field and the hydrodynamic (friction) forces associated with the viscosity of the suspending medium. A large number of theoretical analyses have been presented in the literature for the electrophoretic mobility, with the differences lying primarily in the approximations made in evaluating the electrical interactions. These differences include both the detailed structure of the equilibrium electrical potential (e.g., the use of the low electrical potential, small Debye length, or flat plate approximations) and the distortion of the equilibrium structure associated with the particle and fluid motion during electrophoresis.

The earliest analysis of electrophoresis is due to Smoluchowski and is valid for arbitrary particle shape under conditions where the Debye length (double layer thickness) is much smaller than the characteristic particle size and the potential is assumed to be low (Masliyah, 1994). The Smoluchowski analysis describes the mobility (μ) of the particle as:

$$\mu = \frac{\varepsilon_r \varepsilon_o \zeta}{\eta} \tag{6.1}$$

where ε_r is the relative permittivity (or dielectric constant) of the solution, ε_o is the permittivity of vacuum, η is the fluid viscosity, and ζ is the zeta potential, defined as the electrostatic potential at the plane of shear (slip) (Masliyah, 1994).

If the electrical double layer is much larger than the particle, the electrophoretic mobility (μ) is given by the Debye-Huckel equation assuming that the potential is low:

$$\mu = \frac{2\varepsilon_r\varepsilon_o\zeta}{3\eta} \quad (6.2)$$

The zeta potential for a uniformly charged hard sphere can be expressed in terms of the particle surface charge (q) assuming a low potential as:

$$\zeta = \frac{q}{4\pi R\varepsilon_r\varepsilon_o(1 + \kappa R)} \quad (6.3)$$

where R is the particle radius and κ is the inverse Debye length given by Equation 6.4 (Masliyah, 1994).

$$\kappa = \left(\frac{1}{\varepsilon_r\varepsilon_o k_B T} \sum_{i=1}^N z_i^2 C_{io} \right)^{1/2} \quad (6.4)$$

where k_B is Boltzmann's constant, T is the absolute temperature, and z_i and C_{io} are the valence and bulk concentration of the mobile ions.

Henry (1931) obtained a more complete solution for the electrophoretic mobility that accounts for the distortion of the electric field lines by the presence of the particle, with the resulting expression valid over the entire range of Debye lengths as long as the particle zeta potential is small so that the exponential terms in the Poisson-Boltzmann equation can be approximated using the first term in the Taylor series expansions:

$$\mu = \frac{2\varepsilon_r\varepsilon_o\zeta H(\kappa R)}{3\eta} \quad (6.5)$$

where

$$H(\kappa R) = 1 + \frac{1}{16}(\kappa R)^2 - \frac{5}{48}(\kappa R)^3 - \frac{1}{96}(\kappa R)^4 + \frac{1}{96}(\kappa R)^5 + \frac{1}{8}(\kappa R)^4 \exp[\kappa R] \left(1 - \frac{(\kappa R)^2}{12} \right) \int_{\kappa a}^{\infty} \frac{\exp[-t]}{t} dt \quad (6.6)$$

A number of studies have analyzed the effects of relaxation and electrophoretic retardation on the electrophoretic mobility (e.g., O'brien and White, 1978; Ohshima, 2001). These theoretical developments are not discussed here due to the relatively low surface potential of the PEGylated proteins examined in this study. At surface potentials below 25 mV the relaxation effect on the ion cloud is negligible; this effect is often insignificant even up to surface potentials of 50 mV (Hiemenz and Rajagopalan, 1997). The highest calculated surface potential for the native α -lactalbumin in our experimental studies was 48 mV. The calculated surface potentials of the PEGylated proteins were below 30 mV for all experiments.

There have also been a number of theoretical studies of the electrophoretic behavior of particles with more complex geometries / morphologies. For example, the mobility of non-spherical particles has been examined by Yariv (2005). The mobility of porous particles has been examined by Hill et al. (2003), Cohen and Khorosheva (2001), Ding and Keh (2003), and Bhatt and Sacheti (1994). Several studies have examined the behavior of composite particles containing both electrically neutral and charged components, analogous to the PEGylated proteins examined in this thesis, although the majority of this work has focused on larger particles in which the Smoluchowski analysis is valid (Hill et al., 2003; Keh and Ding, 2002; Lietor-Santos and Fernandez-Nieves, 2005; Ohshima, 1995; Sharp and Brooks, 1985; Yoon, 1990). Jones (1979) examined the effects of polymer length, density, and charge on the electrophoretic mobility of large particles. In this analysis, it was assumed that the Smoluchowski equation could be

followed, the polymer density was constant throughout the polymer layer, and the dielectric constant was similar in the polymer layer and the bulk. The hydrodynamic drag of the molecule was calculated based on the drag of the solid colloid and the drag associated with the density and length of the polymer segments. The electrostatic force was calculated based on the charge on the solid surface and an average charge in the polymer layer, based on the polymer density. By comparing the drag force and the electrostatic force it was determined that at low polymer surface concentration the addition of charged polymer increased the electrostatic forces to a greater degree than the hydrodynamic forces, but the opposite was seen at higher polymer concentrations.

6.2.2 PEGylated Proteins

Despite the extensive prior work on the electrophoretic mobility of a variety of composite objects, it is unclear how to most appropriately describe the electrophoretic mobility of a PEGylated protein due to uncertainties in the actual geometry / structure of the PEGylated species. We examined a number of different physical models in this work, which are conveniently described in two broad groups: (1) models in which the PEG and protein components are used to determine the overall drag while the protein is used to determine the electrophoretic force (Kim and Karrila, 2005; Long and Ajdari, 1996), and (2) models in which the PEGylated protein is treated as a composite sphere with an effective radius determined from the contributions of the PEG and protein to the overall solute volume (Cohen and Khorosheva, 2001; Hill et al., 2003; Sharma and Carbeck, 2005). These different models are described briefly in the following

paragraphs, and are discussed further in the context of the experimental results presented later in this Chapter.

Long and Ajdari (1996) developed a model for the electrophoretic mobility of a composite particle consisting of two spheres connected by a tether. Their analysis assumes that the spheres align with the electrical field (with no rotational diffusion) and that the hydrodynamic drag on each sphere is unaffected by the presence of the other sphere (or tether) with:

$$\omega_i = 6\pi\eta R_i \quad (6.7)$$

where ω_i is the hydrodynamic drag on sphere i , η is the viscosity, and R_i is the radius of sphere i . The overall mobility of a PEGylated protein can be evaluated using this theoretical framework as:

$$\mu = \frac{\omega_{pro}\mu_{pro}}{\omega_{pro} + \omega_{PEG}} = \mu_{pro} \frac{R_{pro}}{(R_{pro} + R_{PEG})} \quad (6.8)$$

where the PEG is assumed to be completely uncharged with a radius R_{PEG} and μ_{pro} is the electrophoretic mobility of the isolated protein as determined by Equation 6.5. Equation 6.8 predicts that the electrophoretic mobility of the PEGylated protein is reduced because of the additional drag associated with the PEG (modeled as a sphere), with no change in the electrical force.

The PEGylated molecule may also be modeled as an effective prolate spheroid formed by the direct linkage of the PEG and protein, without any "tether" as assumed in the model by Long and Ajdari (1996). In this case, we evaluated the effective diameter of the spheroid (g) as the larger of the diameters of the isolated PEG and protein, with the effective length (h) evaluated as the sum of the diameters of the isolated PEG and protein

components. The drag force on a prolate spheroid depends upon the geometry (defined by the ratio h/g) and the orientation of the spheroid with respect to the direction of motion (Kim and Karrila, 2005):

$$\omega = 6\pi\eta(R_{PEG} + R_{Pro})f\left(\frac{h}{g}\right) \quad (6.9)$$

For a freely rotating spheroid, the drag ratio is determined by averaging the drag force over all possible orientations giving:

$$\omega_{Total} = 6\pi\eta(R_{PEG} + R_{Pro})\left[\frac{2}{3}f_g\left(\frac{h}{g}\right) + \frac{1}{3}f_h\left(\frac{h}{g}\right)\right] \quad (6.10)$$

where f_g and f_h refer to the drag force with the motion directed along the short (g) and long (h) axes, respectively. The electrophoretic mobility of the prolate spheroid can be evaluated directly from the drag force assuming that the electric force is unaffected by the presence of the PEG component:

$$\mu = \frac{\omega_{Pro}\mu_{pro}}{\omega_{Total}} = \mu_{pro} \frac{R_{pro}}{(R_{PEG} + R_{Pro})\left(\frac{2}{3}f_g\left(\frac{h}{g}\right) + \frac{1}{3}f_h\left(\frac{h}{g}\right)\right)} \quad (6.11)$$

An alternative approach for evaluating the electrophoretic mobility of a PEGylated protein is to assume the molecule is a single composite sphere. The simplest approach is to assume that the PEG layer is impermeable to the flow, in which case the hydrodynamic drag acts on the exterior surface of the PEGylated protein, while the electrical force is determined by the charge on the surface of the protein. Under these conditions, the electrophoretic mobility can be estimated using Henry's equation with the zeta potential and the Henry correction factor, $H(\kappa R)$ both evaluated at the outer surface of the PEGylated protein (assumed to be the surface of shear). The electrical potential on the surface of shear can be related to the electrical charge at the protein surface ($q_{surface}$)

by solving the linearized form of the Poisson-Boltzmann equation in both the PEG layer and in the bulk solution:

$$\frac{d^2(r\psi_1)}{dr^2} = \kappa_1^2 r\psi_1 \quad (\text{for } a \leq r \leq s) \quad (6.12)$$

$$\frac{d^2(r\psi_2)}{dr^2} = \kappa_2^2 r\psi_2 \quad (\text{for } r \geq s) \quad (6.13)$$

where a is the radius of the protein and s is the radius of the PEGylated protein. The Debye length in regions 1 (6.12) and 2 (6.13) may be different since the "bulk" salt concentrations in the PEG layer and bulk solution can be different due to thermodynamic (partitioning) of the salt between the PEG and aqueous solution. This phenomenon is discussed in more detail subsequently. The general solution to Equation 6.12 and 6.13 can be written as:

$$Ae^{-\kappa_1 r} + Be^{\kappa_1 r} = r\psi_1 \quad (6.14)$$

$$Ce^{-\kappa_2 r} + De^{\kappa_2 r} = r\psi_2 \quad (6.15)$$

The integration constants (A , B , C , and D) in Equations 6.14 and 6.15 are evaluated using the boundary conditions:

$$q_{surface} = 4\pi a^2 \epsilon_1 \epsilon_0 \frac{d\psi_1}{dr} \quad \text{at } r = a \quad (6.16)$$

$$\psi_2 \rightarrow 0 \quad \text{at } r \rightarrow \infty \quad (6.17)$$

$$\psi_1 = \psi_2 \quad \text{at } r = s \quad (6.18)$$

$$\frac{d\psi_1}{dr} = \frac{d\psi_2}{dr} \quad \text{at } r = s \quad (6.19)$$

Equation 6.19 is valid if the electrical permittivity (i.e., dielectric constant) in the PEG and bulk solution are equal. The electrical potential (ζ) at the surface of shear is evaluated from the resulting expression for ψ_1 at $r = s$:

$$\zeta = \frac{e^{a\kappa_1 + s\kappa_1} \kappa_1 q_{surface}}{2\varepsilon_r \varepsilon_o \pi s \left(e^{2a\kappa_1} (\kappa_1 - a\kappa_1^2 - \kappa_2 + a\kappa_1 \kappa_2) + e^{2s\kappa_1} (\kappa_1 + a\kappa_1^2 + \kappa_2 + a\kappa_1 \kappa_2) \right)} \quad (6.20)$$

with the electrophoretic mobility given as:

$$\mu = \frac{e^{a\kappa_1 + s\kappa_1} \kappa_1 q_{surface}}{3\pi\eta \left(e^{2a\kappa_1} (s\kappa_1 - a s \kappa_1^2 - s\kappa_2 + a s \kappa_1 \kappa_2) + e^{2s\kappa_1} (s\kappa_1 + a s \kappa_1^2 + s\kappa_2 + a s \kappa_1 \kappa_2) \right)} H(\kappa_2 s) \quad (6.21)$$

Equation 6.21 has not been presented previously in the literature. However, if the Debye length inside the PEG layer is very large, $\kappa_1 a \rightarrow 0$, Equation 6.21 reduces to:

$$\mu = \frac{q_{surface}}{6\pi\eta s (1 + \kappa_2 s)} H(\kappa_2 s) \quad (6.22)$$

which is equivalent to the expression presented by Sharma and Carbeck (2005) for the electrophoretic mobility of a PEGylated protein. Note that Sharma and Carbeck provided no discussion of the development leading to Equation 6.22 or of the key underlying assumptions, including the limitation that Equation 6.22 is only valid when $\kappa_1 a$ is very small. If the Debye length inside the PEG layer is equal to that in the bulk solution, the electrophoretic mobility given by Equation 6.21 simplifies to:

$$\mu = \frac{e^{a\kappa - s\kappa} q_{surface}}{6\pi\eta s (1 + \kappa a)} H(\kappa s) \quad (6.23)$$

where $\kappa = \kappa_1 = \kappa_2$. Equation 6.23 reduces to Equation 6.22 in the limit of a very thin PEG layer, i.e., when $\kappa(s - a) \rightarrow 0$.

Cohen and Khorosheva (2001) developed a theoretical description of the electrophoretic mobility for a composite object with an inner solid charged surface and an outer uncharged (polymer) layer that was permeable to the surrounding fluid with a constant permeability factor (f_{perm}). Their analysis implicitly assumes that the Debye length and dielectric constant are the same in the polymer and bulk solution. The electrophoretic mobility was evaluated using Smoluchowski's analysis, which is valid when the Debye length is much smaller than the characteristic particle size, with the final result given in Equation 6.24.

$$\mu = \frac{\varepsilon_o \varepsilon_r \zeta_{pro}}{\eta} \frac{\kappa^2 e^{(-f_{perm}(s-a))} - f_{perm}^2 e^{(-\kappa(s-a))}}{\kappa^2 - f_{perm}^2} \quad (6.24)$$

This model was in good agreement with experimental data for the mobility of charged liposomes coated with a thin layer of a neutral polymer, a system in which the Smoluchowski approximation should be valid. Hill et al. (2003) suggested that Equation 6.24 could be extended to molecules of all sizes (with low zeta potentials) by multiplying the bare particle mobility by the factor accounting for both the change in position of the zeta potential and the permeability of the polymer layer.

$$\mu = \frac{2\varepsilon_o \varepsilon_r \zeta_{pro} H(\kappa a)}{3\eta} \frac{\kappa^2 e^{(-f_{perm}(s-a))} - f_{perm}^2 e^{(-\kappa(s-a))}}{\kappa^2 - f_{perm}^2} \quad (6.25)$$

The application of this model to describe the electrophoretic mobility of PEGylated proteins is questionable since the permeability factor for the PEG layer may vary with position (distance from the protein surface) and the Debye length within the PEG layer may be different from that in the bulk solution.

6.3 Materials and Methods

6.3.1 Materials

All experiments were performed using α -lactalbumin PEGylated with mPEG-SPA (activated with succinimidyl propionic acid) or mPEG-SMB (activated with succinimidyl *a*-methylbutanoate) with nominal weight-average molecular weight of 2, 5, 10, 20, or 30 kDa in a 10 mM Bis Tris or 10 mM Tris Glycine buffer. A molar ratio of protein to PEG of approximately 1:4 was used for the 2, 5, and 10 kDa PEG, while a molar ratio of 1:2 was used for the 20 and 30 kDa PEG. More details on the PEGylation reactions are given in Chapters 3 and 4. Acetylated forms of α -lactalbumin were produced as described in Chapter 3.

Bis Tris buffer was prepared as described in Chapter 3. Tris buffer with glycine was prepared by adding 1.21 g/L of Trizma base (Sigma, St. Louis, MO) and 7.507 g/L glycine (Sigma) to deionized water. The pH was adjusted to 8.1 by the addition of KOH, with the ionic strength adjusted by the addition of KCl (Sigma). The pH was measured using a Model 402 Thermo Orion pH meter (Beverly, MA). Solution conductivity was measured using a Model 105 Thermo Orion conductivity meter.

6.3.2 Capillary Electrophoresis

The electrophoretic mobility of the PEGylated and acetylated proteins were determined using the procedure described in Chapter 3. Several different running buffers were examined including 10 mM Tris/Glycine (pH 8.1) and 10 mM Bis Tris (pH 7.0). The current was less than 45 μ A during all experiments, so Joule heating was negligible.

The electrophoretic mobility was calculated from the migration times of the protein (or PEGylated protein) and the neutral marker as:

$$\mu = \frac{L_d}{E_z} \left(\frac{1}{t} - \frac{1}{t_o} \right) \quad (6.26)$$

where L_d is the effective capillary length to the detector, E_z is the applied electric field, and t and t_o are the times for the protein and neutral marker to reach the detector.

6.4 Results and Analysis

6.4.1 Effects of Buffer Additives

A typical electropherogram for the PEGylated α -lactalbumin (formed with the 20 kDa mPEG-SPA) using a running buffer of 10 mM Bis Tris (the buffer used in the PEGylation reaction) are shown in Figure 6.1 (lower electropherogram). The first peak is the neutral marker (mesityl oxide) that was added to the PEGylated sample. The second distinct peak is the PEGylated α -lactalbumin with one 20 kDa branch. The third peak is the native α -lactalbumin. Although it was possible to resolve peaks corresponding to the PEGylated proteins with different numbers of PEG chains and the native protein, there was significant peak asymmetry and the overall resolution was poor using this buffer.

A number of previous studies have shown that the buffer type and composition can strongly influence the overall resolution and separation during capillary electrophoresis (Shibata et al., 2004), both by reducing protein adsorption to the walls of the capillary and by altering the electro-osmotic flow. For example, a number of organic compounds have been used to inhibit protein adsorption (Watzig et al., 1998). Li and Su (2004) used a 1:1 mixture of acetonitrile to 0.025M phosphate for the analysis of

PEGylated RNAase using a silica capillary dynamically coated with PEG. Zwitterionic additives are used to alter the magnitude of the electro-osmotic flow without increasing the conductivity (MacDonald et al., 2005). Also zwitterions have been shown to reduce the binding of positively charged compounds onto negatively charged silica capillaries. For example trimethyl ammonium propylsulfonate was used to improve the resolution of a humanized monoclonal antibody by capillary electrophoresis (Corradini, 1997).

Several different buffer additives were examined as part of this project. Initial efforts were focused on the semi-aqueous (water + acetonitrile) buffer employed by Li et al. (2001) for analysis of PEGylated RNAase. Results were obtained between 10 and 80% acetonitrile, but peak resolution was poor and decreased at high acetonitrile concentrations. Much better results were obtained using added glycine. For example, the upper electropherogram in Figure 6.1 shows results using a 10 mM Bis Tris with 0.1 M glycine added to the buffer. The improvement in performance can be quantified by evaluating the resolution (S):

$$S = \frac{R_{T2} - R_{T1}}{\frac{1}{2}W_1 + \frac{1}{2}W_2} \quad (6.27)$$

where R_{T2} and R_{T1} are the retention times of the two peaks and $\frac{1}{2}W_1$ and $\frac{1}{2}W_2$ are the peak widths at half height, equal to 2.355 times the standard deviation assuming standard Gaussian curves. The resolution between α -lactalbumin and the PEGylated α -lactalbumin with a single 20 kDa PEG chain increased from 2.1 to 4.7 upon addition of the glycine, consistent with results obtained previously using other zwitterionic additives (Corradini, 1997). A similar improvement was seen in the symmetry factor, defined as the ratio of the peak width to the left and right of the peak apex (with the larger value in

the numerator). Thus, a symmetry factor of 1 indicates perfect symmetry, with larger values corresponding to greater degrees of asymmetry. The symmetry factor of the α -lactalbumin peak decreased from 13.6 to 3.6 upon addition of the 0.1 M glycine.

The large improvement in peak resolution and symmetry is probably not simply due to the small change in conductivity (1190 $\mu\text{S}/\text{cm}$ for the Bis Tris alone versus 1310 $\mu\text{S}/\text{cm}$ with 0.1 M glycine) or with the associated change in bulk electroosmotic flow (7% difference between the two buffers). Instead, the improved performance is likely due to competition of the glycine for the silanol groups on the capillary, which reduces the extent of protein adsorption (Bushey and Jorgenson, 1989). As seen in Figure 6.1, the effect of glycine tended to be significantly more pronounced for the more highly substituted PEGylated proteins, which is probably associated with the greater interaction of the silica surface with the PEGylated molecules, caused by the lack of hydrophilic interactions of the PEGylated protein with the buffer solution. This is discussed in more detail in Chapter 10.

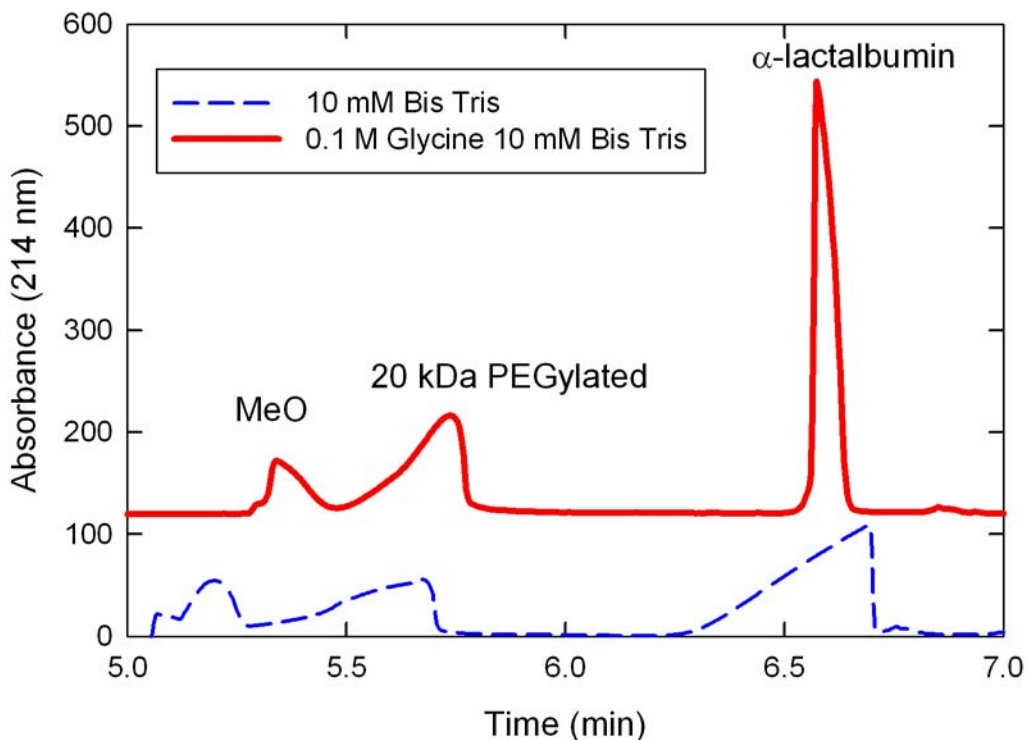


Figure 6.1. Electropherogram of a 20 kDa PEGylated α -lactalbumin with two different running buffers: Bis Tris (pH 7.0, 10 mM), and Bis Tris with Glycine (pH 7.0, 11 mM).

Similar results were obtained with the 5 kDa PEGylated protein when different buffers were employed. The resolution between the first and second PEGylated species in the sample run without glycine was 0.57 compared to 0.76 in the presence of 0.1 M glycine. The symmetry factor for the PEGylated species with one PEG branch was 1.37 without glycine while the sample with glycine had a symmetry factor of 1.12. All of the experimental results presented in the remainder of this Chapter were obtained using 0.1 M glycine as a buffer additive.

To further improve the resolution, the pH of the solution was increased from 7.0 to 8.1 by changing from Bis Tris buffer to a Tris buffer. The higher pH gave slightly

better resolution and reproducibility. Other factors that improve the resolution include an increase in column length. While some experiments in this study were run using a 64.5 cm length column, the majority of the experiments were run using an 80.5 cm column. The column length did not change the overall mobility but it did improve the resolution by nearly a factor of two. Previous studies have shown that increasing the viscosity (by lowering the temperature) can improve the resolution of samples in capillary electrophoresis (Corradini, 1997; Watzig et al., 1998). The resolution between a two 5 kDa branched PEGylated α -lactalbumin and a three 5 kDa branched α -lactalbumin increased from 0.66 to 0.72 by decreasing the solution temperature from 35°C to 25°C, consistent with the expected change in viscosity. However, it was impractical to perform the capillary electrophoresis experiments at lower temperatures due to the inability to obtain consistent temperature control with available cooling systems. All subsequent data reported in this thesis were obtained at 25 °C.

6.4.2 Effects of PEGylation on Protein Mobility

Figure 6.2 shows electropherograms for both the acetylated (lower curve) and PEGylated (upper curve) α -lactalbumin using a 10 mM pH 8.1 Tris-Glycine running buffer at 25 kV. The acetylation and PEGylation reactions both involve the $-\text{NH}_2$ on lysine amino acids; thus, the singly acetylated and PEGylated species each have one less protonated amino group than the native protein. In both cases, the first peak is the neutral marker (mesityl oxide), which is carried to the detector solely by the electroosmotic flow generated within the negatively charged capillary. The small difference in elution times for the mesityl oxide reflects the inherent variability in capillary properties and / or buffer

conditions. The second peak with the acetylated sample corresponds to the native α -lactalbumin, which migrates back against the electroosmotic flow and thus exits at a later time than the neutral marker. Each subsequent peak in the lower curve represents an acetylated α -lactalbumin with one more lysine group capped by reaction with acetic anhydride, resulting in a more negatively charged species. Twelve distinct peaks were easily resolved, corresponding to modification of up to the twelve different lysine residues on the native protein. Only the first four are shown in Figure 6.2 to compare with the PEGylated forms. The nearly evenly spaced peaks produced from the acetylated species have been previously referred to as "rungs" in a "charge ladder" (Carbeck et al., 1998). Note that even the most heavily acetylated species in this system has a molecular weight that is only 3.6% larger than the unmodified α -lactalbumin due to the small size of the ligand.

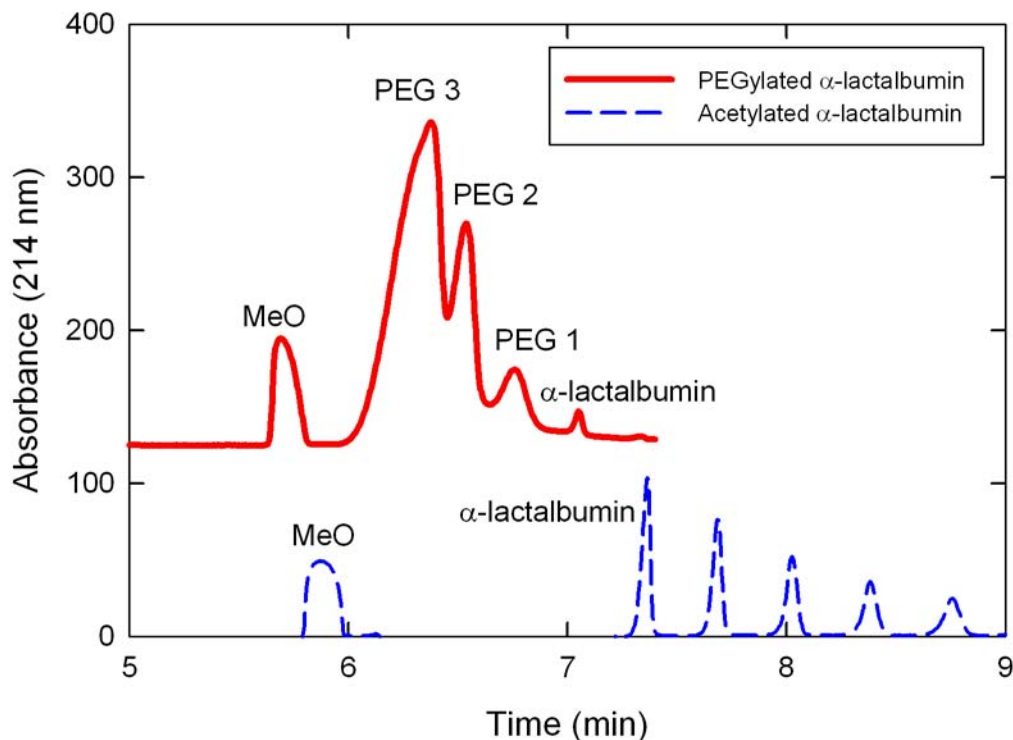


Figure 6.2. Electropherograms of acetylated α -lactalbumin (lower curve) and α -lactalbumin PEGylated with 5 kDa mPEG-SPA (upper curve). The first peak corresponds to the neutral marker (mesityl oxide), while the subsequent peaks in the PEGylated sample correspond to samples with decreasing amount of PEG. The acetylated peaks each differ by one reacted lysine group, with the first peak representing the native α -lactalbumin.

The upper curve in Figure 6.2 shows the electropherogram for the PEGylated α -lactalbumin formed by reaction with 5 kDa mPEG-SPA. Similar results were obtained with the PEGylated protein produced by reaction with mPEG-SMB. In contrast to the data for the acetylated α -lactalbumin, the peaks for the PEGylated species lie between those for the neutral marker and the unmodified α -lactalbumin due to the reduction in the electrophoretic mobility associated with the addition of the large neutral polyethylene glycol chain. Three distinct peaks, each corresponding to a PEGylated species with one

more PEG chain, are easily observable in the electropherogram. A fourth peak, corresponding to α -lactalbumin PEGylated with four PEG chains, appears as a shoulder at $t = 6.22$ min. The peaks for the PEGylated species are much broader than those for the acetylated α -lactalbumin, due primarily to the polydispersity in the mPEG-SPA. It is also possible that the variability in location of attachment of the PEG chain contributes to peak broadening, although this effect was not seen in the results for the acetylated proteins (lower curve).

6.4.3 Electrophoretic Mobility of PEGylated Proteins

6.4.3.1 Effect of the Number of Substitutions

Data such as that shown in Figure 6.2 was used to calculate the electrophoretic mobility of the acetylated and PEGylated species using Equation 6.26. Results are shown in Figure 6.3 for experiments performed with PEGylated α -lactalbumin formed by attachment of PEG with molecular weight of 2, 5, 10, 20, and 30 kDa PEG along with the corresponding results for the acetylated α -lactalbumin. Error bars show the standard deviation of at least three repeat experiments. In each case, the data are plotted as a function of the number of modifications to the native protein; thus, the species with $n = 1$ represents α -lactalbumin with either a single PEG group or a single acetylated lysine. The electrophoretic mobility of the acetylated species increases with increasing number of acetyl groups due to the increase in net negative charge associated with the conversion of the protonated amino group to an amide. The dependence on n is slightly non-linear due to the effects of charge regulation; the increase in negative charge causes an increase in the local H^+ concentration near the protein surface which leads to the slight protonation

of other basic or acidic amino acid residues. This phenomenon is discussed in more detail by Menon and Zydney (2000).

In contrast, the electrophoretic mobility of the PEGylated α -lactalbumin decreases with increasing number of attached PEG groups even though PEGylation also eliminates multiple amine groups (analogous to the acetylation reaction). For example, the mobility of the α -lactalbumin with a single 5 kDa PEG is approximately 34 % smaller than that of the native protein while the mobility of the PEGylated α -lactalbumin with a single 30 kDa PEG is more than 75 % smaller than that of the un-modified α -lactalbumin. The electrophoretic mobility of the PEGylated α -lactalbumin with one 20 kDa PEG chain is slightly smaller than that of the PEGylated protein with two 10 kDa PEG chains which is in turn smaller than that for the PEGylated protein with four 5 kDa PEG chains even though these species all have basically the same molecular weight (and thus the effective size as determined by size exclusion chromatography as discussed in Chapter 5). These differences are a direct result of the change in molecular charge, in addition to size, due to PEGylation.

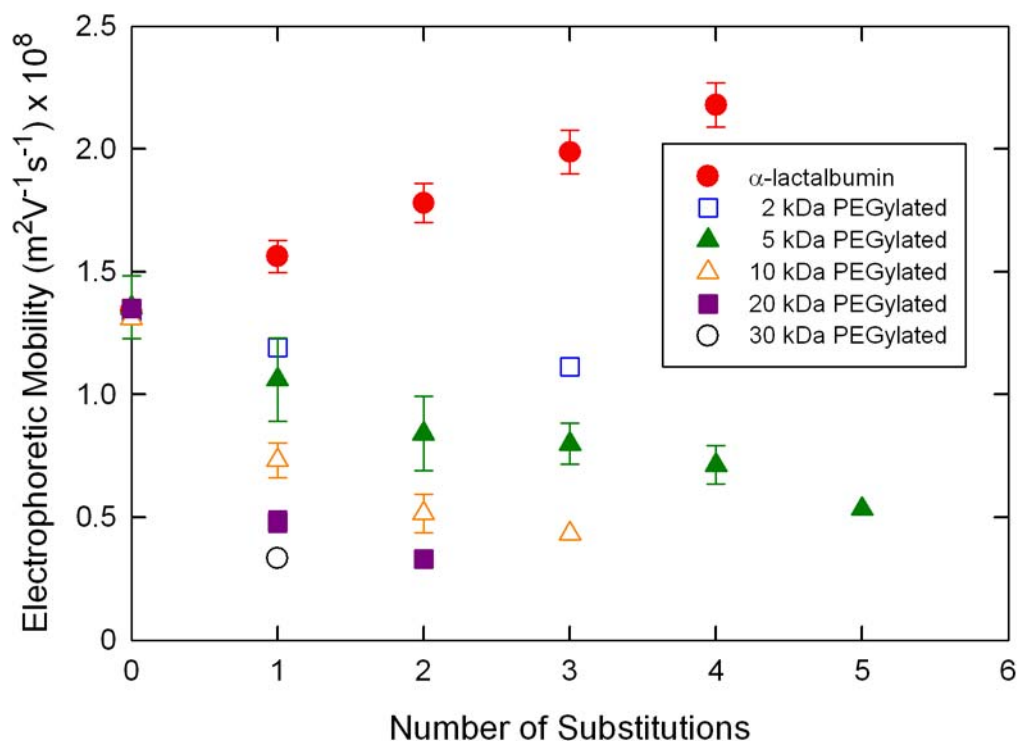


Figure 6.3. Electrophoretic mobility of the acetylated and PEGylated α -lactalbumin in 10 mM pH 8.1 Tris-Glycine running buffer as a function of the number of substituted lysine groups. Error bars represent plus/minus one standard deviation of the experimental data.

The effects of the solution parameters, including the PEG and protein concentrations and the solution viscosity, were tested to ensure that the measured electrophoretic mobility provided a true measure of the actual mobility of the PEGylated proteins. Injection volumes containing either 30 nl or 140 nl showed no dependence of the electrophoretic mobility on the total protein concentration. In addition, the mobility of the α -lactalbumin in the acetylated and PEGylated samples are within 5% of each other. The mobility of the 5 kDa PEGylated α -lactalbumin was unaffected by the concentration of other PEGylated species; there were no differences between data

obtained with mixtures containing different amounts of native α -lactalbumin or with more highly substituted species.

6.4.3.2 Effect of Ionic Strength

Figure 6.4 shows the effect of solution ionic strength on the electrophoretic mobility of α -lactalbumin, the PEGylated α -lactalbumin with a single 5 kDa PEG chain, and the PEGylated α -lactalbumin with four 5 kDa PEG chains. The data were again obtained in a Tris buffer at pH 8.1 with 0.1 M glycine, with the ionic strength varied by addition of KCl. Error bars show the standard deviation of three repeat experiments. The smallest compound, the native α -lactalbumin, had the highest electrophoretic mobility for all ionic strengths while the PEGylated α -lactalbumin with four PEG branches had the lowest mobility. The electrophoretic mobility of each species decreased with increasing ionic strength due to the electrostatic shielding provided by the bulk electrolyte, with the absolute value of slope of the data being slightly greater for the PEGylated α -lactalbumin with a single 5 kDa PEG chain. There was no evidence of any discontinuity in the data (or slope) when the double layer thickness exceeded the thickness of the PEG layer, which was estimated as 1.1 nm for the PEGylated protein with one 5 kDa branch (corresponding to a solution ionic strength of 75 mM) and 3.2 nm for the protein with four 5 kDa branches (corresponding to 9 mM), in both cases assuming that the PEGylated protein consisted of a composite sphere with inner protein core and uniform PEG layer with total radius as determined by the partition coefficient in size exclusion chromatography.

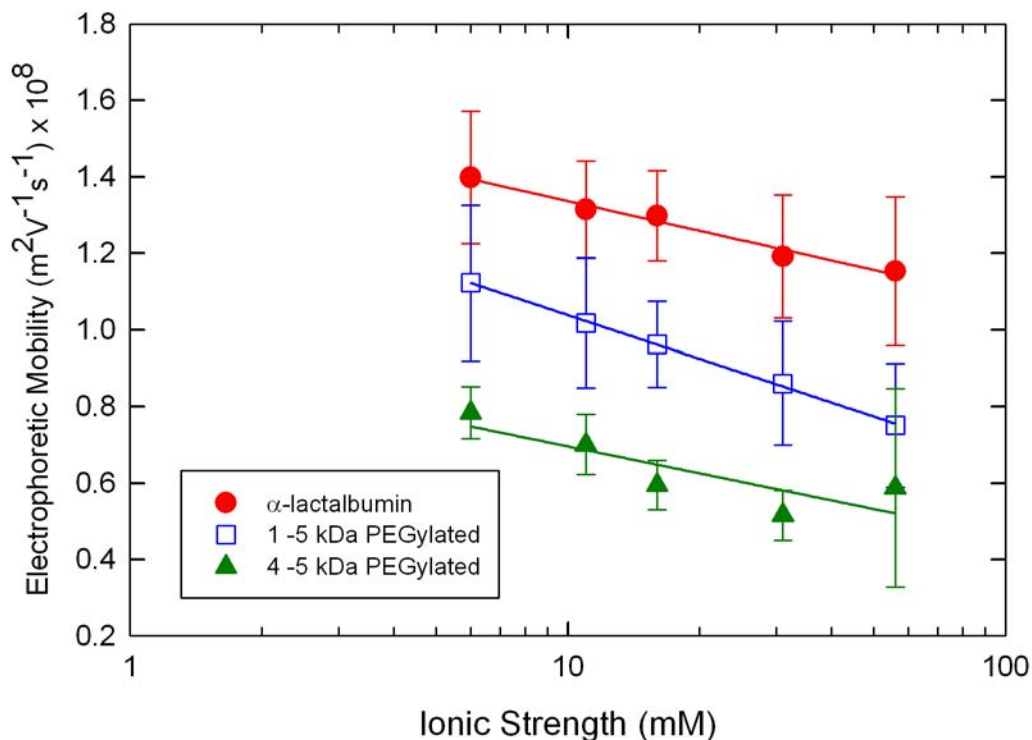


Figure 6.4. The effect of ionic strength on the mobility of α -lactalbumin and PEGylated α -lactalbumin with one 5 kDa PEG or one 20 kDa PEG. Error bars represent plus/minus one standard deviation of the experimental data. Solid curves are spline fits to the data.

Figure 6.5 shows the electrophoretic mobility of three PEGylated proteins with the same hydrodynamic radius (based on the size exclusion chromatography measurements) but with different configurations of attached PEG: PEGylated α -lactalbumin with four 5 kDa branches, PEGylated α -lactalbumin with two 10 kDa branches, and PEGylated α -lactalbumin with one 20 kDa branch. Error bars show the standard deviation of three repeat experiments. The PEGylated α -lactalbumin with four 5 kDa branches has a higher mobility than the PEGylated proteins with one or two added branches, consistent with the increase in net negative charge associated with the reaction

of the additional amino groups with the activated PEG. The effect of ionic strength on the mobility is similar for all 3 species.

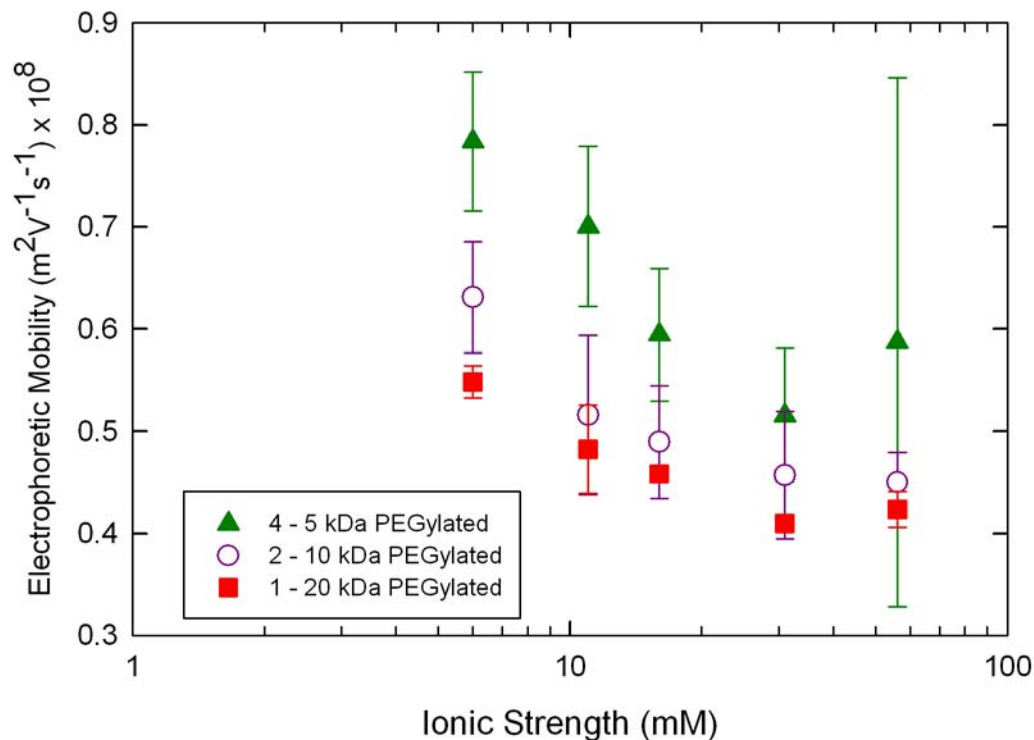


Figure 6.5. The effect of ionic strength on the mobility of PEGylated α -lactalbumin with 20 kDa total PEG molecular weight. Electrophoretic mobility is shown for molecules with one, two, or four branches. Error bars represent plus/minus one standard deviation of the experimental data.

6.4.4 Drag Ratio

In order to account for the change in both size and net charge of the PEGylated proteins, the experimental data in Figure 6.3 were analyzed by calculating the drag ratio, K_D , which is equal to the electrophoretic mobility of the PEGylated α -lactalbumin divided by the mobility of the corresponding acetylated species with the same number of chemical substitutions. Thus, the drag ratio for the PEGylated α -lactalbumin with a

single 10 kDa PEG group was evaluated by normalizing the mobility using data for the singly acetylated protein while the drag ratio for the PEGylated α -lactalbumin with two 5 kDa PEG groups was evaluated by normalizing with data for the doubly acetylated protein. The use of the drag ratio enables the comparison PEGylated proteins with different number of substitution since the change in protein charge is accounted for by the acetylated species (assuming that the presence of the PEG has no effect on the electrical potential other than the elimination of one or more lysine groups). Sharma and Carbeck (2005) used a similar approach to calculate the effective size of PEGylated proteins using capillary electrophoresis.

Experimental data for the drag ratio for the different PEGylated species are shown in Figure 6.6 as a function of the effective protein radius. The error bars are plus/minus one standard deviation as determined from standard propagation of error based on the experimental measurements of the PEGylated and acetylated species. The data collapse to a single curve when plotted based on the drag ratio. For example, the drag ratio for the PEGylated α -lactalbumin with a single 10 kDa PEG chain is 0.44, which is within 10 % of the value for the PEGylated α -lactalbumin having two 5 kDa PEG chains (which is within the standard deviation of the measurements). This is in sharp contrast to the 40% difference in the electrophoretic mobility of these species, which is directly due to the difference in electrical charge associated with the different number of modified lysine groups.

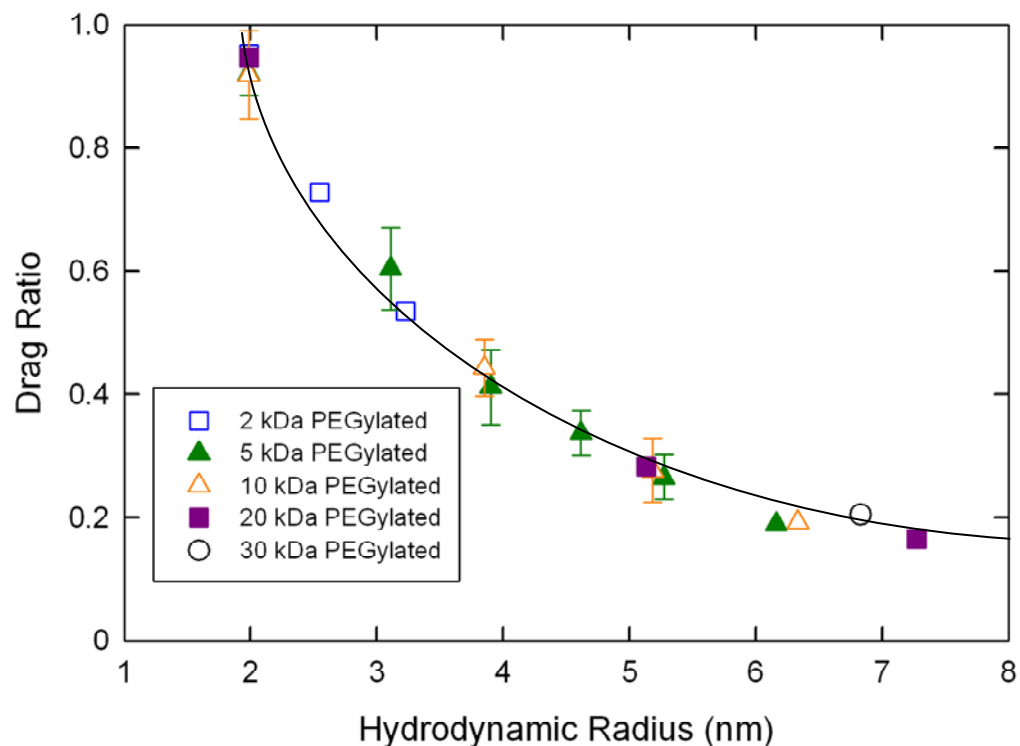
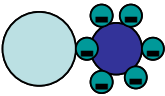
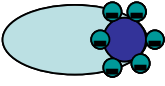
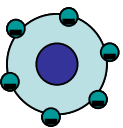
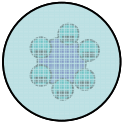


Figure 6.6. Drag coefficient as a function the hydrodynamic radius for PEGylated proteins containing 2, 5, 10, 20 and 30 kDa branches. Error bars represent plus/minus one standard deviation of the experimental data. The solid curve is a spline fit to the data.

The experimental data for the drag ratio were compared with predictions of the different physical models discussed in Section 6.2.2. Theoretical drag ratios were calculated by dividing the mobility of the PEGylated protein (calculated by Equations 6.8, 6.11, 6.22, and 6.23) by the mobility of the un-modified α -lactalbumin as given by Equation 6.5. Since the surface charge for the PEGylated and acetylated molecules was assumed to be the same, the charge term (q) drop out in the evaluation of the drag ratio. The theoretical expressions for the drag ratios for the different physical models are summarized in Table 6.1.

Table 6.1. Theoretical expressions for drag ratios using physical models discussed in Section 6.2.2.

Model #	Model Depiction	Particle Shape	Mobility Equation	Drag Coefficient
1		two spheres	Eq. 6.8	$\frac{R_{pro}}{R_{pro} + R_{PEG}}$
2		prolate sphere	Eq. 6.11	$\frac{R_{pro}}{(R_{pro} + R_{PEG}) \left(\frac{2}{3} f_g + \frac{1}{3} f_h \right)}$
3		sphere	Eq. 6.22	$\frac{H(\kappa_2 s) \left(\frac{a}{s} \right) (1 + \kappa_2 a)}{H(\kappa_2 a) \left(\frac{a}{s} \right) (1 + \kappa_2 s)}$
4		sphere	Eq. 6.23	$\frac{H(\kappa s) a}{H(\kappa a) s} e^{-\kappa(a-s)}$

The calculated values of the drag ratio for the different models are plotted in Figure 6.7 as a function of the hydrodynamic radius, as determined from the partition coefficient in size exclusion chromatography along with the corresponding experimental results from Figure 6.6. The radius of the unmodified protein was 1.99 nm and the Debye length in the bulk solution was 3.07 nm as calculated for a 10 mM ionic strength solution.

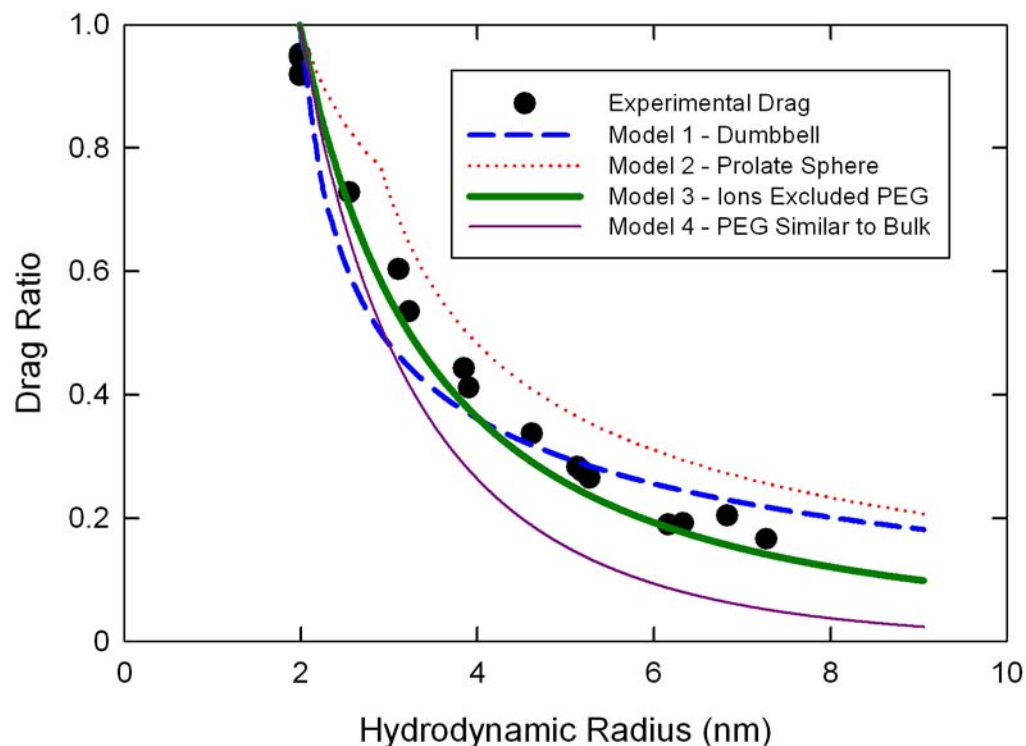


Figure 6.7. Theoretical drag coefficient for PEGylated α -lactalbumin as a function of the PEGylated α -lactalbumin radius. Experimental results are listed for comparison.

The dumbbell model under predicts the experimental data when the PEG is small, but it over predicts the data obtained with large PEG (corresponding to large hydrodynamic radii). The total standard deviation between the experimental data and the model is 0.07. The discrepancies may be due to the inaccurate physical picture of the PEG and protein being attached by a long tether as well as the assumption that the PEG and protein behave as independent spheres with no hydrodynamic interactions. Instead, the fluid flow around the protein is likely to alter the hydrodynamic drag on the PEG and vice versa.

The prolate spheroid model significantly over predicts the drag ratio for all values of the hydrodynamic radius with a total standard deviation from the experimental data of 0.10. The discontinuity in the slope of the model calculations at a hydrodynamic radius of 3.0 nm is due to the evaluation of the effective diameter of the spheroid using the diameter of the protein when the PEG is smaller than the protein and as the diameter of the PEG when the PEG is larger than the protein. In the limit of a very large PEG, the mobility is determined almost entirely by the drag on the PEG, with the predicted drag ratio equal to the value predicted by the dumbbell model (Equation 6.8).

The drag ratio calculated using the composite sphere model in which the Debye length within the PEG layer is the same as that in the bulk solution (Equation 6.23) under predicts the experimental data, suggesting that this model underestimates the electrical force on the PEGylated protein with a total standard deviation of 0.12 compared to the experimental data. In contrast, the model calculations developed in the limit in which the Debye length in the PEG layer is very large are in good agreement with the experimental data over the entire range of hydrodynamic radii (standard deviation of 0.05). This suggests that the polyethylene glycol forms a shell that has a substantially lower ionic strength (larger double layer thickness) than the bulk solution. An analysis of the variance of the model describing the Debye length within the PEG layer as very large (Equation 6.22) compared to the other models, suggests that it is not possible to determine if the dumbbell model (Equation 6.8) is more or less accurate than the model described in Equation 6.22 (within 95% accuracy). In contrast the prolate sphere model (Equation 6.11) and composite sphere model with the Debye length the same as the

Debye length in the bulk (Equation 6.23) do show significant differences compared to the model given by Equation 6.22.

The thermodynamics of PEG-salt systems have been studied quite extensively (Andrews et al., 2005; de Belval et al., 1998; Schmidt et al., 1996; Willauer et al., 2002). These systems tend to phase separate due to the strong "negative" interactions between the salts and the polyethylene glycol. The salt concentration in the PEG phase can be as much as 7 times smaller than the salt concentration in the non-PEG phase (Willauer et al., 2002). Although it is difficult to directly extrapolate these data for PEG-salt systems to the behavior of PEGylated proteins, the results clearly indicate that there may be a significant exclusion of buffer salts from the polyethylene glycol layer in the PEGylated protein.

Figure 6.8 shows the theoretical drag ratio of a PEGylated α -lactalbumin with 20 kDa of PEG as a function κ_2/κ_1 (ratio of the Debye length in the PEG layer to that in the bulk). The results show the drag ratio goes from zero, when the Debye length inside the PEG layer is very small ($\kappa_2/\kappa_1 < 0.1$) to a finite drag ratio associated with an infinitely large Debye length ($\kappa_2/\kappa_1 > 10$). If the salt concentration in the PEG layer is reduced by 7 fold compared to the bulk solution as suggested by Willauer et al. (2002), the ratio of κ_2/κ_1 would be 2.7 and the drag ratio would be 92% of the drag ratio for the 20 kDa PEGylated α -lactalbumin with the salt completely excluded from the PEG layer.

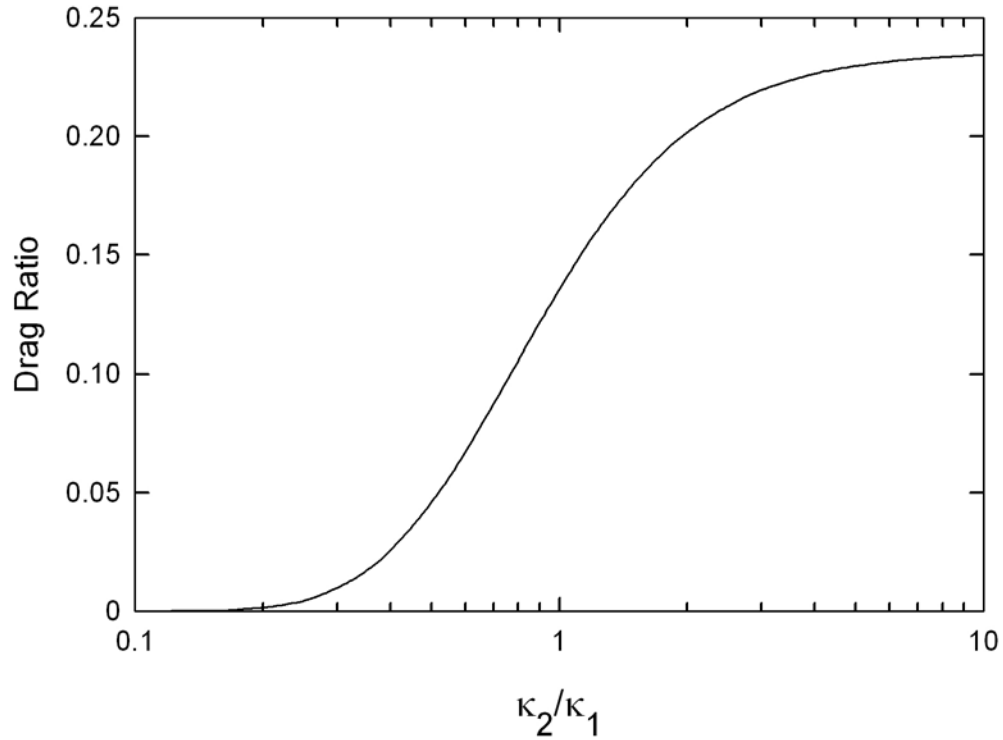


Figure 6.8. Theoretical drag ratio of a 20 kDa PEGylated α -lactalbumin as a function of the κ_2/κ_1 ratio where κ_2 is the inverse Debye length in the bulk fluid and κ_1 is the inverse Debye length in the PEG layer.

6.5 Conclusions

The data presented in this chapter provide an extensive experimental investigation of the use of capillary electrophoresis for the analysis of PEGylated α -lactalbumin. Buffer conditions had a very strong effect on the peak shape and resolution. The use of acetonitrile-water mixtures, as suggested by Li and Su (2004), was largely ineffective for the resolution of PEGylated α -lactalbumin species using a bare fused silica capillary giving very broad and asymmetric peaks. In contrast, the addition of glycine significantly improved the peak symmetry, reduced peak spreading, and increased

resolution between PEGylated species with different numbers of attached polyethylene glycol chains.

PEGylation alters the electrophoretic mobility by increasing the hydrodynamic drag (due to the presence of the PEG chains) and by increasing the net protein charge (through reaction with the $-\text{NH}_2$ of the amino acid lysine). The experimental data for the electrophoretic mobility of the different PEGylated species collapsed to a single curve when plotted as the drag ratio, which is equal to the electrophoretic mobility of the PEGylated α -lactalbumin divided by the mobility of the acetylated protein having the same number of covalently linked lysines. Various models were examined and all showed similar trends to the experimental drag ratio as a function of the hydrodynamic radius. More insight could be obtained into the best possible model by using a larger protein with similar quantities of PEG attached in addition to investigating the effects of salt concentration on the mobility. The experimental drag ratio was best predicted by the model based on Equation 6.22 in which the PEGylated protein was assumed to be a composite sphere with the surface of shear located at the outer radius of the sphere. The electrical potential at the surface of shear was calculated using a simple model in which the Debye length within the PEG layer was very large compared to the Debye length in the bulk solution, with the mobility evaluated using Henry's equation (Equation 6.5). This behavior is consistent with the strong exclusion of charged ions from the polyethylene glycol layer, similar to results reported previously for the thermodynamics of two-phase aqueous systems composed of PEG and salt. This phenomenon could have important implications for understanding the transport and separation characteristics of

PEGylated proteins. Additional studies will be needed to fully characterize this salt partitioning phenomenon and its effect on the physical properties of PEGylated proteins.

Chapter 7

ULTRAFILTRATION CHARACTERISTICS OF PEGYLATED PROTEINS

7.1 Introduction

Ultrafiltration is a potentially attractive alternative to chromatography for the purification of PEGylated proteins. Previous studies comparing ultrafiltration and size exclusion chromatography for concentration and buffer exchange of therapeutic proteins have clearly demonstrated the advantages of using ultrafiltration in terms of both cost and throughput (Kurnik et al., 1995). Previous studies by Edwards et al. (2003) reported limited data on the ultrafiltration of PEGylated soluble Tumor Necrosis Factor Receptor Type I, but there have been no prior quantitative studies examining the detailed transport behavior of PEGylated proteins in ultrafiltration or the potential use of membrane systems for the purification of desired PEGylated products.

This chapter examines the ultrafiltration characteristics of a series of PEGylated proteins with different degrees of PEGylation with the goal of understanding the effects of PEGylation on the protein transmission through semipermeable ultrafiltration membrane. Sieving data were obtained over a range of filtrate flux to examine possible effects of flow-induced elongation on transmission. Results were compared with available theoretical models for the ultrafiltration of hard sphere solutes, with deviations between theory and data analyzed using available models for the transport of flexible polymers during ultrafiltration. The sieving coefficients of the PEGylated proteins

depend not only on the protein size and the total molecular weight of the polyethylene glycol but also on the number and configuration of the polyethylene glycol chains. This is in sharp contrast to the results shown in Chapter 5 in which the partition coefficient in size exclusion chromatography was uniquely determined by the total molecular weight of the polyethylene glycol and protein, independent of the number of PEG chains linked to the protein. These results provide important insights into the physical phenomena governing the ultrafiltration of PEGylated proteins, including the role of macromolecule deformation and / or elongation on the sieving characteristics.

7.2 Materials and Methods

7.2.1 Protein PEGylation

The proteins used in this study included ovalbumin, α -lactalbumin, and bovine serum albumin (BSA), all obtained from Sigma Chemical (St. Louis, MO). Active PEG, in this case, mPEG-SPA or mPEG-SMB with 5 kDa, 10 kDa, and 20 kDa molecular weight, were obtained from Nektar Therapeutics (Huntsville, AL). More information about the proteins and PEG are given in Chapter 3. The PEGylation reactions and ultrafiltration experiments were performed in phosphate buffered saline (PBS) or Tris-EDTA (TE), both at pH 7 and 10 mM total ionic strength. PEGylation reactions were performed using 15 g/L solutions of mPEG-SPA or mPEG-SMB. The molar ratio of mPEG-SPA or mPEG-SMB to protein used in this PEGylation reaction was five to one for the 5 kDa and 10 kDa activated PEG and two to one for the 20 kDa activated PEG. After the reaction was complete the samples were diluted using the desired buffer in a three to one ratio. Additional (unreacted) protein and native (not activated) PEG were

added to the final reaction mixture at a concentration of approximately 3 g/L to allow accurate detection of the protein and PEG in the experiments. The ionic strength was adjusted to 0.15 M by the addition of NaCl after completion of the reaction unless otherwise noted. More details on the PEGylation reaction procedures are given in Chapters 3 and 4.

7.2.2 Ultrafiltration

Ultrafiltration experiments were performed using composite regenerated cellulose Ultracel™ membranes with nominal molecular weight cut-offs of 30 and 100 kDa (Millipore Corp., Bedford, MA). The membrane hydraulic permeability (L_p) was evaluated using Equation 2.8 by measuring the flux of a 150 mM ionic strength PBS or 150 mM TE buffer as a function of transmembrane pressure. The clean Ultracel™ 30 kDa membranes had an average permeability of $(0.60 \pm 0.06) \times 10^{-12}$ m while the clean Ultracel™ 100 kDa membranes had an average permeability of $(2.4 \pm 0.1) \times 10^{-12}$ m. After evaluating the permeability, the stirred cell was filled with a PEGylated protein solution and allowed to sit overnight to ensure equilibrium adsorption. Sieving experiments were performed as described in Section 3.2. The stirring speed, ω , was set to 600 rpm or 1200 rpm depending on the experiment. Samples were analyzed using size exclusion chromatography as reported in Section 3.3. The minimum measurable concentration was 0.02 g/L for the PEG component and 0.002 g/L for the protein component.

7.3 Results

7.3.1 Observed Sieving Behavior

Figure 7.1 shows experimental data for the observed sieving coefficients, defined as the ratio of the solute concentration in the filtrate solution (C_f) to that in the bulk feed (C_b), for a series of PEG molecules with molecular weight ranging from 5 to 35 kDa, for the globular proteins: α -lactalbumin, ovalbumin, and BSA, and for several different PEGylated species generated from reaction of α -lactalbumin (upper panel) or ovalbumin (lower panel) with 5 kDa or 10 kDa mPEG-SPA. The data are plotted as the mean value of the sieving coefficients determined from at least three repeat measurements using different membranes from the same lot, with the error bars representing the calculated values of the standard deviation. All data were obtained at a flux of 13.6 $\mu\text{m/s}$ (50 $\text{L/m}^2/\text{hr}$) using a 0.15 M ionic strength PBS buffer to minimize any electrostatic interactions. The molecular weights of the pure PEG and the various proteins were provided by the manufacturer. The molecular weights of the PEGylated proteins were determined by the sum of the molecular weights of the PEG and protein components after subtracting off the molecular weight of the N-hydroxyl succinimide released as a reaction by-product.

The sieving coefficients for each class of molecules decrease with increasing molecular weight as expected, although the dependence on molecular weight is very different for the PEG, the unmodified proteins, and the PEGylated species. The sieving coefficient at a given molecular weight is greatest for the globular proteins and smallest for the PEG, with the sieving coefficients for the PEGylated proteins lying between these values. These differences in sieving coefficients reflect the different conformations of

the PEG and proteins in solution, with the PEG behaving as a random coil with a larger specific molar volume and radius of gyration than a globular protein of the same molecular weight (Hellberg et al., 1996; Kunitani et al., 1991). The addition of the PEG chains to the globular protein causes a large reduction in the protein sieving coefficient. For example, the observed sieving coefficient for the ovalbumin was more than three times as large as the sieving coefficient of the ovalbumin with one 5 kDa PEG group attached even though these species differ in molecular weight by only 12%.

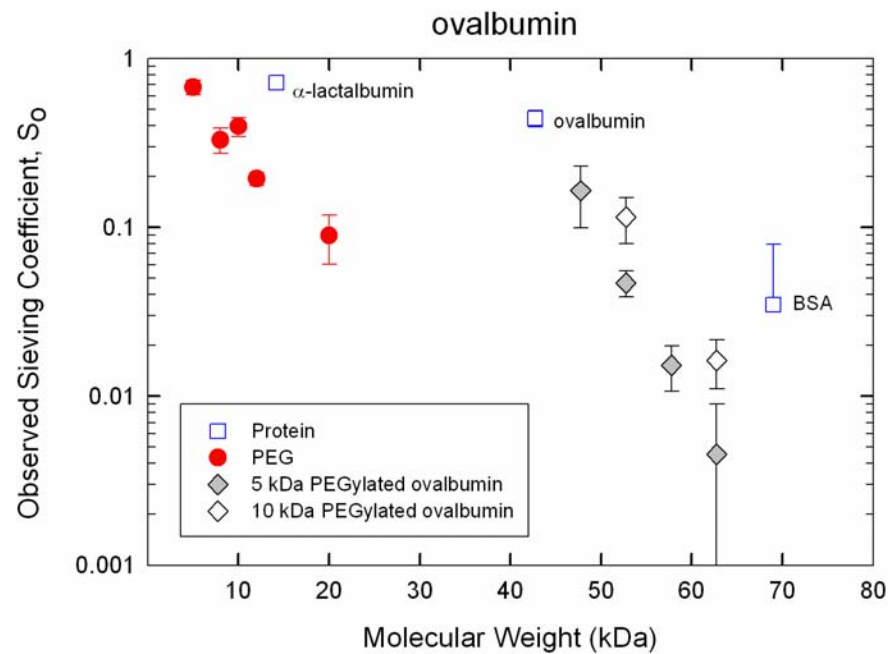
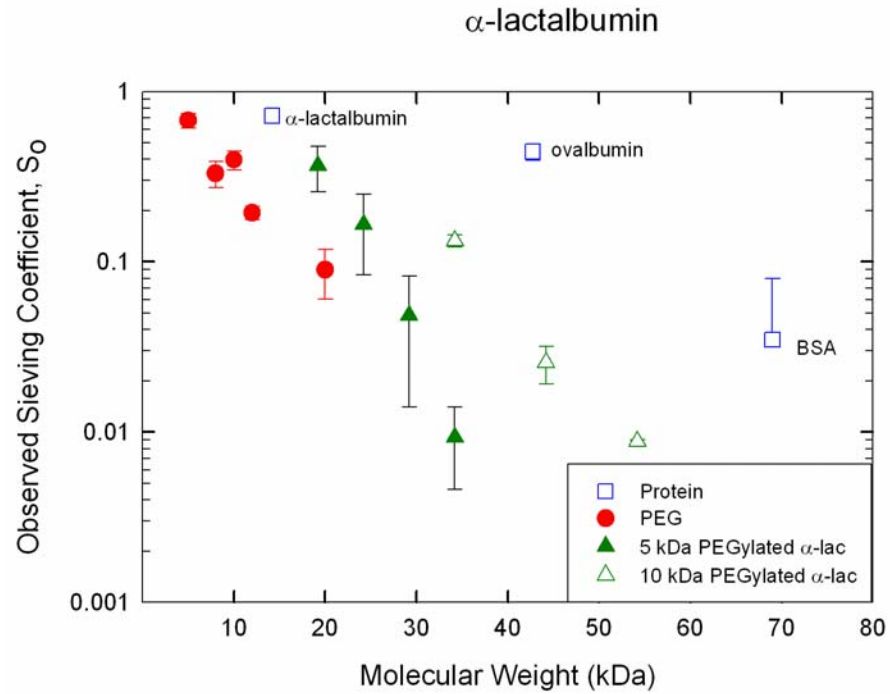


Figure 7.1. The observed sieving coefficient of PEG, protein, and PEGylated proteins as a function of the molecular weight. The upper panel shows the sieving data for PEGylated α -lactalbumin (5 kDa and 10 kDa series) and the lower panel shows the sieving data for PEGylated ovalbumin (5 kDa and 10 kDa series). Error bars represent plus/minus one standard deviation for at least three repeat experiments.

The observed sieving coefficient data from Figure 7.1 are replotted in Figure 7.2 as a function of the effective solute radius as determined from the measured retention volume in size exclusion chromatography (data from Chapter 5). Plotting the data as a function of the effective radius tends to collapse the results to some extent, although there are still significant differences between results for the PEG, proteins, and PEGylated proteins. For example, the 10 kDa polyethylene glycol, the unmodified BSA, and the PEGylated ovalbumin with a 5 kDa PEG chain all have a hydrodynamic radius of approximately 3.3 nm as determined by SEC, but the observed sieving coefficients for these species vary by a factor of ten from approximately 0.003 for the BSA to 0.03 for the PEG alone. These results clearly indicate that there are fundamental differences in the phenomena controlling the partitioning behavior in SEC and the sieving behavior in ultrafiltration.

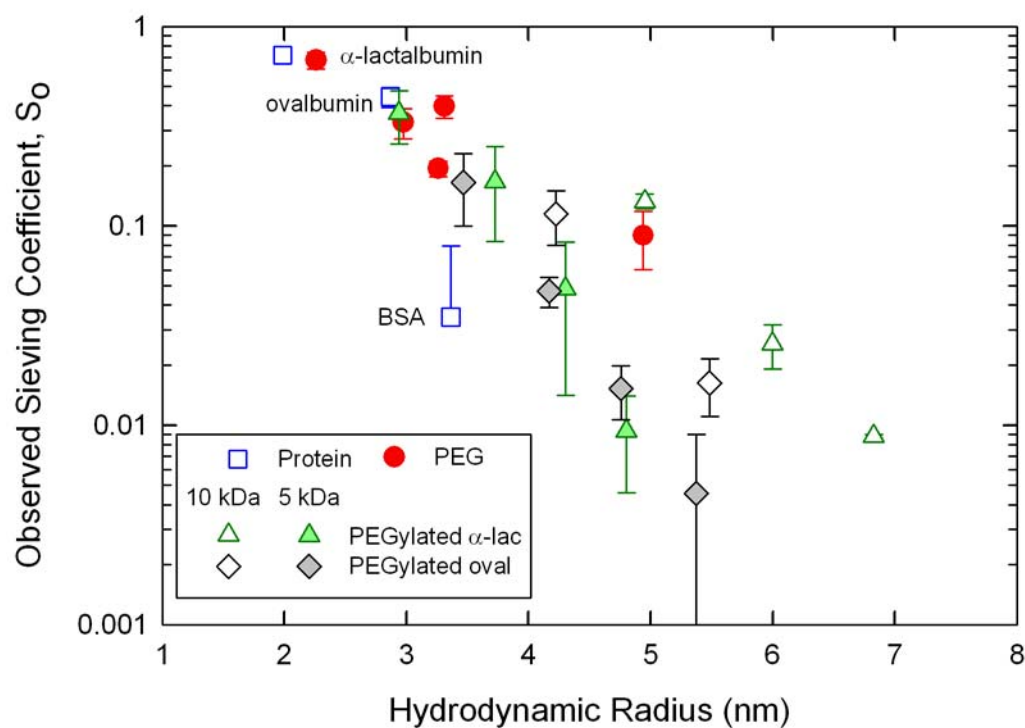


Figure 7.2. The observed sieving coefficient as a function of the effective radius determined by SEC for PEG, globular proteins, and PEGylated proteins. Error bars represent plus/minus one standard deviation for at least three repeat experiments.

7.3.2 Comparison of Different PEG Configurations

Figure 7.3 compares the sieving coefficients of PEGylated α -lactalbumin (upper panel) and ovalbumin (lower panel) produced by covalent attachment of either the 5 kDa or 10 kDa mPEG-SPA, again at a constant flux of 13.8 $\mu\text{m/s}$. In each case, the sieving coefficients of the PEGylated proteins produced from the 10 kDa mPEG-SPA, which have fewer branches for the same total molecular weight, are considerably greater than the sieving coefficients of the PEGylated proteins generated using the 5 kDa mPEG-SPA. For example the PEGylated α -lactalbumin molecule with four 5 kDa branches has an

observed sieving coefficient of 0.01 while the PEGylated α -lactalbumin with two 10 kDa branches has an observed sieving coefficient of 0.13 even though these molecules have nearly identical amounts of protein and PEG and nearly identical partition coefficients based on SEC measurements. Similar results were obtained with the PEGylated ovalbumin, although the magnitude of the difference in sieving coefficients was smaller. This is consistent with the smaller contribution of the PEG chains to the sieving behavior of the larger ovalbumin. These data clearly demonstrate that the configuration of the PEGylated proteins, in this case the number of branches of PEG, and not just the total molecular weight of the added PEG, is an important factor governing the sieving behavior during ultrafiltration. This is discussed in more detail subsequently.

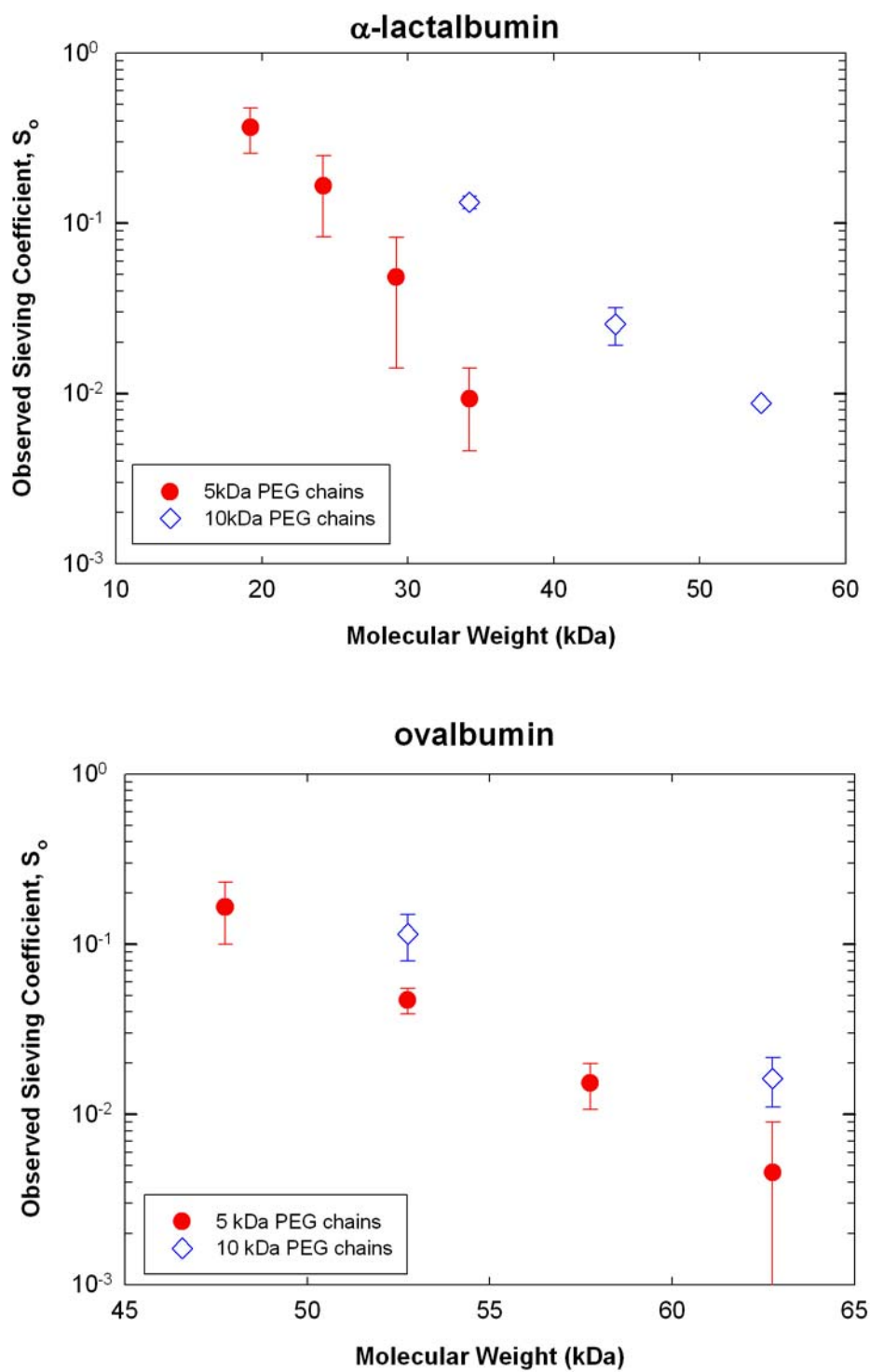


Figure 7.3. The observed sieving coefficient as a function of molecular weight for PEGylated α -lactalbumin (upper panel) and ovalbumin (lower panel) formed using 10 kDa and 5 kDa mPEG-SPA. Error bars represent plus/minus one standard deviation for at least three repeat experiments.

7.3.3 Stagnant Film Model Calculations

One major factor affecting the observed sieving coefficients during ultrafiltration is concentration polarization in the stirred cell. PEGylation changes the degree of concentration polarization due to the change in the bulk diffusion coefficient associated with the increased size of the PEGylated proteins. The effect of concentration polarization in the stirred cell was estimated using the stagnant film model as discussed in Chapter 2 (Zeman and Zydney, 1996). The diffusion coefficients of the PEGylated proteins were calculated using the Stokes-Einstein equation assuming that the hydrodynamic radius R_h of the molecule was equivalent to the experimentally determined radius using SEC.

Figure 7.4 shows the effects of filtrate flux on the observed sieving coefficients of ovalbumin, the 5 kDa PEG, and ovalbumin PEGylated with either one, two, or three 5 kDa PEG chains. In each case, data are shown from 2-4 replicated experiments. The error bars in the x-direction represent the standard deviation in the flux values between experiments while those in the y-direction represent the standard deviation in the observed sieving coefficient. The observed sieving coefficient increases with increasing filtrate flux, consistent with predictions of the classical concentration polarization model. The increase in sieving coefficient for the PEGylated proteins is somewhat greater than that for the ovalbumin and PEG due to the smaller value of the mass transfer coefficient for the larger PEGylated proteins.

The solid curves in Figure 7.4 are model calculations developed using Equations 2.3 - 2.5 with the best fit value of S_a for each species determined by minimizing the sum of the squared residuals between the model and the data. The values of S_a and k_m for the

PEGylated proteins, ovalbumin and 5 kDa PEG are given in Table 7.1. Calculations were performed using a stirring speed of $\omega = 600$ rpm, $\eta = 0.915$ cP, $d = 0.567$, and $A = 0.23$, $b = 1.14$ cm with the hydrodynamic radius of the solutes determined by SEC. For all five molecules, the model calculations properly capture the increase in the observed sieving coefficient with increasing filtrate flux. An analysis of variance of the data suggests that the models are significant ($> 95\%$) for all sets of data and there are no significant “left out terms” for the PEGylated protein models.

Table 7.1. Mass transfer coefficient (k_m) and actual sieving coefficients (S_a) of ovalbumin, PEG, and PEGylated forms of ovalbumin through a 30 kDa Ultracel™ membrane.

Compound	k_m ($\mu\text{m/s}$)	S_a
Ovalbumin	8.21	0.116
5 kDa PEG	9.42	0.379
1 – 5 kDa PEGylated	6.65	0.016
2 – 5 kDa PEGylated	6.01	0.004
3 – 5 kDa PEGylated	5.51	0.001

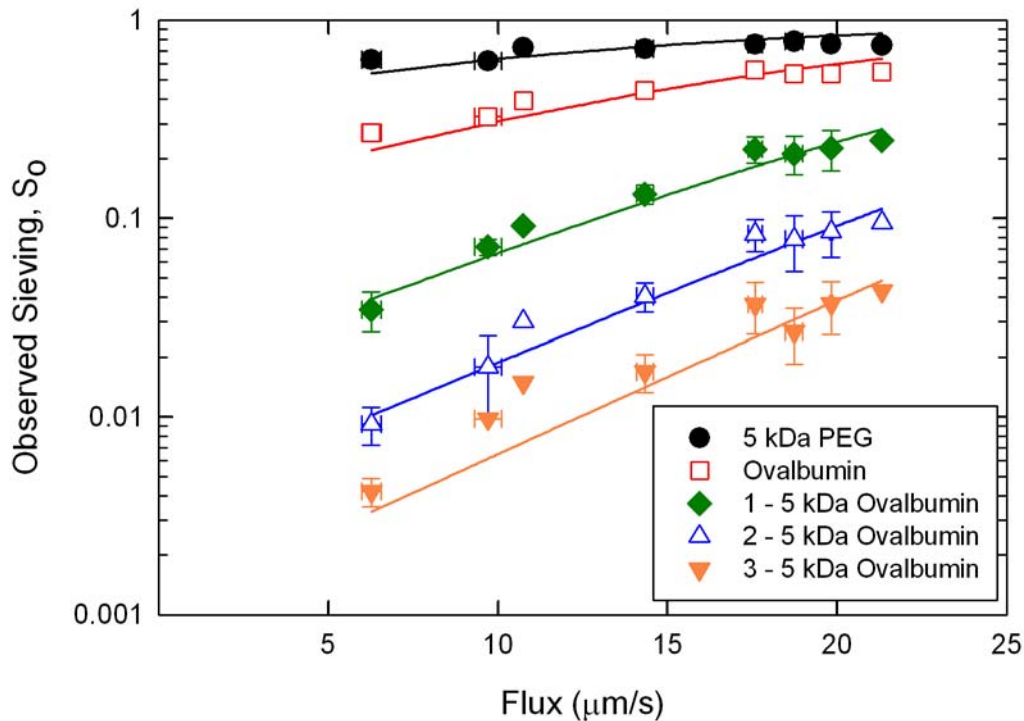


Figure 7.4. Observed sieving coefficient as a function of flux for ovalbumin and PEGylated forms of ovalbumin with 5 kDa PEG branches. Curves are model calculations using the stagnant film theory with best fit values of the actual sieving coefficient given in Table 7.1. Error bars represent plus/minus one standard deviation for at least three repeat experiments.

7.3.4 Model Calculations for a Hard Sphere

The effects of the number and size of the PEG chains on the actual sieving coefficients of the PEGylated α -lactalbumins are examined in Figure 7.5. Results are shown for PEGylated α -lactalbumin with one to four 5 kDa PEG chains and two to four 10 kDa PEG chains through the 30 kDa UltracelTM membrane. Also shown for comparison are data for a series of native (un-PEGylated) proteins: α -lactalbumin, ovalbumin, and bovine serum albumin through the same pore size membrane. In each case, the actual sieving coefficients were determined by fitting the observed sieving

coefficient data to the concentration polarization model as discussed in the previous section. The data are plotted as a function of the effective hydrodynamic radius with the radius of the PEGylated proteins calculated using Equations 5.8 and 5.10. The actual sieving coefficients decrease with increasing effective radius as expected, but the data for PEGylated α -lactalbumins lie uniformly above those for the unmodified proteins, with this discrepancy being most pronounced for the α -lactalbumin PEGylated with the 10 kDa mPEG-SPA.

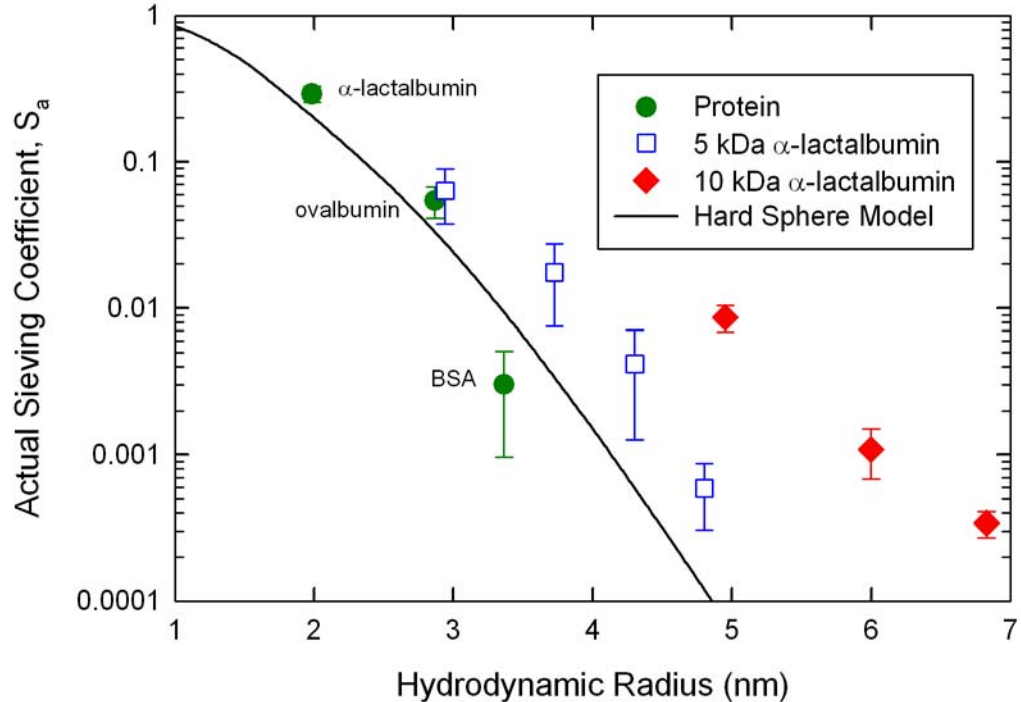


Figure 7.5. Actual sieving coefficient through the 30 kDa Ultracel™ membrane for PEGylated α -lactalbumin formed with 5 kDa and 10 kDa PEG chains. Data for a series of globular proteins, α -lactalbumin, ovalbumin, and bovine serum albumin, are shown for comparison. Results are plotted as a function of the effective radius determined by size exclusion chromatography. Error bars represent plus/minus one standard deviation for at least three repeat experiments.

The solid curve in Figure 7.5 represents the predicted values of the actual sieving coefficient determined using Equations 2.19 – 2.39 for the transport of a hard spherical particle through a cylindrical pore accounting for the effects of convection and diffusion. Electrostatic effects were considered to be negligible. See Sections 2.4 and 2.5 for more details on the theoretical development. Calculations were performed assuming a log-normal pore size distribution with the best fit value of the mean pore size ($\bar{r} = 2.7$ nm) determined by minimizing the sum of the squared residuals between the model and data for the proteins assuming a coefficient of variation of $\sigma/\bar{r} = 0.20$ based on previous studies of the pore size distribution of ultrafiltration membranes (Mehta and Zydney, 2005; Zeman and Zydney, 1996). The fitted pore size distribution was consistent with experimental measurements of the clean membrane permeability, with the calculated value of the permeability using Equation 2.56 within 10 % of the experimental value assuming a membrane thickness of $\delta_m = 1.0$ μm and a porosity of $\varepsilon = 0.5$.

The model is in excellent agreement with the experimental data for α -lactalbumin and ovalbumin, but it over predicts the results for BSA, which may reflect some degree of fouling with this larger protein (Pujar and Zydney, 1998). In contrast, the actual sieving coefficients for the PEGylated proteins were uniformly larger than the model calculations. This was especially true for the 10 kDa PEGylated proteins. For example an α -lactalbumin molecule with one 10 kDa PEG group had a sieving coefficient that was an order of magnitude higher than that of the PEGylated α -lactalbumin molecule with two 5 kDa PEG groups and more than 100 times larger than the model calculation. In addition, the sieving coefficient of immunoglobulin G, a globular protein with approximately the same effective size as the PEGylated α -lactalbumin with 10 kDa of

attached PEG (as determined by SEC), was undetectable under these conditions ($S_0 < 0.01$). These results provide clear evidence that the PEGylated α -lactalbumin behaves as a smaller species during ultrafiltration compared to what would be expected from the partitioning behavior in size exclusion chromatography.

7.3.5 Deviations from the Stagnant Film Model

Figure 7.6 and Figure 7.7 show the observed sieving coefficients of PEGylated α -lactalbumin with 20 kDa of total attached PEG using either four 5 kDa PEG chains, two 10 kDa PEG chains, or a single 20 kDa PEG. The data in Chapter 5 demonstrated that PEGylated proteins having different size PEG chains, but with the same total molecular weight, have identical sizes as determined by size exclusion chromatography, consistent with results presented by Fee (2007). For example, the PEGylated α -lactalbumin with four 5 kDa PEG chains has $R_{\text{eff}} = 5.3$ nm compared to $R_{\text{eff}} = 5.2$ nm for the PEGylated protein with one 20 kDa PEG chain as determined by SEC; this 1% difference in radius is due to the very small difference in total molecular weight of the attached PEG groups (21.0 kDa versus 20.7 kDa) associated with the slight variations in molecular weight of the mPEG-SPA used to form the PEGylated proteins.

Figure 7.6 shows data for α -lactalbumin with four 5 kDa PEG chains and two 10 kDa PEG chains using a 150 mM phosphate buffer with a 30 kDa membrane at a stirring speed of 600 rpm. The error bars represent the standard deviation in these replicated measurements. The sieving coefficients of both PEGylated proteins increase with increasing filtrate flux, however the effect is much more pronounced for the α -lactalbumin with two 10 kDa PEG chains. At very low filtration fluxes (below

6 $\mu\text{m/s}$), the observed sieving coefficients for both proteins are below 0.005. However, at a filtrate flux of 15.5 $\mu\text{m/s}$, the observed sieving coefficient of the PEGylated α -lactalbumin with two 10 kDa PEG chain has increased to nearly $S_o = 0.2$, which is an order of magnitude larger than the sieving coefficient for the PEGylated protein with four 5 kDa PEG chains.

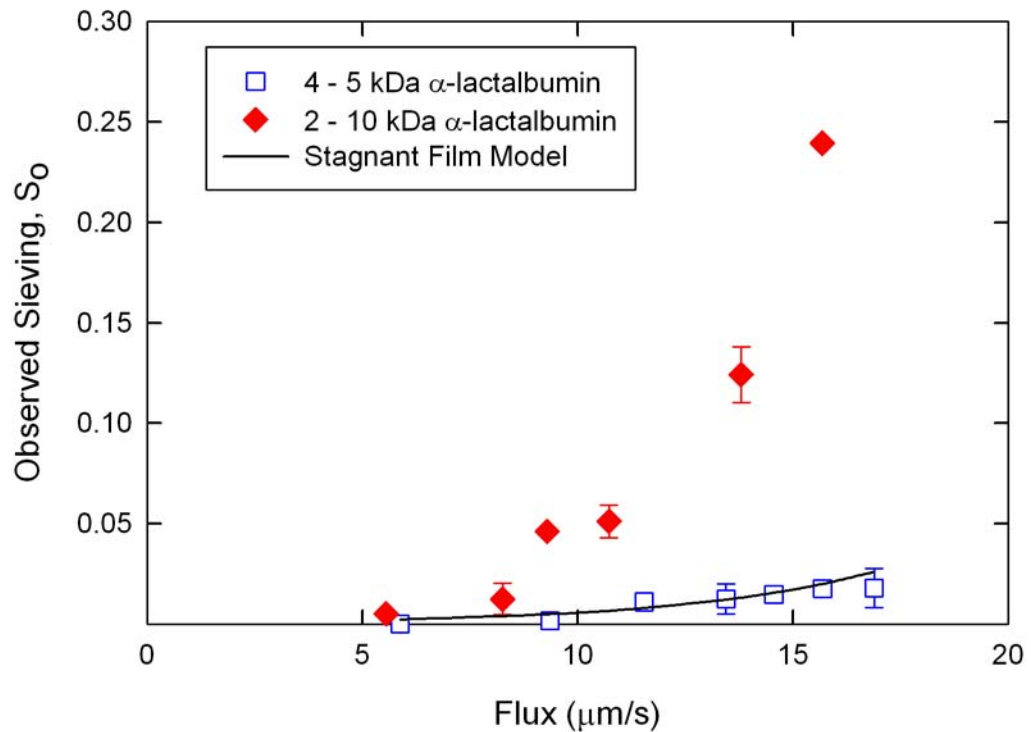


Figure 7.6. Observed sieving coefficient of PEGylated α -lactalbumin with four 5 kDa PEG and two 10 kDa PEG chains through an Ultracel™ 30 kDa membrane at a stirring speed of 600 rpm. The solid curve is the model calculation as described in the text. Error bars represent plus/minus one standard deviation for the experimental data.

The solid curve in Figure 7.6 represents the calculated values of the observed sieving coefficient using the stagnant film model (Equation 2.3) with a mass transfer coefficient of 4.5 $\mu\text{m/s}$ as calculated from Equations 2.4 and 2.5 using a hydrodynamic

radius for the PEGylated protein of 5.2 nm. The actual sieving coefficient was evaluated using the hydrodynamic models described by Equations 2.19-2.39 using the best fit parameters for the membrane determine for the protein data in Figure 7.5. The model calculations are in good agreement with the data for the PEGylated α -lactalbumin with four 5 kDa PEG chains, but dramatically under-predict the results for the PEGylated protein with two 10 kDa PEG chains even though these species have identical size (as determined by SEC) and should thus have very similar diffusivities and mass transfer coefficients.

Figure 7.7 shows corresponding data for the PEGylated α -lactalbumin with four 5 kDa PEG chains and with one 20 kDa PEG chain, in this case obtained using two separate 100 kDa UltracelTM membranes, both cut from a single flat sheet of membrane. At low filtrate flux, the sieving coefficients of the two PEGylated proteins are similar, with $S_o \approx 0.1$ at a filtrate flux of 7 $\mu\text{m/s}$, which is consistent with the very similar values of the effective hydrodynamic radii of the PEGylated proteins. The observed sieving coefficients increase with increasing filtrate flux for both proteins, with the magnitude of this increase being much more pronounced for the protein with one 20 kDa PEG chain. Thus, at a filtrate flux of 30 $\mu\text{m/s}$ the sieving coefficient of the PEGylated α -lactalbumin with one 20 kDa PEG chain is almost twice as large as that for the PEGylated protein with four 5 kDa PEG chains.

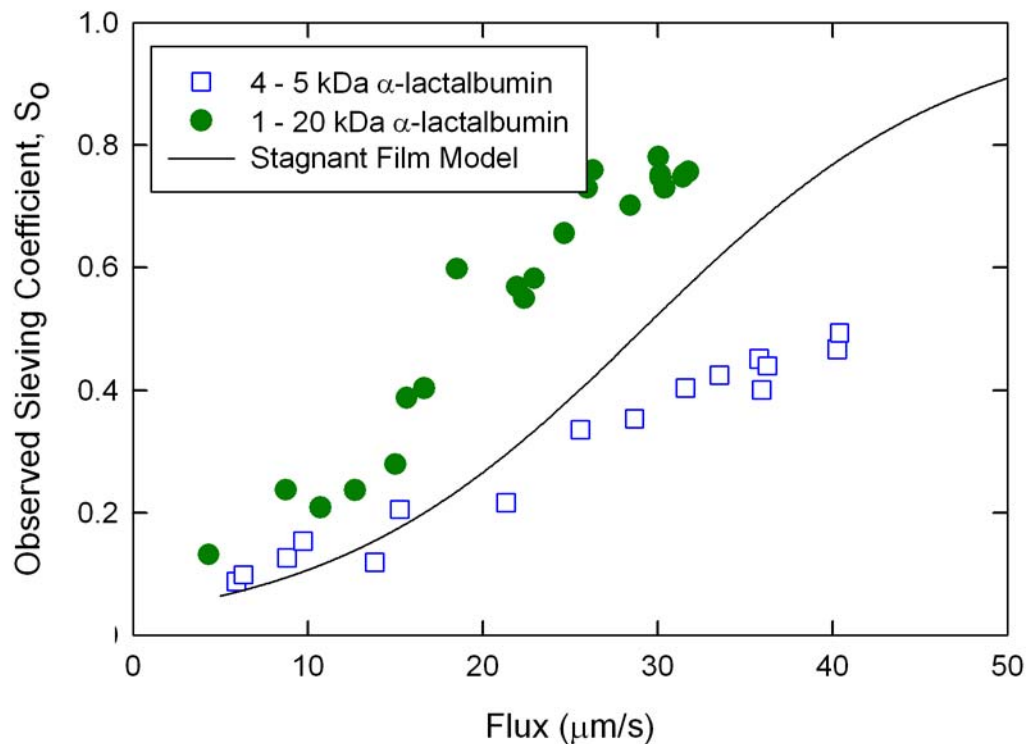


Figure 7.7. Observed sieving coefficients of PEGylated α -lactalbumin with four 5 kDa PEG chains and one 20 kDa PEG chain through an Ultracel™ 100 kDa membrane at a stirring speed of 1200 rpm. The solid curve is the model calculation as described in the text.

The solid curve in Figure 7.7 represents calculations from the stagnant film model, with the mass transfer coefficient calculated as $k_m = 9.0 \mu\text{m/s}$ using Equations 2.4 and 2.5 with $Re = 22,000$ at a stirring speed of 1200 rpm (compared to 600 rpm in Figure 7.6), $d = 0.59$, and $A = 0.285$ based on the correlations presented by Colton (1969). The mass transfer coefficient is larger for this experiment than for the experiment in Figure 7.6, consistent with the higher stirring speed (1200 rpm versus 600 rpm). The best fit value of the actual sieving coefficient was $S_a = 0.038$ as determined by minimizing the sum of the squared residuals for the fluxes below $25 \mu\text{m/s}$

using data for the PEGylated α -lactalbumin with four 5 kDa PEG chains. The model is in good agreement with the data at filtrate flux below about 25 $\mu\text{m/s}$; the discrepancies at higher flux may be due to fouling effects under these conditions. The model significantly under predicts the observed sieving coefficient data for the PEGylated α -lactalbumin with one 20 kDa PEG chain, particularly at high filtrate flux.

The observed sieving coefficient data in Figure 7.6 and 7.7 clearly indicate that the PEGylated proteins having only a single long PEG chain have a greater flux dependence than that predicted by the classical concentration polarization model. This effect could be due to the elongation of the PEG chain at high filtrate flux, which would reduce the effective size of the PEGylated protein and increase its transmission through the ultrafiltration membrane. This effect would not be seen at low filtrate flux where the hydrodynamic forces on the PEG are insufficient to elongate the polyethylene glycol chain. This phenomenon is discussed in more detail in the next two sections.

7.3.6 Scaled Sieving Coefficient

The experimental data in Figure 7.6 and 7.7 have been re-plotted in Figure 7.8 as the scaled sieving coefficient (χ):

$$\chi = \frac{S_o - S_1}{S_2 - S_1} \quad (7.1)$$

S_1 is defined as the observed sieving coefficient for an undeformed protein at the same flux, which was evaluated directly from the model calculations (solid curve) in Figure 7.6 and Figure 7.7. S_2 is defined as the observed sieving coefficient for the PEGylated protein with a fully elongated PEG chain. Experimentally, S_2 is taken as the sieving

coefficient of the native protein which assumes that the fully elongated PEG chain has no influence on the protein transmission. Thus, a scaled sieving coefficient of unity ($\chi = 1$) indicates that the PEGylated protein behaves as if the PEG has no effect on the overall size of the molecule, with the observed sieving coefficient determined entirely by the protein. A scaled sieving coefficient of zero ($\chi = 0$) indicates that the molecule behaves as a hard sphere with an effective radius equal to that of the PEGylated protein as determined by SEC. The scaled sieving coefficients for the PEGylated α -lactalbumin with 10 or 20 kDa PEG chains increase with increasing flux, consistent with the elongation of the PEG associated with the fluid flow. The data for the PEGylated proteins with 10 and 20 kDa PEG nearly collapse to a single curve when plotted in this manner, even though the experiments were performed with different molecular weight cut-off membranes having very different absolute sieving coefficients. The scaled sieving coefficient for the PEGylated α -lactalbumin with four 5 kDa chains stays nearly constant at zero for all fluxes tested, suggesting that the smaller PEG chains do not elongate under these conditions.

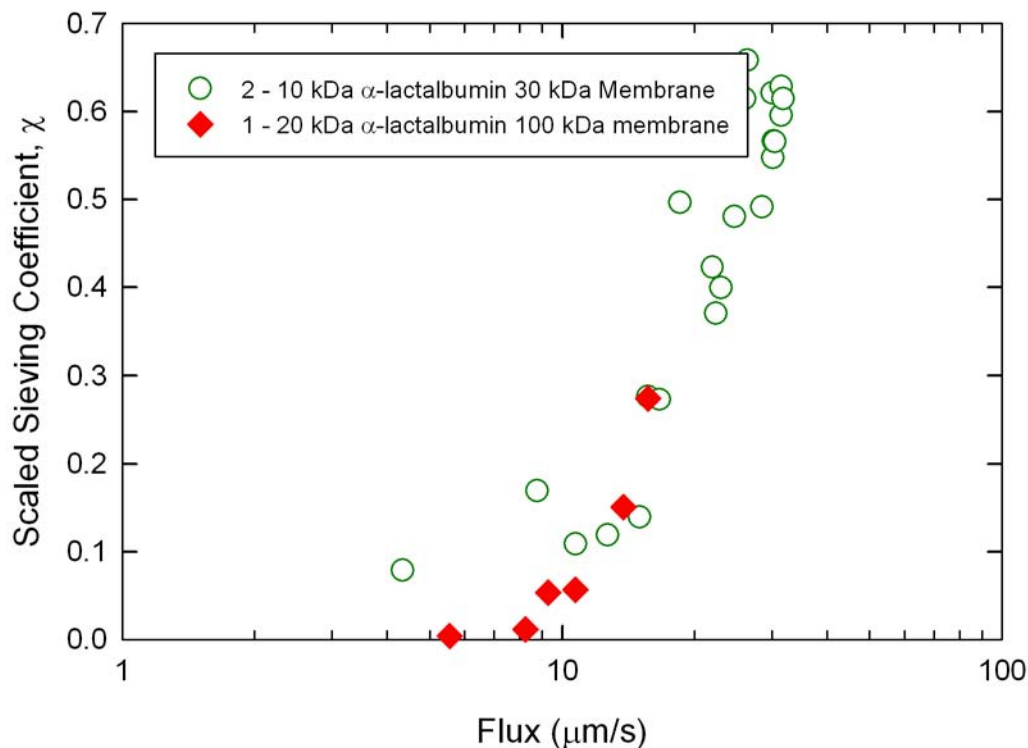


Figure 7.8. Scaled sieving coefficient as a function of flux for PEGylated α -lactalbumin. Data for the protein with two 10 kDa PEGylated samples were obtained using a 30 kDa UltracelTM membrane while that with one 20 kDa PEG was obtained using a 100 kDa UltracelTM membrane.

7.3.7 Deborah Number

In a good solvent, PEG is often described as an "ideal" flexible molecule (Long and Anderson, 1984). As discussed previously, the sieving characteristics of the PEGylated proteins having only a single long PEG chain may be strongly influenced by the flow-induced elongation of the PEG in the vicinity of the pore entrance. The degree of flow-induced deformation is typically characterized in terms of the Deborah number (De) as discussed in Chapter 2. The Deborah number for the PEGylated protein was calculated using the radius of gyration of the PEG in a good solvent, which implicitly

assumes that the elongation of the PEG chain is unaffected by the covalent attachment to the protein. Nguyen and Neel (1983) showed that the relaxation of PEG in a good solvent is well described by the Zimm equation; thus, Equation 2.62 was used to evaluate the relaxation time. The radius of gyration of the PEG chain was determined to be 1.5 times the hydrodynamic radius based on a correlation presented by Kok and Rudin (1981) for linear polyethylene glycol in a good solvent. This gives $R_G = 7.3$ nm for the 20 kDa PEG. The characteristic time for the fluid flow was calculated as the reciprocal of the shear rate as given by Equation 2.61. The mean pore size of the 100 kDa membrane was calculated to be 6.0 nm and the mean pore size of the 30 kDa membrane was calculated to be 2.7 nm based on the measured values of the hydraulic permeability assuming a log-normal pore size distribution with the ratio of the standard deviation to mean pore size equal to 0.20.

The value of the critical Deborah number for the PEGylated protein, defined as the value of De corresponding to $\chi = 0.2$ in Figure 7.8, is approximately 9×10^{-4} for the 10 kDa PEGylated α -lactalbumin using the 30 kDa membrane and 4×10^{-4} for the 20 kDa PEGylated α -lactalbumin using the 100 kDa membrane. These values are much smaller than the typical assumption that elongation becomes significant when $De_{crit} \approx 1$, although there is clear evidence in the literature for significant polymer elongation at $De = 0.05$ (Long and Anderson, 1984; Zeman and Wales, 1981). In addition, Latulippe et al. (2007) found values of De_{crit} around 10^{-3} for the ultrafiltration of plasmid DNA through the same UltracelTM membranes used in this study.

Daoudi and Brochard (1978) hypothesized that there was a sharp transition in polymer transmission at a critical value of the filtrate flux corresponding to a Deborah

number of approximately one. This type of sharp transition has been experimentally observed using a special double-layer membrane that minimized interactions between the flow-fields of adjacent pores (Jin and Wu, 2006). In contrast, Keh (1984) predicted a gradual transition in polymer transmission with increasing filtrate flux. This behavior is consistent with experimental data for polystyrene transmission through both track-etch (Long and Anderson, 1984) and immersion-cast (Beerlage et al., 1996) ultrafiltration membranes. A similar gradual increase in transmission was seen by Latulippe et al. (2007) for ultrafiltration of plasmid DNA, although they attributed this effect to the distributions in membrane pore size and plasmid morphology.

In contrast to these studies of very large polymers, there has been relatively little work on the effects of flow-induced deformation on the ultrafiltration of flexible polymers that are smaller than the membrane pore radius such as the ultrafiltration of PEGylated proteins through the 30 and 100 kDa UltracelTM membranes examined in this thesis. Long and Anderson (1984) obtained data for polystyrene transmission through track-etched membranes with pores that were slightly larger than the radius of gyration of the polymer and found clear deviations from the classical hard-sphere theory when $De \geq 0.1$. However, there was no attempt to develop a quantitative model for polymer transmission under these conditions.

There are several possible explanations for the very small values of the critical Deborah number seen with the PEGylated proteins. First, the critical distance above the membrane pore was set equal to the mean pore radius, which completely neglects the effect of the α -lactalbumin and the detailed geometry of the PEGylated protein. The data in Figure 7.8 would be shifted to much larger Deborah numbers if the calculations had

been performed using a smaller value of the critical distance. Second, the concentration of PEGylated protein at the membrane surface can be quite large due to concentration polarization effects, which would significantly alter both the solution viscosity and the PEG relaxation time, with the latter effect becoming very large when the local concentration exceeds the polymer overlap concentration (Odell et al., 1985). There could also be a significant viscosity difference between the solution immediately upstream of the membrane and that inside of the pore, which would tend to enhance polymer elongation (Chauveteau, 1982). The analysis also neglects the distribution of pore sizes in the Ultracel™ membrane. Finally, the small value of De_{crit} for the PEGylated protein could be directly associated with the covalent attachment of the PEG chain to the α -lactalbumin. Perkins et al. (1997) showed that attachment of a 144 kbp linear DNA to a 0.3 μm rigid bead significantly increased the relaxation time of the DNA due to the restricted motion of the attached end. A similar phenomenon with the PEG chains would cause a shift in the Deborah numbers for the PEGylated proteins, although it is unlikely that this would cause a 3-4 order of magnitude shift in De . It is also possible that the hydrodynamic drag on the α -lactalbumin causes a preferential orientation of the PEGylated protein potentially increasing the extent of elongation of the PEG chain.

7.4 Conclusions

This chapter provides the first quantitative results for the effects of the number and size of the polyethylene glycol chains on the sieving coefficients of different PEGylated proteins. The results clearly demonstrate that PEGylation reduces the sieving coefficient due to the increase in the effective protein size. At low filtrate flux, the

observed sieving coefficient was determined by the size of the base protein and the total molecular weight of the attached PEG, independent of the number of PEG chains, similar to the behavior seen previously for the partition coefficient in size exclusion chromatography. Under these conditions, the PEGylated protein appears to behave as an effective hard sphere, with the measured sieving coefficients in good agreement with model calculations using the effective size determined by SEC.

In contrast to the behavior at low filtrate flux, the observed sieving coefficients at high flux depend on the number of attached PEG chains (in addition to the total molecular weight of the attached PEG). For example, the observed sieving coefficient for the PEGylated α -lactalbumin with four 5 kDa PEG chains at a flux of 16 $\mu\text{m/s}$ was more than an order of magnitude smaller than that for the PEGylated α -lactalbumin with two 10 kDa PEG chains even though these species have the same total mass of attached PEG. This behavior appears to be associated with the deformation of the PEG chains in the converging flow into the membrane pores. This phenomenon was more pronounced for the PEGylated proteins having longer PEG chains; the sieving coefficient for PEGylated α -lactalbumin with one 20 kDa PEG chain was a factor of two larger than that for the PEGylated α -lactalbumin with four 5 kDa chains at high filtrate flux (Figure 7.7) with even greater differences seen between the PEGylated α -lactalbumin with two 10 kDa chains compared to that with four 5 kDa PEG chains (Figure 7.6).

The effect of filtrate flux on the sieving characteristics of the PEGylated proteins was qualitatively similar to that predicted using available models for polymer elongation, but the critical Deborah number was about 4 orders of magnitude smaller than that assumed (or measured) in most previous studies. It is possible that this discrepancy may

be directly related to the covalent attachment of one end of the PEG chain to the protein, causing a large reduction in the polymer relaxation time. Alternatively, the experimental results are consistent with an early orientation (and elongation) of the PEG chain due to the strong hydrodynamic drag on the protein part of the polymer-protein conjugate. Additional studies will be needed to fully understand the effects of molecular flexibility and elongation on the ultrafiltration characteristics of these important second-generation biotherapeutics.

Chapter 8

ULTRAFILTRATION OF PEGYLATED PROTEINS USING CHARGE-MODIFIED MEMBRANES

8.1 Introduction

Ultrafiltration membranes have traditionally been used for the separation of molecules of vastly different sizes such as: (1) cells and / or particles from macromolecule solutions or (2) macromolecules from solvents and buffer components. More recently, several studies have demonstrated that ultrafiltration can also be used for separating solutes that are similar in size by exploiting electrostatic interactions to increase the selectivity (Pujar and Zydney, 1998). The earliest discussions of electrostatic effects in ultrafiltration systems date back to at least 1978 (Malone and Anderson, 1978), although the most extensive work in this area has been conducted over the past decade.

Figure 8.1 shows a schematic of an electrically charged membrane used for the separation of two solutes of similar size, one that is negatively-charged and one that is nearly electrically neutral. The like charged proteins are electrostatically excluded from the membrane pores by an energetic barrier created by the interactions between the charged groups on the protein and membrane. Neutral molecules have much weaker electrostatic interactions with the membrane and are thus able to pass through the membrane pores more readily.

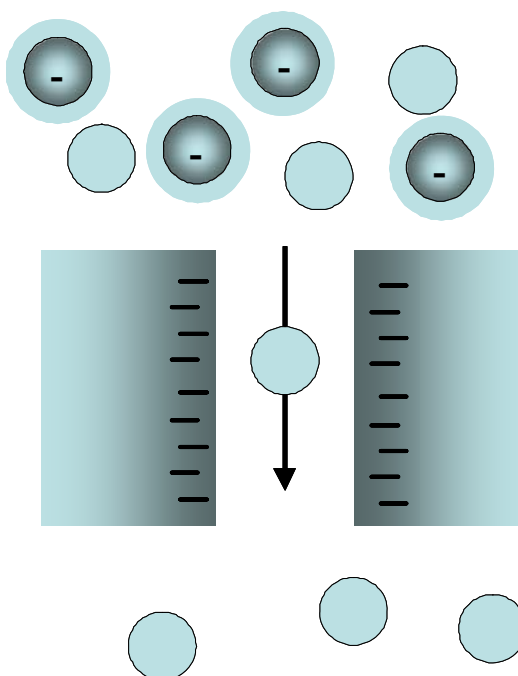


Figure 8.1. Schematic of electrically charged membrane used for the separation of negatively charged molecules from neutral molecules (adapted from Mehta, 2006).

Electrostatic interactions have been successfully exploited for the separation of a variety of protein feedstreams. For example Saksena and Zydney (1994) showed that BSA and IgG could be separated by operating the ultrafiltration device at the isoelectric point of BSA (the pI, or pH at which the protein has no net charge) and at low salt concentrations to enhance the electrostatic repulsion of the IgG. Similar results were obtained by van Reis et al. (1997) in a tangential flow filtration system using an antigen binding fragment of a monoclonal antibody. Van Eijndhoven et al. (1995) were able to separate BSA and hemoglobin by operating at pH 7 where the BSA was negatively charged and the hemoglobin was electrically neutral. The high protein transmission at its isoelectric point is consistent with data obtained in a number of published studies (Balakrishnan and Agarwal, 1996; Ehsani et al., 1996; Nakao et al., 1988; Yang and

Tong, 1997). The use of low ionic strength to enhance electrostatic interactions is also well established (Deen and Smith, 1982; McDonogh et al., 1984; Pujar and Zydney, 1994; Rabiller-Baudry et al., 2000). For example, Pujar and Zydney (1994) found that the sieving coefficient of BSA could be reduced by two orders of magnitude simply by changing the ionic strength from 150 to 1.5 mM. Improved separations have also been achieved by increasing the surface charge density of the membrane (Ebersold and Zydney, 2004a; Mehta and Zydney, 2006). For example, Mehta and Zydney (2006) showed that the transmission of positively-charged cytochrome C could be reduced by a factor of 100 by increasing the zeta potential of the membrane from 0.3 to +6.6 mV.

The partition coefficient for charged spherical solutes in charged cylindrical pores has been evaluated theoretically by Smith and Deen (1980; 1983) and by Lin and Deen (1990) by solving the linearized Poisson-Boltzmann equation. Pujar and Zydney (1994) extended this theoretical framework to account for the effects of charge regulation, the change in protein / membrane charge (or surface potential) due to the electrostatic interactions between the protein and pore. These model calculations are in good qualitative agreement with experiment results for the transport of spherical globular proteins through track-etched (Mitchell and Deen, 1986), polyethersulfone (Burns and Zydney, 1999; Cho et al., 2000; Pujar and Zydney, 1994), polyvinylidene fluoride and polysulfone (Causserand et al., 1996) membranes, and also with data obtained using a series of charge-modified composite regenerated cellulose membrane (Mehta and Zydney, 2006).

The objective of the work described in this chapter is to understand how electrostatic interactions affect the transport of PEGylated proteins during ultrafiltration.

Experiments were designed to explore the influence of pH, ionic strength, and membrane charge on the transport characteristics of PEGylated proteins with different degrees of PEGylation. The results were compared with predictions of available theoretical models, with the protein charge and hydrodynamic radius calculated as described in Chapters 5 and 6 while the membrane properties were evaluated from dextran sieving (Appendix B) and streaming potential measurements (discussed subsequently). The results provide insights into the potential use of electrically-charged membranes for ultrafiltration of PEGylated proteins and also into the underlying physical phenomena governing electrostatic interactions with these protein-polymer conjugates.

8.2 Materials and Methods

8.2.1 Materials

Ultrafiltration experiments were performed with α -lactalbumin, PEG with nominal molecular weights of 5, 10, and 20 kDa, and PEGylated α -lactalbumin with one or more 5, 10, or 20 kDa branches. PEGylated α -lactalbumins were prepared as described in Chapter 3 using a 10 mM Bis Tris buffer. Bis Tris buffers at pH 7.0 were prepared over a range of ionic strengths by addition of KCl, with the molarity of the active buffering species set to 10 mM. Acetate buffer at pH 5.0 with a 10 mM active buffering concentration and total ionic strength of 10 mM was prepared as described in Chapter 3. Bis Tris buffers at pH 6.0 and 7.0 were prepared in the same manner. Buffer exchange was performed using a 10 kDa UltracelTM membrane for a minimum of 10 diavolumes to adjust the solution conditions as described in Chapter 3.

Ultracel™ membranes with either 30 or 100 kDa molecular weight cut-off were used for the ultrafiltration experiments. Negatively-charged versions of these membranes were produced by chemical modification of the base cellulose by attachment of sulfonic acid moieties. More details on the membrane preparation and handling are given in Chapter 3. Charging times ranged from 12 to 24 hours.

8.2.2 Methods

All filtration experiments were performed in the 25 mm diameter stirred ultrafiltration cell (Amicon model 8010) using the procedure described in Chapter 3. The membrane was placed in the bottom of the stirred cell and flushed with at least 40 L/m² of the buffer solution prior to exposure to protein. The membrane hydraulic permeability (L_p) was evaluated by measuring the filtrate flux of buffer as a function of the transmembrane pressure using at least five different pressures between 3.4 and 76 kPa (0.5 and 11 psi). The membrane was then equilibrated with the PEGylated protein solution for 12 hrs. At the start of the ultrafiltration experiment, a minimum of 4 ml of filtrate was passed through the membrane to ensure stable operation; this also served to flush the dead space beneath the membrane in the stirred cell. For each experimental condition, a small filtrate sample was collected followed directly by a small sample of the bulk solution from the stirred cell. The stirred cell was then refilled with the PEGylated protein solution and a repeat measurement obtained. The stirred cell was then emptied and refilled with a 10 mM Bis Tris pH 7.0 buffer to re-evaluate the hydraulic permeability. The process was repeated using solutions of different ionic strength or pH to cover the range of solution conditions.

Size exclusion chromatography was used to analyze the filtrate and bulk samples. Data were obtained with a Superdex 200 G/L (GE healthcare) column with a running buffer of 150 mM KCl, 50 mM phosphate buffered saline at pH 7.0. Peaks for the different PEGylated proteins were easily resolved, although not with baseline resolution. More details on the SEC procedures and data analysis are given in Chapter 3.

8.3 Results

8.3.1 Membrane Charge

The effective surface charge densities of the unmodified and negatively-charged Ultracel™ membranes were determined using streaming potential measurements. The effective zeta potential (ζ) of the membrane was calculated directly from the measured streaming potential using the Helmholtz-Smoluchowski equation (Hunter, 1981):

$$\zeta = \frac{\eta c}{\varepsilon_0 \varepsilon_r} \frac{dE_z}{dP} \quad (8.1)$$

where η is the solution viscosity, c is the conductivity, ε_0 is the permittivity of a vacuum, and ε_r is the relative permittivity of the solution. dE_z/dP is the slope of the measured streaming potential as a function of the applied transmembrane pressure. Note that Equation 8.1 is rigorously valid only when the electrical double layer is very thin relative to the pore radius, a condition that is not typically satisfied in the streaming potential experiments (the double layer thickness in a 10 mM solution is around 3.1 nm compared to the approximately 3.0 nm mean pore radius of the 30 kDa Ultracel™ membranes). Equation 8.1 also assumes that all electrical transport occurs through the electrolyte

solution within the pores; the contributions of surface conduction and conduction through the solid polymer are both neglected.

The effective surface charge density (σ_p) within the membrane pores was then evaluated as (Hunter, 1981):

$$\sigma_p = 4C_o F \kappa^{-1} \text{Sinh}\left(\frac{F\zeta}{2RT}\right) \quad (8.2)$$

where C_o is the bulk ion concentration, F is Faraday's constant, κ^{-1} is the Debye length (defined in Equation 2.17), R is the ideal gas constant, and T is the temperature. Equation 8.2 was developed for a flat surface immersed in a 1:1 electrolyte solution. More detailed information on the derivation of Equations 8.1 and 8.2, as well as a discussion of different approaches to account for the more complex phenomena involved in the streaming potential measurements, is provided by Burns and Zydney (2000).

Figure 8.2 shows typical data for the streaming potential as a function of the transmembrane pressure for 100 kDa UltracelTM membranes that are unmodified, charged for 12 hours, and charged for 24 hours. Data were obtained using a 10 mM Bis Tris buffer at pH 7.0. The non-zero value of the intercept arises from asymmetries in the Ag/AgCl electrodes and has no effect on the results. The data were highly linear, with $r^2 > 0.99$ for all membranes. The data in Figure 8.2 were used to calculate the effective zeta potential and surface charge density yielding values of 7.7 ± 0.1 mV and $1.8 \pm 0.02 \times 10^{-3}$ C/m² for the membrane charged for 24 hrs. This latter value corresponds to approximately 0.01 electronic charge groups per nm² (or 1 electronic charge per 100 nm²), indicating a relatively low coverage of the sulfonic acid moieties. A complete listing of the zeta potentials and average surface charge densities for the different membranes used in this thesis are shown in Table 8.1.

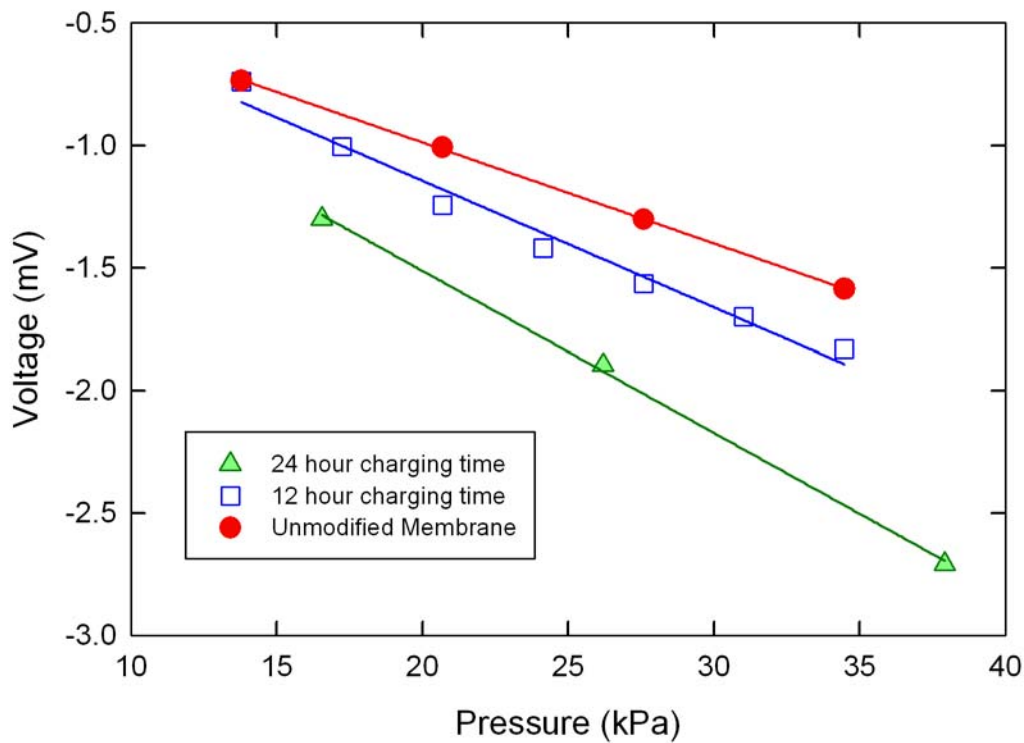


Figure 8.2. Streaming potential as a function of applied transmembrane pressure for the 100 kDa Ultracel™ membranes charged for different periods of time.

Table 8.1. Zeta potential and charge density for 30 kDa and 100 kDa Ultracel™ membranes charged for 0, 12, or 24 hours.

Ultracel™ Membrane	Charging Time (hr)	Buffer Ionic Strength (mM)	Zeta Potential (mV)	Charge Density ($\mu\text{C}/\text{m}^2$)
30 kDa	0	10	-2.6 +/- 0.2	-0.6 +/- 0.04
30 kDa	12	10	-7.9 +/- 0.5	-1.8 +/- 0.1
100 kDa	0	10	-4.2 +/- 0.2	-1.0 +/- 0.05
100 kDa	12	10	-6.1	-1.4
100 kDa	24	10	-7.7 +/- 0.1	1.8 +/- 0.02

8.3.2 Effect of Ionic Strength on Sieving

Figure 8.3 shows the observed sieving coefficient of α -lactalbumin, a 5 kDa PEG, and PEGylated α -lactalbumin with 5 kDa PEG branches as a function of solution ionic strength. Data were obtained with a 100 kDa UltracelTM membrane that was charged for 12 hours (1.4×10^{-3} C/m²). The experiments were performed using a pH 7.0 Bis Tris buffer at a flux of approximately 8 μ m/s (Lower than the fluxes associated with deformation in Chapter 7). The error bars represent plus/minus one standard deviation for three repeat measurements; some error bars lie within the size of the data points and are not shown. The sieving coefficient of the 5 kDa PEG was nearly independent of ionic strength, varying from 0.86 to 0.90 over the entire range of ionic strength. The sieving coefficient of α -lactalbumin increased from 0.50 to 0.93 as the ionic strength increased from 2.3 to 200 mM due to the reduction in electrostatic interactions at high salt concentrations. The ionic strength dependence was even greater for the PEGylated protein with four 5 kDa PEG groups, with S_0 increasing from undetectable levels (approximately 0.1%) to greater than 30% over the same range of ionic strength.

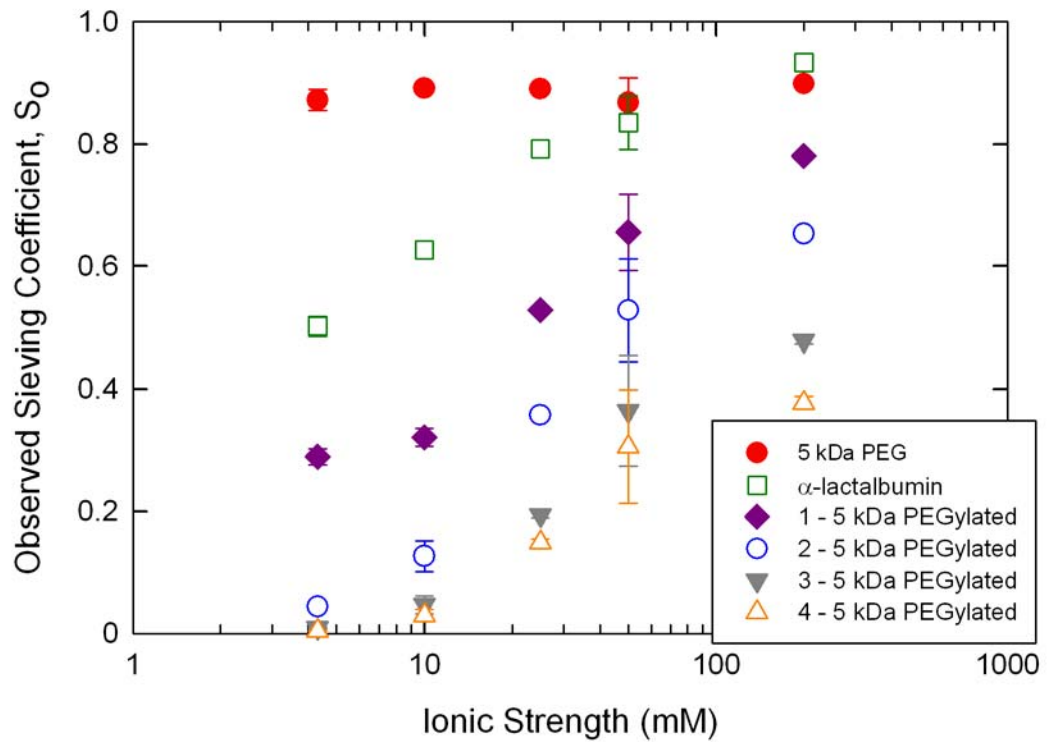


Figure 8.3. Observed sieving coefficient of a 5 kDa PEG, α -lactalbumin, and a PEGylated α -lactalbumin with different numbers of PEG chains as a function of ionic strength at a flux of 8 $\mu\text{m/s}$. Error bars represent plus/minus one standard deviation of the experimental data. Error bars that are smaller than the symbols are not shown.

The sieving data were analyzed using the theoretical model developed by Smith and Deen (1980) for the partitioning of charged spherical solutes into infinitely long cylindrical pores. More details on the theoretical development are given in Chapter 2.

The actual sieving coefficient (S_a) is given as:

$$S_a = (1 - \lambda)^2 K_c \exp\left(\frac{-\psi_E}{k_B T}\right) \quad (8.3)$$

where the term $(1 - \lambda)^2$ describes the steric (hard-sphere) exclusion of the sphere from the region within one solute radius of the pore wall (with λ equal to the ratio of the solute

radius to the pore radius), K_c is the hindrance factor associated with the convection, and

$\left(\frac{\psi_E}{k_B T}\right)$ is the electrostatic energy of interaction:

$$\frac{\psi_E}{k_B T} = A_s \sigma_s^2 + A_{sp} \sigma_s \sigma_p + A_p \sigma_p^2 \quad (8.4)$$

where A_s , A_{sp} , and A_p are given in Equations 2.42 – 2.44 and σ_s and σ_p are the dimensionless surface charge density of the solute and pores, respectively (Equations 2.45 and 2.46). The three terms in Equation 8.4 represent the energy of interaction associated with the distortion of the electrical double layer around the solute, direct charge-charge interactions between the solute and the pore, and the distortion of the electrical double layer adjacent to the pore wall, respectively.

The surface charge densities of both the α -lactalbumin and the PEGylated protein were calculated theoretically from the amino acid sequence using the charge regulation model presented in Appendix C. These calculations implicitly assume that all charges are placed uniformly on the outside of the sphere, consistent with the analysis of the capillary electrophoresis data in Chapter 6 for the proteins in this study. The radius of the PEGylated protein was set equal to the hydrodynamic radius evaluated using the correlation presented by Fee and Van Alstine (2004) as discussed in Chapter 5. The membrane pore size distribution was evaluated from dextran sieving data assuming a log-normal distribution as discussed in Appendix B. The ratio of the standard deviation to the mean pore radius was fixed as $\sigma/\bar{r} = 0.20$, based on previous results (Mehta, 2006) yielding a mean pore radius of 6.0 nm. This value of the pore size is in excellent agreement with the membrane hydraulic permeability measured with the 500 mM Bis Tris buffer, $L_p = 3.2 \times 10^{-12}$ m; the permeability calculated using Equation 2.8 is

2.8 x 10⁻¹² m using a membrane porosity of 50% and a membrane thickness of 1 μm. The small difference between the calculated and measured permeabilities is well within the uncertainties in the values used for the membrane thickness, porosity, and the breadth of the pore size distribution (σ/\bar{r}). A summary of the model parameters is provided in Table 8.2 and Table 8.3.

Table 8.2. Physical properties of α-lactalbumin, PEG, and PEGylated α-lactalbumin in 10 mM pH 7.0 Bis Tris buffer.

Compound	Hydrodynamic Radius (nm)	Diffusion Coefficient (10 ⁻⁶ m ² /s)	Surface Charge (free electron charges)
α-lactalbumin	1.99	7.54	4.67
5 kDa PEG	2.23	6.99	0
5 kDa PEGylated α-lac	3.01	5.64	5.61
5 kDa PEGylated α-lac	3.83	4.86	6.55
5 kDa PEGylated α-lac	4.51	4.39	7.49
5 kDa PEGylated α-lac	5.15	3.99	8.44

Table 8.3. Physical parameters of the 100 kDa Ultracel™ membrane charged for 12 hours.

Pore Radius	nm	6.0
Standard Deviation	nm	1.2
z ratio		0.20
Membrane Thickness	μm	1.0
Surface Charge	C/m ²	1.4×10 ⁻³

The experimental data in Figure 8.3 are compared with the model calculations in Figure 8.4. Results are plotted in terms of the actual sieving coefficient (S_a), which was evaluated directly from the observed sieving coefficient data using the stagnant film to account for the effects of concentration polarization as described in Equation 2.3. The solute mass transfer coefficients were evaluated from Equation 2.4 using the diffusion

coefficients given in Table 8.2, a stirrer speed of 600 rpm, and a flux of 8 $\mu\text{m/s}$. The model calculations are in reasonable agreement with the experimental data for the α -lactalbumin and the PEGylated α -lactalbumin with 1 and 4 PEG chains (all using the same set of model parameters). The model under predicts the data at low ionic strength which could be due to charge regulation effects in the presence of strong electrostatic interactions (Pujar and Zydney, 1997; Burns and Zydney, 2001). The charge regulation effect occur to do the theoretical simplification that the surface charge of the protein and pore are constant when in fact that charge shifts due to the high electrostatic potential between the protein and pore wall.

The model calculations in Figure 8.4 implicitly assume that solute diffusion across the membrane was insignificant compared to the convective transport. The validity of this assumption was examined by calculating the membrane Peclet number:

$$Pe = \frac{J_v \delta}{\varepsilon D_\infty} \frac{\phi K_c}{\phi K_d} \quad (8.5)$$

where K_c and K_d are the hindrance factors for convection and diffusion, respectively. A Peclet number greater than one ($Pe > 1$) indicates that convection is dominant. The values of ϕK_c and ϕK_d were calculated by numerical integration over the log-normal pore size distribution. The calculated values of the membrane Peclet numbers for this experiment ranged from 0.3 to 11, with the smallest Pe for the smaller compounds: α -lactalbumin and the hydrolyzed PEG. Thus, diffusion is probably negligible for the PEGylated proteins, but causes an increase in the calculated values of the actual sieving coefficient for the α -lactalbumin and PEG compared to the results for purely convective transport.

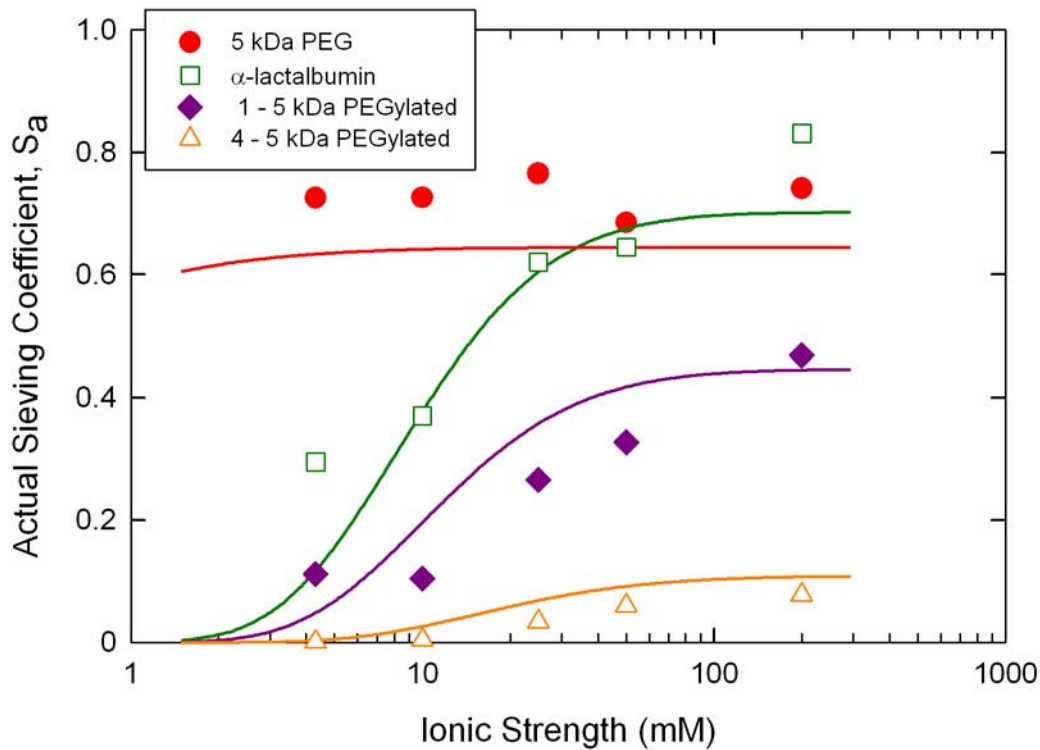


Figure 8.4. Actual sieving coefficient of α -lactalbumin, PEG and, PEGylated α -lactalbumin as a function of ionic strength. Model calculations using the Smith and Deen analysis are shown as solid curves.

In order to examine the model predictions in more detail, a sensitivity analysis was performed to examine the effects of the membrane pore size distribution, membrane surface charge density, and solute size and charge on the calculated values of the actual sieving coefficient. Figure 8.5 shows the effect of the breadth of the pore size distribution, defined by the ratio of the standard deviation to the mean pore size. Results are shown for $z = \sigma / \bar{r} = 0.10, 0.20,$ and 0.30 with a constant pore size of 6.0 nm. The calculated values of the actual sieving coefficient increase with increasing values of σ / \bar{r} due to the increased transport through the largest pores in the distribution. Although it is

difficult to see in Figure 5, the changes in σ/\bar{r} have the greatest relative effect on the actual sieving coefficient for the largest species at the lowest ionic strength. For example, the actual sieving coefficient of the PEGylated α -lactalbumin with four 5 kDa PEG groups varies by more than two orders of magnitude as σ/\bar{r} was increased from 0.1 to 0.3 at an ionic strength of 5 mM but varies by only a factor of 5 at an ionic strength of 200mM.

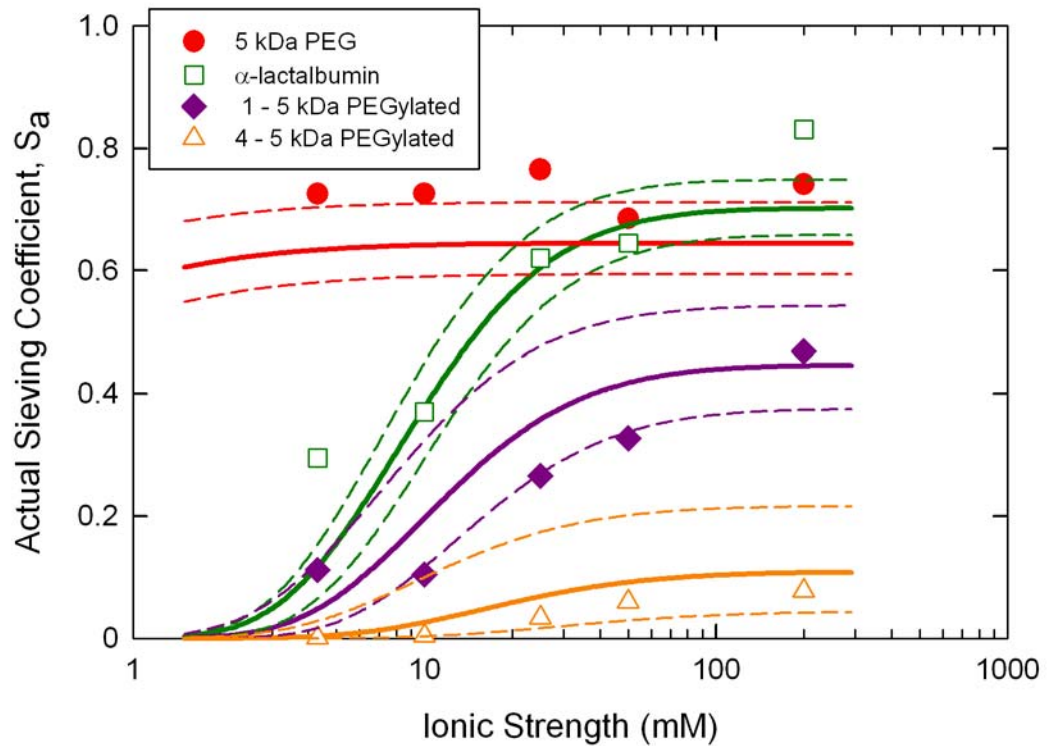


Figure 8.5. Effect of pore size distribution on the calculated values of the actual sieving coefficient of PEG, α -lactalbumin, and PEGylated α -lactalbumin. Dashed curves represent model calculations with $\sigma/\bar{r}=0.10$ and 0.30 ; bold curves represents results with $\sigma/\bar{r}=0.20$.

The effect of the mean pore size on the actual sieving coefficients is shown in Figure 8.6 for calculations with $\sigma/\bar{r}=0.20$. The mean pore size has a strong effect on the sieving coefficient. A 1 nm shift in the mean pore size (using a constant value of $\sigma/\bar{r} = 0.2$) can change the sieving coefficient of the PEGylated α -lactalbumin with four 5 kDa PEGylated groups by up to an order of magnitude with smaller changes in the sieving coefficient for the smaller molecules. The effect of changing the mean pore size is a very weak function of the solution ionic strength. The effects of protein size on the sieving coefficients are similar to the effects of changing the pore size (results not shown) as long as deformation is considered to be negligible. A 15 percent change in the size of the PEGylated α -lactalbumin with four 5 kDa groups caused an increase or decrease in the sieving coefficient by approximately 2 fold, fairly independent of the ionic strength. The changing in sieving coefficient of the smaller molecules was less pronounced.

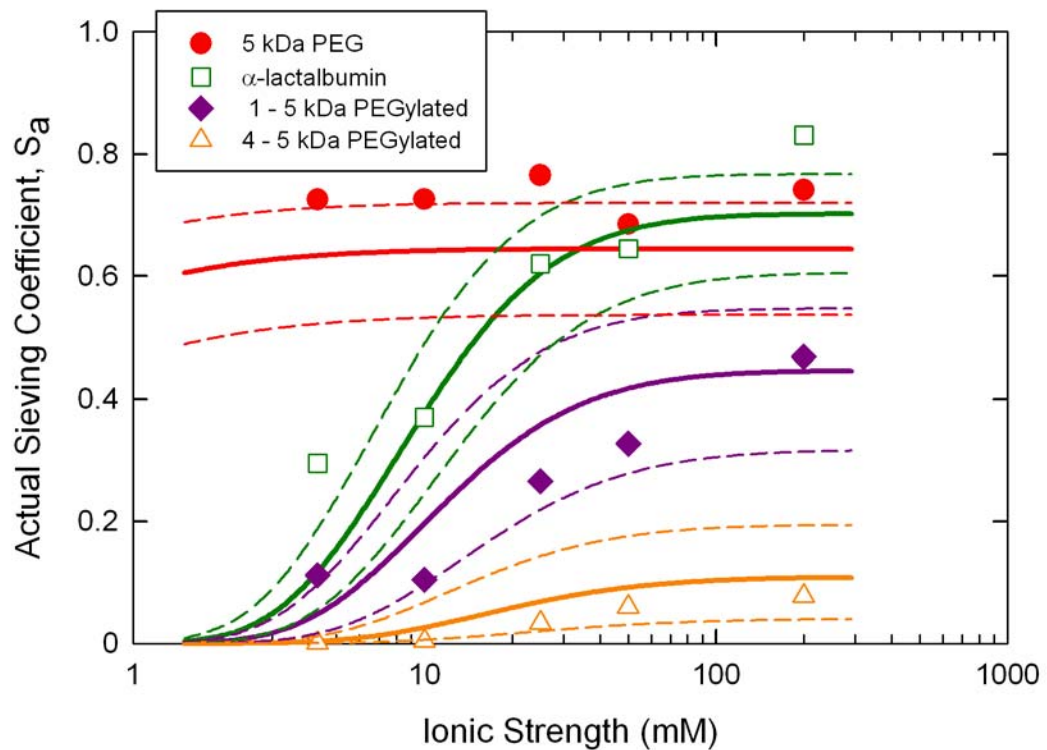


Figure 8.6. Effect of mean pore size on the actual sieving coefficient of PEG, α -lactalbumin, and PEGylated α -lactalbumin. Dashed curves represent model calculations with $\bar{r} = 5.0$ and 7.0 nm. The bold curves represent the model calculation with $\bar{r} = 6.0$ nm.

The effect of the membrane surface charge density on the sieving coefficients is examined in Figure 8.7. At low ionic strength, the sieving coefficient of the α -lactalbumin and the PEGylated proteins decrease with increasing membrane surface charge density due to the increase in electrostatic repulsion. For example, at 5 mM ionic strength, the predicted sieving coefficient for the α -lactalbumin decreases by almost an order of magnitude (from $S_a = 0.30$ to 0.04) as the membrane charge density increases from $0.6 \times 10^{-3} \text{ C/m}^2$ to $3.0 \times 10^{-3} \text{ C/m}^2$. This effect is negligible at high ionic strength due to the shielding provided by the bulk electrolyte. The membrane surface charge density has very little effect on the sieving coefficient of the neutral PEG, although at very low

ionic strength the sieving coefficient does decrease with increasing surface charge density due to the increase in free energy associated with the distortion of the electrical double layer adjacent to the pore wall by the neutral PEG.

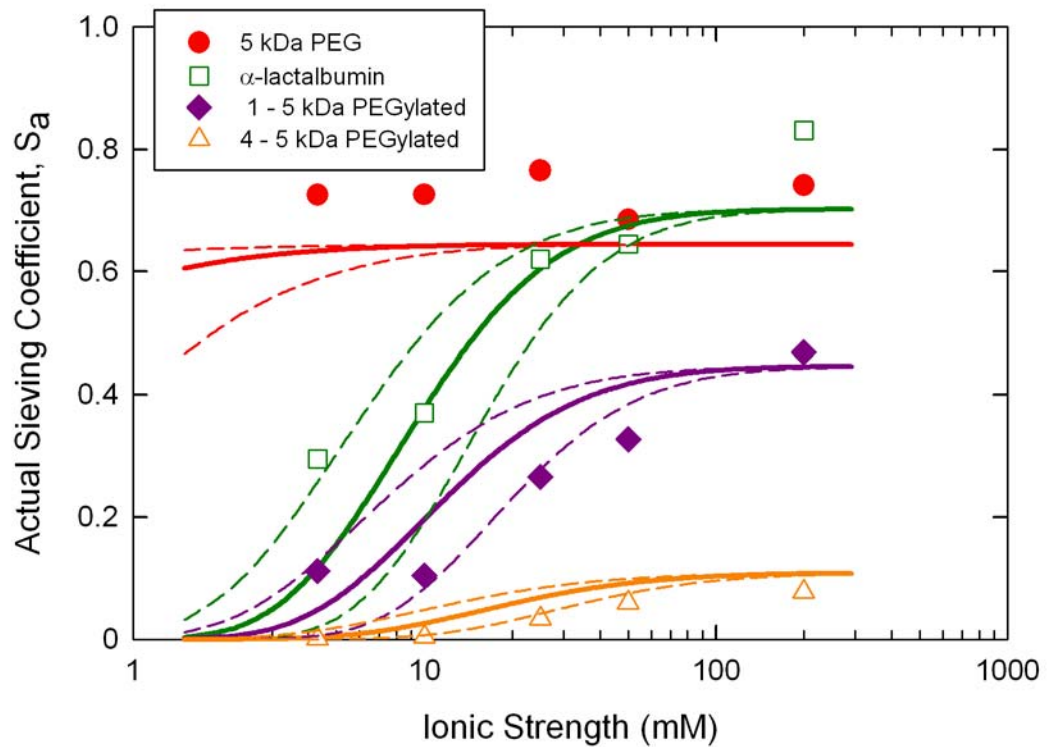


Figure 8.7. Effect of membrane surface charge density on actual sieving coefficient of PEG, α -lactalbumin, and PEGylated α -lactalbumin. Dashed curves represent model calculations with membrane charge of $0.6 \times 10^{-3} \text{ C/m}^2$ and $3.0 \times 10^{-3} \text{ C/m}^2$. The bold curves represent model calculations with membrane charge of $1.3 \times 10^{-3} \text{ C/m}^2$.

The effect of protein surface charge density is examined in Figure 8.8. Simulations were performed in which the net surface charge was either increased or decreased by 15% (approximately 0.5 to 2 charge units) compared to the charge determined from the amino acid sequence. As shown in Figure 8.8, these small changes in protein charge changed the predicted values of the sieving coefficient by less than 20%

even at relatively low ionic strength (< 10mM). Thus, small uncertainties in the protein charge would have no measurable effect on the agreement between the model calculations and experimental results.

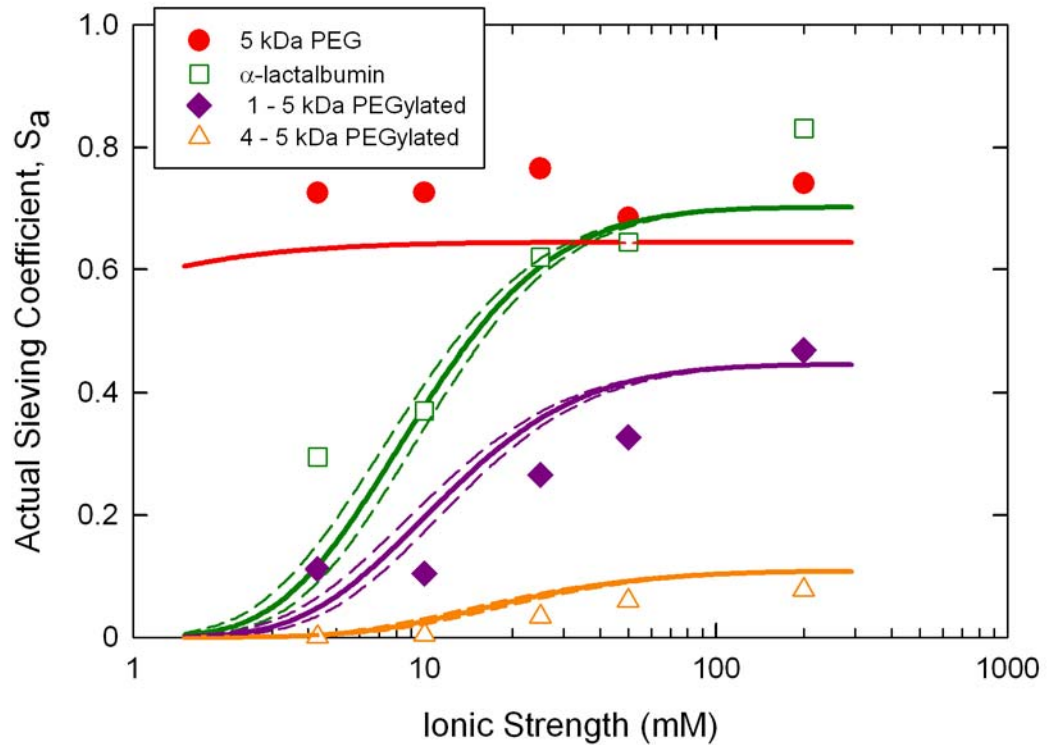


Figure 8.8. Effect of protein surface charge density on the predicted values of the actual sieving coefficient of PEG, α -lactalbumin, and PEGylated α -lactalbumin. Dashed curves represent model calculations in which the solute charge was varied by $\pm 15\%$. The bold curves represent the model calculation in which the solute charge was calculated directly from the published amino acid sequence.

Figure 8.9 shows results for the actual sieving coefficient of 20 kDa PEGylated α -lactalbumin containing four 5 kDa branches, two 10 kDa branches, and one 20 kDa branch as a function of solution ionic strength. In each case, the actual sieving coefficient was calculated directly from the observed sieving coefficient data using the stagnant film model as discussed in Equations 2.3 with $k_m = 3.99 \times 10^{-6}$ m/s for all 3

species based on their identical size as determined by size exclusion chromatography. At high ionic strength, all 3 molecules have nearly identical sieving coefficients. In contrast, the PEGylated protein with a single 20 kDa PEG chain had the largest sieving coefficient at low ionic strength while the PEGylated protein containing four 5 kDa PEG chains had the lowest sieving coefficient under these conditions. This behavior is completely consistent with the differences in net charge of the different PEGylated proteins associated with the PEGylation reaction. The PEGylated α -lactalbumin with four 5 kDa PEG chains has four blocked lysine groups, which eliminates four potential positive charges on the protein surface at pH 7.0 (which is well below the $pK_a = 9.8$ of the lysine amino groups). Thus, the PEGylated α -lactalbumin with four 5 kDa PEG chains will have the greatest net negative charge leading to the greatest electrostatic exclusion at low ionic strength.

The solid curves in Figure 8.9 are model calculations, with the net charge of the different PEGylated proteins evaluated from the amino acid sequence accounting for the elimination of one or more lysine amino groups as discussed in Appendix C. The predicted values of the actual sieving coefficient are identical at high ionic strength since electrostatic interactions are negligible under these conditions. The model correctly predicts the trend in the experimental data for the different PEGylated proteins, but the model tends to over predict the data at intermediate ionic strength and under predicts the experimental results at very low ionic strength. These discrepancies could simply be due to uncertainties in one or more of the model parameters. In addition, the poor agreement at very low ionic strength is likely due to the effects of charge regulation on the protein partition coefficient, with the hydrogen ion concentration in the region between the

negatively-charged protein and the negatively-charged pore being significantly greater than that in the bulk solution due to the very strong electrostatic attraction of the positively-charged H^+ . This causes a shift in the local pH at the protein surface, leading to a reduction in the net negative charge due to the protonation of some of the acidic / basic amino acid residues. There is no clear evidence of any charge shielding by the PEG itself; the model calculations were all performed by assuming that the net protein charge was uniformly distributed over the external surface of the PEGylated protein, analogous to the approach used to describe the electrophoretic mobility in Chapter 6.

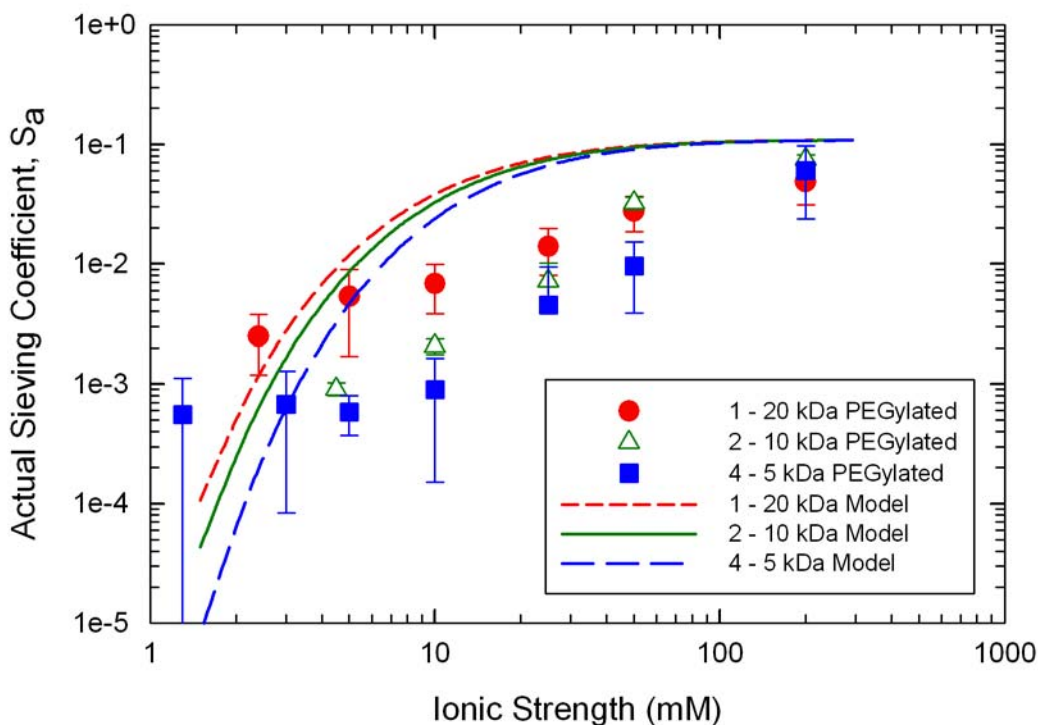


Figure 8.9. Actual sieving coefficient as a function of ionic strength for α -lactalbumin PEGylated with 20 kDa total molecular weight of PEG in one 20 kDa branch, two 10 kDa branches, or four 5 kDa branches. Error bars represent plus/minus standard deviation of at least three repeat experiments. Solid curves are model calculations as described in the text.

8.3.3 Effect of pH on PEGylated Protein Transport

The solution pH controls the protein charge and the diffusion coefficient (Doherty and Benedek, 1974), and it can also alter the protein conformation and degree of fouling (Burns and Zydney, 1999). The effects of pH on the actual sieving coefficient of PEG, α -lactalbumin, and PEGylated α -lactalbumin are shown in Figure 8.10. Data were obtained using a 100 kDa UltracelTM membrane that was charged for 12 hrs to generate an effective charge density of $-1.4 \times 10^{-3} \text{ C/m}^2$. The flux was kept constant at approximately $8 \text{ } \mu\text{m/s}$ and the ionic strength was adjusted to 7 mM by adding KCl to either 10 mM Bis Tris (at pH 6.0 or 7.0) or 10 mM acetate (at pH 5.0) buffer. The hydraulic permeabilities of the clean membranes, evaluated using a 200 mM ionic strength buffer, ranged from $2.8 \times 10^{-12} \text{ m}$ to $3.2 \times 10^{-12} \text{ m}$. The permeability after each experiment was within 15% of the initial flux, suggesting minimal fouling during the ultrafiltration measurements.

The results are plotted as the actual sieving coefficients, which were again calculated directly from the observed sieving coefficient data using the stagnant film model assuming that the mass transfer coefficients are independent of solution pH. The actual sieving coefficients of the α -lactalbumin and PEGylated α -lactalbumins decrease with increasing pH, consistent with the increase in net negative charge on the protein at higher pH. In contrast, the sieving coefficient of the neutral PEG was independent of the solution pH, consistent with the very low pK_a value of the sulfonic acid groups used to generate the charge-modified membrane. The solid curves in Figure 8.10 are the model calculations accounting for electrostatic and hydrodynamic interactions. The pore size distribution was calculated from dextran sieving measurements as $\bar{r} = 5.8 \text{ nm}$ with

$\sigma/\bar{r}=0.2$, while the membrane surface charge density was calculated from zeta potential measurements as $-1.4 \times 10^{-3} \text{ C/m}^2$. The net electronic charge of the α -lactalbumin and PEGylated α -lactalbumins at pH 5, 6, and 7 were calculated based on the amino acid sequence as described previously, with the results summarized in Table 8.4. The model calculations are in good qualitative agreement with the experimental data for all 4 species, properly capturing the effects of solution pH on the transmission of both the α -lactalbumin and the different PEGylated α -lactalbumins.

Table 8.4. Calculated electronic charge (number of free electrons) based on the published amino acid sequence (Brew et al., 1970).

Compound	pH 5.0	pH 6.0	pH 7.0
α -lactalbumin	1.8	3.44	4.65
5 kDa PEG	0	0	0
1-5 kDa PEGylated α -lac	2.54	4.25	5.59
4-5 kDa PEGylated α -lac	4.76	6.83	8.42

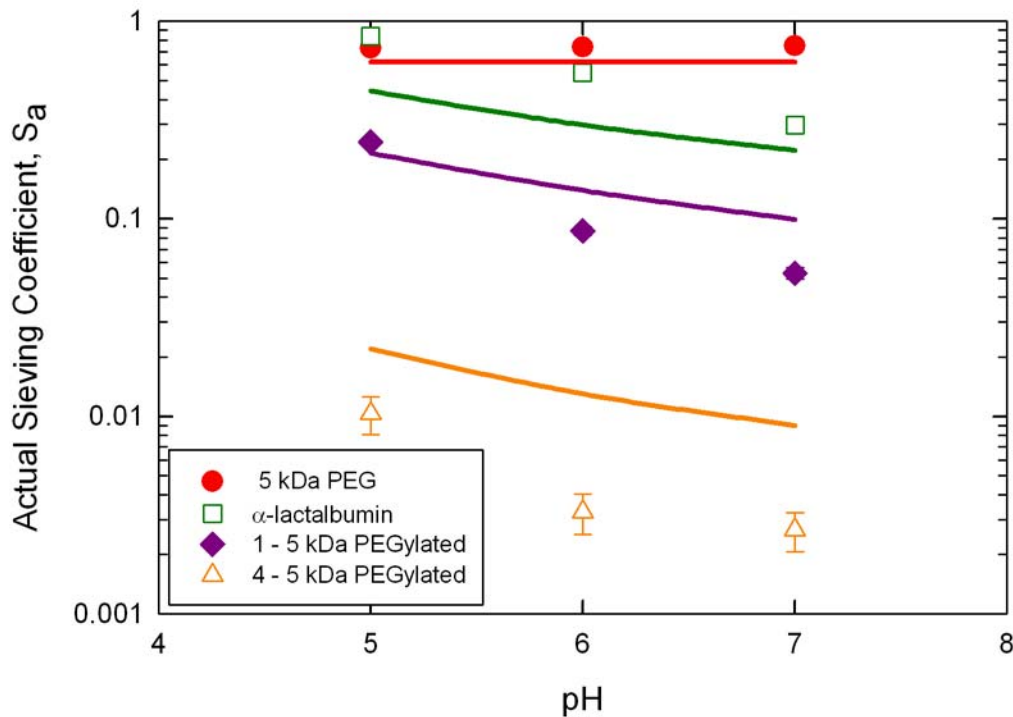


Figure 8.10. The actual sieving coefficient of 5 kDa PEG, α -lactalbumin, and PEGylated α -lactalbumin as a function of pH. Solid curves are model calculations as described in the text.

8.3.4 Effect of Membrane Charge

Figure 8.11 shows the effect of the membrane charging time (12 and 24 hrs) on the actual sieving coefficients of α -lactalbumin, PEGylated α -lactalbumin with one 20 kDa branch, and the 20 kDa PEG alone. In each case, the data points represent the mean values for three repeat measurements with the error bars showing the corresponding standard deviations. At high ionic strength the actual sieving coefficients of the PEGylated protein and the α -lactalbumin were nearly independent of the charging time, consistent with the absence of any significant electrostatic interactions under these conditions. The sieving coefficients of the α -lactalbumin and the PEGylated

α -lactalbumin are smaller for the membrane with the greater charging time, reflecting the increase in electrostatic exclusion of the negatively-charged proteins from the negatively-charged membrane. This effect was most pronounced for the PEGylated protein due to its larger size. There was a small difference in sieving coefficients of the neutral PEG for the membranes charged for 12 and 24 hr, although this difference is likely due to differences in the membrane pore size (variability in the membrane samples) as opposed to any specific electrostatic interactions.

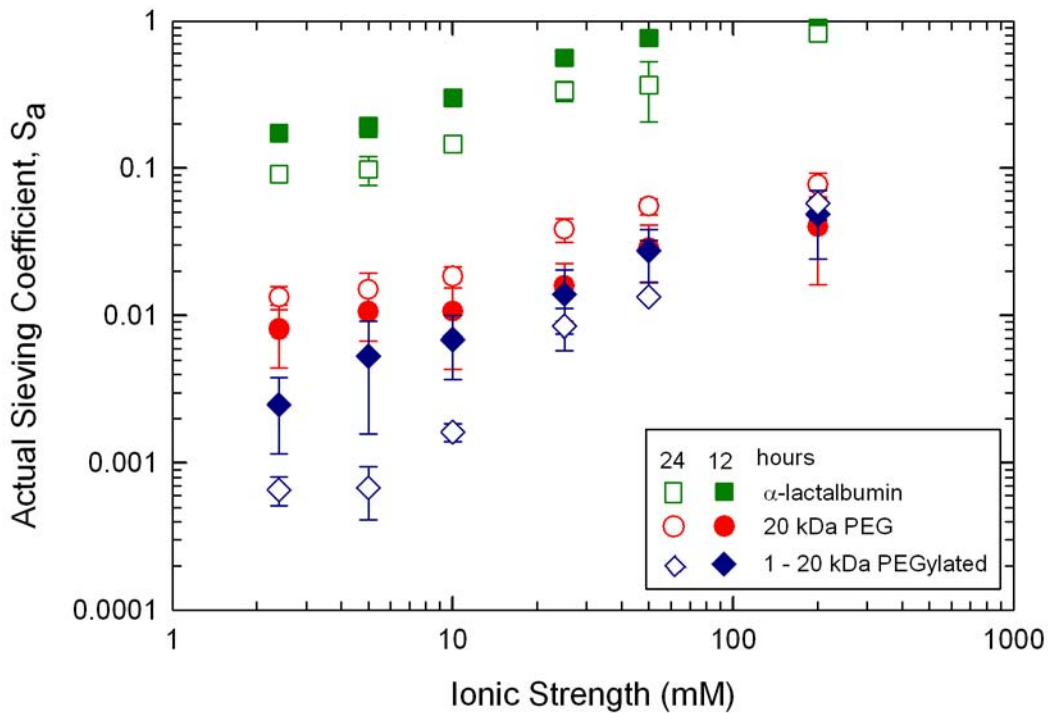


Figure 8.11. Actual sieving coefficient as a function of the solution ionic strength for membranes that were charged for either 12 or 24 hr (charge densities of -1.4×10^{-3} and -1.7×10^{-3} C/m²). Error bars represent plus/minus one standard deviation of the experimental data.

8.4 Conclusions

Although many studies have examined the use of charged-modified membranes for the separation of globular proteins, there have been no prior studies of the effects of membrane charge on the transmission of PEGylated proteins through semipermeable ultrafiltration membranes. The sieving coefficients of the PEGylated proteins increased with increasing solution ionic strength due to the shielding of the electrostatic interactions. For example, the sieving coefficient of the PEGylated α -lactalbumin with four 5 kDa groups was undetectable at a salt concentration of 2.3 mM but increased to almost $S_0 = 0.3$ when the ionic strength of the solution was increased to 200 mM. There was no evidence of any shielding of the electrical charges by the PEG layer that surrounds the protein core; the sieving coefficient data were in good agreement with model calculations developed for a charged sphere in which the net protein charge was assumed to be uniformly distributed over the external surface of the PEGylated protein.

The sieving data for PEGylated proteins having the same total mass of PEG but with different numbers of PEG groups were essentially identical at high ionic strength, consistent with the SEC data showing that these species have identical size, but the results showed significant differences at low salt concentrations. This behavior is consistent with the shift in net protein charge arising from the chemical reaction of different number of lysine amino groups with the activated PEG chains. Thus, the PEGylated protein with four 5 kDa PEG chains has four less lysine amino groups, leading to a significant increase in the net negative charge at pH 7. The experimental results were in good agreement with model calculations accounting for this shift in protein charge. All model parameters were evaluated from independent experimental or

theoretical measurements: the pore size distribution was determined from dextran sieving measurements, the membrane surface charge density was determined from zeta potential measurements, the protein size was determined from the partition coefficient in size exclusion chromatography, and the protein charge was calculated using the amino acid sequence accounting for the loss of lysine amino groups associated with the PEGylation reaction. The model accurately captured all of the key experimental trends, including the effects of solution pH, ionic strength, and membrane charge.

Despite the good qualitative agreement between the model and data, there were some clear deviations, particularly at low ionic strength. This behavior is similar to that seen previously by Pujar and Zydney (1994) and Burns and Zydney (2001) for the sieving behavior of different globular proteins in low ionic strength solutions. Pujar and Zydney (1994) and Burns and Zydney (2001) attributed these discrepancies to the effects of charge regulation. The region between the negatively-charged protein and the negatively-charged pore will have a higher concentration of positively-charged H^+ ions than the bulk solution, leading to a reduction in the local pH near the protein surface. This pH shift can cause the protonation of acidic and basic amino acid residues on the protein, leading to a reduction in the net negative charge on the protein (and a corresponding reduction in the electrostatic repulsion). This effect has been discussed in more detail by Pujar and Zydney (1997) and Ebersold and Zydney (2004b) in the context of globular proteins; the same phenomenon should occur for the PEGylated proteins examined in this work.

The ability to control the transmission of PEGylated proteins by altering the charge on the ultrafiltration membrane can potentially be exploited for enhanced

ultrafiltration processes. For example, it should be possible to use a larger pore size membrane, with larger hydraulic permeability and greater ability to clear small impurities, for concentration and buffer exchange while still maintaining very high rejection of the PEGylated protein due to the strong electrostatic interactions. It should also be possible to use electrically charged ultrafiltration membranes to enhance the separation of charged PEGylated proteins from electrically neutral PEG. This latter problem is discussed in more detail in Chapter 9 of this thesis.

Chapter 9

SEPARATION OF PEGYLATED PROTEINS FROM UNREACTED PRECURSORS

9.1 Introduction

One of the challenges in the production of PEGylated proteins is the need to remove residual polymer, native (un-reacted) protein, and any reaction by-products from the final therapeutic formulation. These separations are required even if the PEGylation reaction is site specific and only produces a single PEGylated product since the PEGylation reaction does not have a 100% yield. Additional purification would typically be required if more than one PEGylated form of the molecule is produced, e.g., reaction at multiple lysine amino groups. This chapter evaluates the feasibility of using ultrafiltration for the separation of un-reacted protein and residual (hydrolyzed) polymer from a model PEGylated protein. Experiments were focused on the purification of an α -lactalbumin molecule PEGylated with one 20 kDa branch.

Sieving coefficients for the PEGylated α -lactalbumin were obtained over a range of pH, ionic strength, and filtrate flux using both neutral and charge-modified UltracelTM membranes with molecular weight cutoffs of 30 and 100 kDa. Optimal separation conditions were identified using the strategies outlined by van Reis et al. (1997) for the development of high performance tangential flow filtration (HPTFF) systems for protein separations. Purification of the PEGylated protein was achieved using a two stage diafiltration process with a final purification factor of 23 and more than 75 % product

yield. The first stage used a neutral membrane to remove the un-reacted protein and any small reaction by-products while retaining the large PEGylated product. The second stage used a negatively-charged membrane to remove the neutral polyethylene glycol while retaining the PEGylated α -lactalbumin due to strong electrostatic interactions. The results clearly demonstrate the potential for using ultrafiltration as a scalable technology platform capable of purifying PEGylated protein products for large-scale manufacturing.

9.2 Materials and Methods

9.2.1 Protein PEGylation

A 20 kDa PEGylated α -lactalbumin solution was created using the procedure given in Chapter 3. Specifically 10 g/L of α -lactalbumin was mixed in a 1 to 2 molar ratio with mPEG-SMB in a Bis Tris buffer (pH 7.0) with 10 mM total ionic strength. After the reaction was complete, the solution was diluted with additional Bis Tris buffer. No additional α -lactalbumin or PEG was added to the solution prior to the beginning of the ultrafiltration experiment. The concentration of each species in the initial ultrafiltration experiments and the actual diafiltration experiments is shown in Table 9.1. Note that the 20 kDa PEG was actually in the hydrolyzed form since all of the activated PEG had undergone hydrolysis (see Chapter 4).

Table 9.1. Feed concentration of 20 kDa PEG, native α -lactalbumin, and PEGylated α -lactalbumin for the ultrafiltration and diafiltration experiments.

	Concentration (g/L)	
	Ultrafiltration Experiments	Diafiltration Experiments
20 kDa PEG	3.5	2.2
Native α -lactalbumin	0.9	0.44
20 kDa PEGylated Protein	0.9	0.56

9.2.2 Ultrafiltration Membranes / Apparatus

Ultrafiltration and diafiltration experiments were performed using UltracelTM composite regenerated cellulose membranes with nominal molecular weight cut-offs of 30 or 100 kDa (Millipore Corp., Bedford, MA) as described in Chapter 3. Negatively charged versions of the 100 kDa membrane were created by covalent attachment of sulfonic acid groups to the surface of the membrane using a base activated chemistry as described in Chapter 3 using a 24 hour reaction time.

9.2.3 Ultrafiltration Sieving Experiments

Ultrafiltration was performed in Amicon 8010 stirred cells as described in Chapter 3. The membrane hydraulic permeability (L_p) was evaluated from Equation 2.8 by measuring the filtrate flux as a function of pressure using a 10 mM Bis Tris buffer. The hydraulic permeability of the charge-modified membrane was also evaluated using a 500 mM Bis Tris / KCl solution, which minimized the contribution of counter-electroosmosis. Each membrane was exposed to the feed solution for at least one hour prior to initiating the ultrafiltration to minimize any transients associated with protein adsorption. The membrane permeability was re-evaluated after this initial adsorption and

then again after protein filtration to provide a measure of the extent of fouling. Sieving experiments were performed as described in Chapter 3 to identify appropriate conditions for separation of the protein, PEG, and PEGylated protein. Small samples of the filtrate and bulk solutions were collected and analyzed using size exclusion chromatography. The flux was varied by adjusting the transmembrane pressure. The ionic strength of the solution was adjusted by addition of KCl to a 10 mM Bis Tris buffer. The solution pH was adjusted by the use of different buffer species: a 10 mM acetate buffer was used at pH 5, a 10 mM Bis Tris buffer was used at pH 6 and 7, and a 10 mM Tris buffer was used at pH 8.5. Specific buffer compositions are given in Chapter 3. In order to reduce the amount of PEGylated protein required for these experiments, the feed solution was reused for multiple experiments by performing a diafiltration to readjust the concentration, pH, and conductivity to the desired values. Diafiltration was performed using a 10 kDa UltracelTM membrane for 10 diavolumes, with the pH, conductivity, and composition of the resulting solution evaluated before use in subsequent ultrafiltration experiments.

9.2.4 Diafiltration

The diafiltration was performed in two stages to separate the PEG, PEGylated protein, and α -lactalbumin. For each stage, a 62 mm diameter membrane was pre-adsorbed with the PEGylated protein feed for at least 12 hrs and then placed in an Amicon 8200 stirred cell with 47 mL solution volume. The first stage diafiltration used a 30 kDa unmodified UltracelTM membrane. The diafiltration reservoir was filled with a 10 mM Bis Tris buffer at pH 7.0 (500 mM ionic strength) that was free of any NHS, PEG,

protein, or PEGylated proteins. The second stage diafiltration used a 100 kDa Ultracel™ membrane that had been charged for 24 hours as described in Chapter 3. The surface charge density of the membrane was estimated as $-1.8 \times 10^{-3} \text{ C/m}^2$ from streaming potential measurements as described in Chapter 8. The diafiltration buffer was 10 mM Bis Tris at pH 7.0 (10 mM ionic strength). Between stages 1 and 2 a 10 diavolume diafiltration was performed to change the buffer ionic strength. All diafiltrations were performed at constant flux. For the 30 kDa membrane the flux was set to $9 \mu\text{m/s}$ while the flux for the 100 kDa membrane was set to $17 \mu\text{m/s}$. Small samples were taken periodically from both the collected filtrate and the stirred cell for subsequent analysis of the solute concentrations.

9.2.5 Assays

The concentrations of the PEGylated protein, the native α -lactalbumin, and the unreacted polyethylene glycol were determined using size exclusion chromatography as described in Chapter 3. The concentrations of PEG and the PEGylated protein could be accurately measured to within 0.02 g/L (with baseline resolution of the peaks) using the RI detector; the α -lactalbumin concentration could be accurately measured to $\pm 0.002 \text{ g/L}$ using the UV detector.

9.3 Results

9.3.1 Sieving Experiments

9.3.1.1 Uncharged Membranes

Initial filtration experiments were used to determine the optimal flux, pH, ionic strength, and membrane for the separation of α -lactalbumin from the singly PEGylated α -lactalbumin. Experiments were focused on the neutral 30 kDa UltracelTM membrane to exploit the large size of the PEGylated protein relative to the native α -lactalbumin.

Data for the effect of filtrate flux on the observed sieving coefficient of the 20 kDa hydrolyzed PEG (3.5 g/L in feed), α -lactalbumin (0.9 g/L), and PEGylated α -lactalbumin (0.9 g/L) are shown in Figure 9.1. The feed solution also contained a small amount of the doubly PEGylated protein (approximately 0.27 g/L), although the presence of this additional component had no effect on the sieving results as determined from experiments employing feed solutions with different levels of the singly and doubly PEGylated products. The unmodified composite regenerated cellulose 30 kDa membrane had a permeability of 6.6×10^{-13} m (evaluated using the 10 mM buffer) while the permeability after exposure to protein was 5.8×10^{-13} m. There was a negligible drop in permeability during the actual filtration experiment, suggesting that there was little membrane fouling beyond some initial protein adsorption.

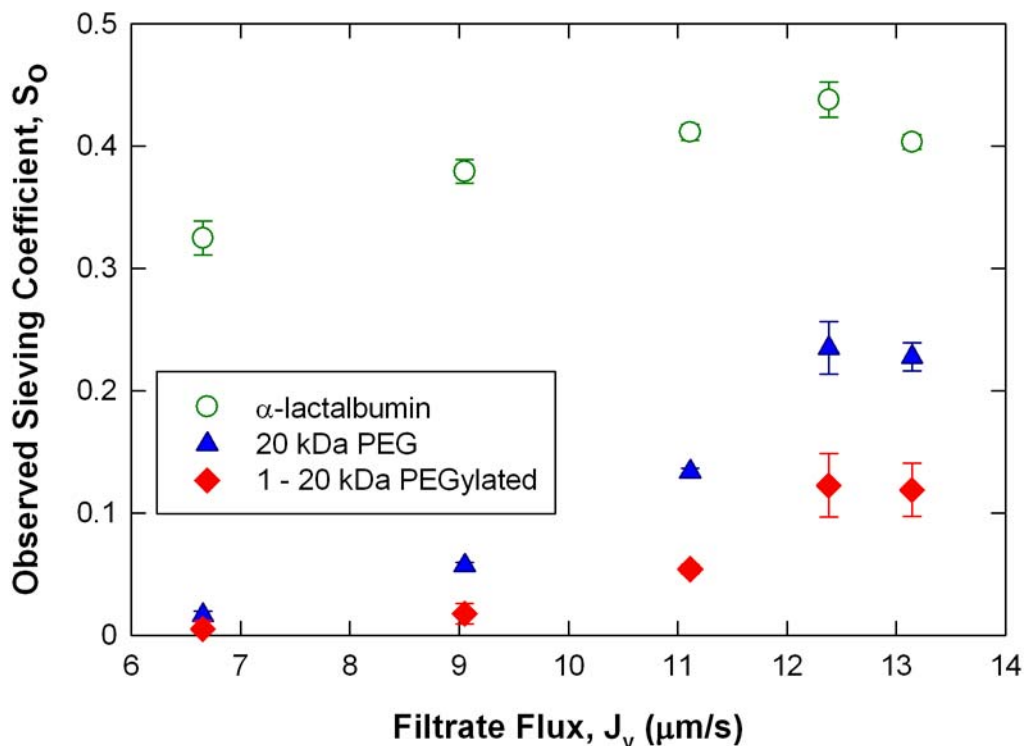


Figure 9.1. Observed sieving coefficients for PEGylated α -lactalbumin, native α -lactalbumin, and 20 kDa polyethylene glycol as a function of filtrate flux through a 30 kDa Ultracel™ membrane at pH 7 and 10 mM total ionic strength. Error bars represent plus/minus one standard deviation of the experimental data.

The symbols in Figure 9.1 represent the mean values of the observed sieving coefficients determined from two repeat experiments using the same membrane with the error bars representing the standard deviation in the data. In some cases, the error bars lay within the size of the symbol and are not shown for clarity. The sieving coefficients for α -lactalbumin were significantly greater than those for the 20 kDa PEG and the PEGylated protein over the entire range of filtrate flux. This behavior is consistent with measurements of the effective solute size as determined by size exclusion chromatography in Chapter 5. The effective radius of the α -lactalbumin [$r_{\text{eff}} = 1.99 \text{ nm}$]

was significantly smaller than that of either the 20 kDa PEG [$r_{\text{eff}} = 4.85 \text{ nm}$] or the PEGylated protein [$r_{\text{eff}} = 5.15 \text{ nm}$]. The increase in sieving coefficient with increasing filtrate flux is consistent with concentration polarization effects associated with the accumulation of retained species at the upstream surface of the membrane. It is also possible that there is some flow-induced deformation or alignment of the PEGylated protein at high filtrate flux as discussed in Chapter 7. In this particular experiment, the sieving coefficient of all species decreased slightly at very high filtrate flux which may be a result of fouling or compaction of the membrane.

In order to quantify the effect of filtrate flux on the separation of the PEG, protein, and PEGylated protein, the data in Figure 9.1 were re-analyzed in terms of the selectivity, which is defined as the ratio of the observed sieving coefficient for the impurity (either α -lactalbumin or the 20 kDa PEG) to that of the desired product, in this case the PEGylated protein. Results are shown in Figure 9.2 for the selectivity of the PEGylated α -lactalbumin from both α -lactalbumin and the PEG. The selectivity with respect to α -lactalbumin (Ψ_{protein}) is greater than 60-fold at a filtrate flux of $7 \mu\text{m/s}$, but it decreases with increasing flux to a value of less than 4 at $J_v = 13 \mu\text{m/s}$. This large reduction in selectivity is a direct result of the greater relative increase in transmission of the PEGylated protein with increasing filtrate, which is consistent with the greater degree of concentration polarization associated with the smaller value of the bulk mass transfer coefficient and / or to the flow-induced deformation of the PEGylated protein at high flux. The selectivity for the separation of the PEGylated protein from the PEG (Ψ_{PEG}) is quite small, with values less than 4 over the entire range of filtrate flux, reflecting the very similar effective size of these two species.

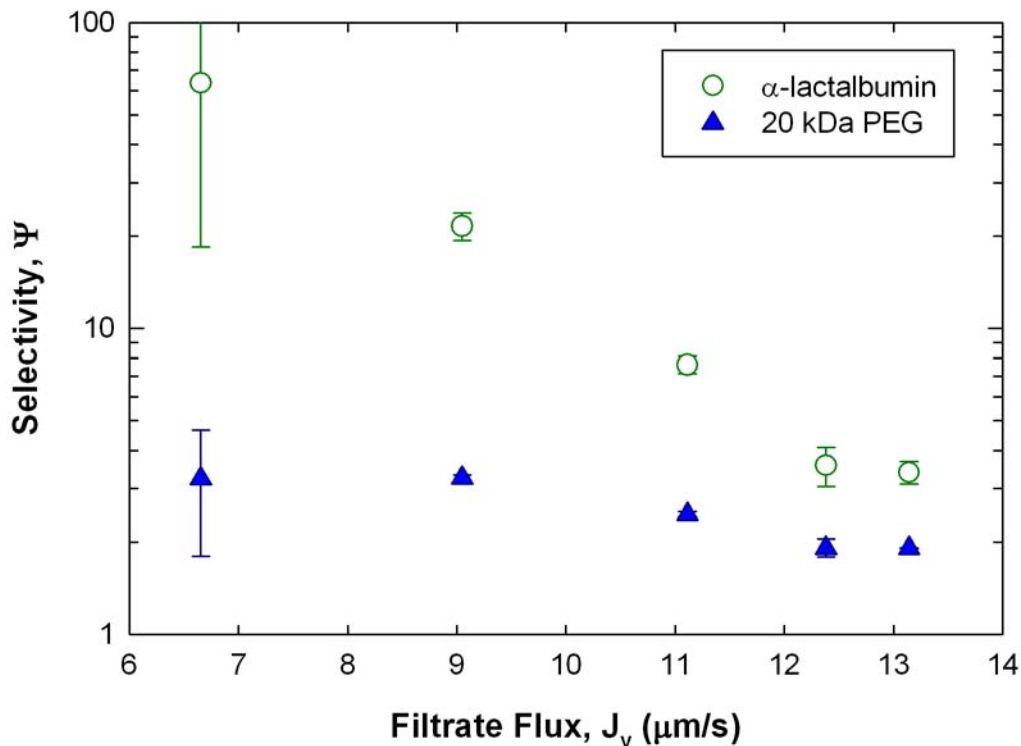


Figure 9.2. Selectivity between the PEGylated protein and α -lactalbumin and between the PEGylated protein and the 20 kDa PEG using the 30 kDa UltracelTM membrane at pH 7 and 10 mM ionic strength. Error bars represent plus/minus one standard deviation of the experimental data.

9.3.1.2 Charged Membrane Separations

A variety of conditions were examined for the separation of the PEGylated protein from the unreacted PEG using the UltracelTM 30 kDa membrane, but none of these provided any significant selectivity due to the very similar size of these species. As discussed in Chapter 8, it is also possible to separate proteins using ultrafiltration by exploiting differences in the net charge of the product and impurity (Burns and Zydney, 2001; Saksena and Zydney, 1994; van Reis et al., 1999). The selectivity under these conditions is a strong function of both the solution ionic strength and the electrical charge

of the solute and the membrane. Since the UltracelTM membrane has very little charge, experiments were performed with an electrically-charged version of the cellulose membrane generated by covalent attachment of a sulfonic acid functionality to the free hydroxyl groups on the base cellulose. Since the attachment of the charged ligand causes a small reduction in the membrane pore size (Mehta and Zydney, 2006), experiments were focused on using a charged-modified 100 kDa composite regenerated cellulose membrane produced by reaction with 3-bromopropanesulfonic acid for 24 hrs. The charged density on the membrane was calculated to be -1.8 mC/m^2 , similar to charge densities determined in previous studies using membranes modified with the same chemistry (Rao and Zydney, 2006). The charge-modified 100 kDa membrane had a permeability of $2.85 \times 10^{-12} \text{ m}$ and $3.22 \times 10^{-12} \text{ m}$, respectively, in the 10 mM and 500 mM buffer. The small increase in permeability at high salt concentrations is due to the reduction in counter electro-osmosis as discussed by Mehta and Zydney (2006), with the appropriate equations describing this phenomenon presented in Chapter 2 (Equations 2.10 – 2.18).

Experimental data for the observed sieving coefficients of the PEGylated protein, the hydrolyzed PEG, and the native α -lactalbumin through the negatively-charged 100 kDa membrane are shown in Figure 9.3 as an explicit function of the solution ionic strength at a filtrate flux of approximately $17 \text{ } \mu\text{m/s}$. The symbols represent the mean value of the observed sieving coefficient determined from four replicated experiments with the error bars representing the standard deviation in the data. The sieving coefficients for all 3 species increase with increasing ionic strength, with the weakest variation in S_0 seen for the un-charged polyethylene glycol. The transmission of the

negatively-charged α -lactalbumin and the negatively-charged PEGylated protein increase significantly at high ionic strength due to the reduction in the electrostatic exclusion of these species from the negatively-charged pores of the charge-modified membrane. The small increase in sieving coefficient of PEG with increasing ionic strength is probably due to the decrease in the thickness of the electrical double layer adjacent to the membrane pore wall at higher salt concentrations; this phenomenon is discussed in more detail by Burns and Zydney (2001). The different electrostatic interactions for the PEG and α -lactalbumin cause the sieving coefficient for the PEG to be greater than that for the α -lactalbumin at low ionic strength (where the electrostatic exclusion of the charged α -lactalbumin is most significant), with the reverse behavior seen at high salt concentrations (where solute transmission is dominated by steric interactions). It is interesting to note that the sieving coefficient of the PEGylated protein is a fairly strong function of the solution ionic strength, increasing by more than a factor of 10 as the ionic strength increases from 1 to 200 mM, even though the PEGylated protein is predominantly polyethylene glycol -- 58% by mass and more than 94 % by volume (Chapter 5). The effect of electrostatic interactions on the sieving characteristics of the PEGylated proteins is discussed in more detail in Chapter 8.

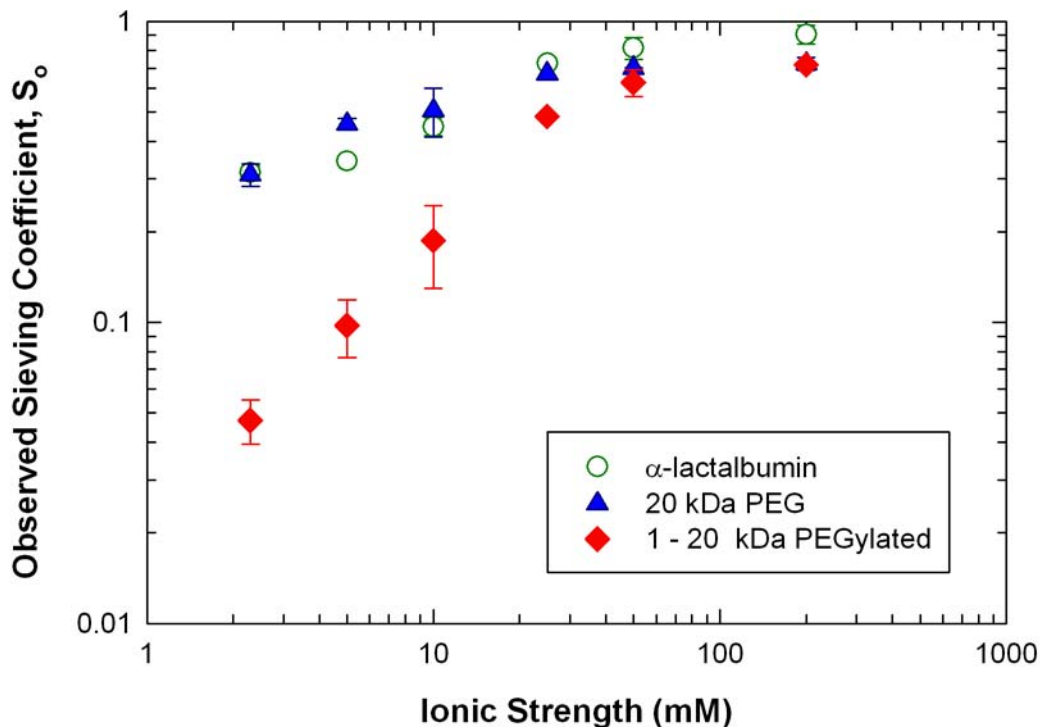


Figure 9.3. Observed sieving coefficients for PEGylated α -lactalbumin, native α -lactalbumin, and hydrolyzed 20 kDa polyethylene glycol as a function of ionic strength using a negatively-charged 100 kDa Ultracel™ membrane at pH 7 and a filtrate flux of 17 $\mu\text{m/s}$. Error bars represent plus/minus one standard deviation of the experimental data.

The selectivity between the PEGylated protein and the PEG and between the PEGylated protein and the unreacted α -lactalbumin was calculated using the data in Figure 9.3 with the results shown in Figure 9.4. The selectivity for the PEGylated protein compared to the PEG was greatest at low ionic strength with a value of approximately 7 for ionic strengths below 5 mM. The selectivity decreased with increasing salt concentration due to the large increase in the sieving coefficient of the PEGylated protein. The selectivity of the PEGylated protein compared to the α -lactalbumin is also highest at low ionic strength due to the very strong effect of salt on the sieving coefficient

of the PEGylated α -lactalbumin. Note that the best selectivity between the PEGylated protein and α -lactalbumin with the 100 kDa membrane (approximately 7 at 2.5 mM ionic strength) is still considerably smaller than that obtained with the unmodified 30 kDa (approximately 25 at the same flux) demonstrating that it is much more effective to exploit size differences, rather than charge differences, in the removal of the small unreacted protein.

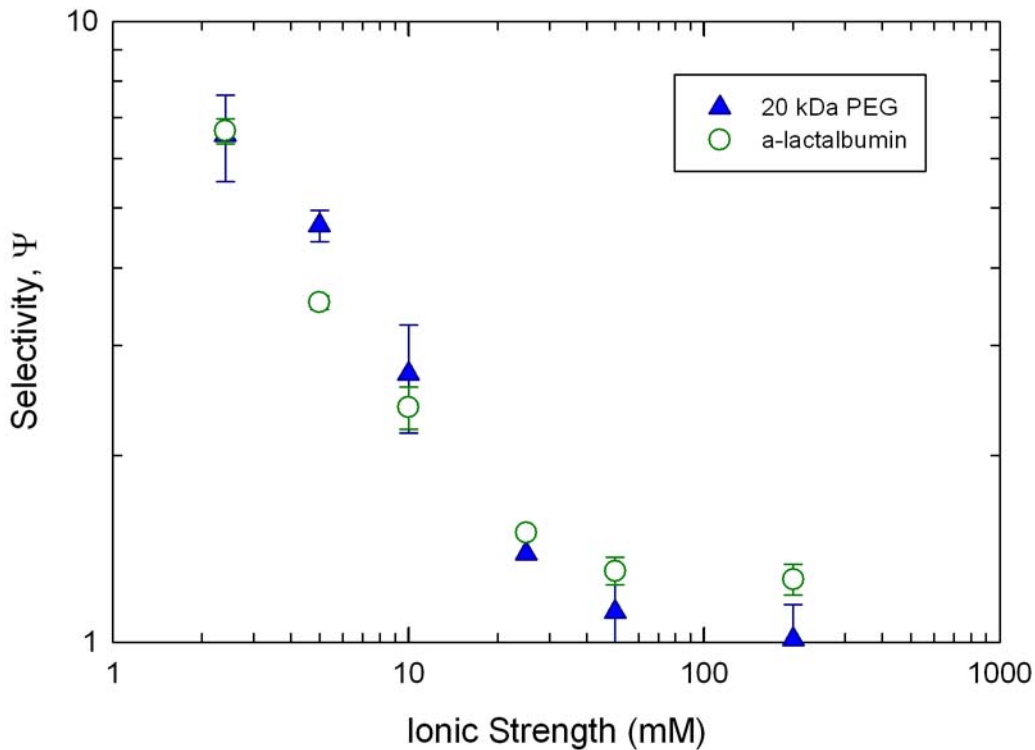


Figure 9.4. Selectivity between the PEGylated protein and α -lactalbumin and between the PEGylated protein and the 20 kDa PEG for the 100 kDa UltracelTM membrane charged for 24 hrs at pH 7 and 17 μ m/s.

The observed sieving coefficients of the PEGylated protein, 20 kDa PEG, and the native α -lactalbumin through the negatively charged 100 kDa membrane are shown in

Figure 9.5 as a function of the solution pH using a 10 mM ionic strength buffer at a filtrate flux of approximately 31 $\mu\text{m/s}$. The sieving coefficients for the PEGylated protein and the α -lactalbumin decrease with increasing pH due to the reduction in electrostatic exclusion associated with the decrease in net charge as one moves closer to the isoelectric point (the pI for α -lactalbumin is 4.6). The sieving coefficient of the PEG is nearly independent of the solution pH in agreement with the data presented in Chapter 8. The small decrease in the sieving coefficient of the PEG at pH 8.5 may be due to a small amount of fouling during that experiment, although the permeability of the membrane showed essentially no change before and after the ultrafiltration. At low pH the net charge on the PEGylated protein is very small; thus, the sieving coefficients of the PEG and PEGylated protein are very similar under these conditions. As the pH increases, the sieving coefficient of the PEGylated protein decreases while that of the PEG remains nearly constant. The net result is that the sieving coefficients of these very similarly sized molecules differ by more than an order of magnitude at pH 8.5.

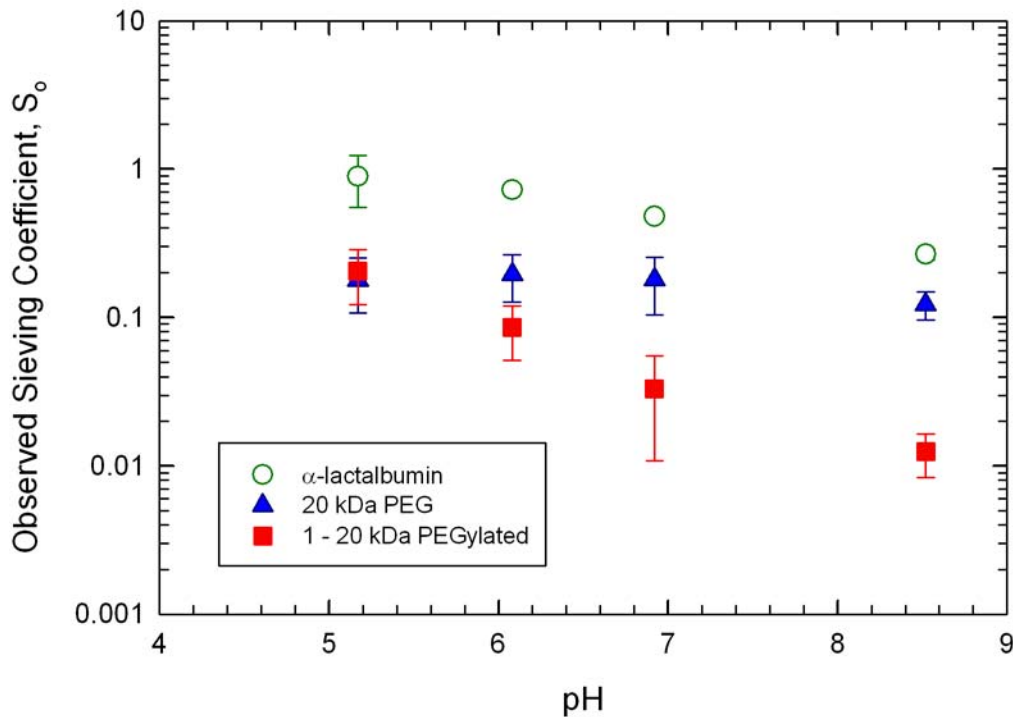


Figure 9.5. Observed sieving coefficient as a function of pH for native α -lactalbumin, PEGylated α -lactalbumin, and 20 kDa PEG through a negatively charged 100 kDa membrane at a flux of 31 $\mu\text{m/s}$. Error bars represent plus/minus one standard deviation of the experimental data.

The selectivity for the PEGylated protein is shown in Figure 9.6 as an explicit function of the pH. The selectivity increases with increasing pH in the range of pH 5.0 to 8.5 due to the increase in the net charge of the protein as the pH increases. The greatest selectivity between the PEGylated protein and the PEG was thus obtained at pH 8.5, conditions which gave the largest electrostatic exclusion of the negatively-charged PEGylated α -lactalbumin. Experiments performed at higher pH showed minimal improvements in selectivity and seemed more susceptible to membrane fouling.

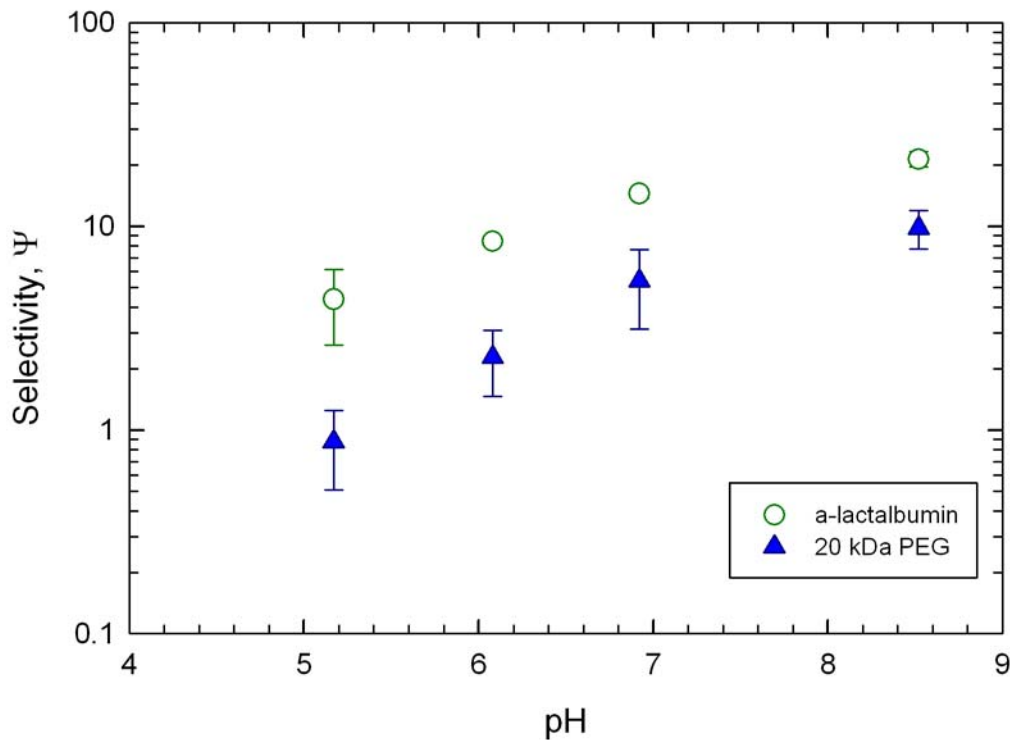


Figure 9.6. Selectivity between the PEGylated protein and α -lactalbumin and between the PEGylated protein and the 20 kDa PEG for the 100 kDa Ultracel™ membrane charged for 24 hrs at 10 mM ionic strength and a flux of 31 $\mu\text{m/s}$. Error bars represent plus/minus one standard deviation of the experimental data.

9.3.2 Diafiltration

Based on the results from the initial ultrafiltration experiments, a two-stage diafiltration process was designed to purify the PEGylated α -lactalbumin from the unreacted precursors, in this case the 20 kDa PEG and the native α -lactalbumin. The first stage was designed to remove the α -lactalbumin and was performed with an un-modified 30 kDa Ultracel™ membrane at a flux of 9 $\mu\text{m/s}$ using a pH 7 Bis Tris buffer with 500 mM ionic strength. The second stage was designed to remove the PEG, with the diafiltration performed using the negatively-charged 100 kDa Ultracel™ membrane at pH

7 and 2.5 mM ionic strength to enhance the electrostatic exclusion of the negatively-charged PEGylated protein from the membrane pores. A buffer pH of 7.0 was chosen instead of 8.5 due to excessive fouling that seemed to occur at high pH over a long time period. A conventional buffer exchange was performed between these processes using the 30 kDa UltracelTM membrane with the 2.5 mM buffer used for the diafiltration.

Experimental data for the normalized concentration of α -lactalbumin, the hydrolyzed PEG, and the PEGylated protein in the retentate solution for the first-stage diafiltration are shown in Figure 9.7 as a function of the number of diavolumes (N), defined as the ratio of the total collected filtrate volume to the constant retentate volume in the stirred cell. In each case, the solute concentration was normalized by the concentration of that species in the feed (0.44 g/L for α -lactalbumin, 2.2 g/L for the PEG, and 0.56 g/L for the PEGylated protein). The concentration of α -lactalbumin decreased rapidly during the diafiltration, dropping to less than 1% of its initial value after only 7 diavolumes. The α -lactalbumin concentration after 9.5 diavolumes was less than 0.003 g/L, which is near the detection limit for the SEC assay. In contrast, the concentration of the PEGylated α -lactalbumin and PEG remained nearly constant throughout the diafiltration, decreasing by less than 5% even after 9.5 diavolumes.

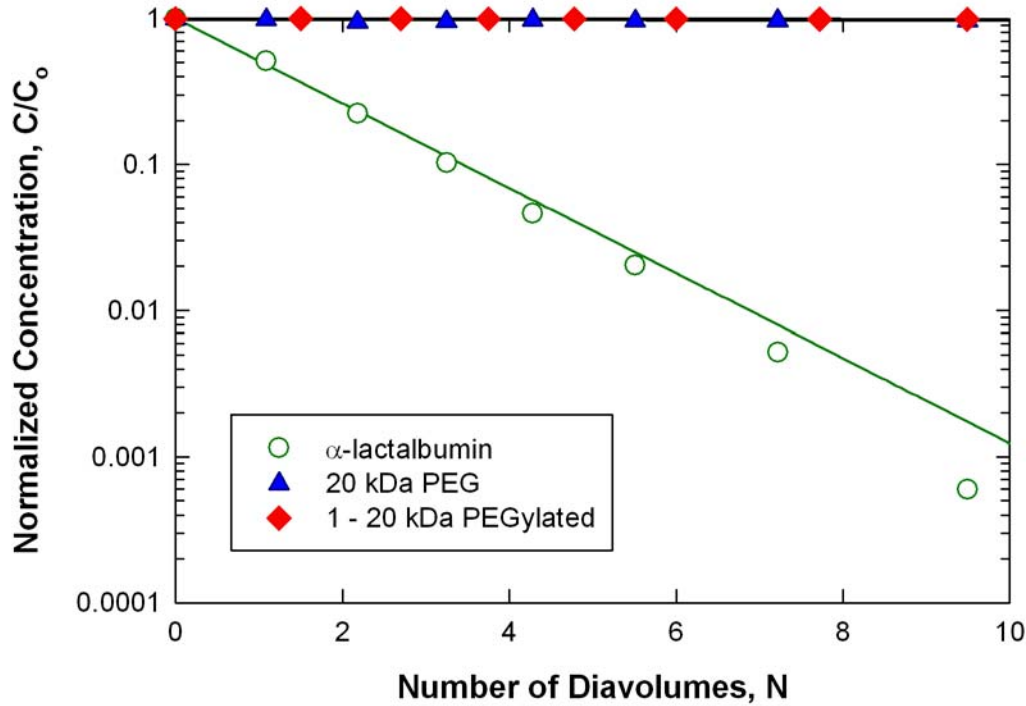


Figure 9.7. Normalized concentrations of the PEGylated α -lactalbumin, native α -lactalbumin, and hydrolyzed 20 kDa polyethylene glycol as a function of the number of diavolumes for a diafiltration performed with a 30 kDa Ultracel™ membrane at pH 7, 500 mM ionic strength, and a filtrate flux of 9 $\mu\text{m/s}$. Solid lines are model calculations using the best fit values of the sieving coefficients as shown in Table 9.2.

The experimental data in Figure 9.7 were analyzed using a simple species mass balance on the diafiltration system:

$$\frac{d(V_{\text{sys}} C)}{dt} = J_v A_{\text{mem}} S_o C \quad (9.1)$$

where V_{sys} is the constant system volume and A_{mem} is the membrane area. Equation 9.1 can be integrated to obtain an expression for the solute concentration in the retentate as a function of the number of diavolumes (N):

$$\frac{C}{C_o} = \exp[-NS_o] \quad (9.2)$$

Equation 9.2 predicts a linear relationship between $\ln(C/C_o)$ and N , consistent with the results in Figure 9.7. The solid lines represent the model calculations, with the best fit value of the observed sieving coefficient determined by minimizing the sum of the squared residuals between the model and data. The simple model provides an excellent fit to the data, indicating that there were no measurable changes in the sieving coefficients over the course of the diafiltration. The constant sieving coefficient is indicative of a lack of fouling of the membrane and that the protein sample is stable.

The best-fit values of the sieving coefficients for the PEG, PEGylated protein, and α -lactalbumin are summarized in Table 9.2. The best-fit value for α -lactalbumin was $S_o = 0.67$, which is considerably larger than the values seen in Figure 9.1 for α -lactalbumin transmission through a separate 30 kDa membrane, while the sieving coefficients of the PEG and PEGylated protein were similar but slightly smaller than the values obtained in the initial experiments. These differences could be due to the inherent variability between membrane samples as well as possible effects of electrostatic interactions; the initial ultrafiltration experiments were performed using a 10 mM ionic strength buffer while the diafiltration was performed using a higher ionic strength buffer (500 mM) to further reduce any electrostatic repulsion of the negatively charged α -lactalbumin (Pujar and Zydney, 1994). In addition, the diafiltration experiments were performed using the larger diameter (62 mm) stirred cell while the initial sieving experiments were performed in a 25 mm diameter cell. Experimental and theoretical correlations indicate that the mass transfer coefficient is considerably larger in the large diameter cell, which would reduce the degree of concentration polarization for the more retained species (Zydney and

Xenopoulos, 2007). This effect could contribute to the very high degree of retention for the PEGylated product ($S_o = 0.001$) during the diafiltration.

Table 9.2. Sieving coefficients for α -lactalbumin, 20 kDa PEG, and PEGylated protein for the first and second stage diafiltration.

Solute	First Stage	Second Stage
α -lactalbumin	0.67	--
20 kDa PEG	0.002	0.24
PEGylated protein	0.001	0.006

The size exclusion chromatograms of the initial feed, at various points within the diafiltration, and the final retentate solution after the first stage diafiltration are shown in Figure 9.8. The initial feed contains a high concentration of α -lactalbumin (retention time of 58.4 min), the PEGylated α -lactalbumin (retention time of 40.8 min), and a small peak for α -lactalbumin conjugated to two 20 kDa PEG chains (retention time of 35.1 min). The presence of the doubly PEGylated protein had no affect on the sieving results of the α -lactalbumin or first PEGylated species. The PEG is not apparent in this chromatogram since the PEG has no absorbance at 280 nm. The α -lactalbumin peak is essentially absent in the chromatogram for the final retentate, consistent with the very high degree of purification achieved during the diafiltration.

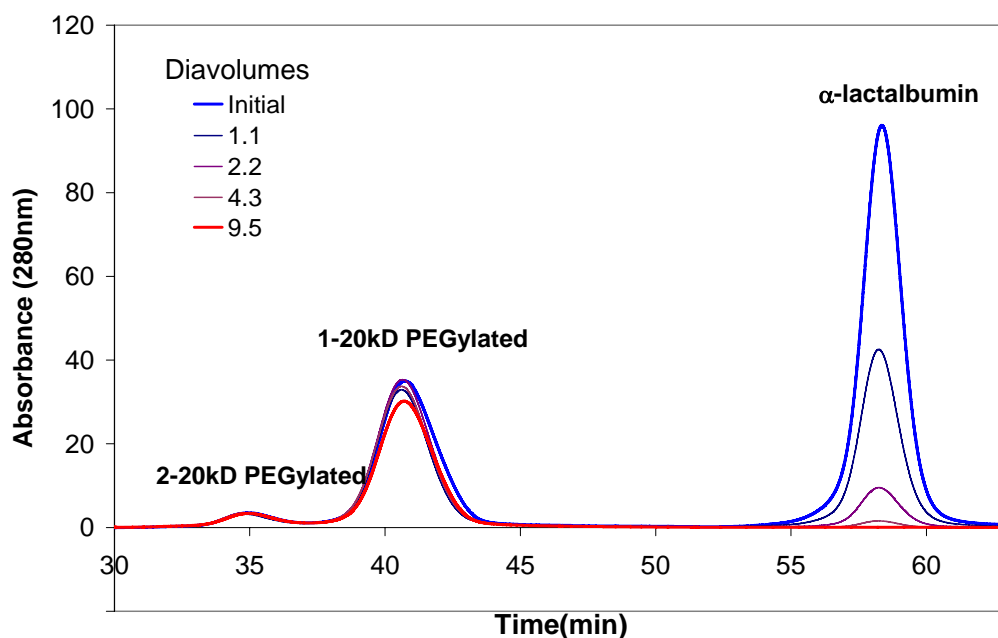


Figure 9.8. Size exclusion chromatograms showing the initial feed and final retentate for the first-stage diafiltration using a 30 kDa Ultracel™ membrane at pH 7, 500 mM ionic strength, and a filtrate flux of 9 $\mu\text{m/s}$. Detection is by UV at 280 nm.

After the first stage diafiltration, the ionic strength of the retentate solution was reduced by buffer exchange to achieve the desired conditions for the second-stage diafiltration. This was performed with a 30 kDa membrane using 10 diavolumes of a 10 mM Bis Tris (2.5 mM ionic strength with no additional KCl) at pH 7.0 as the diafiltration buffer at a flux of 7 $\mu\text{m/s}$. The ionic strength and pH of the final solution were measured and found to be identical (within experimental error) to that of the diafiltrate buffer. The retentate solution was then transferred to a second stirred cell housing a negatively-charged 100 kDa membrane. The concentrations of PEG and PEGylated protein in the feed to the second stage diafiltration were 1.76 g/L and 0.48 g/L, respectively. This corresponds to overall yields based on the initial feed of 80% and 85%, respectively, due

to the combined losses associated with the first-stage diafiltration, the buffer exchange, and the solution transfer. The dominant contribution to the yield loss (greater than one-half) occurred during the solution transfer due to the very small volumes involved in these experiments.

Experimental data for the normalized concentrations of PEG and the PEGylated protein during the second-stage diafiltration using the negatively-charged 100 kDa membrane are shown in Figure 9.9. In this case, the concentrations were normalized using the initial solute concentrations at the start of the second diafiltration, which were evaluated immediately after the system had reached stable operation. No results are shown for the α -lactalbumin since its concentration in the second stage was too low to determine accurately. The PEG concentration decreased throughout the diafiltration, dropping to less than 7% of the initial value after 15 diavolumes. The PEGylated protein was strongly retained by the negatively-charged membrane, with the concentration decreasing by less than 10% even after 15 diavolumes. The final product at the end of the two-stage diafiltration contained 0.44 g/L of PEGylated α -lactalbumin (compared to the initial concentration of 0.56 g/L in the feed), with only 0.086 g/L of PEG and undetectable (less than 0.002 g/L) concentrations of the un-reacted α -lactalbumin.

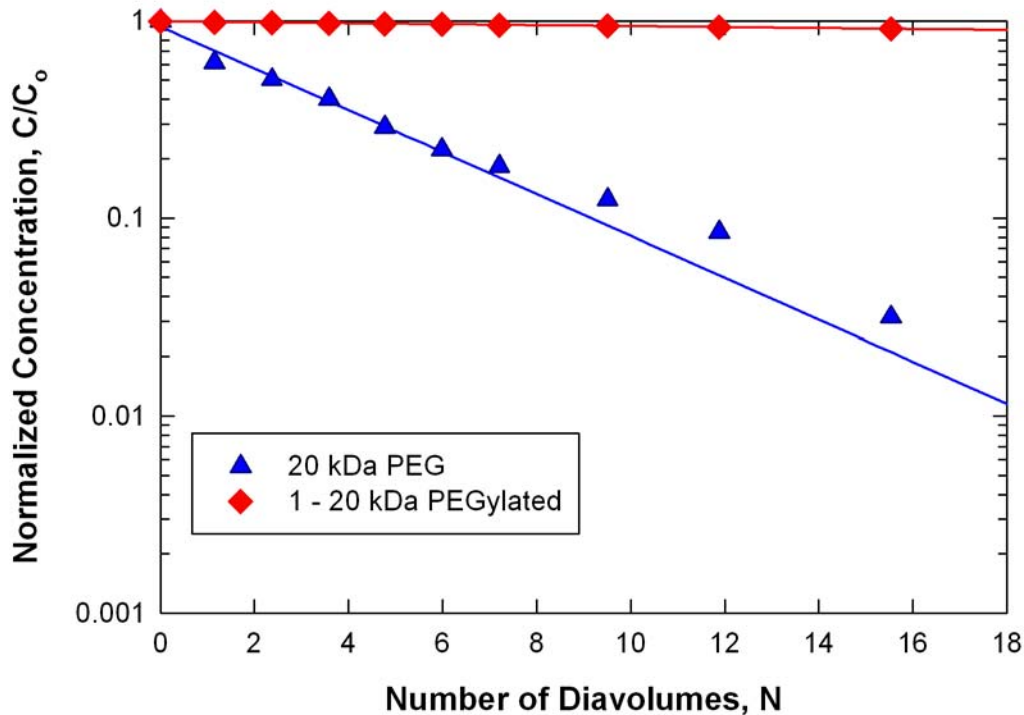


Figure 9.9. Normalized concentrations of the PEGylated α -lactalbumin and free 20 kDa polyethylene glycol as a function of the number of diavolumes for a diafiltration performed with a negatively-charged 100 kDa Ultracel™ membrane at pH 7, 2.5 mM total ionic strength, and a filtrate flux of 21 $\mu\text{m/s}$. Solid lines are model calculations using the best fit values of the sieving coefficients shown in Table 9.2.

The solid lines in Figure 9.9 are the model calculations evaluated from Equation 9.2 using the best fit values of the sieving coefficients determined by linear regression of the data for $\ln(C/C_0)$ versus N (see final column in Table 9.2). These sieving coefficients were significantly smaller than the values determined in the initial sieving experiments (Figure 9.3), which is probably due to the smaller degree of concentration polarization in the 62 mm diameter stirred cell. Note that the initial permeability of the membrane used for the diafiltration was also about 13% less than that for the membrane used in the

ultrafiltration experiments, which is consistent with the smaller solute transmission seen during the diafiltration.

9.3.3 Purification – Yield Analysis

In order to examine the separation performance of this system in more detail, the experimental data for the first-stage diafiltration (Figure 9.7) were re-plotted in terms of the yield of the PEGylated protein as a function of the purification factor (P) in Figure 9.10. The product yield (Y) was evaluated as the ratio of the concentration of the PEGylated protein in the retentate solution to that in the feed since the retentate volume remains constant during the diafiltration. The product yield can also be evaluated theoretically in terms of the selectivity (ψ) as discussed by van Reis and Saksena (1997):

$$P = Y^{1-\psi} \tag{9.3}$$

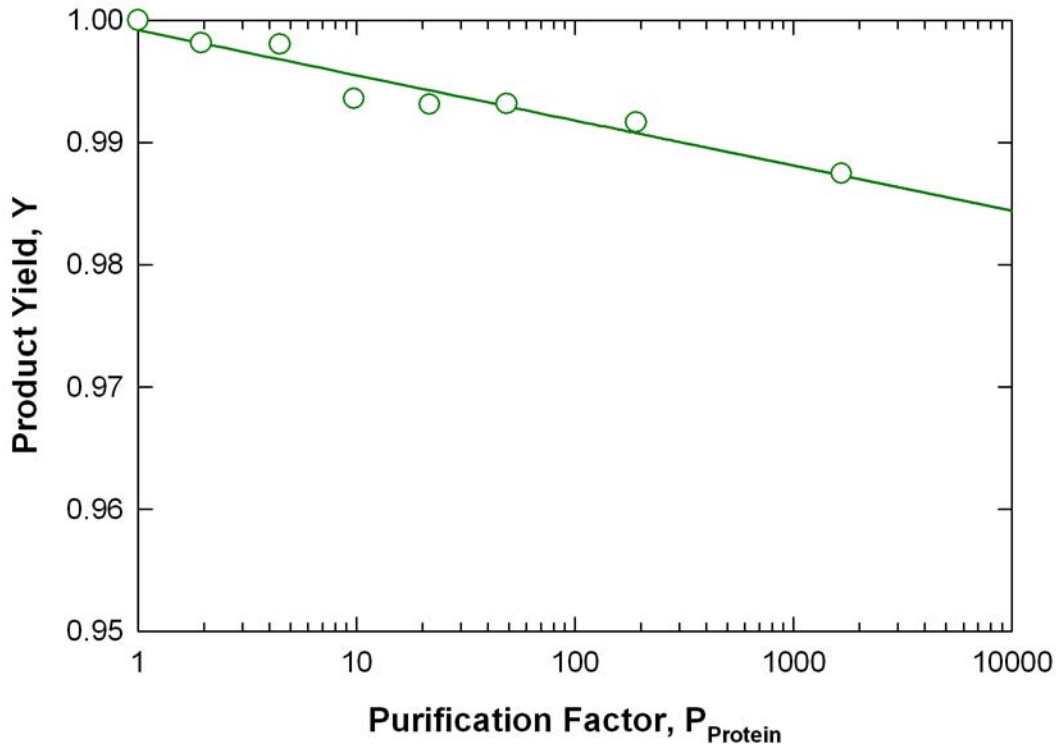


Figure 9.10. Yield versus purification factor for the PEGylated α -lactalbumin based on native α -lactalbumin as the impurity. Data for a diafiltration using a 30 kDa Ultracel™ membrane at pH 7, 500 mM ionic strength, and a filtrate flux of 9 $\mu\text{m/s}$. The solid curve is the model calculation using a selectivity of $\Psi_{\text{protein}} = 530$.

The solid curve in Figure 9.10 represents the model calculation evaluated using Equation 9.3 with a selectivity of 530 based on the values in Table 9.2. The process begins with a 100% product yield (all of the PEGylated protein is contained in the retentate) and a purification factor of 1, corresponding to the data point in the upper left hand corner of the graph. The purification factor increases throughout the diafiltration due to the removal of the impurity, with the product yield decreasing slightly because of the slow leakage of the product through the membrane. The model is in excellent agreement with the experimental data over the entire diafiltration using this single (constant) value of Ψ_{protein} . The final results of the first diafiltration provided an

experimental purification factor greater than 1000 with respect to the native protein with more than 98% product yield. Extrapolation of the model to higher diavolumes using Equation 9.3 suggests that this diafiltration process could have provided purification factors greater than 10^5 while still maintaining a product yield above 97 %.

Figure 9.11 shows the yield - purification factor behavior for the second-stage diafiltration, where the purification factor is defined using the 20 kDa PEG as the impurity of interest. The scatter in the data arises from errors in the evaluation of the PEG concentration by the SEC assay due to the use of the RI detector. The UV detector used to analyze the PEGylated protein and the α -lactalbumin had much greater sensitivity and accuracy. There were also small fluctuations in the retentate volume during the second-stage diafiltration, which would have minimal effect on the overall impurity removal but could easily have caused some of the scatter seen in Figure 9.11. The second-stage diafiltration provided more than 15-fold purification of the desired PEGylated protein with greater than 90% yield. The solid curve in Figure 9.11 is the model calculation evaluated from Equation 9.3 using a selectivity of 43 based on the best fit values of the sieving coefficients (Table 9.2). The model is in good agreement with the data and suggests that a purification factor greater than 100 could have been obtained with a product yield of 87% by using approximately 20 diavolumes.

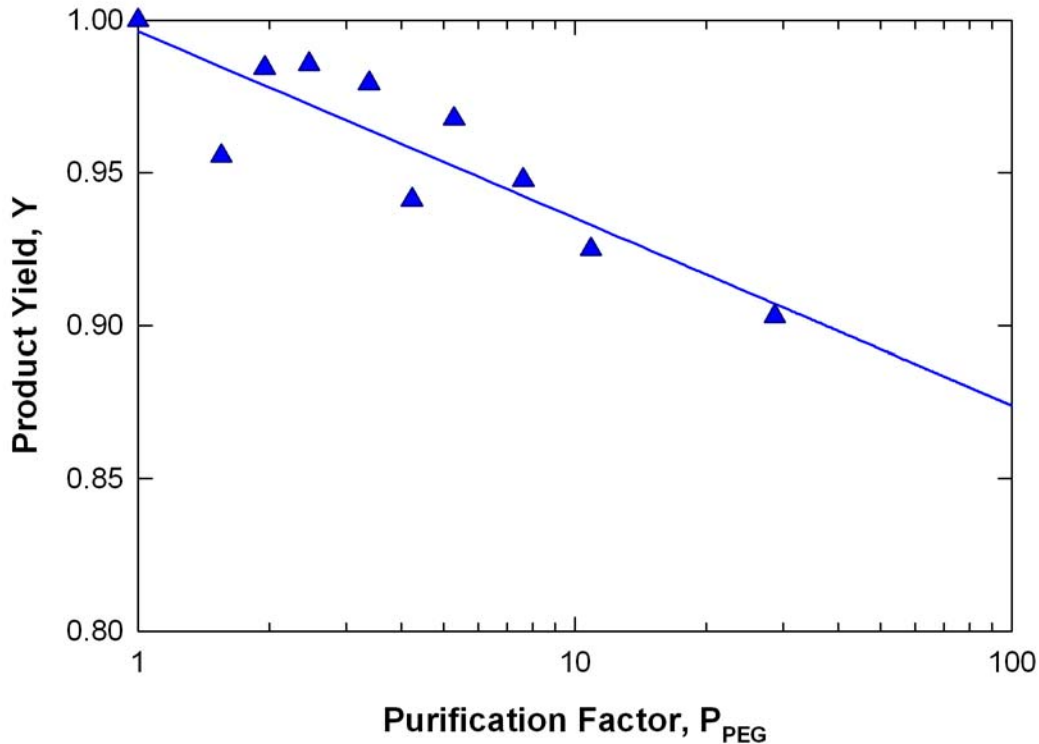


Figure 9.11. Yield versus purification factor for the PEGylated α -lactalbumin based on the 20 kDa PEG as the impurity. Data for a diafiltration using a negatively-charged 100 kDa Ultracel™ membrane at pH 7, 2.5 mM ionic strength, and a filtrate flux of 21 $\mu\text{m/s}$. Solid curve is a model calculation using a selectivity of $\Psi_{PEG} = 43$.

9.4 Conclusions

One of the critical challenges in the commercial development of protein-polymer conjugates as second-generation biotherapeutics is the need to remove unreacted precursors from the desired product. The results obtained in this chapter provide the first quantitative demonstration that it is possible to use a two-stage diafiltration system for the purification of a PEGylated protein, with nearly complete removal of the native (unreacted) protein and a 25-fold reduction in the concentration of the PEG. The overall product yield for this process was greater than 75%, with much of the loss occurring

during transfer of the feed between the membrane stages, an effect that would be much less significant at larger scale. The high degree of purification obtained in the two-stage system was achieved by exploiting differences in both the size and electrical charge of the PEGylated protein. The unreacted protein was very effectively removed in the first stage by a size-based separation using an Ultracel™ membrane in which the separation was driven by the very large size of the PEGylated protein. The unreacted PEG was then removed in the second stage using a negatively-charged Ultracel™ membrane that provided high retention of the negatively-charged PEGylated product while allowing the neutral PEG to pass into the filtrate.

A small scaled stirred cell system can be used as a basis for larger scale diafiltration systems. Tangential flow membranes such as the Pellicon XL and hollow fiber membrane systems tend to have higher mass transfer coefficients than the stirred cell set-ups that will limit concentration polarization. Thus it is expected that the sieving coefficients of the larger PEG and PEGylated protein may be smaller in the large scale system. The difference in mass transfer coefficients will increase the selectivity of the PEG and PEGylated protein for the first stage operation and most likely have little effect on the selectivity of the second stage since the size of the PEG and PEGylated proteins are similar.

It is difficult to compare the purification and yield data obtained in this chapter with previous work using chromatographic separations due to the lack of experimental detail in most published studies. Arduini et al. (2004) used size exclusion chromatography to purify PEGylated rat interferon- β from the native protein with purification factors greater than 99%, which is similar to the results obtained in this study

during the first-stage diafiltration. No data were provided for the removal of the unreacted PEG, which may reflect the very similar size (and thus very difficult separation) of these species using size exclusion chromatography. Brumeanu et al. (1995) examined the purification of two different antigenized immunoglobulins conjugated with polyethylene glycol using a combination of size exclusion followed by anion exchange chromatography. The size exclusion chromatography provided relatively little removal of the free PEG, consistent with the similar size of the PEG and PEGylated proteins, but the anion exchange step was able to reduce the concentration of PEG to nearly undetectable levels. The overall purification factor was above 100, but no data were provided on the product yield and it is difficult to compare results for this large antigenized immunoglobulin (MW > 120 kDa) with those obtained in this study using the 14 kDa α -lactalbumin.

The design and optimization of the two-stage diafiltration for the purification of the PEGylated protein requires the proper selection of the membrane pore size, membrane surface charge, solution pH, ionic strength, and filtrate flux. The data obtained with the PEGylated α -lactalbumin showed that removal of the native protein was relatively easy based on the large increase in effective size associated with the attachment of the polyethylene glycol chain. Selectivities greater than 500 were obtained using a commercially available 30 kDa UltracelTM membrane simply by operating at relatively low filtrate flux (7 - 10 $\mu\text{m/s}$). In contrast, the separation between the PEGylated protein and the PEG was much more challenging, requiring proper selection of the membrane charge and solution conditions to exploit differences in the electrostatic interactions. For example, reducing the ionic strength from 200 mM to 2.4 mM caused

the selectivity between the PEGylated α -lactalbumin and PEG to increase by nearly an order of magnitude.

Although the PEGylated α -lactalbumin used in these studies is a model system with no clinical applications, the physical characteristics of this system are very similar to those encountered in the production of actual PEGylated proteins. For example PegasysTM (Roche), a recombinant interferon α -2a, contains 44 kDa of PEG added to the 19.2 kDa protein through a single amide bond (Foser et al., 2003). Human granulocyte colony stimulating factor has a molecular weight of 18.8 kDa, only slightly larger than that of α -lactalbumin, and animal trials of PEGylated forms of this molecule have been performed with total molecular weight ranging from 81 to 150 kDa (Niven et al., 1994). PegvisomantTM (Pfizer) is composed of a 22 kDa protein with 20 – 24 kDa of PEG (Parkinson et al., 2003), which is very similar to the molecular weights of the PEGylated α -lactalbumin used in this study. Future studies will be needed to evaluate the economics and performance characteristics of the membrane process relative to that of alternative separation technologies for the large-scale commercial purification of clinically-relevant protein-polymer conjugates.

Chapter 10

FOULING AND CONCENTRATION POLARIZATION DURING ULTRAFILTRATION OF PEGYLATED PROTEINS

10.1 Introduction

One of the critical issues in the application of membrane technology for protein purification is membrane fouling, the largely irreversible adsorption and/or deposition of solutes on and within the membrane. Previous studies of protein fouling in ultrafiltration and microfiltration have clearly demonstrated the importance of solution conditions (Burns and Zydney, 2001; Fane et al., 1983; Jones and O'Melia, 2001; Palacio et al., 2003; Palecek and Zydney, 1994), membrane chemistry (Ho and Zydney, 2001; Hosch and Staude, 1996; Iordanskii, 1996; Ko and Pellegrino, 1992; Matthiasson, 1983; Nakatsuka and Michaels, 1992; Nystrom, 1989), and protein properties (Kelly et al., 1993; Kelly and Zydney, 1994; 1995; 1997; Palecek and Zydney, 1994) on both the rate and extent of fouling. For example, Jones and O'Melia (2001) showed that the flux decline during ultrafiltration of bovine serum albumin (BSA) through regenerated cellulose membranes was greatest at a pH equal to the protein isoelectric point (pI). Similar results were obtained by Fane et al. (1983), with maximum BSA adsorption to polyethersulfone membranes at pH near the pI and at high ionic strength, which the authors attributed to changes in the electrostatic interactions between the protein and

membrane surface. Several studies have clearly demonstrated that fouling is also greater on membranes with less hydrophilic characteristics (Nakatsuka and Michaels, 1992).

Protein fouling during ultrafiltration is often described in terms of the effects of pore blockage, pore constriction, and cake formation (Mochizuki and Zydney, 1992; Palacio et al., 2003 and 2002; Robertson and Zydney, 1990; Zeman and Zydney, 1996). The filtrate flux is written using Darcy's law:

$$J_v = \frac{\Delta P_{TM} - \sigma_o \Delta \Pi}{\mu(R_m + R_c)} \quad (10.1)$$

where ΔP_{TM} is the transmembrane pressure, σ_o is the osmotic reflection coefficient, $\Delta \Pi$ is the osmotic pressure difference across the membrane, R_m is the resistance associated with the membrane (including the effects of pore blockage and pore constriction), and R_c is the hydraulic resistance associated with the cake layer. The membrane resistance is often approximated using the Hagen-Poiseuille equation for laminar flow through a membrane consisting of a uniform array of cylindrical pores:

$$R_m = \frac{8\delta}{n\pi r_p^4} \quad (10.2)$$

where n is the number of pores, δ is the membrane thickness, and r_p is the pore radius. Fouling due to pore blockage reduces the number of pores (n) while pore constriction reduces the pore radius (r_p). Pore constriction usually occurs in relatively larger pores compared to the size of the solute molecules while pore blockage and cake formation are usually more important for large solutes. However, even small proteins can block pores of microfiltration membranes due to the presence of trace amounts of large aggregates (Kelly et al., 1993). More details on these models are given by Hermia (1982) and Zeman and Zydney (1996).

The objective of this chapter was to evaluate the effects of PEGylation on the filtrate flux and fouling characteristics during ultrafiltration of a model PEGylated protein using both fully and partially retentive regenerated cellulose and polyethersulfone membranes. Experiments were performed using PEGylated bovine serum albumin as a model protein, with the native (un-PEGylated) BSA used for comparison. The results are analyzed in terms of the underlying physical properties of the PEGylated proteins as determined by liquid chromatography (Chapter 5), dynamic light scattering (Chapter 5), capillary electrophoresis (Chapter 6), and reverse phase chromatography (discussed subsequently). The filtration behavior with the cellulose membranes was dominated by concentration polarization effects, with the lower flux for the PEGylated protein solutions associated with the smaller bulk mass transfer coefficient. Significant fouling was observed with the polyethersulfone membranes. Greater fouling was seen with the PEGylated protein due to its increased size, greater hydrophobicity, and lower electrostatic interactions, all of which are directly associated with the attached poly(ethylene glycol) chains. These results provide important insights into the ultrafiltration characteristics of PEGylated proteins.

Much of the experimental data presented in this chapter were obtained by Dr. Boksoon Kwon, a postdoctoral researcher who spent several months at Penn State collaborating on this project.

10.2 Materials and Methods

10.2.1 Protein PEGylation

Bovine serum albumin was used as a model protein for this set of experiments due to the extensive prior literature on BSA fouling in both ultrafiltration and microfiltration (Ghosh and Cui, 1999; Nabe et al., 1997; Palacio et al., 2003). PEGylated BSA, formed by attachment of a single 12 kDa PEG to the free sulfhydryl group on BSA, was provided by Pfizer in a 20 mM Bis Tris propane solution containing 10 mM NaCl. BSA was also PEGylated in our laboratory using 5 kDa mPEG-SMB as described in Chapter 3. Conjugation was performed by adding activated PEG in a 6 to 1 molar ratio to 12 g/L BSA dissolved in a 10 mM Bis Tris buffer solution at pH 7.0. These solutions were diluted with 10 mM Bis Tris buffer (MP Biomedicals, Solon, Ohio) to obtain the desired protein concentration, with the appropriate amount of KCl added to achieve the desired 10 mM ionic strength. Additional HCl was added in select experiments to reduce the pH.

10.2.2 Ultrafiltration

Ultrafiltration experiments were conducted using UltracelTM composite regenerated cellulose membranes and BiomaxTM polyethersulfone membranes, both provided by Millipore Corporation (Bedford, MA). The handling and preparation of these membranes is described in Chapter 3. All filtration experiments were performed in 25 mm diameter stirred ultrafiltration cells (Millipore Corp., Bedford, MA). A Model 8010 cell (effective area of 4.1 cm²) was used with the 30 and 100 kDa membranes while Model 8003 (effective area of 0.9 cm²) was used with the 300 kDa membranes; the

smaller volume cell was used with the larger molecular weight cut-off membranes to reduce the amount of protein needed for experiments with these higher flux membranes. Prior to each experiment the hydraulic permeability was evaluated using Equation 2.8 based on the measured values of the filtrate flux as a function of the transmembrane pressure. The zeta potential of the membrane (ζ) was evaluated from streaming potential measurements obtained with a 10 mM Bis Tris buffer containing 10 mM KCl at pH 7 as described in Chapter 8.

After measuring the permeability of the clean membrane, the stirred cell and solution reservoir were emptied and rapidly refilled with a solution containing either the native or PEGylated BSA. The system was re-pressurized, and the filtrate flux was measured as a function of time using timed collection at constant pressures between 14 and 140 kPa (corresponding to 2 and 20 psi). Samples were obtained periodically from both the bulk and filtrate solutions for subsequent analysis by either UV spectrophotometry or size exclusion chromatography (SEC). At the completion of the ultrafiltration, the stirred cell was emptied and gently rinsed to remove any labile protein. Rinsing was done by filling the stirred cell with DI water (2 times) and stirring at 600 rpm for about two minutes in the absence of any applied transmembrane pressure. This procedure was then repeated using Bis Tris buffer instead of DI water. The device was then filled with fresh Bis Tris buffer and re-pressurized, and the buffer flux was evaluated as a function of time to obtain a measure of the extent of irreversible fouling.

Protein adsorption studies on regenerated cellulose (UltracelTM) and polyethersulfone (BiomaxTM) membranes were performed by simply soaking the membrane in the protein solution for approximately 12 hours. The membrane was then

gently rinsed as described above to remove any labile protein prior to evaluating the permeability. The extent of adsorption was determined based on the difference in the permeability of the membrane before and after soaking the membrane in protein solution.

10.2.3 Protein Characterization

The molecular weight of the BSA and PEGylated BSA solutions were determined by size exclusion chromatography using an Agilent 1100 HPLC system with a Superdex 200 column as described in Chapter 3. Protein detection was by UV absorbance at 280 nm, with the UV detector used in series with an Agilent 1100 series refractive index detector to detect any free PEG.

Protein electrophoretic mobilities were determined using a G1600A High Performance Capillary Electrophoresis instrument as described in Chapter 3. Fused silica capillaries (inner diameter = 50 μm , total length = 80.5 cm) were used with an applied voltage of 25 kV and a running buffer of 10 mM Bis Tris at pH 7.0.

Hydrophobic interactions of the BSA and PEGylated BSA were characterized by reverse-phase HPLC using a SymmetryTM 300 C4 column (4.6 mm \times 50 mm, 30 nm pore size, 5 μm particle size from Waters, Milford, MA) as described in Chapter 3. The molecules were eluted with a linear gradient between water and acetonitrile each with 0.1% TFA.

10.3 Results

10.3.1 Regenerated Cellulose Membranes

Typical experimental data for the normalized filtrate flux as a function of time for the ultrafiltration of BSA and the 12 kDa PEGylated BSA through 100 kDa nominal molecular weight cut-off Utracel™ membranes at a constant pressure of 35 kPa (5 psi) and 140 kPa (20 psi) are shown in the top and bottom panels of Figure 10.1. A separate membrane was used for each protein / pressure. Two repeat experiments with the 12 kDa PEGylated BSA are shown at the higher pressure, with the measured flux being nearly identical (within 10%) throughout the ultrafiltration. The reproducibility was excellent for both the native and PEGylated BSA for all experimental conditions tested. In each case, the data are normalized by the buffer flux evaluated immediately prior to the protein ultrafiltration at the same transmembrane pressure. The filtrate flux at 35 kPa was slightly greater for the 12 kDa PEGylated BSA although the differences were relatively small. For both the protein and PEGylated protein, there was a small decline in flux over the course of the filtration, with the flux decreasing by about 40%. The average sieving coefficients for both proteins at 35 kPa were greater than 0.9; thus, there was relatively little accumulation of protein in the stirred cell during these experiments. Immediately after each protein filtration experiment, the stirred cell was emptied and re-filled with 10 mM Bis Tris buffer. The filtrate flux for the protein-free buffer (shown as the second set of data immediately after the protein ultrafiltration) was approximately 5~13% smaller than the buffer flux evaluated with the clean membrane ($J_0 = 122 \mu\text{m/s}$), suggesting that

there was relatively little irreversible protein fouling during the ultrafiltration experiments with the Ultracel™ membranes under these conditions.

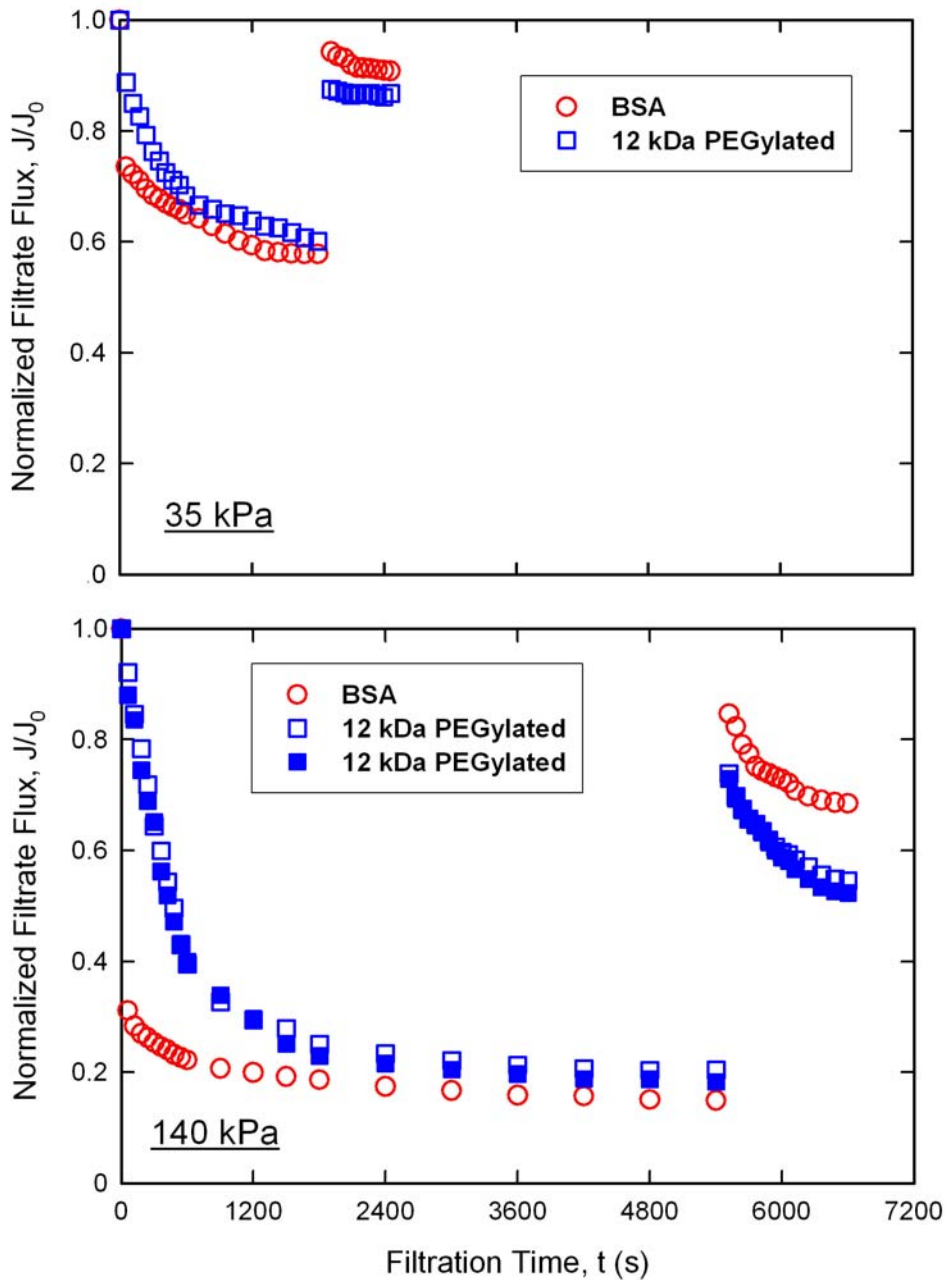


Figure 10.1. Flux decline for ultrafiltration of 1 g/L solutions of native BSA and the 12 kDa PEGylated BSA at pH 7 and 10 mM ionic strength through 100 kDa Ultracel™ membranes at a constant pressure of 35 kPa (upper panel) and 140 kPa (lower panel). Data for $t > 1800$ s (upper panel) and $t > 5400$ s (lower panel) are the buffer flux through the fouled membranes.

The results at a pressure of 140 kPa (bottom panel in Figure 10.1) are qualitatively similar to those at 35 kPa, with the flux for the 12 kDa PEGylated BSA being significantly greater than that for the native BSA over the first 1500 s and then remaining approximately 6 % larger at $t > 2400$ s. However, the rate of flux decline was much more pronounced at the higher pressure, with the flux for the 12 kDa PEGylated BSA decreasing by nearly a factor of 5 over the 90 minute ultrafiltration. The final fluxes for both the 12 kDa PEGylated BSA and the native BSA were similar to those obtained at the lower pressure (despite the large differences in the normalized flux). For example, the flux with the 12 kDa PEGylated BSA at $\Delta P = 35$ kPa was $75 \mu\text{m/s}$ compared to $78 \mu\text{m/s}$ at the higher pressure. The lack of any significant dependence on the applied pressure is consistent with the classical concentration polarization phenomenon, with the steady-state flux determined by the balance between the convective flow towards the membrane and the rate of mass transfer back into the bulk solution. The sieving coefficient of the 12 kDa PEGylated BSA was slightly smaller at 140 kPa ($S_o = 0.85$) compared to that at 35 kPa ($S_o = 0.94$), with similar results for the BSA.

The buffer flux after protein ultrafiltration at 140 kPa began at a value similar to that for the clean membrane, but there was a distinct decline in buffer flux over the next 20 min. The final (essentially steady-state) buffer flux through the membrane that was used to filter the 12 kDa PEGylated BSA was $208 \mu\text{m/s}$, which is 44 % smaller than the buffer flux through the clean membrane. The small decline in buffer flux with time may reflect the slow compression of a protein deposit on the membrane surface, with the data

clearly suggesting that the deposit formed with the 12 kDa PEGylated BSA was less permeable than the deposit formed with the native BSA.

Additional insights into the contributions of fouling and concentration polarization were obtained using 30 kDa Ultracel™ membranes that were fully retentive to both BSA and the PEGylated BSA. Filtrate flux data at 120 kPa (18 psi) are shown in Figure 10.2. In contrast to the results in Figure 10.1, the greatest filtrate flux was obtained with the native BSA, with the flux at $t = 60$ min approximately twice that for the 12 kDa PEGylated BSA. This is exactly opposite the results seen with the 100 kDa membrane where the 12 kDa PEGylated BSA had the greatest flux (top and bottom panels of Figure 10.1). The buffer flux after the protein ultrafiltration was nearly equal to that of the clean membrane for the BSA, while the membrane that was used to filter the 12 kDa PEGylated BSA showed a significant amount of fouling (approximately 40% reduction in buffer flux). The fouling seen with the 12 kDa PEGylated BSA may be related to the hydrophobicity of the PEGylated protein, something that is discussed in more detail in the next section.

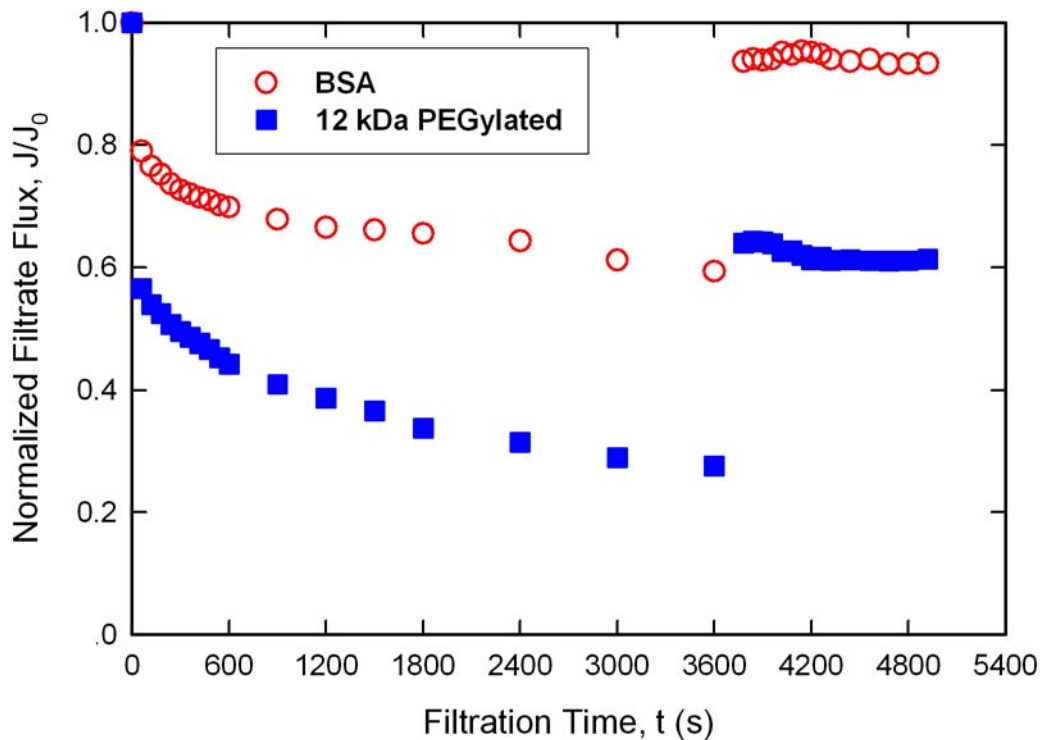


Figure 10.2. Flux decline for ultrafiltration of 1 g/L solutions of native BSA and the 12 kDa PEGylated BSA at pH 7 and 10 mM ionic strength through 30 kDa Ultracel™ membranes at a constant pressure of 120 kPa. Data for $t > 3600$ s are the buffer flux through the fouled membranes.

The higher flux for the BSA relative to the PEGylated BSA through the 30 kDa membrane is likely due to differences in concentration polarization arising from the reduction in protein diffusion coefficient associated with the attachment of the poly ethylene glycol. From the results in Chapter 5, the hydrodynamic radii of the BSA and the 12 kDa PEGylated BSA are 3.3 nm and 5.1 nm as determined using size exclusion chromatography. This difference in protein size would correspond to a difference in mass transfer coefficient (k_m) of approximately 20 % between BSA and the 12 kDa PEGylated BSA assuming that the diffusion coefficient varies as $1/R_h$ and that k_m varies

as $D_\infty^{2/3}$ based on available correlations for mass transfer in stirred cells (discussed in Chapter 2). This reduction in mass transfer coefficient should lead to a corresponding decrease in the filtrate flux as given by Equation 2.2. In contrast, the long-time flux with BSA ($J_v = 58 \mu\text{m/s}$) was more than a factor of two larger than that obtained with the 12 kDa PEGylated BSA, which is likely due to the greater degree of fouling with the 12 kDa PEGylated BSA (as shown by the lower buffer flux through the fouled membrane).

The results for the Ultracel™ membranes are summarized in Table 10.1, which also shows data for a corresponding set of experiments performed with the 5 kDa PEGylated BSA generated in our laboratory. This PEGylated BSA had an average effective size of about 5.3 nm (determined by size exclusion chromatography), which is greater than that of the 12 kDa PEGylated BSA due to the attachment of approximately three PEG chains per protein. The membrane resistance (R_m) is simply equal to the reciprocal of the clean membrane permeability. The resistance of the fouling layer (R_f) was determined from the resistance of the fouled membrane (determined after rinsing with DI water and buffer to remove any labile protein from the boundary layer) subtracting off the resistance of the clean membrane. The fouling resistance thus accounts for the increase in resistance due to both internal membrane fouling and the formation of a stable cake / gel layer on the membrane surface. The resistance of the polarization layer (final column in Table 10.1) was evaluated from the steady-state protein flux (J_{ss}) using the resistance in series model:

$$R_p = \frac{\Delta P}{\mu J_{ss}} - R_m - R_f \quad (10.3)$$

Table 10.1. Membrane, fouling layer, and polarization resistances through Ultracel™ membranes.

Ultracel™ Membranes	Pressure (kPa)	Protein	J_{ss} ($\times 10^5$ m/s)	J_B ($\times 10^5$ m/s)	R_m ($\times 10^{-11}$ m ⁻¹)	R_f ($\times 10^{-11}$ m ⁻¹)	R_p ($\times 10^{-11}$ m ⁻¹)
30 kDa	140	BSA	5.8	9.1	13.3	0.8	8.1
	120	12 kDa PEG-BSA	2.7	6.0	13.0	8.4	26.1
	130	5kDa PEG-BSA	4.0	9.0	12.9	1.2	17.8
100 kDa	34	BSA	7.0	11.1	3.0	0.3	1.9
	35	12 kDa PEG-BSA	7.4	10.7	2.9	0.4	1.5
	39	5kDa PEG-BSA	4.6	11.7	2.9	0.2	4.7
	140	BSA	7.1	26.0	3.8	1.8	14.9
	130	12 kDa PEG-BSA	7.8	20.7	3.8	3.2	11.6
	130	5kDa PEG-BSA	4.8	29.7	3.7	1.2	24.9

The resistance of the fouling layer on the 30 kDa membranes is lowest for the experiment with BSA and highest for the experiment with the 12 kDa PEGylated BSA, with similar behavior seen for the 100 kDa membrane. The R_f values for the experiments with BSA and the 5 kDa PEGylated BSA are much larger with the 100 kDa membrane, which probably reflects the presence of both internal and external fouling of the larger pore size membrane. This effect was not seen with the 12 kDa PEGylated BSA; the reason for this difference is unclear. The polarization layer resistances for the 5 and 12 kDa PEGylated BSA with the 30 kDa membrane were both significantly greater than that for BSA, which is consistent with the smaller mass transfer coefficients for the PEGylated proteins. The 5 kDa PEGylated BSA had the highest R_p for the 100 kDa membrane; however, the R_p values for BSA and the 12 kDa PEGylated BSA for the 100 kDa membrane were similar, which may simply reflect the very low degree of protein retention (around 10 %) with the 100 kDa Ultracel™ membranes.

10.3.2 Polyethersulfone Membranes

Filtrate flux data for BSA and PEGylated BSA through 100 kDa Biomax™ polyethersulfone membranes are shown in Figure 10.3 for ultrafiltration at a constant pressure of 28 kPa (4 psi). This slightly lower pressure was used to achieve approximately the same initial buffer flux ($J_0 = 125 \mu\text{m/s}$) as that for the Ultracel™ membranes at 35 kPa (top panel of Figure 10.1). In contrast to the data with the 100 kDa Ultracel™ membrane, the filtrate flux was greater for the BSA. In addition, the buffer flux through the Biomax™ membranes after protein ultrafiltration was approximately a factor of two smaller than the buffer flux through the clean membranes, indicating that there was a significant amount of fouling during ultrafiltration through the Biomax™ membranes. The extent of fouling for the Biomax™ membranes with the BSA and PEGylated BSA were similar, with somewhat greater fouling seen for the membrane used to filter the 12 kDa PEGylated BSA. The average sieving coefficient of the BSA was 0.09 while the sieving coefficient of the 12 kDa PEGylated BSA was 0.22, even though the PEGylated protein is approximately 35 % larger than the native BSA. This difference may be due to the greater degree of concentration polarization of the 12 kDa PEGylated BSA associated with the smaller mass transfer coefficient of the larger molecule in addition to possible deformation of the PEGylated protein (discussed in Chapter 7). The significantly smaller sieving coefficients of the BSA and PEGylated BSA for the Biomax™ membrane compared to the Ultracel™ membrane is probably a result of the higher degree of fouling with the Biomax™ membranes.

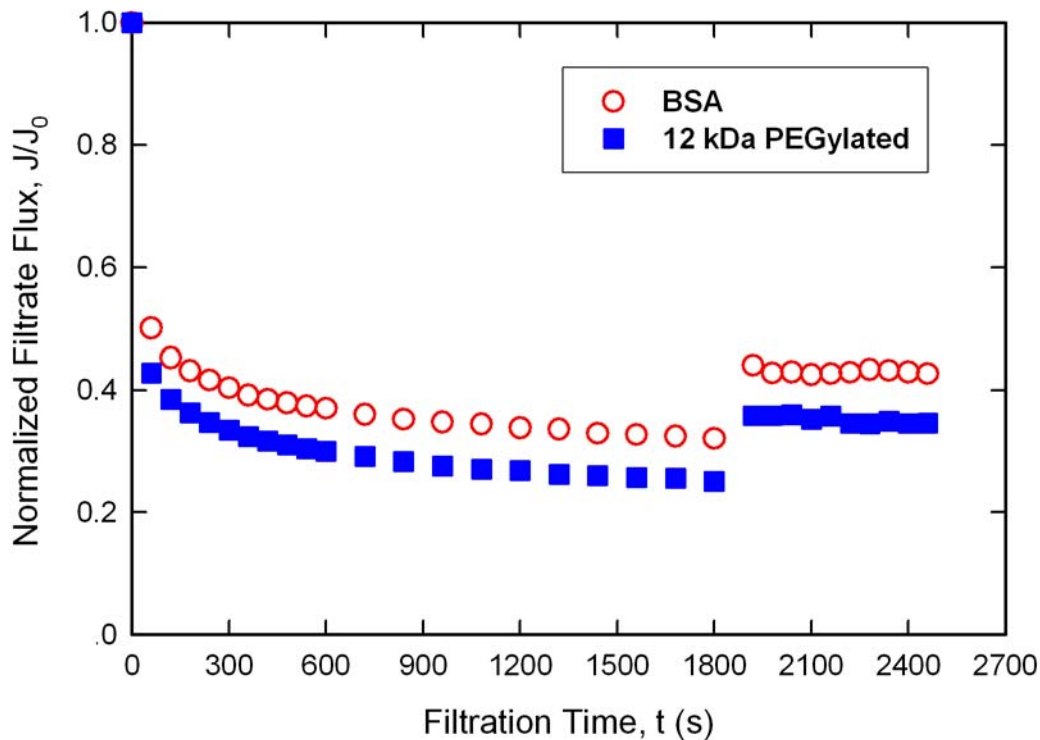


Figure 10.3. Flux decline for ultrafiltration of 1 g/L solutions of native BSA and the 12 kDa PEGylated BSA at pH 7 and 10 mM ionic strength through 100 kDa Biomax™ membranes at a constant pressure of 28 kPa. Data for $t > 1800$ s are the buffer flux through the fouled membranes.

Similar data for protein ultrafiltration through the 300 kDa Biomax™ membrane are shown in Figure 10.4. Protein transmission through the 300 kDa membrane was quite high, with greater than 90% transmission of both BSA and the PEGylated BSA. The filtrate flux data for the 300 kDa membrane were qualitatively similar to the results for the 100 kDa membrane, with the greatest flux seen with BSA. However, the buffer flux after protein ultrafiltration show distinct differences; the membrane used with BSA had a buffer flux that was 2.7 times the value obtained with the membrane used with the 12 kDa PEGylated BSA. These data clearly indicate that the PEGylated protein causes

much greater fouling than the native BSA during ultrafiltration through the larger pore size 300 kDa Biomax™ membrane.

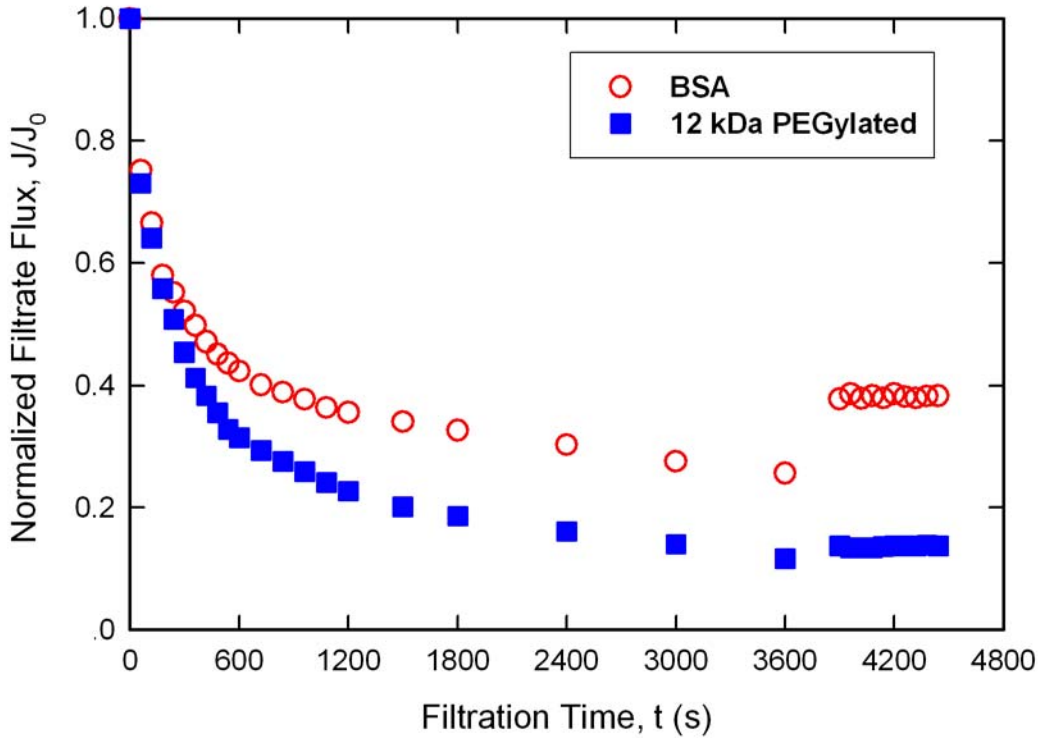


Figure 10.4. Flux decline for ultrafiltration of 1 g/L solutions of native BSA and the 12 kDa PEGylated BSA at pH 7 and 10 mM ionic strength through the 300 kDa Biomax™ membranes at a constant pressure of 14 kPa. Data for $t > 3600$ s are the buffer flux through the fouled membranes.

The calculated values of the membrane resistance (R_m), the fouling layer resistance (R_f), and the polarization layer resistance (R_p) for the experiments with the 100 kDa and 300 kDa Biomax™ membranes are shown in Table 10.2. The polarization layer resistance for the 100 kDa membrane is lowest for the BSA and greatest for the 5 kDa PEGylated BSA, consistent with the differences in the effective size (and mass transfer coefficients) of these proteins: $R_h = 3.3$ nm for BSA, 5.1 nm for the 12 kDa PEGylated

BSA, and 5.3 nm for the 5 kDa PEGylated BSA as determined by size exclusion chromatography. Similar behavior is seen with the 300 kDa membrane, although the polarization layer resistance is quite small due to the relatively low degree of protein retention with this large pore size membrane. The fouling layer resistance is greatest for the 12 kDa PEGylated BSA and lowest for the BSA on both the 100 and 300 kDa membranes, which is similar to the behavior seen with the Ultracel™ membranes.

Table 10.2. Membrane, fouling layer, and polarization resistances for ultrafiltration experiments with Biomax™ membranes

Biomax™ Membranes	Pressure (kPa)	Protein	J_{ss} ($\times 10^5$ m/s)	J_B ($\times 10^5$ m/s)	R_m ($\times 10^{-11}$ m ⁻¹)	R_f ($\times 10^{-11}$ m ⁻¹)	R_p ($\times 10^{-11}$ m ⁻¹)
100kDa	28	BSA	4.1	5.4	2.3	3.0	1.7
	28	12 kDa PEG-BSA	3.1	4.3	2.3	4.4	2.6
	33	5kDa PEG-BSA	3.0	4.6	2.3	3.9	3.3
300kDa	14	BSA	8.2	12.2	0.5	0.7	0.6
	14	12 kDa PEG-BSA	3.8	4.5	0.4	2.8	0.6
	14	5kDa PEG-BSA	5.9	9.2	0.4	1.1	0.9

Although the greater fouling of the PEGylated proteins may be due, at least in part, to the increase in size (and therefore retention) caused by the attachment of the polyethylene glycol chain, the large difference in R_f values for the 300 kDa Biomax™ membranes (which had little retention even for the large PEGylated proteins) suggests that size may not be the dominant factor governing this behavior. Further insights into the fouling characteristics were obtained using reverse phase chromatography, which provides a measure of the relative hydrophobicity (balance of van der Waals and hydrogen bonding forces) of a protein. Results are shown in Figure 10.5 for BSA and the 12 kDa PEGylated BSA using a C4 column. The PEGylated protein eluted considerably

after the native BSA, corresponding to a greater acetonitrile concentration, indicating that the BSA had a stronger interaction with hydrophilic mobile phase than the PEGylated BSA. Similar results have been reported by Hu et al. (2005) for PEGylated hemoglobin and by Zhang et al. (2007) for PEGylated insulin. This behavior is also consistent with previous studies of polyethylene glycol adsorption to hydrophobic surfaces, which have clearly demonstrated that PEG chains do have a significant hydrophobic character (Leininger et al., 2004; Pagac et al., 1997).

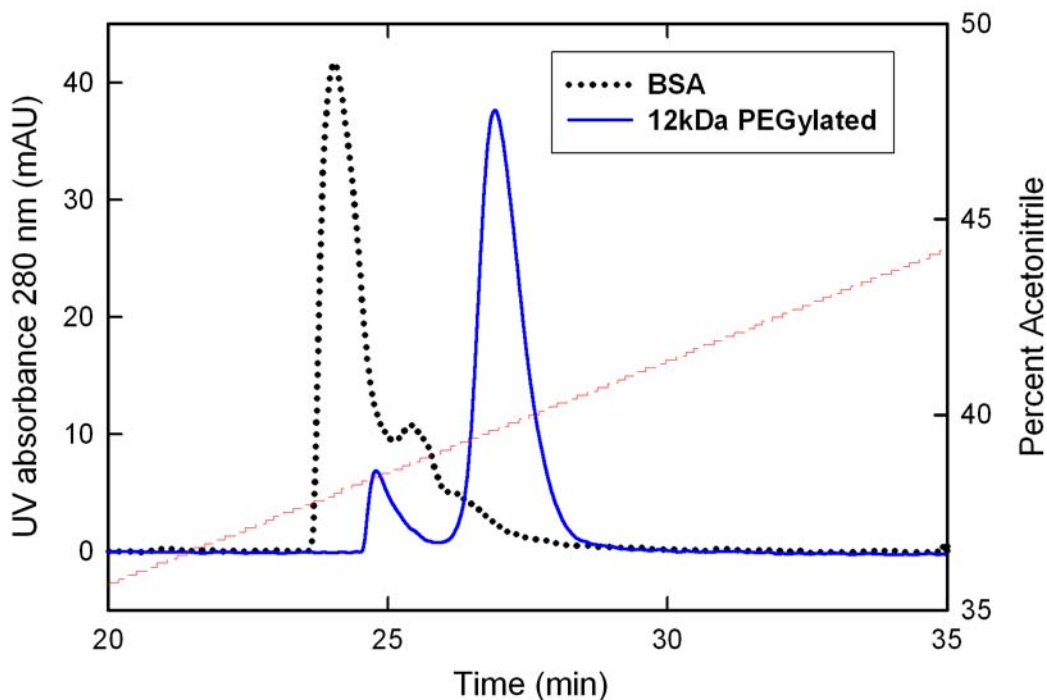


Figure 10.5. Reverse phase chromatography for BSA and the 12 kDa PEGylated BSA on a C4 column using a gradient of trifluoroacetic acid (TFA) in water and TFA in acetonitrile.

The greater hydrophobicity of the PEGylated protein compared to the native BSA may be the cause of the greater degree of fouling seen during ultrafiltration of the

PEGylated BSA through the more hydrophobic Biomax™ polyethersulfone membranes. Additional insights into the effect of the protein hydrophobicity were obtained by measuring the extent of protein adsorption to the polyethersulfone membranes. In this case, the hydraulic permeability was evaluated before and after soaking the membrane in 1 g/L solutions of the different proteins for 24 hr at pH 7 (in the absence of any ultrafiltration). BSA adsorption caused a 43% reduction in the permeability of the 100 kDa Biomax™ membrane, while the 12 kDa PEGylated BSA caused a 51% reduction in permeability, consistent with the greater hydrophobicity of the PEGylated protein. In contrast, the permeability of the Ultracel™ membranes were largely unaffected by adsorption of either BSA or PEGylated BSA; the permeability after protein adsorption was always within 10% of the clean membrane permeability.

10.3.3 Electrostatic Interactions

In addition to hydrophobicity, previous studies have clearly demonstrated the importance of electrostatic interactions on membrane fouling (Palacio et al., 2003). In order to explore these effects, ultrafiltration experiments were performed at various ionic strengths and solution pH with results at pH 4.8 (near the isoelectric point of native BSA) and pH 7 (where BSA has a significant negative charge) shown in Figure 10.6 for both BSA (top panel) and the 5 kDa PEGylated BSA (bottom panel). The filtrate flux with the native BSA was a strong function of solution conditions, with the greatest flux attained at pH 7 and low salt concentration, conditions which maximize electrostatic interactions. In addition, the extent of membrane fouling was also a function of solution conditions, with the membrane used at the protein isoelectric point having the smallest buffer flux after

the protein ultrafiltration. In contrast, the flux and fouling characteristics of the 5 kDa PEGylated BSA (bottom panel) were largely independent of solution conditions, indicating that the poly(ethylene glycol) chains significantly reduce the effects of electrostatic interactions on protein adsorption.

The results from the membrane fouling experiments are consistent with the data obtained in Chapter 6 for the electrophoretic mobility, with the mobility of the PEGylated proteins decreasing as the size of the molecule increases (due to the addition of the PEG chains). For example the electrophoretic mobility of BSA was $-15 \pm 1 \times 10^{-9} \text{ m}^2 \text{ V}^{-1} \text{ s}^{-1}$, which is approximately 40% larger than the electrophoretic mobility of the two PEGylated proteins ($-11 \pm 1 \times 10^{-9} \text{ m}^2 \text{ V}^{-1} \text{ s}^{-1}$ for the 12 kDa PEGylated BSA and $-10 \pm 1 \times 10^{-9} \text{ m}^2 \text{ V}^{-1} \text{ s}^{-1}$ for the 5 kDa PEGylated BSA) using a Bis Tris pH 7.0 and 10 mM ionic strength buffer.

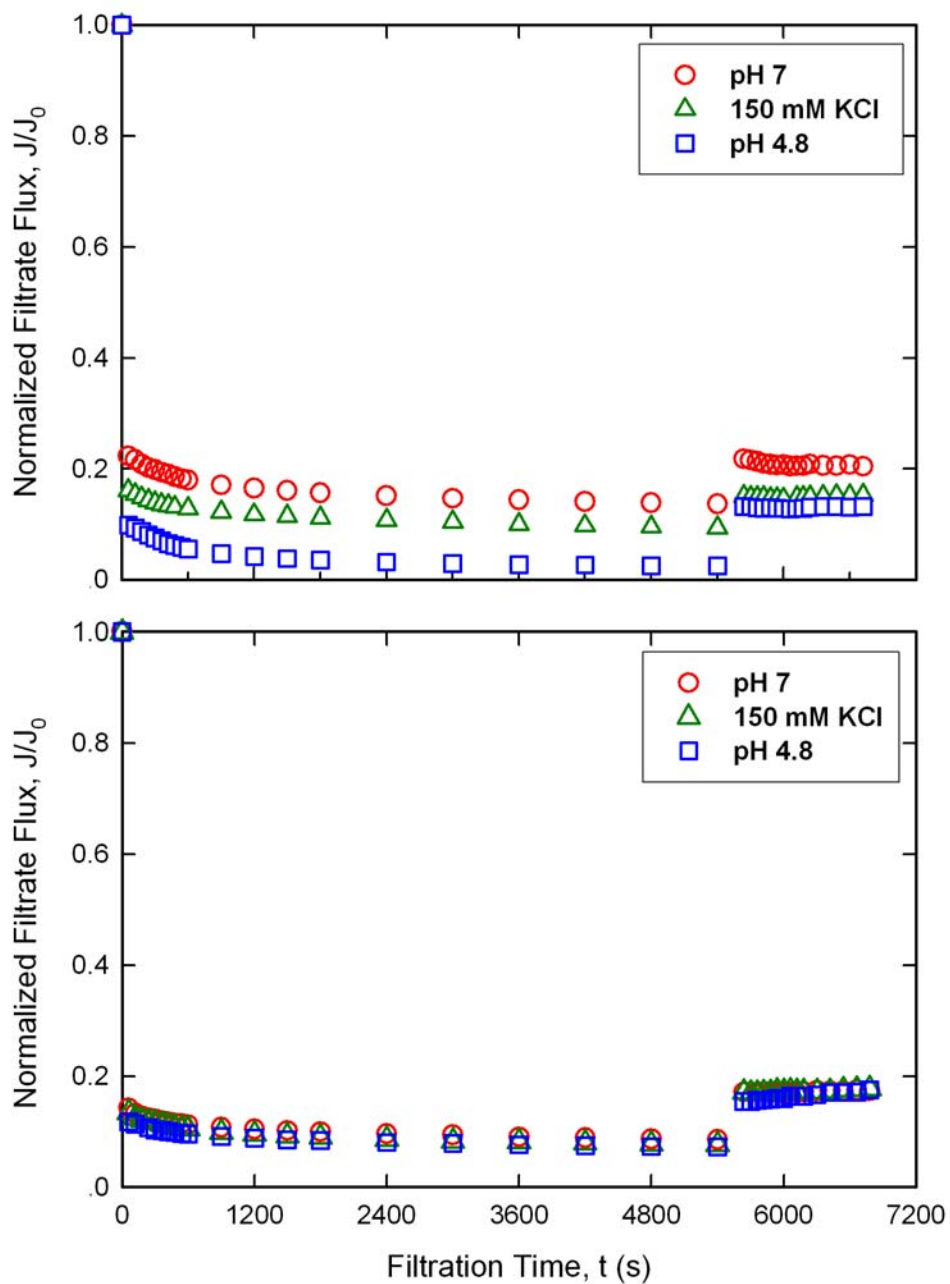


Figure 10.6. Effect of solution pH and salt concentration on the flux decline for BSA (top panel) and the 5 kDa PEGylated BSA (bottom panel) through 100 kDa Biomax™ membranes at a constant pressure of 103 kPa. Data for $t > 5400$ s are the buffer flux through the fouled membranes.

10.4 Conclusions

The data obtained in this chapter provide the first experimental results for the effects of PEGylation on the fouling characteristics during ultrafiltration using hydrophilic regenerated cellulose (UltracelTM) membranes and more hydrophobic polyethersulfone (BiomaxTM) membranes. There was relatively little fouling of the UltracelTM membranes by the BSA or PEGylated BSA, with the flux dominated by concentration polarization effects. In this case, the increase in size of the PEGylated protein caused an increase in the extent of protein retention and a reduction in the protein mass transfer coefficient, both of which contribute to a lower value of the filtrate flux. There was some protein fouling of the UltracelTM membranes at high pressures, particularly with the PEGylated BSA, which is consistent with the greater hydrophobicity and greater retention of the PEGylated protein.

The filtration behavior with the BiomaxTM membranes was more complex. There was a considerable amount of protein fouling with the polyethersulfone BiomaxTM membranes under all conditions. The greater fouling seen with the PEGylated BSA is likely due to the greater size and hydrophobic interactions, both of which are a direct result of the attached poly(ethylene glycol) chains. For example, the resistance of the fouling layer formed on the 300 kDa membrane with the 12 kDa PEGylated BSA was 8 times that of the fouling layer formed with native BSA. In addition, the PEG shields electrostatic interactions between the proteins and membrane, significantly reducing the effects of solution pH and salt concentration on protein adsorption and fouling compared to that observed with the native protein. Future studies will be needed to determine the

implications of this increase in fouling on membrane cleaning / regeneration and membrane lifetime.

The increase in hydrophobic interactions of the PEGylated proteins is somewhat counterintuitive since PEG is typically considered to be hydrophilic (Li and Kao, 2003; Makino et al., 1999; Shi et al., 2007). However, the increase in elution time for the PEGylated BSA on the C4 column was very significant, and this behavior is consistent with previous results using PEGylated hemoglobin (Hu et al., 2005) and PEGylated insulin (Zhang et al., 2007). This increase in hydrophobic interactions could have significant implications in the downstream processing of PEGylated proteins, particularly for filtration steps that utilize hydrophobic membranes that are more susceptible to fouling by hydrophobic species.

Chapter 11

CONCLUSIONS AND FUTURE WORK

11.1 Introduction

There is a growing clinical interest in the use of PEGylated recombinant proteins with enhanced stability, half-life, and bioavailability. One of the critical issues in the large-scale commercial production of these second generation biotherapeutics is the need for high resolution and high throughput purification processes. This thesis provides the first comprehensive study of the use of membrane ultrafiltration to purify PEGylated proteins. The experimental and theoretical studies clearly demonstrated the importance of both steric (size-based) and electrostatic interactions in determining the transmission of PEGylated proteins through semipermeable ultrafiltration membranes. Sieving coefficient data were in good agreement with model calculations with key physical parameters evaluated independently using size exclusion chromatography and capillary electrophoresis. Data from small-scale ultrafiltration experiments were used to design a two-stage diafiltration process that provided effective purification of the PEGylated product from unreacted protein and hydrolyzed polyethylene glycol. The following subsections summarize the key results and conclusions from each chapter of this thesis. Recommendations for future work are also discussed.

11.2 PEGylation Reactions

PEGylated proteins were produced using PEG activated n-hydroxylsuccinimide esters (mPEG-SPA or mPEG-SMB) which react with terminal amine groups (primarily on the lysine amino acids). Reactions were performed over a range of experimental conditions, with the data analyzed using a simple kinetic model assuming that the rate of each reaction was first order in each reactant. The rate constants for the PEGylation reactions decreased as more PEG was added to the protein due to the lower accessibility and / or reactivity of the subsequent PEGylation sites. The mPEG-SPA had significantly higher rate constants for the PEGylation reaction than the mPEG-SMB, but the rates of hydrolysis of the activated PEGs were similar. The yield of PEGylated protein was increased by using high concentrations of the protein and PEG reactants while keeping the molar ratio of PEG to protein constant, although the selectivity for a given PEGylated protein product, e.g., the singly PEGylated species, was largely unaffected by the reactant concentrations. The extent of reaction was relatively independent of pH and ionic strength, although more detailed analysis would be needed to quantify the dependence of the rate constants on solution conditions. These reaction studies were used to identify robust conditions for the production of a PEGylated protein solution with consistent composition, which was critical for use in the characterization and separation experiments performed throughout the rest of the thesis.

Two different reaction schemes were examined to potentially increase the selectivity for production of the desired, typically the singly, PEGylated protein product. A fed-batch reaction system was examined in which PEG was added to the reactor in small consecutive increments. The fed-batch and batch systems were predicted to

provide equivalent yield of the singly PEGylated protein using the first-order kinetic model, and this was confirmed experimentally using a 10 kDa mPEG-SPA. Data were also obtained using a combined reaction-separation scheme in which the PEGylated protein and unreacted PEG were separated from the protein (α -lactalbumin), which was collected in the filtrate and recycled for additional reaction. Model calculations showed that this type of reaction-separation process has the potential to provide higher yields of a desired singly PEGylated product compared to the more highly substituted PEGylated species. However, the selectivity for the singly PEGylated species was only marginally increased by using the reaction-separation scheme due to the incomplete separation of the PEGylated product, PEG, and unreacted α -lactalbumin by the diafiltration process.

11.3 Size Characterization

The experimental studies in Chapter 5 examined the effects of PEGylation on the effective protein size using size exclusion chromatography and dynamic light scattering. The addition of one or more PEG chains greatly increased the effective size of the protein, with the effective size of the PEGylated protein depending only on the molecular weight of the protein and total added PEG, independent of the configuration of the PEG chains (i.e., the number of PEG branches). A simple empirical correlation was developed for the effective size based on the molecular weight of the PEG and protein components. It was also possible to analyze the size of the PEGylated protein using simple geometric models, but data for additional proteins (including PEGylated proteins formed with very small PEG adducts) would be needed to identify the most appropriate geometric description.

The hydrodynamic radii of the PEGylated proteins were also determined by dynamic light scattering. The results were in agreement with the size determined by size exclusion chromatography, demonstrating the viability of the two methods. However, the dynamic light scattering measurements were only successful when using fairly pure feed solutions consisting of only a single PEGylated species, e.g., a protein with only one PEG chain. Light scattering data obtained with mixtures of proteins with different extents of PEGylation or with significant amounts of un-reacted PEG or protein were difficult to interpret and did not provide any useful information on the size (or size distribution) of the PEGylated proteins.

11.4 Charge Characterization

Capillary electrophoresis was used to examine the electrophoretic mobility of the PEGylated proteins with the data used to develop a better understanding of the surface charge characteristics of these protein-polymer conjugates. The mobility of the PEGylated α -lactalbumin decreased upon the addition of one or more PEG groups. In contrast, data obtained with acetylated proteins, formed by reaction of acetic anhydride with the same lysine amino groups involved in PEGylation, showed an increase in the electrophoretic mobility with increasing degree of acetylation. The change in mobility associated with PEGylation is caused by both the increase in size, and thus the hydrodynamic drag, and also the increase in net negative charge due to the removal of one or more positively-charged amines on the lysine residues. For the conditions examined in this study, the increase in hydrodynamic drag dominated the increase in

charge, resulting in a significant reduction in the electrophoretic mobility for the PEGylated proteins.

The experimental data for the electrophoretic mobility were analyzed by calculating the drag ratio, defined as the electrophoretic mobility of the PEGylated protein to the corresponding mobility of the acetylated molecule with the same number of substitutions. Data for the drag ratio of the different PEGylated proteins collapse to a single curve when plotted as a function of the hydrodynamic radius evaluated from size exclusion chromatography. The experimental values for the electrophoretic mobility were in good agreement with a simple model in which the PEGylated protein is treated as a composite sphere, with the electrical potential at the surface of shear evaluated by solving the linearized Poisson-Boltzmann equation under conditions where the Debye length in the PEG layer is much larger than the Debye length in the bulk solution. This model was mathematically equivalent to assuming that the electrical charges on the protein core were simply distributed on the external surface of the PEGylated protein as proposed previously by Sharma and Carbeck (2005). The large value of the Debye length in the PEG layer is consistent with thermodynamic data on the partitioning of salts in aqueous two-phase systems employing salt – PEG mixtures, although future studies will be required to quantify the importance of salt partitioning in determining the physical properties of PEGylated proteins. The electrophoretic mobility data provide no evidence of charge shielding by the PEG groups (beyond the elimination of positively-charged lysine amino groups due to the PEGylation reaction itself).

11.5 Ultrafiltration and PEG Elongation Effects

Experimental data were obtained for the sieving coefficients for a series of PEGylated proteins through different pore size ultrafiltration membranes. At low filtrate flux, PEGylation reduces the protein sieving coefficient due to an increase in the effective size associated with the long PEG chains. This effect is quite dramatic due to the very open structure of the PEG (compared to that of a globular protein). For example, the sieving coefficient of PEGylated α -lactalbumin with a single 5 kDa PEG chain (total molecular weight of 19.6 kDa) is more than a factor of 4 smaller than that of the native protein (MW = 14.6 kDa) when using a 30 kDa UltracelTM membrane at a flux of 6 $\mu\text{m/s}$. The measured sieving coefficients at low filtrate flux are in good agreement with available hydrodynamic models for hard sphere solutes, with the effective size of the PEGylated protein determined from the measured partition coefficient in size exclusion chromatography.

In contrast to the behavior at low filtrate flux, the sieving coefficient at high flux depends on the number of attached PEG chains in addition to the total molecular weight of the PEGylated protein. It is important to recognize that a higher degree of sieving is observed than expected based on the results predicted by the hard sphere model for PEGylated molecules with long PEG chains. This behavior appears to be associated with the deformation of the PEG chains in the converging flow into the membrane pores. Deformation of the PEGylated proteins is not observed in a capillary electrophoresis system with a similar or higher velocity than that found in the ultrafiltration system. In ultrafiltration, PEGylated proteins with a greater number of PEG branches have smaller sieving coefficients than the corresponding proteins with the same total molecular weight

of PEG but with fewer PEG groups due to the greater elongation of the long PEG chains. For example, the observed sieving coefficient through a 30 kDa UltracelTM membrane for the PEGylated α -lactalbumin with four 5 kDa PEG chains at a flux of 16 $\mu\text{m/s}$ was more than an order of magnitude smaller than that for the PEGylated α -lactalbumin with two 10 kDa PEG chains even though these species have the same total mass of attached PEG and thus the same effective size as determined by size exclusion chromatography.

The effect of filtrate flux on the sieving characteristics of the PEGylated proteins was consistent with that predicted using available models for polymer elongation developed from a simple scaling analysis based on the time constant for the flow field and the characteristic time for polymer relaxation. However, the critical Deborah number for elongation of the PEGylated proteins was about 4 orders of magnitude smaller than that expected based on the scaling analysis. It is possible that this discrepancy may be directly related to the covalent attachment of one end of the PEG chain to the protein, which could cause a large reduction in the polymer relaxation time. Alternatively, the experimental data are consistent with an early orientation (and elongation) of the PEG chain due to the strong hydrodynamic drag on the protein part of the polymer-protein conjugate. Additional studies will be needed to fully understand the effects of molecular flexibility and elongation on the ultrafiltration characteristics of these important second-generation biotherapeutics.

11.6 Ultrafiltration and Electrostatic Effects

Although a number of previous studies have shown the importance of electrostatic interactions during protein ultrafiltration using charged membranes, the data obtained in Chapter 8 provide the first experimental measurements of electrostatic effects during ultrafiltration of PEGylated proteins. Experiments were performed using negatively charged membranes generated by covalent attachment of sulfonic acid groups to the base cellulose membrane. Data were obtained over a range of ionic strength, solution pH, and membrane surface charge density to control the magnitude of the electrostatic interactions. The transmission of the PEGylated proteins was drastically reduced when using the negatively-charged membranes at low ionic strength due to the strong electrostatic repulsion under these conditions. For example, decreasing the ionic strength from 200 to 2.3 mM caused more than a two order of magnitude reduction in the sieving coefficient of the PEGylated α -lactalbumin with four 5 kDa PEGylated groups; there was no significant change in the sieving coefficient of the neutral PEG over the same conditions. Similar effects were seen in response to changes in solution pH and membrane charging time.

The sieving coefficient data for the PEGylated proteins were in good agreement with model predictions accounting for the change in free energy arising from the partitioning of a charged sphere into a charged cylindrical pore. The key model parameters were all determined using independent experimental measurements or theoretical analyses: the membrane pore size distribution was evaluated from dextran sieving profiles, the membrane surface charge density was evaluated from streaming potential measurements, the protein charge was evaluated from the amino acid sequence

(as confirmed by measurements of the electrophoretic mobility), and the effective protein size was evaluated from the partition coefficient in size exclusion chromatography. The model does tend to slightly under predict the sieving coefficient at low ionic strength, which could be due to errors in some of the key model parameters, e.g., the presence of some very large pores (beyond that predicted by the log-normal pore size distribution). Alternatively, this discrepancy might reflect underlying simplifications in the theoretical model. In particular, the model neglected the effects of charge regulation, which can lead to changes in protein (and membrane) surface charge due to the change in local pH arising from the preferential partitioning of the positively-charged H^+ ions into the region of high negative electrical potential between the PEGylated protein and the pore wall.

The ability to control the transmission of PEGylated proteins by altering the surface charge on the ultrafiltration membrane can potentially be exploited for enhanced ultrafiltration processes. For example, it should be possible to use a larger pore size membrane, with larger hydraulic permeability and greater ability to clear small impurities, for enhanced concentration and buffer exchange. In this case, the use of a negatively-charged membrane would provide the high rejection of the negatively charged PEGylated protein needed to minimize loss of valuable product due to the strong electrostatic repulsion between the PEGylated protein and the membrane pores.

11.7 Purification of PEGylated Proteins

The separation of PEGylated proteins from unreacted precursors is often a critical step in the overall purification of PEGylated protein products. Previous studies have focused on the use of ion exchange chromatography, but the dynamic binding capacity for PEGylated proteins is typically very small due to the steric hindrance provided by the long PEG chains (Pabst et al., 2007). Size exclusion chromatography does provide good resolution for the purification of PEGylated proteins, but preparative size exclusion chromatography systems tend to be cumbersome and expensive. The results obtained in Chapter 9 of this thesis provide the first demonstration that ultrafiltration can be used to purify a PEGylated protein, in this case PEGylated α -lactalbumin, from the unreacted protein and PEG precursors.

Purification of the singly PEGylated α -lactalbumin was performed using a diafiltration mode in which the impurities were washed through the membrane and into the filtrate solution by continuous addition of diafiltration buffer. The appropriate conditions for performing the diafiltration were determined from measurements of the selectivity obtained using small scale total recycle experiments for: (a) the PEGylated protein and the α -lactalbumin and (b) the PEGylated protein and the hydrolyzed PEG. For example, high selectivities between the PEGylated protein and the α -lactalbumin were obtained at a filtrate flux of 9 $\mu\text{m/s}$ using a 150 mM Bis Tris buffer and a standard 30 kDa UltracelTM membrane to exploit the large size difference between these species. The relatively low flux minimized concentration polarization effects and the elongation of the PEG chains, both of which would tend to compromise the selectivity. It was not possible to obtain high selectivities between the PEG and PEGylated protein using purely

size-based separation, but these species could be separated using a negatively charged membrane at low salt concentrations to exploit differences in electrostatic interactions.

A two-stage separation process was designed and tested for the purification of the PEGylated α -lactalbumin. The first stage removed the native α -lactalbumin using a 30 kDa UltracelTM membrane, while the second stage removed the PEG using a charged 100 kDa UltracelTM membrane. Selectivities of over 500 were obtained between the PEGylated protein and the native α -lactalbumin in the first stage since these species have very different effective sizes. Selectivities of more than 40 were obtained between the PEGylated protein and the PEG in the second stage due to the strong electrostatic exclusion of the negatively charged PEGylated α -lactalbumin. The two-stage diafiltration provided a final product solution that had undetectable levels of the un-reacted α -lactalbumin and more than a 25-fold reduction in the concentration of hydrolyzed PEG. The final yield (recovery) of the desired PEGylated protein was approximately 75%. Much of the product loss occurred during transfer of the feed between the two membrane stages, an effect that would be much less significant in larger scale applications of this type of membrane separation. The yield and purification results for both stages were in good agreement with model calculations developed from simple mass balances assuming constant sieving coefficients for all species throughout the diafiltration. The yield-purification analysis provides an appropriate framework for the optimization of membrane processes for the purification of PEGylated proteins. These results clearly demonstrate the feasibility of using ultrafiltration systems for the purification of PEGylated protein products, and they provide initial guidelines for the design of these membrane systems.

11.8 Membrane Fouling

One of the important aspects to consider in the design and operation of ultrafiltration devices is membrane fouling. The experimental data presented in Chapter 10 provide the first published results comparing the fouling characteristics of a PEGylated protein with that of the native protein. Experiments were performed with bovine serum albumin using both composite regenerated cellulose and polyethersulfone membranes. There was very little fouling of the cellulose membranes with either the native BSA or the PEGylated BSA. Instead, most of flux decline during ultrafiltration was associated with concentration polarization effects associated with the build-up of a concentrated region of retained protein above the membrane. Concentration polarization effects were more pronounced with the PEGylated BSA due to the reduction in back mass transfer rates associated with the smaller diffusion coefficient for the large PEGylated species. Some fouling was observed for the PEGylated proteins at the highest filtrate flux when using the cellulose membranes, although this may simply be related to the greater retention of the large PEGylated proteins.

In contrast to the data with the composite regenerated cellulose membranes, there was significant fouling during ultrafiltration through the polyethersulfone membranes, with the extent of fouling being greater for the PEGylated BSA. This increase in fouling appears to be related to the lack of hydrophilic interactions between the PEGylated protein and buffer solution (as determined using reverse phase chromatography) and to the reduced electrostatic repulsion between the negatively charged polyethersulfone membrane and the negatively charged protein attributed to the attached PEG chains. This

physical picture is consistent with experimental data obtained over a limited range of solution pH and ionic strength. The fouling behavior for the PEGylated BSA was nearly independent of solution conditions while fouling by the un-modified BSA was significantly reduced at pH well above the isoelectric point of the protein and at low ionic strength, conditions that enhance the electrostatic repulsion.

The increase in hydrophobic interactions of the PEGylated proteins is somewhat counterintuitive since PEG is typically considered to be hydrophilic (Li and Kao, 2003; Makino et al., 1999; Shi et al., 2007). However, the increase in elution time for the PEGylated BSA on the C4 reverse phase column was very significant, and this behavior is consistent with previous results obtained with a number of other PEGylated proteins. This increase in hydrophobic interactions could have significant implications in the downstream processing of PEGylated proteins, particularly for filtration steps that utilize hydrophobic membranes that are more susceptible to fouling by hydrophobic species.

11.9 Recommendations

Although the experimental studies and theoretical analyses presented in this thesis provide important insights into the physical characteristics and ultrafiltration properties of PEGylated proteins, there are a number of areas that are ripe for additional studies. This includes work on the underlying properties and structure of the PEGylated proteins as well as efforts to enhance the production and purification of these valuable second-generation therapeutic products. Increasing the yield of the desired PEGylated species such as a molecule with a single PEG branch can improve the overall effectiveness of the drug.

The limited experimental data obtained in this thesis for the production of PEGylated proteins using a combined reaction-separation system demonstrate that it is possible to increase the selectivity for the desired PEGylated species by rapidly separating the PEGylated protein from the reactants as the product is formed. Effective implementation of this approach would require the development of an appropriate separation strategy that would be able to effectively and rapidly separate both the PEG and the un-reacted protein from the PEGylated protein as the product is formed. This might be possible using the negatively charged composite regenerated cellulose membranes that were used in the second stage of the two-stage diafiltration process examined in Chapter 9. However, high selectivities between the PEG and the PEGylated protein required the use of low ionic strength solutions and relatively high pH to enhance the electrostatic exclusion of the negatively charged PEGylated product while allowing the neutral PEG to pass into the filtrate. The optimization of this process would thus require a more detailed understanding of the effects of solution pH and ionic strength on both the intrinsic kinetics of the PEGylation reactions and the ultrafiltration characteristics of the PEGylated protein. These studies should be performed with a range of PEGylated proteins so that general strategies can be developed for the enhanced production of desired PEGylated products.

The effective size of the PEGylated proteins is a critical factor influencing the separation characteristics and the biological properties of these biomolecules. The effective size in this thesis was evaluated by measuring the partition coefficient in size exclusion chromatography and by measuring the diffusion coefficient using dynamic light scattering. These studies showed no measurable differences in the effective size

determined using these two methods even though the effects of the PEG layer might well be different in these systems. For example, large PEGylated proteins should be able to enter even very small pores in an SEC resin because of the conformational flexibility of the PEG, a phenomenon that could have a significant effect on the size determined by size exclusion chromatography. Future studies with more highly purified versions of the PEGylated proteins, covering a wider range of PEG molecular weight and protein size, might be able to identify differences in the effective size determined using different experimental methods. It would also be desirable to perform these experiments over a range of solution ionic strength and pH since these factors may also have different effects on the diffusion coefficient and the partition coefficient.

The electrophoretic mobility data for the PEGylated α -lactalbumin were well described using a very simple model in which the protein charge was assumed to be located on the external surface of an effective sphere, consistent with a strong exclusion of the salt from the PEG layer surrounding a protein core. Previous studies of salt partitioning in aqueous two-phase systems employing PEG clearly demonstrate that different salts can have very different interactions in these PEG-water systems. Future studies should examine the effect of different salts on the electrophoretic mobility to develop a more quantitative understanding of the role of salt partitioning on the properties of the PEGylated protein. These experiments should be performed over a wide range of solution ionic strength and extents of PEGylation to fully explore the electrophoretic mobility behavior. These results would also make it possible to verify the predictions of the simple model developed in this thesis for the surface potential of the PEGylated protein in terms of the radius of the protein core and the PEG layer as well as

the size of the Debye length within the PEG region. It might also be possible to complement these studies of electrophoretic mobility with other direct or indirect measures of the surface charge, e.g., by using titration or dye-binding studies.

The ultrafiltration experiments performed in this thesis indicate that the PEGylated proteins tend to behave as effective hard spheres at low filtrate flux but there is clear evidence that these molecules can deform with the flow when the ultrafiltration is performed at high filtrate flux. However, the onset of PEG elongation appears to occur at a much lower filtrate flux than would be expected based on simple scaling models (assuming a critical Deborah number of order one). Additional experimental and theoretical studies are clearly needed to develop a more quantitative understanding of the effects of molecular flexibility / elongation on the ultrafiltration characteristics of PEGylated proteins. Experiments performed using membranes with very well defined pore structure, such as the Nuclepore track-etched membranes that have very uniform cylindrical pores, could provide important insights by providing greater control of the flow due to the much lower porosity and more uniform pore size for these membranes. It would also be useful to perform a series of experiments with PEG molecules having different branched structures which should have very different elongational properties than the linear PEG chains examined in this thesis.

It would also be very appropriate to try to directly examine the physical properties of different PEGylated proteins in response to elongation forces. For example, single molecule studies have been performed using DNA to directly observe the stretching of the DNA polymer in response to both well-defined flow fields (e.g., in microfluidic devices) and direct mechanical forces (e.g., using DNA molecules tethered at one end to

a solid surface). It might be possible to perform analogous experiments using PEGylated proteins or to add fluorescent tags to the surface of the protein and to the free end of the PEG chain and to then track the distance between these tags through measurements of the interactions between the excitation / fluorescence (FRET). These studies would provide important insights into the physical structure of the PEGylated proteins that could then be used to develop a more fundamental understanding of the ultrafiltration behavior.

All of the fouling experiments performed in this thesis used PEGylated BSA, and most of the data was with a singly PEGylated form of this protein having a 12 kDa PEG chain. Additional studies are needed to develop a more fundamental understanding of the fouling mechanisms of PEGylated proteins. These studies should be performed using a range of proteins with different extents of PEGylation, with both fully-retentive and semi-permeable ultrafiltration membranes. The hydrophobic nature of these molecules may be better quantified by examining changes in Gibbs free surface excess energy in addition to the reverse phase chromatography that was used in this thesis. These studies would help identify the importance of hydrophobicity in determining the fouling behavior of these PEGylated species.

There is also clinical interest in the use of protein-polymer conjugates formed with polymers other than polyethylene glycol. It would be very interesting to extend the studies using PEGylated proteins performed in this thesis to other related systems. This would involve both ultrafiltration experiments as well as different characterization studies, including size exclusion chromatography, and capillary electrophoresis as was done in this thesis. These results could be used to develop a much more quantitative understanding of the relationship between the physical properties of these novel protein-

polymer conjugates and their behavior during ultrafiltration. These studies would not only be of importance for the development of separation strategies for different therapeutic products, they may also provide a broader fundamental understanding of the general behavior of protein-polymer conjugates.

REFERENCES

- Abuchowski, A.; McCoy, J.; Palczuk, N.; van Es, T.; Davis, F., Effect of Covalent Attachment of Polyethylene Glycol on Immunogenicity and Circulating Life of Bovine Liver Catalase. *The Journal of Biological Chemistry* **1977a**, 252, (11), 3582-3586.
- Abuchowski, A.; van Es, T.; Palczuk, N.; Davis, F., Alteration of Immunological Properties of Bovine Serum Albumin by Covalent Attachment of Polyethylene Glycol. *Journal of Biological Chemistry* **1977b**, 252, (11), 3578-3581.
- Amgen, Inc. *Neulasta (Pegfilgrastim)*; FDA Approved Document: Thousand Oaks, CA, **2008**; FDA Approved Document #NDC 55513-190-01.
- Anderson, J. R.; Quinn, J. A., Restricted Transport in Small Pores: A Model for Steric Exclusion and Hindered Particle Motion. *Biophysical Journal* **1974**, 14, (2), 130-150.
- Andrews, B. A.; Schmidt, A. S.; Asenjo, J. A., Correlation for the Partition Behavior of Proteins in Aqueous Two-Phase Systems: Effect of Surface Hydrophobicity and Charge. *Biotechnology and Bioengineering* **2005**, 90, (3), 380-390.
- Arduini, R. M.; Li, Z.; Rapoza, A.; Gronke, R.; Hess, D., M.; Wen, D.; Miatkowski, K.; Coots, C.; Kaffashan, A.; Viseux, N.; Delaney, J.; Domon, B.; Young, C. N.; Boynton, R.; Chen, L. L.; Chen, L.; Betzenhause, M.; Miller, S.; Gill, A.; Pepinsky, R. B.; Hochman, P. S.; Baker, D. P., Expression, Purification, and Characterization of Rat Interferon-Beta and Preparation of an N-Terminally PEGylated Form with Improved Pharmacokinetic Parameters. *Protein Expression and Purification* **2004**, 34, 229-242.
- Arpicco, S.; Dosio, F.; Bolognesi, A.; Lubelli, C.; Brusa, P.; Stella, B.; Ceruti, M.; Cattel, L., Novel Poly(Ethylene Glycol) Derivatives for Preparation of Ribosome-Inactivating Protein Conjugates. *Bioconjugate Chemistry* **2002**, 13, (4), 757-765.
- Asahina, Y.; Izumi, N.; Umeda, N.; Hosokawa, T.; Ueda, K.; Doi, F.; Tsuchiya, K.; Nakanishi, H.; Matsunaga, K.; Kitamura, T.; Kurosaki, M.; Uchihara, M.; Higaki, M.; Miyake, S., Pharmacokinetics and Enhanced PKR Response in Patients with Chronic Hepatitis C Treated with Pegylated Interferon Alpha-2b and Ribavirin. *Journal of Viral Hepatitis* **2007**, 14, 396-403.
- Azarkan, M.; Maes, D.; Bouckaert, J.; Thi, M.-H. D.; Wyns, L.; Looze, Y., Thiol Pegylation Facilitates Purification of Chymopapain Leading to Diffraction Studies at 1.4 Angstrom Resolution. *Journal of Chromatography A* **1996**, 749, (1-2), 69-72.

- Azarkan, M.; El Moussaoui, A.; van Wuytswinkel, D.; Dehon, G.; Looze, Y., Fractionation and Purification of the Enzyme Stored in the Latex of *Carica Papaya*. *Journal of Chromatography B* **2003**, 790, 229-238.
- Bailon, P.; Berthold, W., Polyethylene Glycol-Conjugated Pharmaceutical Proteins. *Pharmaceutical Science and Technology Today* **1998**, 1, (8), 352-356.
- Bailon, P. S. Erythropoietin Conjugates. US Patent 6583272, Hoffmann-LaRoche Inc. 2000.
- Bairoch, A.; Apweiler, R.; Wu, C. H.; Barker, W. C.; Boeckmann, B.; Ferro, S.; Gasteiger, E.; Huang, H. L., R.; Magrane, M., Nucleic Acids Res 33(D154-D159). *The Universal Protein Resource (UniProt)* **2005**, P00711, P01012, P02769.
- Balakrishnan, M.; Agarwal, G. P., Protein Fractionation in a Vortex Flow Filter. I: Effect of System Hydrodynamics and Solution Environment on a Single Protein Transmission. *Journal of Membrane Science* **1996**, 112, (1), 47-74.
- Baran, E.; Ozer, N.; Hassirci, V., Solid-Phase Enzyme Modification Via Affinity Chromatography. *Journal of Chromatography B* **2003**, 794, 311-322.
- Beerlage, M. A. M.; Heijnen, M. L.; Mulder, M. H. V.; Smolders, C. A.; Strathmann, H., Non-Aqueous Retention Measurements: Ultrafiltration Behaviour of Polystyrene Solutions and Colloidal Silver Particles. *Journal of Membrane Science* **1996**, 113, (2), 259-273.
- Beerlage, M. A. M.; Peeters, J. M. M.; Nolten, J. A. M.; Mulder, M. H. V.; Strathmann, H., Hindered Diffusion of Flexible Polymers through Polyimide Ultrafiltration Membranes. *Journal of Applied Polymer Science* **2000**, 75, 1180-1193.
- Bentley, M. D.; Xuan, Z.; Xiaoming, S.; Lihong, G. Sterically Hindered Poly(Ethylene Glycol) Alkanoic Acids and Derivatives Thereof. US Patent 6737505, Nektar Therapeutics. 2004.
- Besselink, G. A. J.; Beugeling, T.; Bantjes, A., N-Hydroxysuccinimide-Activated Glycine-Sepharose. *Applied Biochemistry and Biotechnology* **1993**, 43, 227-246.
- Beynon, R.; Easterby, J., *Buffer Solutions Basics*. 1 ed.; Oxford University Press Inc.: New York, 1996.
- Bhatt, B. S.; Sacheti, N., Flow Past a Porous Spherical Shell Using the Brinkman Model. *Journal of Physics D: Applied Physics* **1994**, 27, 37-41.
- Blanch, H. W.; Clark, D. S., *Biochemical Engineering*. Marckel Dekker: New York, 1997.

- Bohonak, D. M., Performance of Virus Filtration Membranes: Effects of Membrane Morphology and Operating Mode. Ph.D. Dissertation, The Pennsylvania State University, University Park, PA, 2006.
- Bowen, R. W.; Jenner, F., Theoretical Descriptions of Membrane Filtration of Colloids and Fine Particles: An Assessment and Review. *Advances in Colloid and Interface Science* **1995**, 56, 141-200.
- Branca, C.; Magazu, S.; Maisano, G.; Migliardo, F.; Migliardo, P.; Romeo, G., Hydration Study of PEG/Water Mixtures by Quasi Elastic Light Scattering, Acoustic and Rheological Measurements. *Journal of Physical Chemistry B*. **2002**, 106, 10272-10276.
- Brenner, H.; Gaydos, L. J., The Constrained Brownian Movement of Spherical Particles in Cylindrical Pores of Comparable Radius: Models of the Diffusive and Convective Transport of Solute Molecules in Membranes and Porous Media. *Journal of Colloid and Interface Science* **1977**, 58, (2), 312-356.
- Brew, K.; Castellino, F. J.; Vanaman, T. C.; Hill, R. L., The Complete Amino Acid Sequence of Bovine α -Lactalbumin. *The Journal of Biological Chemistry* **1970**, 245, (17), 4570-4582.
- Brookhaven, Instruments Corporation, DLS Basics. www.bic.com/DLSbasics (accessed May 15, 2007).
- Brumeanu, T. D.; Zaghoulani, H.; Bona, C., Purification of Antigenized Immunoglobulins Derivatized with Monomethoxypolyethylene Glycol. *Journal of Chromatography A* **1995**, 696, 219-225.
- Bungay, P. M.; Brenner, H., The Motion of a Closely Fitting Sphere in a Fluid Filled Tube. *International Journal of Multiphase Flow* **1973**, 1, 25-56.
- Burns, D.; Zydney, A. L., Effect of Solution pH on Protein Transport through Ultrafiltration Membranes. *Biotechnology and Bioengineering* **1999**, 64, (1), 27-37.
- Burns, D., Electrostatic Interactions in Protein Transport Using Ultrafiltration Membranes: Effects of Solution Conditions and Membrane Charge. Ph.D. Dissertation, University of Delaware, Newark, DE, 2000.
- Burns, D.; Zydney, A. L., Contributions to Electrostatic Interactions on Protein Transport in Membrane Systems. *American Institute of Chemical Engineers Journal* **2001**, 47, (5), 1101-1114.

- Bushey, M. M.; Jorgenson, J. W., Capillary Electrophoresis of Proteins in Buffers Containing High Concentrations of Zwitterionic Salts. *Journal of Chromatography A* **1989**, 480, 301-310.
- Butler, M., Animal Cell Cultures: Recent Achievements and Perspectives in Production of Biopharmaceuticals. *Applied Microbiology and Biotechnology* **2005**, 68, (3), 283.
- Caliceti, P.; Salmaso, S.; Walker, G.; Bernkop-Schnurch, A., Development and *in vivo* Evaluation of an Oral Insulin-PEG Delivery System. *European Journal of Pharmaceutical Sciences* **2004**, 22, 315-323.
- Caliceti, P.; Schiavon, O.; Veronese, F., M., Biopharmaceutical Properties of Uricase Conjugated to Neutral and Amphiphilic Polymers. *Bioconjugate Chemistry* **1999**, 10, 638-646.
- Caliceti, P.; Schiavon, O.; Veronese, F., M., Immunological Properties of Uricase Conjugated to Neutral Soluble Polymers. *Bioconjugated Chemistry* **2001**, 12, 515-522.
- Caliceti, P.; Veronese, F., M., Pharmacokinetic and Biodistribution Properties of Poly(Ethylene Glycol) - Protein Conjugates. *Advanced Drug Delivery Reviews* **2003**, 55, (10), 1261-1277.
- Callis, P. R.; Davidson, N., Hydrodynamic Relaxation Times of DNA from Decay of Flow Dichroism Measurements. *Biopolymers* **1969**, 8, (3), 379-390.
- Caravella, J. A.; Carbeck, J. D.; Duffy, D. C.; Whitesides, G. M.; Tidor, B., Long-Range Electrostatic Contributions to Protein-Ligand Binding Estimated Using Protein Charge Ladders, Affinity Capillary Electrophoresis and Continuum Electrostatic Theory. *Journal of the American Chemical Society* **1999**, 121, 4340-4347.
- Carbeck, J. D.; Severs, J. C.; Gao, J.; Wu, Q.; Smith, R. D.; Whitesides, G. M., Correlation between the Charge of Proteins in Solution and in the Gas Phase Investigated by Protein Charge Ladders, Capillary Electrophoresis, and Electrospray Ionization Mass Spectrometry. *Journal of Physical Chemistry B*. **1998**, 102, 10596-10601.
- Causserand, C.; Meireles, M.; Aymar, P., Protein Transport through Charged Porous Membranes. *Chemical Engineering Research and Design: Transactions of the Institution of Chemical Engineers* **1996**, 74, (A1), 113-122.
- Chamow, S. C.; Kogan, T. P.; Venuti, M.; Gadek, T.; Harris, R. J.; Peers, D. H.; Mordenti, J.; Shak, S.; Ashkenazi, A., Modification of CD4 Immunoaderin with Monomethoxypoly(Ethylene Glycol) Aldehyde Via Reductive Alkylation. *Bioconjugate Chemistry* **1994**, 5, 133-140.

- Chapman, A., PEGylated Antibodies and Antibody Fragments for Improved Therapy: A Review. *Advanced Drug Delivery Reviews* **2002**, 54, 531-545.
- Chaturvedi, B. K.; Ghosh, A. K.; Ramachandran, M. K.; Trivedi, M. K.; Hanra, M.; Misra, B. M., Preparation, Characterization and Performance of Polyethersulfone Ultrafiltration Membranes. *Desalination* **2000**, 133, 31-40.
- Chauveteau, G., Rodlike Polymer Solution Flow through Fine Pores: Influence of Pore Size on Rheological Behavior. *Journal of Rheology* **1982**, 26, (2), 111-142.
- Cheang, B.; Zydney, A. L., Separation of Alpha-Lactalbumin and Beta-Lactoglobulin Using Membrane Ultrafiltration. *Biotechnology and Bioengineering* **2003**, 83, (2), 201-209.
- Cho, J.; Amy, G.; Pellegrino, J., Membrane Filtration of Natural Organic Matter: Factors and Mechanisms Affecting Rejection and Flux Decline with Charged Ultrafiltration Membrane. *Journal of Membrane Science* **2000**, 164, 89-110.
- Chowdhury, S. K.; Doleman, M.; Johnston, D., Fingerprinting Proteins Coupled with Polymers by Mass Spectrometry: Investigation of Polyethylene Glycol-Conjugated Superoxide Dismutase. *American Society for Mass Spectrometry* **1995**, 6, 478-487.
- Chrysina, E. D.; Brew, K.; Acharya, K. R., Crystal Structures of Apo- and Holo- Bovine Alpha-Lactalbumin at 2.2 - Angstrom Resolution Reveal an Effect of Calcium on Inter-Lobe Interactions. *Journal of Biological Chemistry* **2000**, 275, 37021-37029.
- Cleveland, C. T.; Seacord, T. F.; Zander, A., Standardized Membrane Pore Size Characterization by Polyethylene Glycol Rejection. *Journal of Environmental Engineering* **2002**, 399-407.
- Cohen, J. A.; Khorosheva, V. A., Electrokinetic Measurement of Hydrodynamic Properties of Grafted Polymer Layers on Liposome Surfaces. *Colloids and Surfaces A: Physicochemical and Engineering Aspects* **2001**, 195, 113-127.
- Colton, C., Permeability and Transport Studies in Batch and Flow Dialyzers with Applications to Hemodialysis. Ph.D. Dissertation, Massachusetts Institute of Technology, Boston, MA, 1969.
- Corradini, D., Buffer Additives Other Than the Surfactant Sodium Dodecyl Sulfate for Protein Separations by Capillary Electrophoresis. *Journal of Chromatography B* **1997**, 699, 221-256.

- Corradini, D.; Bevilacqua, L.; Nicoletti, I., Separation of Basic Proteins in Bare Fused-Silica Capillaries with Diethylenetriamine Phosphate Buffer as the Background Electrolyte Solution. *Chromatographia Supplement* **2005**, 62, S43- S50.
- Daoudi, S.; Brochard, F., Flow of Flexible Polymer Solutions in Pores. *Macromolecules* **1978**, 11, (4), 751-758.
- de Belval, S.; le Breton, B.; Huddleston, J. G.; Lyddiatt, A., Influence of Temperature Upon Protein Partitioning in Poly(Ethylene Glycol) - Salt Aqueous Two-Phase Systems Close to the Critical Point with Some Observations Relevant to the Partitioning of Particles. *Journal of Chromatography B* **1998**, 711, 19-29.
- Deen, W. M.; Smith, F. G., Hindered Diffusion of Synthetic Polyelectrolytes in Charged Microporous Membranes. *Journal of Membrane Science* **1982**, 12, 217-237.
- Deen, W., Hindered Transport of Large Molecules in Liquid-Filled Pores. *AIChE Journal* **1987**, 33, (9), 1409-1425.
- Deiters, A.; Cropp, T. A.; Summerer, D.; Mukherji, M.; Schultz, P. G., Site-Specific PEGylation of Proteins Containing Unnatural Amino Acids. *Bioorganic and Medicinal Chemistry Letters* **2004**, 14, 5743-5745.
- Delgado, C.; Francis, G. E.; Fisher, D., The Uses and Properties of PEG-Linked Proteins. *Critical Reviews in Therapeutic Drug Carrier Systems*. **1992**, 9, (3-4), 249-304.
- Denisov, G. A., Theory of Concentration Polarization in Cross-Flow Ultrafiltration Gel-Layer Model and Osmotic-Pressure Model. *Journal of Membrane Science* **1994**, 91, 173-187.
- Digilio, G.; Barbero, L.; Bracco, C.; Corpillo, D.; Esposito, P.; Piquet, G.; Silvio, T.; Silvio, A., NMR Structure of Two Novel Polyethylene Glycol Conjugates of the Human Growth Hormone-Releasing Factors, hGRF(1-20)-NH₂. *Journal of the American Chemical Society* **2003**, 125, 3458-3470.
- Ding, J. M.; Keh, H. J., Electrophoretic Mobility and Electric Conductivity in Dilute Suspensions of Charge-Regulating Composite Spheres. *Langmuir* **2003**, 19, 7226-7239.
- Doherty, P.; Benedek, G. B., The Effect of Electric Charge on the Diffusion of Macromolecules. *Journal of Chemical Physics* **1974**, 61, (12), 5426-5434.
- Ebersold, M. F.; Zydney, A. L., The Effect of Membrane Properties on the Separation of Protein Charge Variants Using Ultrafiltration. *Journal of Membrane Science* **2004a**, 243, 379-388.

- Ebersold, M. F.; Zydney, A. L., Use of Protein Charge Ladders to Study Electrostatic Interactions During Protein Ultrafiltration. *Biotechnology and Bioengineering* **2004b**, 85, (2), 166-176.
- Edwards, C. K.; Martin, S., W.; Seely, J.; Kinstler, O.; Buckel, S.; Bendele, A.; Cosenza, M. E.; Feige, U.; Kohno, T., Design of PEGylated Soluble Tumor Necrosis Factor Receptor Type I (PEG sTNF-RI) for Chronic Inflammatory Diseases. *Advanced Drug Delivery Reviews* **2003**, 55, 1315-1336.
- Ehsani, N.; Parkkinen, S.; Nystrom, M., Fractionation of Natural and Model Egg-White Protein Solutions with Modified and Unmodified Polysulfone UF Membranes. *Journal of Membrane Science* **1996**, 123, (1), 105-119.
- Enzon Pharmaceuticals, Inc. *Adagen (Pegademase Bovine) Injection*; FDA Approved Document: 00117USB Bridgewater, NJ, 2008.
- Ernst and Young Switzerland, Global Biotechnology Report 2008. Bern, Switzerland, **2008**, <http://www2.eycom.ch/media/mediareleases/releases/20080520/en.aspx> (accessed Jul 10, 2008).
- Esposito, P.; Barbero, L.; Caccia, P.; Caliceti, P.; D'Antonio, M.; Piquet, G.; Veronese, F., M., PEGylation of Growth Hormone-Releasing Hormone (GRF) Analogues. *Advanced Drug Delivery Reviews* **2003**, 55, 1279-1291.
- Fane, A. G.; Fell, C. J. D.; Suki, A., The Effect of pH and Ionic Environment on the Ultrafiltration of Protein Solutions with Retentive Membranes. *Journal of Membrane Science* **1983**, 16, 195-210.
- Fee, C. J., Size-Exclusions Reaction Chromatography (SERC): A New Technique for Protein PEGylation. *Biotechnology and Bioengineering* **2003**, 82, (2), 200-206.
- Fee, C. J.; Van Alstine, J. M., Prediction of the Viscosity Radius and the Size Exclusion Chromatography Behavior of PEGylated Proteins. *Bioconjugate Chemistry* **2004**, 15, 1304-1313.
- Fee, C. J.; Van Alstine, J., M., PEG-Proteins: Reaction Engineering and Separation Issues. *Chemical Engineering Science* **2006**, 61, 924-939.
- Fee, C. J., Size Comparison between Proteins PEGylated with Branched and Linear Poly(Ethylene Glycol) Molecules. *Biotechnology and Bioengineering* **2007**, 98, (4), 725-731.
- Food and Drug Administration, FDA, Search for Brand and Generic Drugs. <http://www.accessdata.fda.gov/scripts/cder/drugsatfda/index.cfm>. (accessed May 25, 2008)

- Foser, S.; Schacher, A.; Weyer, K. A.; Brugger, D.; Dietel, E.; Marti, S.; Schreitmuller, T., Isolation, Structural Characterization, Antiviral Activity of Positional Isomers of Monopegylated Interferon Alpha-2a (PEGasys). *Protein Expression and Purification* **2003**, 30, 78-87.
- Francis, G. E.; Fisher, D.; Delgado, C.; Malik, F.; Gardiner, A.; Neale, D., PEGylation of Cytokines and Other Therapeutic Proteins and Peptides: The Importance of Biological Optimization of Coupling Techniques. *International Journal of Hematology* **1998**, 68, 1-18.
- Gao, J.; Whitesides, G. M., Using Protein Charge Ladders to Estimate the Effective Charges and Molecular Weights of Proteins in Solution. *Analytical Chemistry* **1997**, 69, 575-580.
- Ghosh, R.; Cui, Z. F., Purification of Lysozyme Using Ultrafiltration. *Biotechnology and Bioengineering* **1999**, 68, (2), 191-203.
- Granath, K. A., Solution Properties of Branched Dextrans. *Journal of Colloid and Interface Science* **1958**, 13, 308.
- Grigsby, J. J.; Blanch, H. W.; Prausnitz, J. M., Diffusivities of Lysozyme in Aqueous MgCl₂ Solutions from Dynamic Light-Scattering Data: Effect of Protein and Salt Concentrations. *Journal of Physical Chemical B*. **2000**, 104, 3645-3650.
- Grubisic, Z.; Rempp, P.; Benoit, H., A Universal Calibration for Gel Permeation Chromatography. *Polymer Letters* **1967**, 5, 753-759.
- Hall, T.; Wood, D.; Smith, C., Preparative and Analytical Chromatography of Pegylated Myelopoietin Using Monolithic Media. *Journal of Chromatography A* **2004**, 1041, 87-93.
- Hamidi, M.; Azadi, A.; Rafiei, P., Pharmacokinetic Consequences of Pegylation. *Drug Delivery* **2006**, 13, 399-409.
- Harris, J. M.; Antoni, K. Poly(Ethylene Glycol) and Related Polymers Monosubstituted with Propionic and Butanoic Acids and Functional Derivatives Thereof for Biotechnical Applications. US Patent 5672662, Shearwater Polymers Inc. 1997.
- Harris, J. M.; Martin, N.; Modi, M., Pegylation - a Novel Process for Modifying Pharmacokinetics. *Clinical Pharmacokinetics* **2001**, 40, (7), 539-551.
- He, X-H.; Shaw, P-C.; Tam, S.-C., Reducing the Immunogenicity and Improving the *In Vivo* Activity of Trichosanthin by Site-Directed Pegylation. *Life Sciences* **1999**, 65, (4), 355-368.

- Hellberg, U.; Ivarsson, J.-P.; Johansson, B.-L., Characteristic of Superdex Prep Grade Media for Gel Filtration of Proteins and Peptides. *Process Biochemistry* **1996**, 31, (2), 163-172.
- Henry, D. C., The Cataphoresis of Suspended Particles. Part I. The Equation of Cataphoresis. *Proceedings of the Royal Society of London. Series A: Containing Papers of a Mathematical and Physical Character* **1931**, 133, (821), 106-129.
- Heredia, K.; Maynard, H., Synthesis of Protein-Polymer Conjugates. *Organic and Biomolecular Chemistry* **2007**, 5, 45-53.
- Hermia, J., Constant Pressure Blocking Filtration Laws - Application to Power-Law Non-Newtonian Fluids. *Transactions of the Institution of Chemical Engineers* **1982**, 60, (3), 183-187.
- Hiemenz, P.; Rajagopalan, R., *Principles of Colloid and Surface Chemistry*. 3rd ed.; Marcel Dekker Inc.: New York, NY, 1997.
- Hill, R. J.; Saville, D. A.; Russel, W. B., Electrophoresis of Spherical Polymer-Coated Colloidal Particles. *Journal of Colloid and Interface Science* **2003**, 258, 56-74.
- Hinds, K.; Kim, S. W., Effects of PEG Conjugation on Insulin Properties. *Advanced Drug Delivery Reviews* **2002**, 54, 505-530.
- Ho, C.-C.; Zydney, A. L., Protein Fouling of Asymmetric and Composite Microfiltration Membranes. *Industrial and Engineering Chemistry Research* **2001**, 40, (5), 1412-1421.
- Hosch, J.; Staude, E., Preparation and Investigation of Chemically Modified Porous Polyamide Ultrafiltration Membranes. *Journal of Membrane Science* **1996**, 121, 71-82.
- Howell, J. A., *Membranes in Bioprocessing: Theory and Applications*. Chapman and Hall: London, England, 1993
- Hu, T.; Prabhakaran, M.; Acharya, A. S.; Manjula, B. N., Influence of the Chemistry of Conjugation of Poly(Ethylene Glycol) to Hb on the Oxygen-Binding and Solution Properties of the Peg-Hb Conjugate. *Biochemical Journal* **2005**, 392, 555-564.
- Hunter, R. J., *Zeta Potential in Colloid Science: Principles and Applications*. Academic Press: New York, NY, 1981.
- Iordanskii, A. L. Markin, V.S.; Razumovskii, L. P.; Kosenko, R. Yu.; Tarasova, N.A.; Zaikov, G. E., Diffusion Model of Protein Adsorption and Effect of Protein Layer Composition on Water Permeability for Ultrafiltration Membranes. *Desalination* **1996**, 104, 113-118.

- Jiang, Y.-Y.; Chen, J.; Hong, M.-H.; Pei, Y.-Y., Study on Preparation and Purification of PEGylated Beta-Lactoglobulin. *Chinese Pharmaceutical Journal* **2005**, 40, (14), 1110-1113.
- Jin, F.; Wu, C., Observation of the First-Order Transition in Ultrafiltration of Flexible Linear Polymer Chains. *Physical Review Letters* **2006**, 96, (23), 237801.
- Johnson, C.; Royal, M.; Moreadith, R.; Bedu-Addo, F.; Advant, S.; Wan, M.; Conn, G., Monitoring Manufacturing Process Yields, Purity and Stability of Structural Variants of PEGylated Staphylokinase Mutant SY161 by Quantitative Reverse-Phase Chromatography. *Biomedical Chromatography* **2003**, 17, (5), 335-344.
- Jones, I. S., A Theory of Electrophoresis of Large Colloid Particles and Adsorbed Polyelectrolyte. *Journal of Colloid and Interface Science* **1979**, 68, (3), 451-461.
- Jones, K. L.; O'Melia, C. R., Ultrafiltration of Protein and Humic Substances: Effect of Solution Chemistry on Fouling and Flux Decline. *Journal of Membrane Science* **2001**, 193, 163-173.
- Junfeng, L.; Da, X.; Shaoxin, L., Study on Molecular Interactions of Bovine Serum Albumin in Electrolyte Solutions by Dynamic Light Scattering. *Proceedings of SPIE: Optics in Health Care and Biomedical Optics: Diagnostics and Treatment II* **2005**, 5630, 630-638.
- Jungbauer, A., Chromatographic Media for Bioseparation. *Journal of Chromatography A* **2005**, 1065, 3-12.
- Keh, H. J., Characteristics of Transport of Macromolecules through Porous Media. Ph.D. Dissertation, Carnegie-Mellon University, Pittsburgh, PA. 1984.
- Keh, H. J.; Ding, J. M., Electrophoretic Mobility and Electric Conductivity of Suspensions of Charge-Regulating Colloidal Spheres. *Langmuir* **2002**, 18, 4572-4583.
- Kelly, S. T.; Senyo, O. W.; Zydney, A. L., Influence of Protein Aggregates on the Fouling of Microfiltration Membranes During Stirred Cell Filtration. *Journal of Membrane Science* **1993**, 80, (2), 175-187.
- Kelly, S. T.; Zydney, A. L., Effects of Intermolecular Thiol-Disulfide Interchange Reactions on BSA Fouling During Microfiltration. *Biotechnology and Bioengineering* **1994**, 44, (8), 972-982.
- Kelly, S. T.; Zydney, A. L., Mechanisms for BSA Fouling During Microfiltration. *Journal of Membrane Science* **1995**, 107, 115-127.

- Kelly, S. T.; Zydney, A. L., Protein Fouling During Microfiltration: Comparative Behavior of Different Model Proteins. *Biotechnology and Bioengineering* **1997**, 55, (1), 91-100.
- Ko, M. K.; Pellegrino, J., Determination of Osmotic Pressure and Fouling Resistances and Their Effects on Performance of Ultrafiltration Membranes. *Journal of Membrane Science* **1992**, 74, 141-157.
- Khayet, M.; Matsuura, T., Determination of Surface and Bulk Pore Sizes of Flat Sheet and Hollow-Fiber Membranes by Atomic Force Microscopy, Gas Permeation and Solute Transport Methods. *Desalination* **2003**, 158, 57-64.
- Kim, K. J.; Fane, A. G.; Aim, R. B.; Liu, M. G.; Jonsson, G.; Tessaro, I. C.; Broek, A. P.; Bargeman, D., A Comparative Study of Techniques Used for Porous Membrane Characterization: Pore Characterization. *Journal of Membrane Science* **1994**, 87, 35-46.
- Kim, S.; Karrila, S., *Microhydrodynamics: Principles and Selected Applications*. Dover Publications: Mineola, NY, 2005.
- Kim, T. H.; Lee, H.; Park, T. G., Pegylated Recombinant Human Epidermal Growth Factor (rhEGF) for Sustained Release from Biodegradable PLGA Microspheres. *Biomaterials* **2002**, 23, (11), 2311-2317.
- Kinstler, O.; Molineux, G.; Treuheit, M.; Ladd, D.; Gegg, C., Mono-N-Terminal Poly(Ethylene Glycol) - Protein Conjugates. *Advanced Drug Delivery Reviews* **2002**, 54, 477-485.
- Klotz, L. C.; Zimm, B. H., Retardation Times of Deoxyribonucleic Acid Solutions. II. Improvements in Apparatus and Theory. *Macromolecules* **1972**, 5, (4), 471-481.
- Kodera, Y.; Ayako, M.; Misao, H.; Nishimura, H.; Ishii, A.; Ueno, T.; Inada, Y., Pegylation of Proteins and Bioactive Substances for Medical and Technical Applications. *Progress in Polymer Science* **1998**, 23, 1233-1271.
- Kok, C. M.; Rudin, A., Relationship between the Hydrodynamic Radius and the Radius of Gyration of a Polymer in Solution. *Macromolecule Chemistry* **1981**, 2, 655-659.
- Kopelman, R.; Xu, H.; Yan, F.; Monson, E.; Tang, W., Preparation and Characterization of Poly(Ethylene Glycol) - Coated Stober Silica Nanoparticles for Biomedical Applications. *Proceedings of SPIE: Biomedical Nanotechnology Architectures and Applications*; **2002**, 4626, 383-393.

- Koumenis, I. L.; Shahrokh, Z.; Leong, S.; Hsei, V.; Deforge, L.; Zapata, G., Modulating Pharmacokinetics of an Anti-Interleukin-8f(aB')₂ by Amine-Specific PEGylation with Preserved Bioactivity. *Journal of Pharmaceutics* **2000**, 198, (1), 83-95.
- Kunitani, M.; Dollinger, G.; Johnson, D.; Kresin, L., On-Line Characterization of Polyethylene Glycol-Modified Proteins. *Journal of Chromatography* **1991**, 588, 125-137.
- Kurnik, R. T.; Yu, A. W.; Blank, G. S.; Burton, A. R.; Smith, D.; Athalye, A. M.; van Reis, R., Buffer Exchange - Using Size - Exclusion Chromatography Countercurrent Dialysis and Tangential Flow Filtration - Models, Development, and Industrial Application. *Biotechnology and Bioengineering* **1995**, 45, (2), 149-157.
- Latulippe, D.; Ager, K.; Zydney, A., Flux-Dependent Transmission of Supercoiled Plasmid DNA through Ultrafiltration Membranes. *Journal of Membrane Science* **2007**, 294, 169-177.
- Lee, C.-M.; Choi, Y.; Huh, E. J.; Lee, K. Y.; Song, H.-C.; Sun, M. J.; Jeong, H.-J.; Cho, C.-S.; Bom, H.-S., Polyethylene Glycol (PEG) Modified ^{99m}Tc-HMPAO-Liposome for Improving Blood Circulation and Biodistribution: The Effect of the Extent of PEGylation. *Cancer Biotherapy and Radiopharmaceuticals* **2005**, 20, (6), 620-628.
- Lee, E. K.; Lee, J. D., Solid-Phase, N-Terminus-Specific Mono-Pegylation of Recombinant Interferon-Alpha-2a: Purification Characterization and Bioactivity. In *International Symposium on the Separation of Proteins, Peptides and Polynucleotides.*, Aachen, Germany, 2004.
- Lee, H.; Park, T. G., Preparation and Characterization of Mono-Pegylated Epidermal Growth Factor: Evaluation of *In Vitro* Biological Activity. *Pharmaceutical Research* **2002a**, 19, (6), 845-851.
- Lee, H.; Park, T. G., A Novel Method for Identifying PEGylation Sites of Protein Using Biotinylated PEG Derivatives. *Journal of Pharmaceutical Sciences* **2003**, 92, (1), 97-103.
- Lee, K. C.; Moon, C.; Cheol, S.; Park, M. O.; Lee, J. T.; Na, D.; Yoo, S. D.; Lee, H. S.; Deluca, P., Isolation, Characterization, and Stability of Positional Isomers of Mono-PEGylated Salmon Calcitonins. *Pharmaceutical Research* **1999a**, 16, (6), 813-818.
- Lee, K. C.; Tak, K. K.; Park, M. O.; Lee, J. T.; Woo, B. H.; Yoo, S. D.; Lee, H. S.; Deluca, P., Preparation and Characterization of Polyethylene-Glycol-Modified Salmon Calcitonins. *Pharmaceutical Development and Technology* **1999b**, 4, (2), 269-275.

- Lee, S.; Park, G.; Amy, G.; Hong, S.-K.; Moon, S.-H.; Lee, D.-H.; Cho, J., Determination of Membrane Pore Size Distribution Using Fractional Rejection of Nonionic and Charged Macromolecules. *Journal of Membrane Science* **2002b**, 201, 191-201.
- Leininger, N. F.; Gainer, J. L.; Kirwan, D. J., Effect of Aqueous PEG and PPG Solvents on Reaction Selectivity and Gibbs Energies. *AIChE Journal* **2004**, 50, (2), 511-517.
- Li, J.; Kao, W. J., Synthesis of Polyethylene Glycol (PEG) Derivatives and PEGylated-Peptide Biopolymer Conjugates. *Biomacromolecules* **2003**, 4, 1055-1067.
- Li, W.; Yi, Z.; Lin, B.; Su, Z., Characterization of Polyethylene Glycol-Modified Proteins by Semi-Aqueous Capillary Electrophoresis. *Journal of Chromatography A* **2001**, 905, 299-307.
- Li, W.; Wang, Y.; Zhu, X.; Li, M.; Su, Z., Preparation and Characterization of PEGylated Adducts of Recombinant Human Tumor Necrosis Factor- α from *Escherichia Coli*. *Journal of Biotechnology* **2002**, 92, 251-258.
- Li, W.; Su, Z., Quantitatively Investigating Monomethoxypolyethylene Glycol Modification of Protein by Capillary Electrophoresis. *Journal of Biochemical and Biophysical Methods* **2004**, 59, 65-74.
- Li, X.; Zhang, X.; Liu, Q., Determination of Molecular Weight Distribution of the PEGylated Bovine Hemoglobin (PEG-bHb). *Artificial Cells, Blood Substitutes and Biotechnology* **2005**, 33, 13-25.
- Li, X.-Q.; Lei, J.-D.; Su, Z.-G.; Ma, G.-H., Comparison of Bioactivities of Monopegylated rhG-CSF with Branched and Linear mPEG. *Process Biochemistry* **2007**, 42, 1625-1631.
- Lietor-Santos, J. J.; Fernandez-Nieves, A., Electrophoresis of Larger Polyelectrolyte-Coated Colloidal Particles. *Physical Review E* **2005**, 71, 042401-1 - 042401-4.
- Lin, N. P.; Deen, W. M., Effects of Long-Range Polymer-Pore Interactions on the Partitioning of Linear Polymers. *Macromolecules* **1990**, 23, (11), 2947-2955.
- Liu, Y.-H.; Tasarbopoulos, A.; Wylie, D.; Cannon-Carlson, S.; Lee, S.; Gitlin, G.; Youngster, S.; Bausch, J.; Voloch, M.; Pramanik, B. N. In *Mass Spectrometric Study of PEG12000-rhIFN Alpha-2b: Characterization of PEGylated Protein Product and Determination of PEGylation Site*, 50th ASMS Conference on Mass Spectrometry and Allied Topics; ASMS: Orlando, FL, 2002; pp 373-374.

- Long, D.; Ajdari, A., Electrophoretic Mobility of Composite Objects in Free Solution: Application to DNA Separation. *Electrophoresis* **1996**, 17, (6), 1161-1166.
- Long, T., D.; Anderson, J., R., Flow-Dependent Rejection of Polystyrene from Microporous Membranes. *Journal of Polymer Science - Physics Edition* **1984**, 22, 1261-1281.
- MacDonald, A.; Sheppard, M.; Lucy, C., Enhancement of Electroosmotic Flow Using Zwitterionic Additives. *Electrophoresis* **2005**, 26, 4421-4428.
- Makino, K.; Umetsu, M.; Goto, Y.; Nakayama, A.; Suhara, T.; Tsujii, J.; Kikuchi, A.; Ohshima, H.; Sakurai, Y.; Okano, T., Interaction Between Charged Soft Microcapsules and Red Blood Cells: Effects of PEGylation of Microcapsule Membranes Upon Their Surface Properties. *Colloids and Surfaces B: Biointerfaces* **1999**, 13, 287-297.
- Malone, D. M.; Anderson, J., Hindered Diffusion of Particles through Small Pores. *Chemical Engineering Science* **1978**, 33, 1429-1440.
- Manjula, B. N.; Tsai, A.; Upadhy, R.; Perumalsamy, K.; Smith, P. K.; Malavalli, A.; Vandegriff, K.; Winslow, R. M.; Intaglietta, M.; Prabhakaran, M.; Friedman, J. M.; Acharya, A. S., Site-Specific PEGylation of Hemoglobin at cys-93(b): Correlation between the Colligative Properties of the PEGylated Protein and the Length of the Conjugated PEG Chain. *Bioconjugate Chemistry* **2003**, 14, (2), 464-472.
- Martinez-Gomez, M. A.; Carril-Aviles, M. M.; Sagrado, S.; Villanueva-Camanas, R. M.; Medina-Hernandez, M. J., Characterization of Antihistamine-Human Serum Protein Interactions by Capillary Electrophoresis. *Journal of Chromatography A* **2007**, 1147, 261-269.
- Masliyah, J. H., *Electrokinetic Transport Phenomena*. Alberta Oil Sands Technology and Research Authority: Edmonton, Alta, 1994.
- Matthiasson, E., The Role of Macromolecular Adsorption in Fouling of Ultrafiltration Membranes. *Journal of Membrane Science* **1983**, 16, 23-36.
- McDonogh, R. M.; Fell, C. J. D.; Fane, A. G., Surface Charge and Permeability in the Ultrafiltration of Non-Flocculating Colloids. *Journal of Membrane Science* **1984**, 21, 285-294.
- McGoff, P.; Baziotis, A. C.; Maskiewicz, R., Analysis of Polyethylene Glycol Modified Superoxide Dismutase by Chromatographic, Electrophoretic, Light Scattering, Chemical, and Enzymatic Methods. *Chemical Pharmaceutical Bulletin* **1988**, 36, (8), 3079-3090.

- Mehta, A.; Zydney, A. L., Permeability and Selectivity Analysis for Ultrafiltration Membranes. *Journal of Membrane Science* **2005**, 249, 245-249.
- Mehta, A., Performance Characteristics of Charged Ultrafiltration Membranes: Fundamental Studies and Applications. Ph.D. Dissertation, The Pennsylvania State University, University Park, PA, 2006.
- Mehta, A.; Zydney, A. L., Effect of Membrane Charge on Flow and Protein Transport During Ultrafiltration. *Biotechnology Progress* **2006**, 22, 484-492.
- Mehvar, R., Recent Trends in the Use of Polysaccharides for Improved Delivery of Therapeutic Agents: Pharmacokinetics and Pharmacodynamic Perspectives. *Current Pharmaceutical Biotechnology* **2003**, 4, 283-302.
- Menon, M.; Zydney, A. L., Measurement of Protein Charge and Ion Binding Using Capillary Electrophoresis. *Analytical Chemistry* **1998**, 70, 1581-1584.
- Menon, M. K.; Zydney, A. L., Determination of Effective Protein Charge by Capillary Electrophoresis: Effects of Charge Regulation in the Analysis of Charge Ladders. *Analytical Chemistry* **2000**, 72, 5714-5717.
- Michallet, M.; Maloisel, F.; Delain, M.; Hellmann, A.; Rosas, A.; Silver, R. T.; Tandler, C., Pegylated Recombinant Interferon Alpha-2b vs Recombinant Interferon Alpha-2b for the Initial Treatment of Chronic-Phase Myelogenous Leukemia: A Phase III Study. *Leukemia* **2004**, 18, 309-315.
- Millipore, Corporation. *Ultracel Ultrafiltration Disc*. Billerica, MA, 2008a
<http://www.millipore.com/catalogue/item/pltk15005> (accessed June 10, 2008)
- Millipore, Corporation. *Ultrafiltration Membranes: Ultrafiltration Membranes for Macromolecules, Product Selection Guide*; Billerica, MA, 2008b.
- Mirasol, F., US Biotechs Lead Global Industry. *Chemical Market Reporter* **2005**, 268, (3), 38-39.
- Mitchell, B. D.; Deen, W. M., Effect of Concentration on the Rejection Coefficients of Rigid Macromolecules in Track-Etch Membranes. *Journal of Colloid and Interface Science* **1986**, 113, (1), 132-142.
- Miyamoto, D.; Oishi, M.; Kojima, K., Completely Dispersible PEGylated Gold Nanoparticles under Physiological Conditions: Modification of Gold Nanoparticles with Precisely Controlled PEG-B-Polyamine. *Langmuir* **2008**, 24, (9), 5010-5017.

- Mochizuki, S.; Zydney, A. L., Effect of Protein Adsorption on the Transport Characteristics of Asymmetric Ultrafiltration Membranes. *Biotechnology Progress* **1992**, 8, 553-561.
- Mochizuki, S.; Zydney, A. L., Theoretical Analysis of Pore Size Distribution Effects on Membrane Transport. *Journal of Membrane Science* **1993**, 82, 211-227.
- Molek, J.; Zydney, A. L., Ultrafiltration Characteristics of Pegylated Proteins. *Biotechnology and Bioengineering* **2006**, 95, (3), 474-482.
- Molek, J. R.; Zydney, A. L., Separation of PEGylated α -Lactalbumin from Unreacted Precursors and Byproducts Using Ultrafiltration. *Biotechnology Progress* **2007**, 23, 1417-1424.
- Monkarsh, S.; Spence, C.; Porter, J.; Palleroni, A.; Nalin, C.; Rosen, P.; Bailon, P., Isolation of Positional Isomers of MonoPoly(ethylene glycol)ylated Interferon/Alpha-2a and the Determination of Their Biochemical and Biological Characteristics. In *Poly(Ethylene Glycol) Chemistry and Biological Applications*, Harris, M. Z., Samuel, Ed. American Chemical Society: San Francisco, 1997; Vol. 680, pp 207-215.
- Moreadith, R.; Collen, D., Clinical Development of PEGylated Recombinant Staphylokinase (PEG-SAK) for Bolus Thrombolytic Treatment of Patients with Acute Myocardial Infarction. *Advanced Drug Delivery Reviews* **2003**, 55, 1337-1345.
- Muller, H.-J.; Loning, L.; Horn, A.; Schwabe, D.; Gunkel, M.; Schrappe, M.; von Schutz, V.; Henze, G.; Da Palma, J. C.; Vierira Pinheiro, J. P.; Winkelhorst, M.; Boos, J., Pegylated Asparaginase (OncasparTM) in Children with ALL: Drug Monitoring in Reinduction According to the ALL/NHL-BFM 95 Protocols. *British Journal of Haematology* **2000**, 110, 379-384.
- Na, D. H.; Park, M. O.; Choi, S. Y.; Kim, Y. S.; Lee, S. S., Identification of the Modifying Sites of Mono-PEGylated Salmon Calcitonins by Capillary Electrophoresis and MALDI-TOF Mass Spectrometry. *Journal of Chromatography B* **2001**, 754, 259-263.
- Na, D. H.; Youn, Y. S.; Lee, K. C., Optimization of the PEGylation Process of a Peptide by Monitoring with Matrix-Assisted Laser Desorption/Ionization Time-of-Flight Mass Spectrometry. *Rapid Communication Mass Spectrometry* **2003**, 17, (19), 2241-4.
- Na, D. H.; Youn, Y. S.; Park, E. J.; Lee, J. M.; Cho, O. R.; Lee, K. R.; Lee, S. D.; Yoo, S. D.; DeLuca, P. P.; Lee, K. C., Stability of PEGylated Salmon Calcitonin in Nasal Mucosa. *Journal of Pharmaceutical Science* **2004**, 93, (2), 256-261.

- Na, D. H.; Park, E. J.; Jo, Y. W.; Lee, K. C., Capillary Electrophoresis Separation of High Molecular Weight Poly(ethylene glycol)-Modified Proteins. *Analytical Biochemistry* **2008**, 373, 207-212.
- Nabe, A.; Staude, E.; Belfort, G., Surface Modification of Polysulfone Ultrafiltration Membranes and Fouling by BSA Solutions. *Journal of Membrane Science* **1997**, 133, 57-72.
- Nakajima, A.; Miyasaka, T.; Sakai, K.; Tsukahara, T., Determination of Effective Charge Density of Hollow-Fiber Dialysis Membranes and Its Effects on Phosphate Ion Permeability. *Journal of Membrane Science* **2001**, 187, 129-139.
- Nakao, S.; Osada, H.; Kurata, H.; Tsuru, T.; Kimura, S., Separation of Proteins by Charged Ultrafiltration Membranes. *Desalination* **1988**, 70, (1-3), 191-205.
- Nakaoka, R.; Tabata, Y.; Yamaoka, T.; Ikada, Y., Prolongation of the Serum Half-Life Period of Superoxide Dismutase by Poly(Ethylene Glycol) Modification. *Journal of Controlled Release* **1997**, 46, 253-262.
- Nakatsuka, S.; Michaels, A., Transport and Separation of Proteins by Ultrafiltration through Sorptive and Non-Sorptive Membranes. *Journal of Membrane Science* **1992**, 69, 189-211.
- Newman, J. S., *Electrochemical Systems*. Prentice-Hall: Englewood Cliffs, NJ, 1991.
- Nguyen, Q. T.; Neel, J., Characterization of Ultrafiltration Membranes. Part IV. Influence of the Deformation of Macromolecular Solutes on the Transport through Ultrafiltration Membranes. *Journal of Membrane Science* **1983**, 14, 111-128.
- Nijs, M.; Azarkan, M.; Smolders, N.; Brygier, J.; Vincentelli, J.; Petiau-de Vries, G. M.; Duchateau, J.; Looze, Y., Preliminary Characterization of Bovine Beta-Lactoglobulin after Its Conjugation to Polyethylene Glycol. *Biotechnology and Bioengineering* **1997**, 54, (1), 40-49.
- Niven, R. W.; Whitcomb, K. L.; Shaner, L.; Ralph, L. D.; Habberfield, A. D.; Wilson, J. V., Pulmonary Absorption of Polyethylene Glycolated Recombinant Human Granulocyte-Colony-Stimulating Factor (PEG rhG-CSF). *Journal of Controlled Release* **1994**, 32, (2), 177-189.
- Nystrom, M., Fouling of Unmodified and Modified Polysulfone Ultrafiltration Membranes by Ovalbumin. *Journal of Membrane Science* **1989**, 44, 183-196.
- O'brien, R. W.; White, L. R., Electrophoretic Mobility of a Spherical Colloidal Particle. *Journal of the Chemical Society – Faraday Transactions II* **1978**, 74, 1607-1626.

- Odell, J. A.; Keller, A.; Miles, M. J., Assessment of Molecular Connectedness in Semi-Dilute Polymer Solutions by Elongational Flow. *Polymer* **1985**, 26, 1219-1226.
- Ogez, J. R.; Hodgdon, J., C.; Beal, M. P.; Builder, S. E., Downstream Processing of Proteins: Recent Advances. *Biotechnology Advances* **1989**, 7, 467-488.
- Ohshima, H., Electrophoresis of Soft Particles. *Advances in Colloid and Interface Science* **1995**, 62, 189-235.
- Ohshima, H., Approximate Analytic Expression for the Electrophoretic Mobility of a Spherical Colloidal Particle. *Journal of Colloid and Interface Science* **2001**, 239, 587-590.
- Olson, K.; Gehant, R.; Mukku, V.; O'Connell, K.; Tomlinson, B.; Totpal, K.; Winkler, M., Preparation and Characterization of Poly(Ethylene Glycol)ylated Human Growth Hormone Antagonist. In *Poly(Ethylene Glycol) Chemistry and Biological Applications*, Harris, M. Z., Samuel, Ed. American Chemical Society: San Francisco, 1997; Vol. 680, pp 170-181.
- Opong, W. S.; Zydney, A. L., Diffusive and Convective Protein Transport through Asymmetric Membranes. *AIChE Journal* **1991**, 37, (10), 1497-1510.
- Orsatti, L.; Veronese, F., An Unusual Coupling of Poly(Ethylene Glycol) to Tyrosine Residues in Epidermal Growth Factor. *Journal of Bioactive and Compatible Polymers* **1999**, 14, 429-436.
- Pabst, T., M.; Buckley, J. J.; Ramasubramanian, N.; Hunter, A., Comparison of Strong Anion-Exchangers for the Purification of a PEGylated Protein. *Journal of Chromatography A* **2007**, 1147, 172-182.
- Pagac, E. S.; Prieve, D. C.; Solomentsev, Y.; Tilton, R. D., A Comparison of Polystyrene-Poly(Ethylene Oxide) Diblock Copolymer and Poly(Ethylene Oxide) Homopolymer Adsorption from Aqueous Solution. *Langmuir* **1997**, 13, 2993-3001.
- Palacio, L.; Ho, C.-C.; Zydney, A. L., Application of a Pore-Blockage - Cake - Filtration Model to Protein Fouling During Microfiltration. *Biotechnology and Bioengineering* **2002**, 79, (3), 260-270.
- Palacio, L.; Ho, C.-C.; Pradanos, P.; Hernandez, A.; Zydney, A. L., Fouling with Protein Mixtures in Microfiltration: BSA-Lysozyme and BSA-Pepsin. *Journal of Membrane Science* **2003**, 222, 41-51.
- Palecek, S. P.; Zydney, A. L., Hydraulic Permeability of Protein Deposits Form During Microfiltration: Effect of Solution pH and Ionic Strength. *Journal of Membrane Science* **1994**, 95, 71-81.

- Parkinson, C.; Scarlett, J. A.; Trainer, P. J., Pegvisomant in the Treatment of Acromegaly. *Advanced Drug Delivery Reviews* **2003**, 55, (10), 1303-1314.
- Paugh, J.; Lafrance, J. C. *Meeting the Challenge: U.S. Industry Faces the 21st Century: The U.S. Biotechnology Industry*; U.S. Department of Commerce, Office of Technology Policy - Technology Administration: 1997.
- Pecora, R., *Dynamic Light Scattering: Applications of Photo Correlation Spectroscopy* Plenum Press: New York, NY, 1985.
- Perkins, T. T.; Smith, D. E.; Chu, S., Single Polymer Dynamics in an Elongational Flow. *Science* **1997**, 276, 2016-2021.
- Peters, T. J., *All About Albumin: Biochemistry Genetics, and Medical Applications*. Academic Press: San Diego, CA, 1996.
- Pettit, D.; Nightlinger, N.; Goetze, A.; Gombotz, W., Site Protected PEGylation of Recombinant (P75) Tumor Necrosis Factor Receptor. *American Chemical Society, Polymer Preprints, Division of Polymer Chemistry* **1997**, 38, (1), 574-575.
- Pfizer, Inc.; (OSI)Eyeteck, Inc. *Macugen (Pegaptanib Sodium Injection)*; FDA Approved Document: NDC 68782-001-01 New York, NY, 2006.
- Piedmonte, D. M.; Treuheit, M., Formulation of Neulasta[®] (Pegfilgrastim). *Advanced Drug Delivery Reviews* **2008**, 60, 50-58.
- Pike, E. R.; Abbiss, J. B., *Light Scattering and Photon Correlation Spectroscopy*. Kluwer Academic Publishers: Dordrecht, 1997.
- Piquet, G.; Gatti, M.; Barbero, L.; Traversa, S.; Caccia, P.; Esposito, P., Set-up of Large Laboratory-Scale Chromatographic Separations of Poly(Ethylene Glycol) Derivatives of the Growth Hormone-Releasing Factor 1-29 Analogue. *Journal of Chromatography A* **2002**, 944, 141-148.
- Pujar, N. S.; Zydney, A. L., Electrostatic and Electrokinetic Interactions During Protein Transport through Narrow Pore Membranes. *Industrial and Engineering Chemistry Research* **1994**, 33, (10), 2473-2482.
- Pujar, N. S., Electrostatic and Electrokinetic Interactions During Protein Filtration Using Semi-Permeable Membranes. Ph.D. Dissertation, University of Delaware, Newark, DE, 1996.

- Pujar, N. S.; Zydney, A. L., Charge Regulation and Electrostatic Interactions for a Spherical Particle in a Cylindrical Pore. *Journal of Colloid and Interface Science* **1997**, 192, 338-349.
- Pujar, N. S.; Zydney, A. L., Electrostatic Effects on Protein Partitioning in Size-Exclusion Chromatography and Membrane Ultrafiltration. *Journal of Chromatography A* **1998**, 796, 229-238.
- Rabiller-Baudry, M.; Chaufer, B.; Aimar, P.; Bariou, B.; Lucas, D., Application of a Convection-Diffusion-Electrophoretic Migration Model to Ultrafiltration of Lysozyme at Different pH Values and Ionic Strengths. *Journal of Membrane Science* **2000**, 179, 163-174.
- Rang, H. P., *Pharmacology*. 4th ed.; Chuchhill Livingstone: New York, NY, 2001.
- Rao, S., Protein Separation Using Affinity Ultrafiltration with Small Charged Ligands. Ph.D. Dissertation, The Pennsylvania State University, University Park, PA, 2007.
- Rao, S.; Zydney, A. L., High Resolution Protein Separations Using Affinity Ultrafiltration with Small Charged Ligands. *Journal of Membrane Science* **2006**, 280, 781-789.
- Ratledge, C.; Kristiansen, B., Back to Basics: Basic Biotechnology. *Chemistry in Britain* **2001**, 37, (8), 44.
- Rautenbach, R.; Holtz, H., Effect of Concentration Dependence of Physical Properties of Ultrafiltration. *German Chemical Engineering* **1980**, 3, 180-185.
- Reddy, R.; Modi, M.; Pedder, S., Use of PEGinterferon α -2a (40kD) (PEGasys) for the Treatment of Hepatitis C. *Advanced Drug Delivery Reviews* **2002**, 54, 5710586.
- Roberts, M. J.; Harris, J. M., Attachment of Degradable Poly(Ethylene Glycol) to Proteins has the Potential to Increase Therapeutic Efficacy. *Journal of Pharmaceutical Science* **1998**, 87, (11), 1440-1445.
- Roberts, M. J.; Bentley, M. D.; Harris, J. M., Chemistry for Peptide and Protein PEGylation. *Advanced Drug Delivery Reviews* **2002**, 54, 459-476.
- Robertson, B. C.; Zydney, A. L., Protein Adsorption in Asymmetric Ultrafiltration Membranes with Highly Constricted Pores. *Journal of Colloid and Interface Science* **1990**, 134, (2), 563-575.
- Rouse, P. E., A Theory of the Linear Viscoelastic Properties of Dilute Solutions of Coiling Polymers. *Journal of Chemical Physics* **1953**, 21, (7), 1272-1280.

- Safi, S.; Asfari, Z.; Hagege, A., Characterization of Protein Conjugates Using Capillary Electrophoresis. *Journal of Chromatography A* **2007**, 1173, 159-164.
- Saksena, S.; Zydney, A. L., Effect of Solution pH and Ionic Strength on the Separation of Albumin from Immunoglobulins (IgG) by Selective Filtration. *Biotechnology and Bioengineering* **1994**, 43, 960-968.
- Saksena, S.; Zydney, A. L., Pore Size Distribution Effects on Electrokinetic Phenomena in Semipermeable Membranes. *Journal of Membrane Science* **1995**, 105, (3), 203-215.
- Sato, H., Enzymatic Procedure for Site-Specific Pegylation of Proteins. *Advanced Drug Delivery Reviews* **2002**, 54, (4), 487-504.
- Schiavon, O.; Caliceti, P.; Ferruti, P.; Veronese, F., M., Therapeutic Proteins: A Comparison of Chemical and Biological Properties of Uricase Conjugated to Linear or Branched Poly(Ethylene Glycol) and Poly(N-Acryloylmorpholine). *II Farmaco* **2000**, 55, (4), 264-269.
- Schmidt, A. S.; Andrews, B. A.; Asenjo, J. A., Correlations for the Partition Behavior of Proteins in Aqueous Two-Phase Systems: Effect of Overall Protein Concentration. *Biotechnology and Bioengineering* **1996**, 50, (6), 617-626.
- Schock, G.; Miquel, A.; Birkenberger, R., Characterization of Ultrafiltration Membranes: Cut-Off Determination by Gel Permeation Chromatography. *Journal of Membrane Science* **1989**, 41, 55-67.
- Shah, T. N.; Foley, H. C.; Zydney, A. L., Performance Characteristics of Nanoporous Carbon Membranes for Protein Ultrafiltration. *Biotechnology Progress* **2007**, 23, 1157-1162.
- Sharma, U.; Negin, R.; Carbeck, J. D., Effects of Cooperativity in Proton Binding on the Net Charge of Proteins in Charge Ladders. *Journal of Physical Chemistry B*. **2003**, 107, 4653-4666.
- Sharma, U.; Carbeck, J. D., Hydrodynamic Radius Ladders of Proteins. *Electrophoresis* **2005**, 25, 2086-2091.
- Sharp, K. A.; Brooks, D. E., Calculation of the Electrophoretic Mobility of a Particle Bearing Bound Polyelectrolyte Using the Nonlinear Poisson-Boltzmann Equation. *Biophysical Journal* **1985**, 47, 563-566.
- Shi, Q.; Su, Y.; Zhu, S.; Li, C.; Zhao, Y.; Jiang, Z., A Facile Method for Synthesis of Pegylated Polyethersulfone and Its Application in Fabrication of Antifouling Ultrafiltration Membrane. *Journal of Membrane Science* **2007**, 303, 204-212.

- Shibata, H.; Nakagawa, S.; Mayumi, T.; Tsutsumi, Y., Development of Novel Drug Delivery System (DDS) Technologies for Proteomic-Based Drug Development. *Biological Pharmaceutical Bulletin* **2004**, 27, (10), 1483-1488.
- Shibata, H.; Nakagawa, S.; Tsutsumi, Y., Optimization of Protein Therapies by Polymer-Conjugation as an Effective DDS. *Molecules* **2005**, 10, (1), 162-180.
- Singh, S.; Khulbe, K. C.; Matsuura, T.; Ramamurthy, P., Membrane Characterization by Solute Transport and Atomic Force Microscopy. *Journal of Membrane Science* **1998**, 142, 111-127.
- Snider, J.; Neville, C.; Yuan, L.-C.; Bullock, J., Characterization of the Heterogeneity of Polyethylene Glycol-Modified Superoxide Dismutase by Chromatographic and Electrophoretic Techniques. *Journal of Chromatography* **1992**, 599, 141-155.
- Smith, F. G.; Deen, W. M., Electrostatic Double-Layer Interactions for Spherical Colloids in Cylindrical Pores. *Journal of Colloid and Interface Science* **1980**, 78, (2), 444-465.
- Smith, F. G.; Deen, W. M., Electrostatic Effects on the Partitioning of Spherical Colloids between Dilute Bulk Solution and Cylindrical Pores. *Journal of Colloid and Interface Science* **1983**, 91, (2), 571-590.
- Smith, K. A.; Colton, C.; Merrill, E. W.; Evans, L. B., Determination of True Membrane Permeability from a Single Measurement. *Chemical Engineering Progress Symposium* **1968**, 84, (64), 45.
- Smith, M., Molecular Weights of Proteins and Some Other Materials Including Sedimentation, Diffusion and Frictional Coefficients and Partial Specific Volumes. In *Handbook of Biochemistry*, 2nd ed.; Sober, H., Ed. The Chemical Rubber Co.: Cleveland, OH, 1970.
- Stein, P.; Leslie, A. G.; Finch, J. T.; Carrell, R. W., Crystal Structure of Uncleaved Ovalbumin at 1.95 Angstrom Resolution. *Journal of Molecular Biology* **1991**, 221, (3), 941-959.
- Subramanian, G., *Bioseparation and Bioprocessing*. 2nd ed.; Wiley-VCH: Weinheim, Germany, 1998; Vol. 1.
- Sugio, S.; Kashima, A.; Mochizuki, S.; Noda, M.; Kobayashi, K., Crystal Structure of Human Serum Albumin at 2.5 Angstrom Resolution. *Protein Engineering* **1999**, 12, (6), 439-446.
- Tan, Y.; Sun, X.; Xu, M.; An, Z.; Tan, X.; Tan, X.; Han, Q.; Miljkovic, D. A.; Yang, M.; Hoffman, R. M., Polyethylene Glycol Conjugation of Recombinant Methionase for Cancer Therapy. *Protein Expression and Purification* **1998**, 12, (1), 45-52.

- Teraoka, I., Calibration of Retention Volume in Size Exclusion Chromatography by Hydrodynamic Radius. *Macromolecules* **2004**, 37, (17), 6632-6639.
- Thompson, D. S.; Gill, S. J., Polymer Relaxation Times from Birefringence Relaxation Measurements. *Journal of Chemical Physics* **1967**, 47, (12), 5008-5017.
- Ton, G. N.; Fine, J. P.; Kwon, G. S., Methoxypoly(Ethylene Glycol)-Conjugated Carboxypeptidase a for Solid Tumor Targeting Part 1: Synthesis and Characterization. *Journal of Controlled Release* **2005**, 104, 129-139.
- Torchilin, V.; Trubetskoy, V., S., Which Polymers Can Make Nanoparticulate Drug Carriers Long-Circulating? *Advanced Drug Delivery Reviews* **1995**, 16, 141-155.
- UCB Group, Inc. *Cimzia (Certolizumab Pegol)*; FDA Approved Document: 1736 Smyrna, GA, 2008.
- van der Auwera, P.; Platzer, E.; Xu, Z. X.; Schulz, R.; Feugeas, O.; Capdeville, R.; Edwards, D. J., Pharmacodynamics and Pharmacokinetics of Single Doses of Subcutaneous Pegylated Human G-CSF Mutant (Ro 25-8315) in Healthy Volunteers: Comparison with Single and Multiple Daily Doses of Filgrastim. *American Journal of Hematology* **2001**, 66, 245-251.
- van Eijndhoven, R. H. C. M.; Saksena, S.; Zydney, A. L., Protein Fractionation Using Electrostatic Interactions in Membrane Filtration. *Biotechnology and Bioengineering* **1995**, 48, 408-414.
- van Reis, R.; Gadam, S.; Frautschy, L.; Orlando, S.; Goodrich, E.; Saksena, S.; Kuriyel, R.; Simpson, C.; Pearl, S.; Zydney, A. L., High Performance Tangential Flow Filtration. *Biotechnology and Bioengineering* **1997**, 56, (1), 71-82.
- van Reis, R.; Saksena, S., Optimization Diagram for Membrane Separations. *Journal of Membrane Science* **1997**, 129, 19-29.
- van Reis, R.; Brake, J.; Charkoudian, J.; Burns, D.; Zydney, A. L., High-Performance Tangential Flow Filtration Using Charged Membranes. *Journal of Membrane Science* **1999**, 159, 133-142.
- van Reis, R. Charged Filtration Membranes and Uses Therefor. US Patent 7001550, Genentech Inc, 2006.
- Veronese, F., M., Peptide and Protein PEGylation: A Review of Problems and Solutions. *Biomaterials* **2001**, 22, 405-417.

- Veronese, F. M.; Sacca, B.; Polverino de Laureto, P.; Sergi, M.; Caliceti, P.; Schiavon, O.; Orsolini, P., New PEGs for Peptide and Protein Modification, Suitable for Identification of the PEGylation Site. *Bioconjugate Chemistry* **2001**, 12, (1), 62-70.
- Verwey, E. J. W., *Theory of the Stability of Lyophobic Colloids: The Interaction of Sol Particles Having an Electric Double Layer*. Elsevier Publishing Co.: New York, NY, 1948.
- Vestling, M.; Murphy, C.; Fenselau, C., Characterization of PEGylated Superoxide Dismutase. In *Techniques in Protein Chemistry 3rd Ed.*, Academic Press: San Diego, CA, 1992; pp 477-485.
- Vincentelli, J.; Paul, C.; Azarka, M., Evaluation of the Polyethylene Glycol-KF-Water System in the Context of Purifying PEG-Protein Adducts. *International Journal of Pharmaceutics* **1999**, 176, (2), 241-249.
- Walsh, G. G., Biopharmaceutical Benchmarks. *Nature Biotechnology* **2006**, 24, (7), 769.
- Wang, Y.; Youngster, S.; Grace, M.; Bausch, J.; Borden, R.; Wyss, D., Structural and Biological Characterization of Pegylated Recombinant Interferon Alpha-2b and Its Therapeutic Implications. *Advanced Drug Delivery Reviews* **2002**, 54, 547-570.
- Watzig, H.; Degenhardt, M.; Kunkel, A., Strategies for Capillary Electrophoresis: Method Development and Validation for Pharmaceutical and Biological Applications. *Electrophoresis* **1998**, 19, 2695-2752.
- Willauer, H. D.; Huddleston, J. G.; Rogers, R. D., Solute Partitioning in Aqueous Biphasic Systems Composed of Polyethylene Glycol and Salt: The Partitioning of Small Neutral Organic Species. *Industrial and Engineering Chemistry Research* **2002**, 41, 1892-1904.
- Working, P., K.; Newman, M. S.; Johnson, J.; Cornacoff, J. B., Safety of Poly(Ethylene Glycol) and Poly(Ethylene Glycol) Derivatives. In *ACS Symposium Series 680: Poly(Ethylene Glycol) Chemistry and Biological Applications*, Harris, M. J.; Zalipsky, S., Eds. ACS Symposium Series: San Francisco, CA, 1997.
- Wu, X.; Liu, X.; Xiao, Y.; Huang, Z.; Xiao, J.; Lin, S.; Cai, L.; Feng, W.; Li, X., Purification and Modification by Polyethylene Glycol of a New Human Basic Fibroblast Growth Factor Mutant-hbFGF^{ser25,87,92}. *Journal of Chromatography A* **2007**, 1161, 51-55.
- Wylie, D.; Voloch, M.; Lee, S.; Liu, Y.; Cannon-Carlson, S.; Cutler, C.; Pramanik, B., Carboxyalkylated Histidine Is a pH-Dependent Product of Pegylation with SC-PEG. *Pharmaceutical Research* **2001**, 18, (9), 1354-1360.

- Yamamoto, Y.; Tsutsumi, Y.; Yoshioka, Y.; Nishibata, T.; Kobayashi, K.; Okamoto, T.; Mukai, Y.; Shimizu, T.; Nakagawa, S.; Nagata, S.; Mayumi, T., Site-Specific PEGylation of a Lysine-Deficient TNF-Alpha with Full Bioactivity. *Nature Biotechnology* **2003**, 21, (5), 546-552.
- Yang, M. C.; Tong, J. H., Loose Ultrafiltration of Proteins Using Hydrolyzed Polyacrylonitrile Hollow Fiber. *Journal of Membrane Science* **1997**, 132, (1), 63-71.
- Yang, K.; Basu, A.; Wang, M.; Chintala, R.; Hsieh, M.-C.; Liu, S.; Hua, J.; Zhang, Z.; Zhou, J.; Li, M.; Phyu, H.; Petti, G.; Mendez, M.; Janjua, H.; Peng, P.; Longley, C.; Borowski, V.; Mehlig, M.; Filpula, D., Tailoring Structure-Function and Pharmacokinetic Properties of Single Chain Fv Proteins by Site-Specific PEGylation. *Protein Engineering* **2003**, 16, (10), 761-770.
- Yariv, E., Induced-Charge Electrophoresis of Nonspherical Particles. *Physics of Fluids* **2005**, 17, 051702-4.
- Yoon, B. J., Electrophoretic Motion of Spherical Particles with a Nonuniform Charge Distribution. *Journal of Colloid and Interface Science* **1990**, 142, (2), 575-581.
- Youn, Y. S.; Na, D. H.; Yoo, S. D.; Song, S.-C.; Lee, K. C., Chromatographic Separation and Mass Spectrometric Identification of Positional Isomers of Polyethylene Glycol-Modified Growth Hormone Releasing Factor (1-29). *Journal of Chromatography A* **2004**, 1061, 45-49.
- Youn, Y. S.; Jung, J. Y.; Oh, S. H.; Yoo, S. D.; Lee, K. C., Improved Intestinal Delivery of Salmon Calcitonin by Lys18-Amine Specific PEGylation: Stability, Permeability, Pharmacokinetic Behavior and *In Vivo* Hypocalcemic Efficacy. *Journal of Controlled Release* **2006**, 114, 334-342.
- Young, M. E.; Carroad, P. A.; Bell, R. L., Estimation of Diffusion Coefficients of Proteins. *Biotechnology and Bioengineering* **1980**, 22, 947-955.
- Yun, Q.; Chen, T.; Zhang, G.; Bi, J.; Ma, G.; Su, Z., Novel Polyethylene Glycol Derivative Suitable for the Preparation of Mono-PEGylated Protein. *Biotechnology Letters* **2005a**, 27, 213-217.
- Yun, Q.; Yang, R. E.; Chen, T.; Bi, J.; Ma, G.; Su, Z., Reproducible Preparation and Effective Separation of PEGylated Recombinant Human Granulocyte Colony-Stimulating Factor with Novel "PEG-Pellet" PEGylation Mode and Ion-Exchange Chromatography. *Journal of Biotechnology* **2005b**, 118, 67-74.

- Yun, Q.; Xing, W.; Ma, G.; Su, Z., Preparation and Characterization of Mono-PEGylated Consensus Interferon by a Novel Polyethylene Glycol Derivative. *Journal of Chemical Technology and Biotechnology* **2006**, 81, 776-781.
- Zalipsky, S., Chemistry of Polyethylene Glycol Conjugates with Biologically Active Molecules. *Advanced Drug Delivery Reviews* **1995**, 16, 157-182.
- Zeman, L.; Wales, M., Steric Rejection of Polymeric Solutes by Membranes with Uniform Pore Size Distribution. *Separation Science and Technology* **1981**, 16, (3), 275-290.
- Zeman, L. J.; Zydney, A. L., *Microfiltration and Ultrafiltration : Principles and Applications*. Marcel Dekker: New York, 1996; p 350-379.
- Zhang, M.; Zhang, Y.; Zhu, S.-Y.; Li-Fang, W.; Dou, H.-Z.; Yin, C.-H., Synthesis and Chromatographic Separation of Monomethoxypolyethylene Glycol Modified Insulin. *Separation Science and Technology* **2007**, 42, (4), 789-801.
- Zimm, B. H., Dynamics of Polymer Molecules in Dilute Solution: Viscoelasticity, Flow Birefringence, and Dielectric Loss. *Journal of Chemical Physics* **1956**, 24, (2), 269-278.
- Zulkali, M. M. D.; Ahmad, A. L.; Derel, C. J. C., Membrane Application in Proteomic Studies: Preliminary Studies on the Effect of pH, Ionic Strength and Pressure on Protein Fractionation. *Desalination* **2005**, 179, 381-390.
- Zydney, A. L., Stagnant Film Model for Concentration Polarization in Membrane Systems. *Journal of Membrane Science* **1997**, 130, (1-2), 275-281.
- Zydney, A. L.; Xenopoulos, A., Improving Dextran Tests for Ultrafiltration Membranes: Effect of Device Format. *Journal of Membrane Science* **2007**, 291, 180-190.

Appendix A

Nomenclature

A_{mem}	= membrane area (m ²)
A_p	= coefficient describing the pore double layer in the energy of interaction (-)
A_s	= coefficient describing the solute double layer in the energy of interaction (-)
A_{sp}	= coefficient describing the solute-pore term in the energy of interaction (-)
A	= constant in mass transfer coefficient calculation (-)
A	= coefficient in light scattering calculation (chapter 5 only) (-)
a	= hydrodynamic radius (m)
a_n	= expansion coefficient for K_S and K_T (-)
a_{pro}	= radius of the protein (m)
b	= radius of the stirred cell (m)
b_n	= expansion coefficient for K_S and K_T (-)
C	= local solute concentration (g/L)
C_b	= bulk solute concentration (g/L)
C_f	= filtrate solute concentration (g/L)
C_i	= ion concentration (mol/L)
C_o	= initial solute concentration in diafiltration (g/L)
C_s	= solute concentration in the pore (g/L)
$\langle C_s \rangle$	= radially averaged concentration (g/L)
C_w	= wall solute concentration (g/L)
c	= solution conductivity (S/cm)
D_i	= ion diffusion coefficient (m ² /s)
D_∞	= solute diffusivity (m ² /s)
De	= Deborah number (-)
d	= constant in mass transfer coefficient correlation (-)
E_z	= applied electric field (V)
F	= Faraday constant (C/mol)

f	= frictional coefficient (kg/s)
f_g	= drag force coefficient with the motion along the short (a) axes (-)
f_h	= drag force coefficient with the motion along the long (b) axes (-)
f_{perm}	= permeability factor (m^{-1})
G	= hydrodynamic lag coefficient (-)
G	= homodyne intensity-intensity auto correlation function (Chapter 5 only) (-)
g	= effective spheroid diameter (the larger diameter of the PEG or protein) (m)
H	= Henry correction factor (-)
h	= spheroid length (equal to the diameters of the PEG and protein component) (m)
I	= ionic strength (mol/L)
I_1	= modified Bessel Function of the first kind of order 1 (-)
I_2	= modified Bessel Function of the first kind of order 2 (-)
J_v	= filtrate flux (m/s)
K	= enhanced drag coefficient (-)
K_a	= dissociation constant (-)
K_c	= hindrance factor for convection (-)
K_d	= hindrance factor for diffusion (-)
K_s	= hydrodynamic function describing convection
K_t	= hydrodynamic function describing convection and diffusion
K_l	= modified Bessel Function of the second kind of order 1 (-)
k_B	= Boltzmann's constant (J/K)
k_i	= kinetic rate constant for PEGylation reactions ($mol^{-1}min^{-1}$)
k_m	= solute mass transfer coefficient (m/s)
L_d	= length of the capillary to detector (m)
L_p	= hydraulic permeability (m)
MW	= solute molecular weight (Da)
N	= number of diavolumes (-)
\bar{N}_s	= average solute flux through pore (m/s)
$\langle N_s \rangle$	= radially averaged solute flux (m/s)
n	= number of pores (-)
n_i	= total number of titratable species (-)

n_0	= refractive index of the medium (-)
n_{RI}	= total RI response (-)
dn/dc	= specific RI response (nRIU/g/L)
P	= purification factor (-)
Pe	= Peclet number (-)
Q_p	= flow rate through a single pore (m^3/s)
q	= charge on a particle (C)
q	= scattering vector (Chapter 5 only) (-)
q_p	= constant surface charge density of the pore (C/m^2)
q_s	= constant surface charge density of the solute (C/m^2)
$q_{surface}$	= charge of the protein surface (C)
R	= ideal gas constant ($J\ mol^{-1}\ K^{-1}$)
R_h	= protein hydrodynamic radius (m)
R_G	= radius of gyration (m)
R_{PEG}	= hydrodynamic radius of PEG (m)
R_{Pro}	= hydrodynamic radius of protein (m)
R_p	= particle radius (m)
R_i	= radius of sphere i (m)
R_{eff}	= effective hydrodynamic radius (m)
R_T	= retention times in capillary electrophoresis (s)
R_m	= resistance associated with the membrane (m^{-1})
R_c	= resistance of the cake layer (m^{-1})
R_f	= resistance of the fouling layer (m^{-1})
R_p	= resistance of the polarization layer (m^{-1})
Re	= Reynolds number (-)
r	= radial position within the pore (m)
r_i	= number of dissociated groups (-)
r_p	= pore radius (m)
\bar{r}	= mean pore radius (m)
S	= peak resolution (-)
S_a	= actual sieving coefficient (-)

S_o	= observed sieving coefficient (-)
Sh	= Sherwood number (-)
S_I	= observed sieving coefficient for an undeformed protein (-)
S_2	= observed sieving coefficient for the PEGylated protein at very high flux (-)
s	= radius of the PEGylated protein (m)
T	= absolute temperature (K)
t	= time needed for solute to reach capillary electrophoresis detector (s)
t_o	= time needed for neutral marker to reach capillary electrophoresis detector (s)
t_o	= initial time (light scattering – Chapter 5 only) (s)
V	= fluid velocity (m/s)
\bar{V}	= average fluid velocity through the membrane (m/s)
$\langle V \rangle$	= radially averaged velocity (m/s)
V_i	= interstitial (excluded) volume (L)
V_{sys}	= system volume (L)
V_r	= retention volume of the species of interest (L)
V_v	= total void volume (L)
V_σ	= dimensionless interaction energy (-)
v_z	= axial velocity (m/s)
$\frac{1}{2}W$	= peak width at half height (s)
Y	= product yield (-)
z	= distance above the membrane (m)
z_i	= ion valence (-)

Greek Symbols

β	= dimensionless radial position (-)
β_0	= prefactor in the autocorrelation function (-)
χ	= scaled sieving coefficient (-)
ΔP	= transmembrane pressure (kPa)
$\Delta \Pi$	= osmotic pressure difference across the membrane (kPa)
δ	= membrane thickness (m)

ε	= porosity of the membrane (-)
ε_0	= permittivity of a vacuum ($\text{C}^2 \text{N}^{-1} \text{m}^{-2}$)
ε_r	= relative permittivity (-)
Φ	= electrical potential at specific radial position (V)
Φ_r	= electrical potential at the surface of the pore (V)
ϕ	= equilibrium partition coefficient (-)
Γ	= correlator time delay (s^{-1})
γ	= inverse of characteristic time for fluid flow (s^{-1})
η	= solution viscosity (kg m s^{-1})
$[\eta_0]$	= intrinsic viscosity (L/g)
κ^{-1}	= Debye length (m)
λ	= ratio of the solute to pore radii (-)
λ	= wavelength of light (Chapter 5 only) (m)
λ_0	= wavelength of excitation light in a vacuum (m)
μ	= electrophoretic mobility ($\text{m}^2 \text{V}^{-1} \text{s}^{-1}$)
μ_{pro}	= electrophoretic mobility of a native protein ($\text{m}^2 \text{V}^{-1} \text{s}^{-1}$)
θ	= scattering angle (-)
ρ_e	= local charge density (C m^{-3})
σ	= standard deviation of the pore size distribution (-)
σ_0	= osmotic reflection coefficient (-)
σ_s	= dimensionless solute surface charge density (-)
σ_p	= dimensionless pore surface charge density (-)
τ	= dimensionless pore size (-)
τ	= time step for dynamic light scattering (Chapter 5 only) (s)
τ_0	= time scale for polymer relaxation (s)
ν	= kinematic viscosity (m^2/s)
ω	= stirring speed (s^{-1})
ω_i	= hydrodynamic drag on sphere i (kg/s)
Ψ	= selectivity (-)

ψ = electrical potential energy of interaction (J)

ψ_o = electrical potential at the surface of the protein (V)

$\left\langle \frac{\partial \Psi}{\partial z} \right\rangle$ = radially averaged potential energy (J/m)

ζ = zeta potential (V)

Appendix B

ANALYSIS OF MEMBRANE PORE SIZE USING POLYDISPERSED DEXTRANS

Many methods exist to characterize the pore size of ultrafiltration membranes; some of these include permeation tests, solute transport tests and visual analysis. Permeation tests can be performed using a solvent (either liquid or gas) that is able to enter all the pores. The permeation along with the Hagan- Poiseuille equation (Equation 2.9) is used to determine the average pore size. Visual analysis methods include examining the membrane using techniques such as atomic force microscopy (Khayet and Matsuura, 2003) or scanning electron microscopy (Chaturvedi, et al., 2000). While visual analysis can provide a good understanding of pore structure at the surface, determining the internal pore structure using visual methods is much more difficult due to the additional preparation steps needed to visualize the surface. The disadvantage of this method is that flow-through and dead-end pores cannot be differentiated. One of the most common techniques used for pore characterization for ultrafiltration membranes is a solute transport analysis. This technique has the advantage that the sieving coefficient of a range of molecular sizes can be examined instead of a simple solvent flow. The disadvantage of using the solute transport analysis is that the results must be fit to a pore size distribution to obtain information about a mean pore size. Dextrans (Kim, et al., 1994; Schock, et al., 1989; Zydney and Xenopoulos, 2007) are a very common solute used for membrane characterization, but PEG (Chaturvedi, et al., 2000; Cleveland, et al.,

2002) or polystyrenes (Beerlage, et al., 2000) have also be used. Membrane characterization studies have also been performed using charged solutes such as natural organic matter (Lee, et al., 2002), though the use of such compounds can be difficult to analyze due to both electrostatic and hydrodynamic effects. In this appendix the procedure to calculate the mean pore size and the extent of pore size distribution will be summarized. A computer program used to perform the calculations is given at the end of this appendix.

To determine the pore size distribution, an ultrafiltration sieving test with a polydispersed dextran was performed as described in Chapter 3. The filtrate and bulk samples of the dextran solution were analyzed using size exclusion chromatography with a TOSOH G2000SW or G3000SW column, depending on the range of dextran molecular weight used. The sieving coefficient of the dextrans at fixed retention time values, each corresponding to approximately 5% of the peak width of the polydispersed dextran were analyzed. Figure B.1 shows an example of the experimental results obtain for the sieving coefficient of a polydispersed dextran as a function of molecular weight in a 100 kDa UltracelTM membrane that had been charged-modified for 24 hours. The results are plotted as the actual sieving coefficient determined from the observed sieving coefficient and the stagnant film model (Equation 2.3) as a function of molecular weight determined from a calibration of the retention time in the SEC system. These results were obtained at a flux of 19.3 $\mu\text{m/s}$.

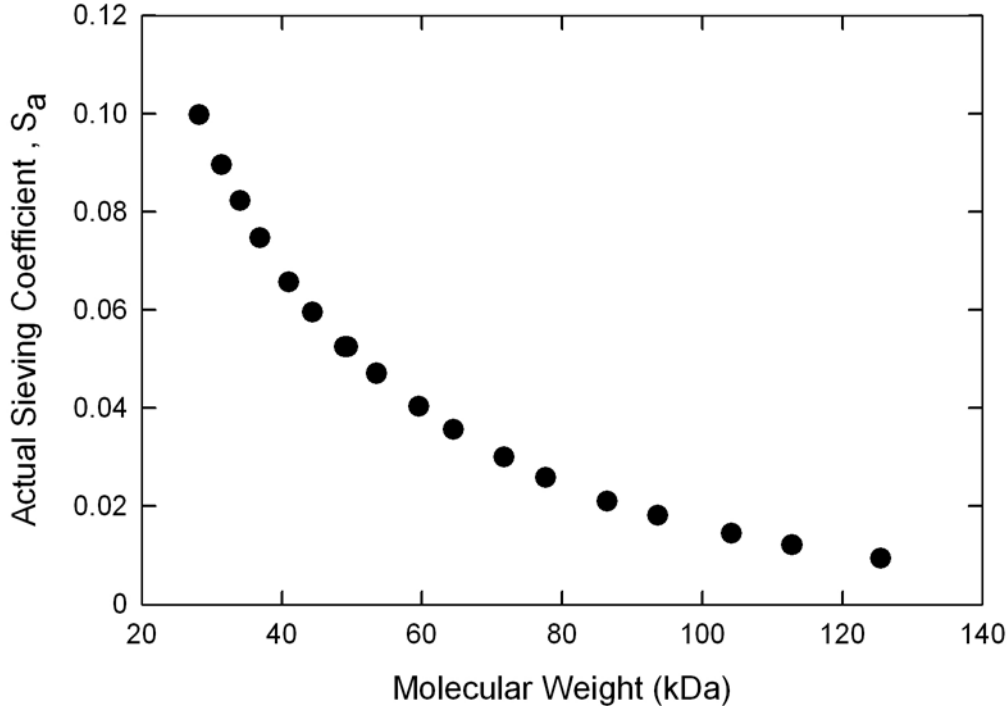


Figure B.1. Actual sieving coefficient as a function of the dextran molecular weight in a 100 kDa Ultracel™ membrane that was charged modified for 24 hours.

The hydrodynamic models described in Chapter 2 are used to calculate the actual sieving coefficient as a function of the solute radii over a range of mean pore sizes and pore distribution ratio. A sample of the computer calculations for this analysis is shown in at the end of this appendix. It was assumed that the pore sizes follow a log normal pore size distribution. Previous studies have often used a value of 0.10- 0.5 for the ratio of the standard deviation to the mean pore radius (Mehta and Zydney, 2005).

The results of the theoretical calculations are compared to the experimental values of the actual sieving coefficient for molecular weights over a range of mean pore size and pore size distributions. The squared residuals between the experimental and theoretical data are determined. Figure B.2 shows the sum of squared residuals (SSR) between the theoretical values and the experimental sieving coefficients of the polydispersed dextrans

in a 100 kDa membrane that has been charged modified for 24 hours as a function of the mean pore size and ratio of pore size distribution to mean pore size (z). Low residuals indicate a high correlation between the experimental and the theoretical data. Though a SSR of zero indicates no error between the theory and experimental data, a SSR of 0.004 is the limit of to which the experimental data can be compared to the theory for this particular experiment.

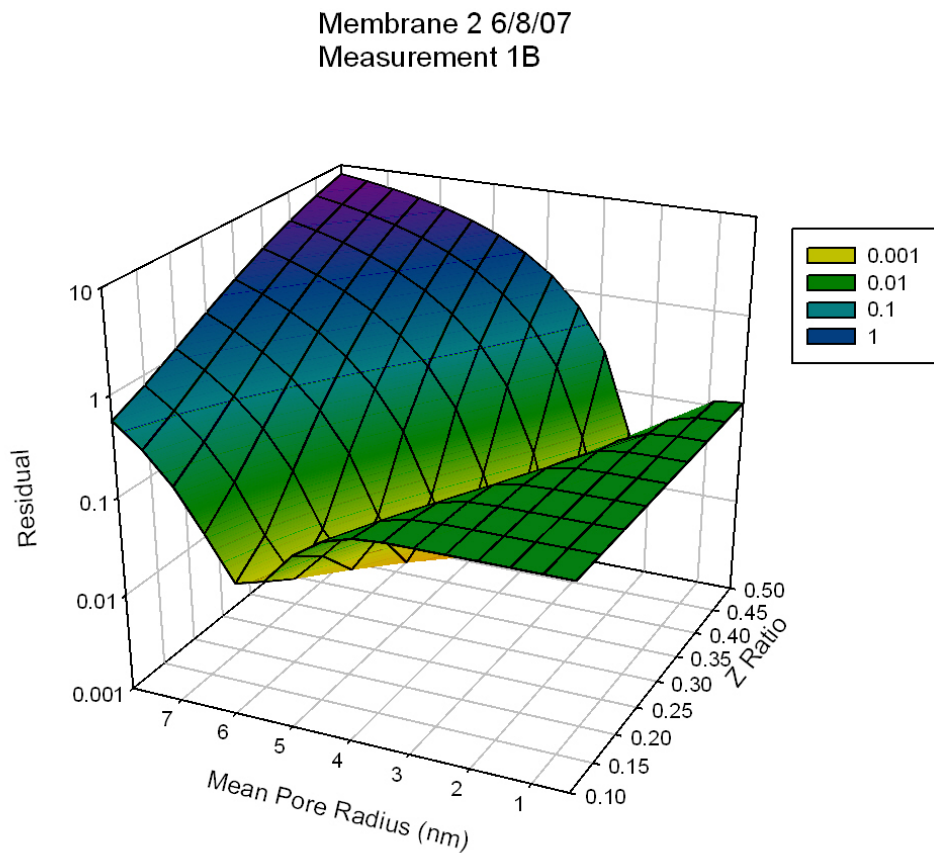


Figure B.2. Sum of squared residuals (SSR) between the theoretical and experimental actual sieving coefficient for various values of mean pore radius and Z ratio.

Figure B.2 shows there is a tradeoff between the higher pore size and the lower pore distribution to which the data can be correlated. In most of the membranes tested there were many combinations of mean pore radius and z ratios that provide similar fits.

Computer Program (Software: Mathematica 6.0)

(*Computer program to determine the best fit pore size and pore size distribution from polydispersed dextran sieving data*)

(*Experimental Conditions*)

$\epsilon = 0.5$; (*membrane void fraction*)

$\delta m = .5 * 10^{-6}$; (*membrane thickness, m*)

$Jv = 1.439 * 10^{-5}$; (*Flux ,m/s*)

$\mu = .001$; (*viscosity, kg/m/s*)

(*Constants for hydrodynamic drag*)

$a_1 = -73/60$;

$a_2 = 77293/50400$;

$a_3 = -22.5083$;

$a_4 = -5.6117$;

$a_5 = -0.3363$;

$a_6 = -1.216$;

$a_7 = 1.647$;

$b_1 = 7/60$;

$b_2 = -2277/50400$;

$b_3 = 4.0180$;

$b_4 = -3.9788$;

$b_5 = -1.9215$;

$b_6 = 4.392$;

$b_7 = 5.006$;

(*Loop parameters*)

i = 0;
Finalz = 100;
FinalMeanRad = 100;
FinalResidualSum = 100;
FinalPerm = 100;
LoopCount = 1;
Residual = 0;

ResidualList = {};
zlist = {};
Rlist = {};
Tot = 0;

(*Experimental data*)

(*Dextran molecular weights used*)

MWKD = {125.5, 112.8, 104.1, 93.6, 86.4, 77.7, 71.7, 64.5, 59.5, 53.5,
49.4, 44.4, 43.9, 41.0, 36.8, 34.0, 31.4, 28.2};
MW = MWKD * 1000;

(*Experimental Actual Sieving Coefficients*)

Sexp = {0.00560, 0.00747, 0.00930, 0.01172, 0.01404, 0.01732, 0.02042,
0.02473, 0.02878, 0.03439, 0.03973, 0.04710, 0.05036, 0.05670,
0.06600, 0.07377, 0.08222, 0.09234};

(*Do Loop to form matrix of residuals*)

```

Do {
  Do { i = 0;
    Residual = 0;
    Do { i = i + 1;
      { InitMW = Part[MW, i];
        Dinf = 7.667 * 10-9 * InitMW-0.47752;
        (*diffusion coefficient for Dextran from molecular weight*)
        Rs = (1.3806503 * 10-23 * (23 + 273.15)) / (6 * π * 0.001 * Dinf) * 109;
        (*hydrodynamic radius from molecular weight*)
        λ = Rs / r;
        φ = (1 - λ)2;

        Ks =  $\frac{9}{4} * \pi^2 * (2)^{0.5} (1 - \lambda)^{-2.5} * \left( 1 + \sum_{k=1}^2 b_k (1 - \lambda)^k \right) +$ 
               $\sum_{k=0}^4 (b_{k+3}) * (\lambda)^k;$ 

        Kt =  $\frac{9}{4} * \pi^2 * (2)^{0.5} (1 - \lambda)^{-2.5} * \left( 1 + \sum_{k=1}^2 a_k (1 - \lambda)^k \right) +$ 
               $\sum_{k=0}^4 (a_{k+3}) * (\lambda)^k;$ 

        Kc =  $\frac{(2 - \phi) * Ks}{2 * Kt};$ 
        Kd = 6 * π / Kt;
      }
    }
  }
}

```

Sinf =

$$\left(\text{NIntegrate} \left[\phi * \text{Kc} * \frac{1}{r * (2 * \pi)^{0.5}} (\text{Log}[1 + (z)^2])^{-0.5} * \right. \right. \\ \left. \left. \text{Exp} \left[- \left(\text{Log} \left[\frac{1}{R_*} (r * (1 + (z)^2)^{0.5}) \right] \right)^2 / (2 * \text{Log}[1 + (z)^2]) \right] * r^4, \right. \right. \\ \left. \left. \{r, (R_s + 0.1), \infty\} \right] \right) / \\ \left(\text{NIntegrate} \left[\frac{1}{r * (2 * \pi)^{0.5}} (\text{Log}[1 + (z)^2])^{-0.5} * \right. \right. \\ \left. \left. \text{Exp} \left[- \left(\text{Log} \left[\frac{1}{R_*} (r * (1 + (z)^2)^{0.5}) \right] \right)^2 / (2 * \text{Log}[1 + (z)^2]) \right] * r^4, \{r, 0, \infty\} \right] \right);$$

sdif =

$$\left(\text{NIntegrate} \left[\phi * \text{Kd} * \frac{1}{r * (2 * \pi)^{0.5}} (\text{Log}[1 + (z)^2])^{(-0.5)} * \right. \right. \\ \left. \left. \text{Exp} \left[- \left(\text{Log} \left[\frac{1}{R_*} (r * (1 + (z)^2)^{0.5}) \right] \right)^2 / (2 * \text{Log}[1 + (z)^2]) \right] * r^4, \{r, (R_s + 0.1), \infty\} \right] \right) / \\ \left(\text{NIntegrate} \left[\frac{1}{r * (2 * \pi)^{0.5}} (\text{Log}[1 + (z)^2])^{(-0.5)} * \right. \right. \\ \left. \left. \text{Exp} \left[- \left(\text{Log} \left[\frac{1}{R_*} (r * (1 + (z)^2)^{0.5}) \right] \right)^2 / (2 * \text{Log}[1 + (z)^2]) \right] * r^4, \{r, 0, \infty\} \right] \right);$$

Pem = **Sinf** / (**Sdif** * **e**) * (**Jv** * **δm** / **Dinf**) ; (*Peclet number*)

Sa = **Sinf** * **e** (**Pem**) / (**Sinf** + **e** (**Pem**) - 1) ;
(*Actual Sieving coefficient*)

Residual = **Residual** + (**Sa** - **Sexp**[[**i**]])² ;

$$\begin{aligned}
L_p = & \left(\left(\frac{\epsilon}{\delta m * (10)^9 * 8} \right) * \text{NIntegrate} \left[\frac{1}{r * (2 * \pi)^{0.5}} (\text{Log}[1 + (z)^2])^{(-0.5)} * \right. \right. \\
& \left. \left. \text{Exp} \left[- \left(\text{Log} \left[\frac{1}{R_*} (r * (1 + (z)^2)^{0.5} \right] \right) \right]^2 / (2 * \text{Log}[1 + (z)^2]) \right] * r^4, \{r, 0, \infty\} \right] \right) / \\
& \left(\text{NIntegrate} \left[\frac{1}{r * (2 * \pi)^{0.5}} (\text{Log}[1 + (z)^2])^{(-0.5)} * \right. \right. \\
& \left. \left. \text{Exp} \left[- \left(\text{Log} \left[\frac{1}{R_*} (r * (1 + (z)^2)^{0.5} \right] \right) \right]^2 / (2 * \text{Log}[1 + (z)^2]) \right] * r^2, \{r, 0, \infty\} \right] \right) * \\
& (10)^{-9}; \\
& \left. \right\}, \{\text{LoopCount}, 18\} \};
\end{aligned}$$

ResidualList = Append[ResidualList, Residual];

zlist = Append[zlist, z];

Rlist = Append[Rlist, R_*];

Finalz = If[Residual < FinalResidualSum, z, Finalz];

FinalMeanRad = If[Residual < FinalResidualSum, R_*, FinalMeanRad];

FinalPerm = If[Residual < FinalResidualSum, Lp, FinalPerm_];

FinalResidualSum = If[Residual < FinalResidualSum, Residual, FinalResidualSum];

}, {z, .1, .6, .05}];

}, {R_*, .4, 8, .5}];

Arraycomp = {ResidualList, zlist, Rlist};

TranArray = Transpose[Arraycomp];

Export["ToGraph.csv", TranArray]

Appendix C

CHARGE REGULATION THEORY

The net electrostatic charge on a protein can be estimated directly from the amino acid sequence, the pH, and the solution ionic strength. The number of dissociated acid and basic amino residues is calculated from the pK_a^i value for each amino acid as shown for a carboxylic acid residue in Equation C.1.

$$K_a^i = \frac{[R-COO^-][H^+]}{[R-COOH]} \quad (\text{C.1})$$

Equation C.1 can be rewritten in terms of the pH and the number of dissociated groups (r_i)

$$pH = pK_{\text{int}}^i + \log \frac{r_i}{(n_i - r_i)} \quad (\text{C.2})$$

where $pH = -\log_{10}[H^+]$, $pK_{\text{int}}^i = -\log_{10}[K_{\text{int}}^i]$, and n_i is the total number of titratable species. The local concentration of $[H^+]$ at the protein surface (required in Equations C.1 and C.2) can be related to the bulk H^+ concentration assuming a Boltzmann distribution:

$$H^+ = H_{\text{bulk}}^+ \exp[-(e\psi_o / k_B T)] \quad (\text{C.3})$$

where e is the charge of an electron ($1.602 \cdot 10^{-19}$ C), k_B is Boltzmann's constant, T is the temperature, and ψ_o is the electrical potential at the surface of the protein. The surface potential for a hard sphere is directly proportional to the net protein charge (z):

$$\psi_o = \frac{ez}{4\pi\epsilon_o\epsilon_r a(1 + \kappa a)} \quad (\text{C.4})$$

where ε_0 is the permittivity of a vacuum, ε_r is the relative permittivity, a is the protein radius, and κ is the inverse Debye length. The protein charge is equal to the difference between the maximum number of positive charges (N-terminal, histidine, lysine, arginine) and the sum of all the dissociated groups:

$$z = z_{\max}^+ - \sum_i r_i \quad (\text{C.5})$$

Equations C.2 to C.5 are solved iteratively to evaluate the net protein charge as a function of the bulk pH and the solution ionic strength (which determines the Debye length). The development of these equations is discussed in more detail by Menon and Zydney (2000).

Table C.1 shows the number of each type of ionizable amino acid present in the protein α -lactalbumin molecule along with the corresponding pK_a . The net charge for each PEGylated and acetylated α -lactalbumin species was calculated by removing one lysine group for each covalent linkage. It is implicitly assumed that the net charge of the PEGylated and acetylated α -lactalbumin with the same number of substitutions was equal.

Table C.1. Number and pK_a values for the dissociable amino acids in α -lactalbumin (Brew, et al., 1970)

Chart of Residues	n_i	pK_a^i
C terminal	1	2.16
N terminal	1	9.87
Asp (D)	9	3.9
Glu (E)	8	3.9
His (H)	3	6.04
Lys (K)	12	10.54
Tyr (Y)	4	10.35
Arg (R)	0	12.48

It is important to note that the net charge evaluated from Equations C.2 to C.5 completely ignores the possible effects of ion binding to the protein, a phenomenon

which is known to be important for bovine serum albumin (Menon and Zydney, 1998) but has not been studied in any detail for α -lactalbumin. In addition, the analysis ignores the detailed distribution of charge groups over the protein surface, with each amino acid residue of a given type assumed to have identical pK_a and thus identical degrees of protonation. More sophisticated models for calculating protein charge are available (Sharma et al., 2003), but those analyses require very detailed information about the protein structure.

Figure C.1 shows the theoretical charge of the α -lactalbumin as a function of pH for α -lactalbumin and α -lactalbumin with one or two primary amines removed from the system. The number of positive charges on the protein is high at low pH and goes through the point of zero charge at the isoelectric point of the protein. Most electrophoresis experiments were performed at pH 8 where the charge of the α -lactalbumin and the substituted α -lactalbumin molecules differ by approximately one charge unit. At very high pH, all of the ionizable groups become neutral or positively charged so no difference exists between the different substituted groups.

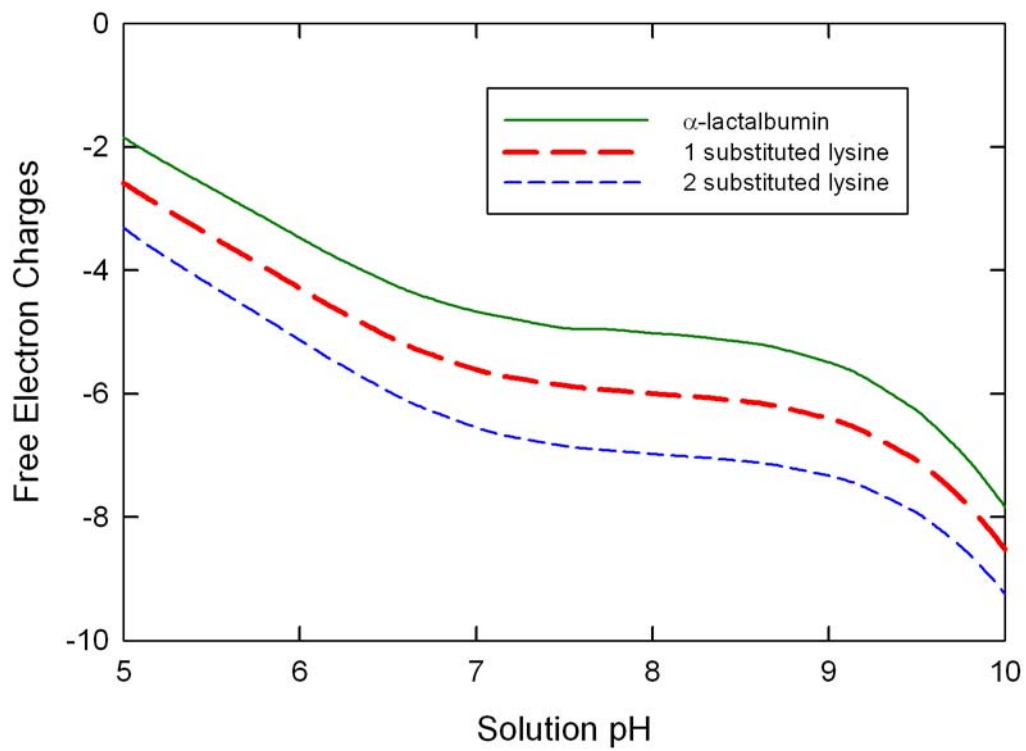


Figure C.1. Calculated net charge of α -lactalbumin and an α -lactalbumin with 1 or 2 substituted lysine groups as a function of the solution pH.

VITA
Jessica Molek

EDUCATION

Pennsylvania State University, University Park, Pennsylvania

Doctor of Philosophy in **CHEMICAL ENGINEERING**

Dec. 2008

Lafayette College, Easton, Pennsylvania

May 2003

Bachelor of Science in **CHEMICAL ENGINEERING**

Minor in Environmental Science

ACADEMIC RESEARCH EXPERIENCE

Doctoral Research

Nov. 2003 to Aug. 2008

Advisor: Dr. Andrew Zydney, The Pennsylvania State University

Thesis Title: Ultrafiltration of PEGylated Proteins.

Undergraduate Research

Aug. 2002 to May 2003

Advisor: Dr. Javad Tavakoli, Lafayette College

Thesis Title: Effect of Feed Composition on the Deactivation of Palladium Catalyst.

INDUSTRIAL EXPERIENCE

Graduate Intern (Genentech Inc, South San Francisco, CA.)

July 2006 to Jan. 2007

Supervisor: Nuno Fontes

Explored the use of ultrafiltration membranes for the separation of therapeutic proteins from host cell protein impurities using scaleable equipment.

Process Engineering Intern (Procter and Gamble, Mehoopany, PA)

May 2002 to Aug. 2002

Supervisor: Michael Lennon

Led projects on the optimization of a vacuum system on a papermachine. Managed a group effort on the reductions of fires occurring on the papermachine.

TEACHING EXPERIENCE

Laboratory Teaching Assistant

(Pennsylvania State University) Aug. 2005 to Dec. 2005

Mass Transfer Teaching Assistant

(Pennsylvania State University) Aug. 2004 to Dec. 2004

PUBLICATIONS

Latulippe, D.; Molek, J.; Zydney, A., *Industrial and Engineering Chemistry Research*. Expected publication date Mar. **2009**

Kwon, B.; Molek, J. R.; Zydney, A. L., *Journal of Membrane Science*. Vol 319 No 1-2. Jul. **2008**. pp. 206-213.

Molek, J. Zydney, A. *Biotechnology Progress*. Vol 23. Dec. **2007**. pp. 1417-1424.

Molek, J. Zydney, A. *Biotechnology and Bioengineering*. Vol 95, No. 3. Oct. **2006**. pp. 474-482.

ORAL PRESENTATIONS/ CONFERENCE PROCEEDINGS

Molek, J. Zydney, A. "Purification of PEGylated Proteins Using Charged Ultrafiltration

Membranes," North American Membrane Society Meeting, Orlando, FL, May 2007.

Fontes, N. Molek, J. Van Reis, R. "HPTFF for industrial-scale non-affinity MAB purification," North American Membrane Society Meeting, Orlando, FL, May 2007

Molek, J. Zydney, A. "Ultrafiltration of PEGylated Proteins," American Institute of Chemical Engineers Annual Meeting, San Francisco, CA, Sept. 2006.

Molek, J. Zydney, A. "Ultrafiltration of PEGylated Proteins," American Chemical Society National Meeting, San Francisco, CA, Sept. 2006.

Molek, J., Zydney, A. "Separation of PEGylated Proteins," North American Membrane Society Meeting, Providence, RI, June 2005.

SELECTED AWARDS

General Electric Faculty of the Future Fellowship, Jan. 2008, Aug. 2003

Harry G. Miller Fellowship in Engineering, Jan. 2008

NAMS Student Poster and Travel Award, May 2005, May 2007

National Science Foundation Graduate Research Fellowship, Aug. 2003